INTERNATIONAL STUDIES AND EVALUATIONS IN THE FIELD OF

ENGINEERING

December 2024

EDITORS

PROF. DR. COŞKUN ÖZALP

PROF. DR. SELAHATTN BARDAK

SERÜVEN YAYINEVİ

Genel Yayın Yönetmeni / Editor in Chief • C. Cansın Selin Temana

Kapak & İç Tasarım / Cover & Interior Design • Serüven Yayınevi

Birinci Basım / First Edition • © Aralık 2024

ISBN • 978-625-5955-67-8

Serüven Yayınevi / Serüven Publishing
Türkiye Adres / Turkey Address: Kızılay Mah. Fevzi Çakmak 1. Sokak
Ümit Apt No: 22/A Çankaya/ANKARA
Telefon / Phone: 05437675765
web: www.seruvenyayinevi.com
e-mail: seruvenyayinevi@gmail.com

Baskı & Cilt / Printing & Volume
Sertifika / Certificate No: 47083

INTERNATIONAL RESEARCH AND EVALUATIONS IN THE FIELD OF ENGINEERING

EDITORS

PROF. DR. COŞKUN ÖZALP

PROF. DR. SELAHATTN BARDAK

SERÜVEN YAYINEVİ

Contents

Chapter 1

DETERMINATION OF LAND CONSOLIDATION SUCCESS CRITERIA: ISPARTA YENIŞARBADEMLI GÖLYAKA EXAMPLE

Ömer ACAR[1]

1 Ögr. Gör., Kahramanmaraş Sütçü İmam Üniversitesi, Göksun Meslek Yüksekokulu, Mimarlık ve Şehir Planlama Bölümü, oacar@ksu.edu.tr, Orcid No: 0000-0002-2382-8594

ENTRANCE

Land plays a role as a material, elemental, and spatial carrier for the socio-economic activities of human society (Esina, 2009; Long, 2014; Li & Li, 2017; Long & Qu, 2018; Qu and Long, 2018; Long et al., 2019). In this context, the economic and social development processes of rural areas are built on three basic factors: population, land (land use and natural resources) and industry (production and economic activities) (Ge et al., 2018a; Long et al., 2018; Tu and Long, 2017). These factors are considered as the basic elements that shape the dynamics of rural development and play a key role in ensuring the sustainability of rural life (Ge et al., 2018b).

In terms of restructuring rural areas and achieving sustainable development goals, coordination of human-land relations is of critical importance (Toklu, 2010; Albaladejo et al., 2021). 2030 In this context, land consolidation, beyond being just a regulatory tool, fulfills many vital functions compatible with the multidimensional goals of rural revitalization. Land consolidation practices undertake a wide range of strategic roles such as ensuring food security in rural areas, improving the living environment, encouraging intensive and scientific use of resources, and coordinating rural development (Li et al., 2017; Long et al., 2010; Long, 2014; Long and Tu, 2018). This process also functions as a mechanism for eliminating economic, social and environmental imbalances in rural areas. Effective implementation of land consolidation allows increasing agricultural production efficiency, optimizing land use patterns and redesigning the spatial order of rural areas (Long et al, 2012). Thus, it becomes possible to manage the natural and human resources of rural areas in a sustainable manner, while significant progress is being made in achieving the multiple goals of rural development. Therefore, land consolidation emerges as both a strategic component of rural development and a fundamental tool supporting the sustainability of this development.

The concept of land consolidation first emerged in Germany in 1343 (Demetriou et al., 2012; Kocur-Bera et al., 2023). Until the 17th century, it was implemented to increase agricultural production by combining scattered parcels (Van Dijk, 2007). In the 18th and 19th centuries, with the influence of the industrial revolution, it was aimed to intensify agricultural production in England, establish large agricultural enterprises and increase productivity, but it caused enterprises with small parcels to lose their land. This process brought about modernization in agriculture and increased production (Humphries, 1990; Allen, 1992). In the 20th century, with the widespread use of consolidation projects, agricultural machinery, and irrigation systems, agricultural productivity gained importance. In the post-World War II period, state-supported programs were used to consolidate fragmented lands in European countries (Van Dijk, 2007).

Successful projects were produced to increase agricultural productivity through consolidation in countries such as the Netherlands, Germany, and Denmark (Demetriou, 2013). In the 20th century, consolidation projects began to take into account not only economic but also environmental and social factors (Vitikainen, 2004; Jürgenson, 2016). They were integrated with rural development and agricultural reform, especially in developing countries (Zhou et al., 2020). Countries with an economy based on agriculture aimed to solve both economic and social problems with consolidation efforts (Uzun and Yomralıoğlu, 2005; Karaman and Gokalp, 2018). Today, land consolidation projects are addressed within the framework of environmental sustainability, water resource management and digitalization in agriculture (Ercan, 2024; Robinson, 2024). More efficient planning is made by using Geographic Information Systems and satellite technologies (Köseoğlu and Gündoğdu, 2004; Guo et al., 2020). Historically, land consolidation projects have shifted from economic efficiency to environmental and social sustainability. While initially carried out to increase agricultural production, today they have evolved into a multidimensional structure such as rural development, natural resource management and adaptation to modern technologies. They have been shaped in line with different purposes depending on economic, political and technological developments.

MATERIAL METHOD

In this study, numerical and attribute data, which are the basis of registration, belonging to the Gölyaka neighborhood land consolidation study included in the Isparta Yenişarbademli Şehit Hüseyin Gökhan Eriç Dam Irrigation Land Consolidation and In-Farm Development Services Project were used (Figure 1). 4 neighborhoods and approximately 2300 hectares of land were included in the arrangement in the project area. The data belonging to the project area were obtained from Adalya Engineering Consultancy Services Construction Real Estate Limited Company. LiCAD, LiTOP 7, ArcMap 10.5, and NetCAD 8.5 software were used in the analysis, calculations, and creation of thematic maps within the scope of the study.

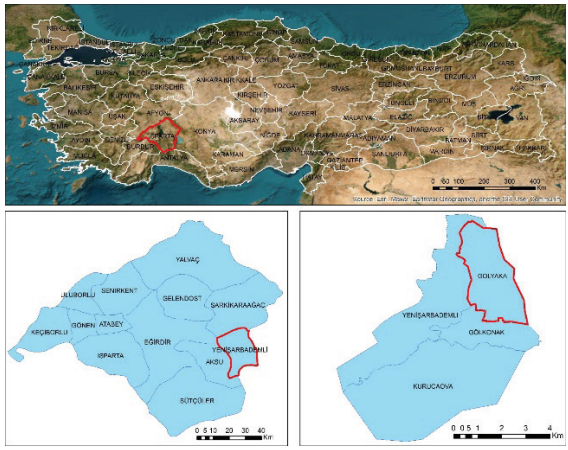

Figure 1. Gölyaka Neighborhood Location Map

Within the scope of the study, the pre-consolidation and post-consolidation status of the Gölyaka Neighborhood was evaluated. The distribution of parcels according to their sizes, the geometric shapes of the parcels, and the direct utilization rates from the transportation network were examined. Within the scope of the regulation, the interruption rate due to newly opened roads, irrigation, and drainage systems, as well as the consolidation rate, which is among the success criteria of the project, were calculated.

FINDINGS

There are a total of 1266 businesses within the scope of the Gölyaka Neighborhood consolidation project. Before the project, a total of 529.80 hectares of the parcel area, 3731 parcels, and the average parcel size of these parcels were calculated as 1.42 decares. After the project, a total of 493.73 hectares of the parcel area, 1915 parcels, and the average parcel size of these parcels were calculated as 2.58 decares (Table 1).

Table 1. Gölyaka Neighborhood Project Summary

	Before the Project	**After the Project**
Parcel Area (ha)	529.80	493.73
Number of Parcels	3731	1915
Average Parcel Size (da)	1.42	2.58

The general situation map of the Gölyaka Neighborhood is given in Figure 2. The parcels are small in area and are numerous. Since there are many parcels that are excluded from consolidation among the parcels, the general situation map was created in two sections (Figures 2-3-4). As can

be seen in situation map number 1 of the project area shown in Figure 3, the parcels are not suitable for agricultural mechanization because they are long and thin.

Figure 2. General Situation Map of Gölyaka District Before Consolidation

Figure 3. *Gölyaka District Number 1 Pre-Consolidation Situation Map*

Figure 4. *Gölyaka District Number 2 Pre-Consolidation Situation Map*

The general situation map of Gölyaka District after the consolidation is shown in Figure 5. When compared with the situation map before consolidation, the changes in the shape and size of the parcels can be noticed on the maps (Figures 5-6-7). It is seen that the parcels, which were thin and long before consolidation, were formed more uniformly after consolidation (Figure 6).

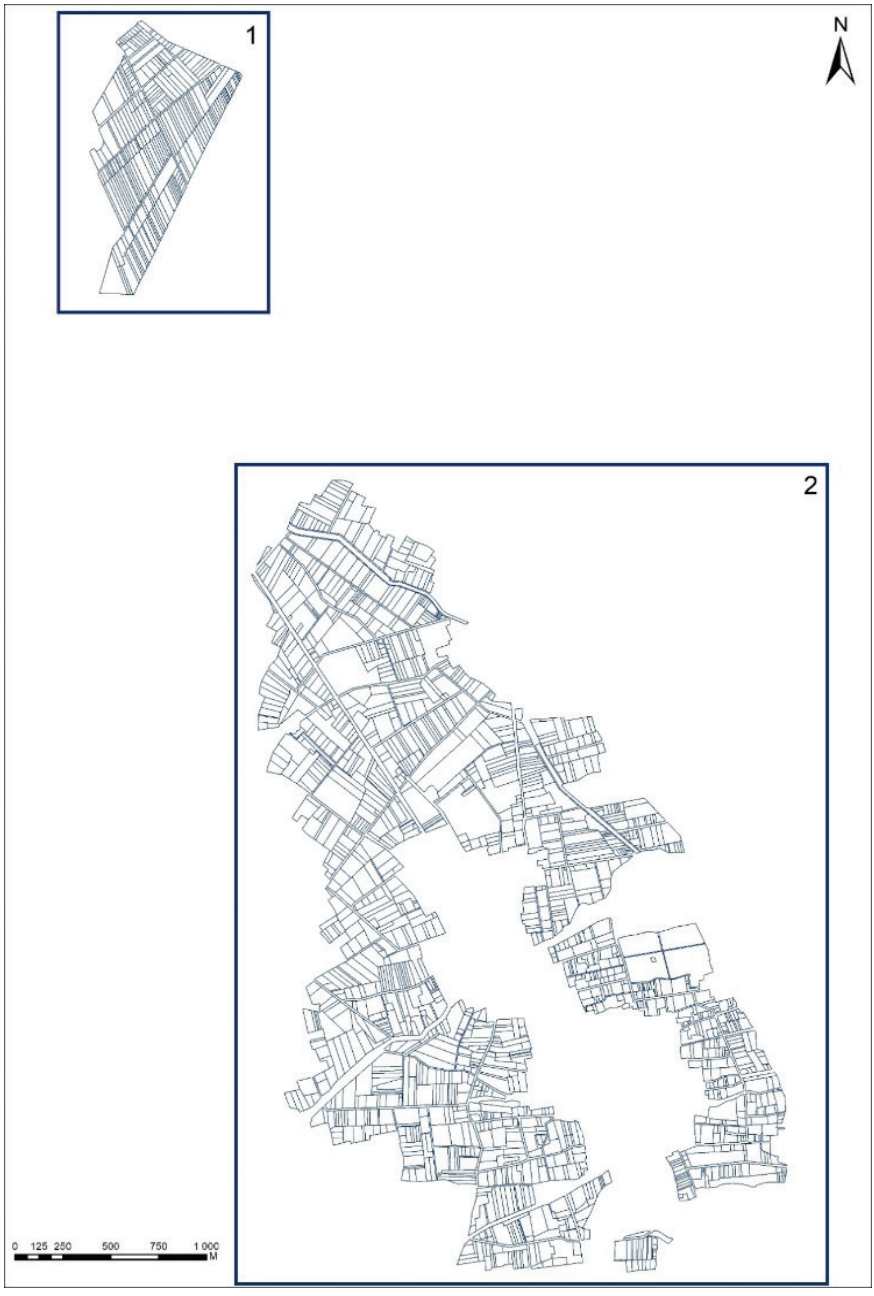

Figure 5. *Gölyaka Mahallesi 1 Numaralı Bölge Toplulaştırma Sonrası Durum Haritası*

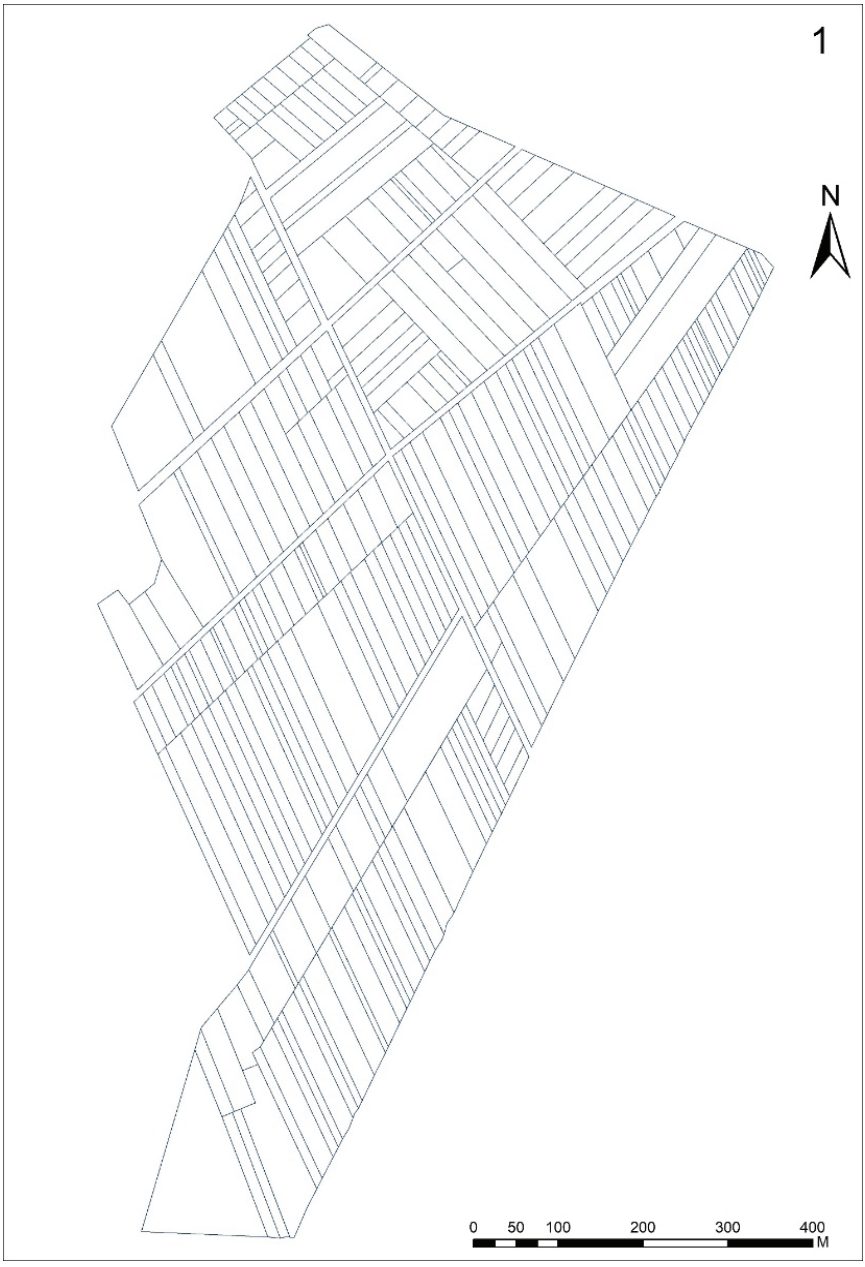

Figure 6. *Gölyaka Mahallesi 1 Numaralı Bölge Toplulaştırma Sonrası Durum Haritası*

Figure 7. *Gölyaka Mahallesi 2 Numaralı Bölge Toplulaştırma Sonrası Durum Haritası*

When the distribution of parcels in the project area according to parcel sizes is examined, the areal density of the parcels before and after the project is in the range of 0-5 decares (Table 2). Increases were detected in

the average size of the parcels' area groups. It is predicted that the increase in the average parcel size will increase agricultural production efficiency.

Table 2. *Distribution According to Gölyaka Neighborhood Parcel Sizes*

	Before Consolidation			After Consolidation		
Parcel Groups (Da)	**Number of parcels**	**%**	**Average Plot Size (Da)**	**Number of parcels**	**%**	**Average Plot Size (Da)**
0 - 5	3670	98.37	1.25	1770	92.43	1.92
6 - 10	44	1.18	7.42	118	6.16	7.84
11 - 20	11	0.29	16.19	14	0.73	14.74
21 - 50	5	0.13	26.93	12	0.63	29.13
51 - 100	1	0.03	58.88	1	0.05	58.38
Total	**3731**	**100.00**	**1.42**	**1915**	**100.00**	**2.58**

While parcel geometry is among the criteria affecting agricultural mechanization, the appropriate parcel geometry for agricultural production should be rectangular, with an aspect ratio between 1/3 and 1/7. The most appropriate geometric shape for agricultural production is rectangular. In the order of parcel shape suitability, square, trapezoid, amorphous, and triangular took their place in the literature after rectangle. (Acar and Akdeniz, 2023). In the parcel shape analysis conducted in the study area, it is seen that the number of rectangular parcels increased from approximately 33% to 39%, an increase of 6%. The number of trapezoidal parcels increased by 1%. The number of triangular parcels decreased by 5%, and the number of square-shaped parcels decreased by 1%. When the number of amorphous parcels was evaluated before and after the project, it was determined to decrease by a small amount (Table 3).

Table 3. *Gölyaka Neighborhood Parcel Shapes*

Parcel Shape	**Before Project**		**After Project**	
	Pieces	**%**	**Pieces**	**%**
Triangle	308	8.26	50	2.61
Square	121	3.24	32	1.67
Rectangle	1216	32.59	755	39.43
Trapezoid	1602	42.94	841	43.92
Shapeless	484	12.97	237	12.38
Total	**3731**	**100.00**	**1915**	**100.00**

The transportation network must be sufficient for the machines used in agricultural production to be used optimally (Acar & Bengin, 2018). One thousand eight hundred sixty-five parcels were excluded from the arrangement in the project area. Of the parcels included in the arrangement within the scope of consolidation, 1816 parcels do not have direct frontage to the road transportation network. One thousand nine hundred fifteen parcels directly benefit from the transportation network (Figures 8-9-10). When considered proportionally, approximately 49% of the parcels included in the arrangement do not have frontage to the transportation network and, therefore, provide transportation through the parcels that directly benefit from the transportation network. All of the parcels included in the arrangement after consolidation were planned so that they could directly benefit from the transportation network.

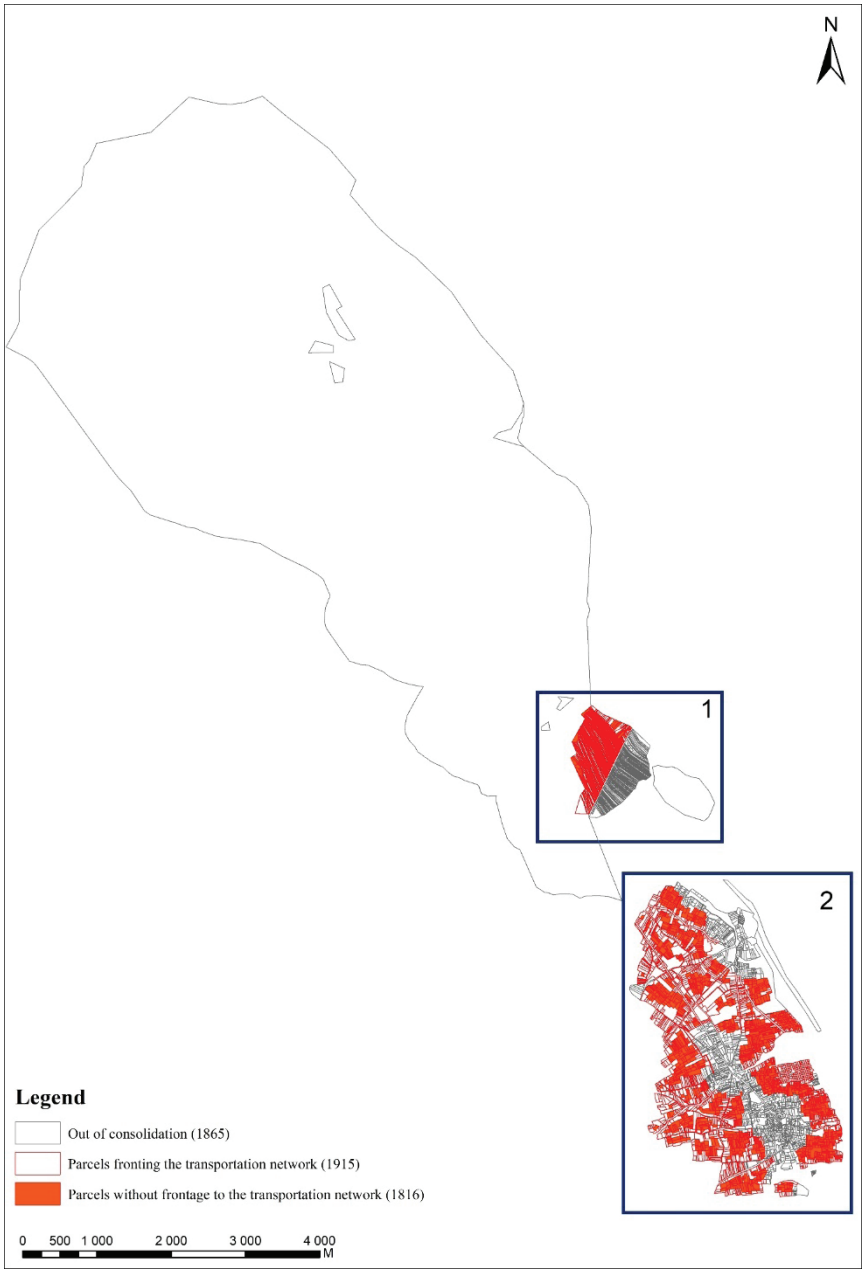

Figure 8. *Gölyaka District Transportation Network General Situation Map*

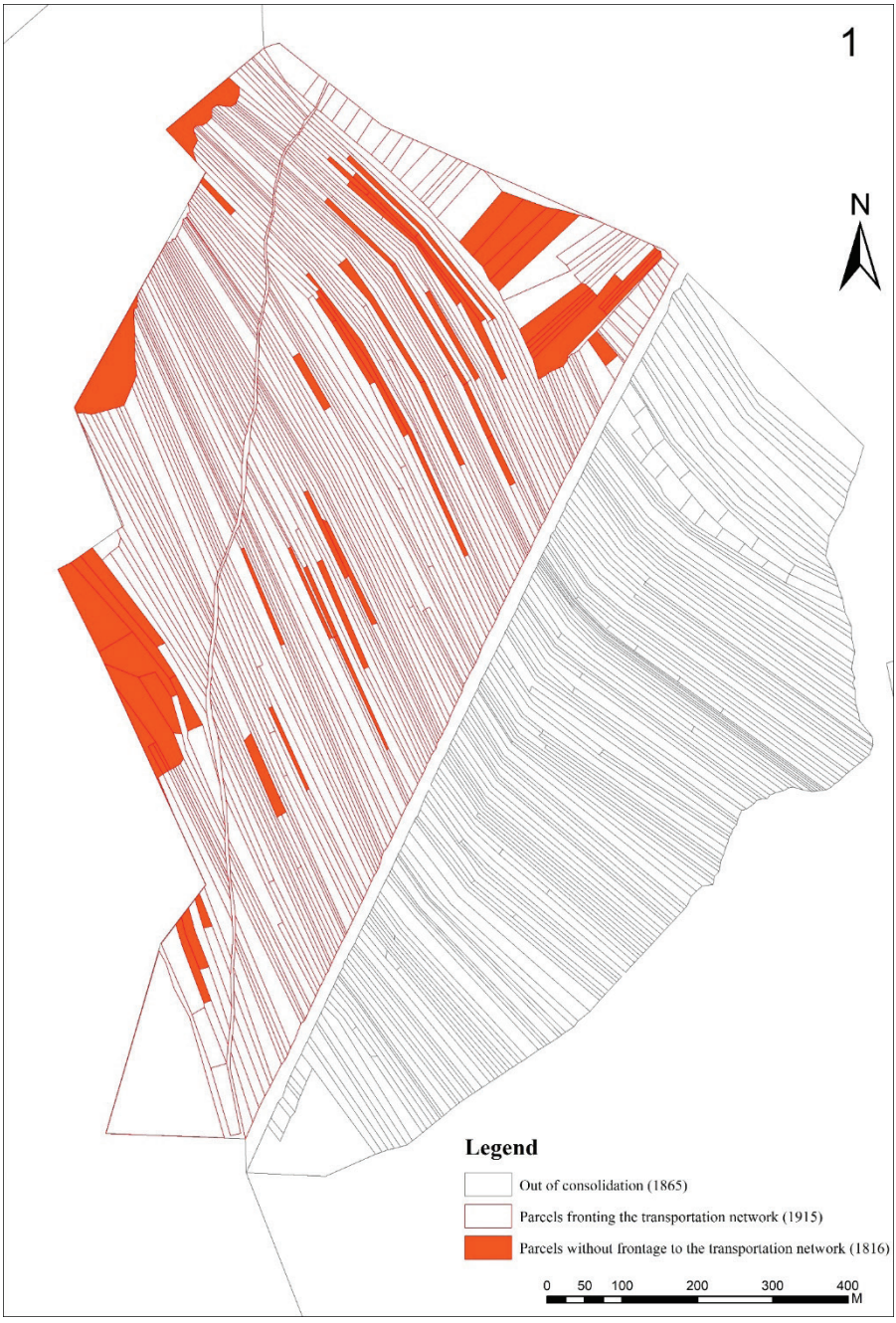

Figure 9. *Gölyaka District Number 1 Transportation Network Map*

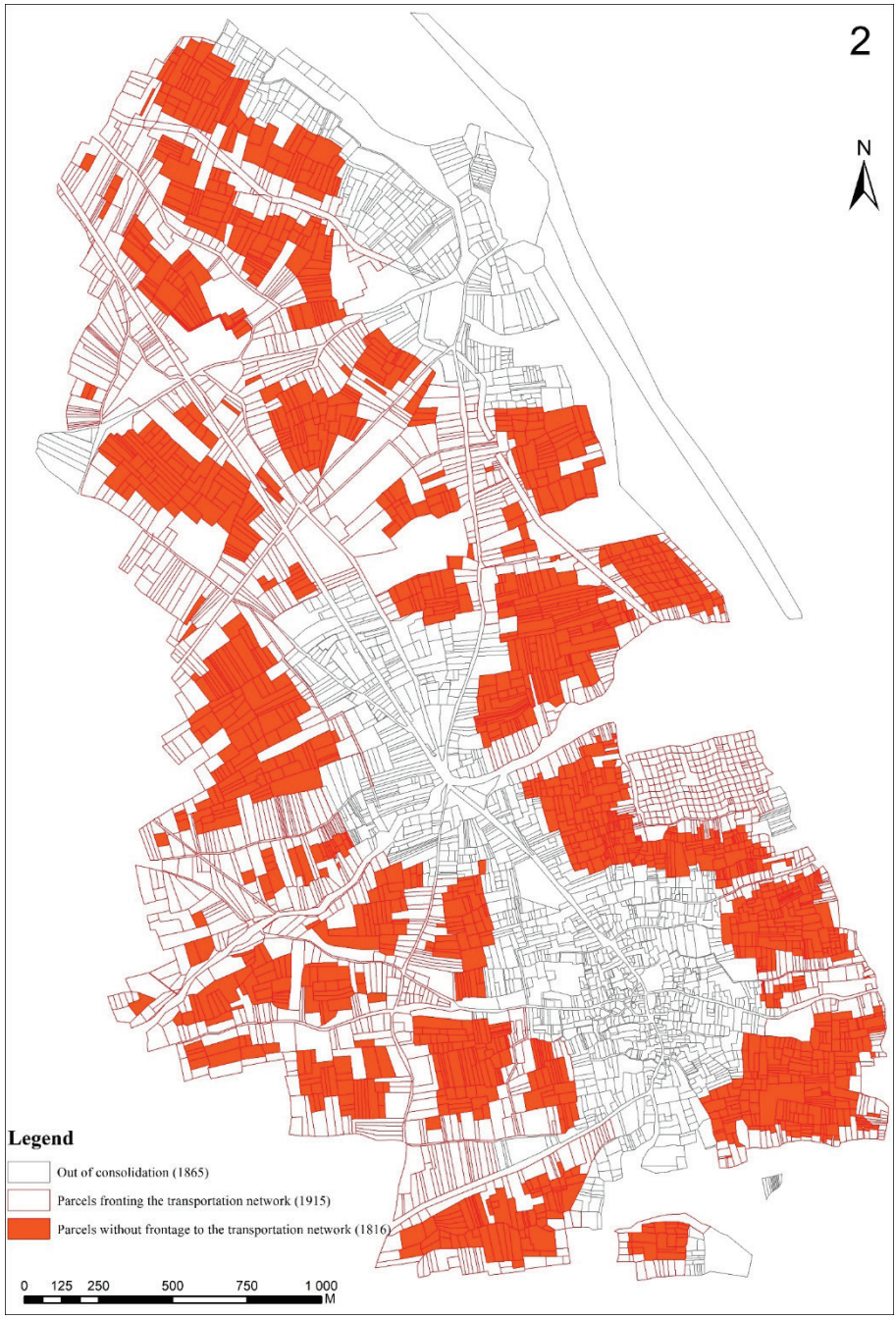

Figure 10. *Gölyaka District Number 2 Transportation Network Map*

Inland consolidation projects, a proportional deduction is made from all parcels subject to regulation to provide space for common facilities (such as newly opened roads and irrigation systems) established within the

project's scope. The consolidation legislation stipulates that up to 10% of the deduction rate can be made free of charge (Acar, 2023). The deduction rate within the scope of the regulation made in the study area was calculated as 6.91%, and this rate was deducted from all parcels included in the regulation.

The consolidation rate is used to evaluate the success criterion of consolidation projects. In the project area, 3731 parcels were included in the regulation before and completed with 1915 parcels after the regulation. A consolidation rate of 48.67% was reached in the project area, and registration procedures were carried out.

CONCLUSION

Land consolidation projects allow spatial changes on a parcel basis in agricultural production areas. Along with the locations of the parcels, arrangements are also made in their shapes and sizes. Geometric shapes in agricultural areas are considered an adequate criterion in production costs from plowing to harvesting operations. It is known that the parcel geometry, being in the most ideal shape for agricultural production, minimizes labor and fuel costs. The strong transportation network of agricultural production areas contributes to minimizing areal losses and ensuring social peace. In agricultural areas with insufficient transportation networks, transportation is provided through other parcels, and sometimes, this situation can cause hostility between farmers. In this context, it is important to evaluate consolidation projects' contribution to agricultural production and conduct post-project research. In the study area, there has been an increase in the number of rectangular and trapezoidal parcels.

In contrast, the geometric shapes of the parcels have decreased compared to the pre-project period. The rectangular shape has the highest increase and is the most suitable shape for agricultural production. At the same time, the change in the project area has shown a slight tendency in this direction. The failure to fully correct the parcel geometry is due to the distorted geometric structure of the neighborhood outer borders, the fixed facilities on the land of the owners, and the road and irrigation systems not being constructed linearly. In the studies carried out, border correction for the outer border of the project area will contribute significantly to the correction of parcel geometries.

A consolidation rate of 48.67% was achieved in the project carried out in the Gölyaka neighborhood. Scattered and fragmented lands belonging to the same enterprise were combined, showing its effect in geometric shapes. The average parcel size in the project area increased from 1.42 decares to 2.58 decares; approximately 82% was achieved. By bringing the parcels

together, the total parcel border length is reduced, and the usable area for agricultural production is increased.

As a result of the analyses made, we can say that the Gölyaka land consolidation and in-field development services project is successful. It is foreseen that positive benefits will be provided when the pre-project and post-project situations are compared with the arrangement made. Although the contribution of consolidation projects to the reduction of agricultural production costs is seen immediately, the benefit to be provided in production efficiency may take some time. Providing more detailed information to farmers in the project area during the interview phase and explaining in more detail the benefits and opportunities that consolidation efforts will provide to farmers will contribute to increasing the project success rate.

REFERENCES

Acar, Ö. (2023). Balıkesir- Manyas – Akçaova Köyü Toplulaştırma Projesi Teknik Analizi. Fazıl Nacar (Ed.), Mekansal Bilgi ve Analiz (s. 32-47). Bidge Yayınları, ISBN: 978-625-6707-28-3

Acar, Ö., Bengin, E. (2018). Yozgat (Baştürk Köyü) Arazi Toplulaştırma Projesinin Bölgesel Kalkınma Açısından Değerlendirilmesi, III. Uluslararası Bozok Sempozyumu, 3-5 Mayıs, Bozok Üniversitesi, Yozgat.

Acar, Ö., ve Akdeniz, H. B., (2023). Arazi Toplulaştırma Projelerinin Parsel Şekil Değişimine Etkisinin Analizi: Manyas/Salur Mahallesi Örneği, Türkiye. Tarımsal Eski Sorunlara Yeni Yaklaşımlar (s. 81–101). İksad yayınevi. https://doi.org/10.5281/zenodo.8373721

Albaladejo, J., Díaz-Pereira, E., & de Vente, J. (2021). Eco-holistic soil conservation to support land degradation neutrality and the sustainable development goals. Catena, 196, 104823.

Allen, R. C. (1992). Enclosure and the yeoman: the agricultural development of the South Midlands 1450-1850. Oxford University Press.

Demetriou, D. (2013). The development of an integrated planning and decision support system (IPDSS) for land consolidation. Springer Science & Business Media.

Demetriou, D., Stillwell, J., & See, L. (2012). Land consolidation in Cyprus: why is an integrated planning and decision support system required?. Land use policy, 29(1), 131-142.

Ercan, O. (2024). Agricultural land-based functional model for effective rural land management in Türkiye. Journal of Agricultural Sciences, 30(3), 526-545.

Esina, E. (2009). Arazi Yönetimi. Yüksek lisans tezi, Selçuk Üniversitesi Fen Bilimleri Enstitüsü, Jeodezi ve Fotogrametri Mühendisliği Ana Bilim Dalı, Konya

Ge D, Long H, Zhang Y et al., 2018a. Analysis of the coupled relationship between grain yields and agricultural labor changes in China. Journal of Geographical Sciences, 28(1): 93–108.

Ge D, Long H, Zhang Y et al., 2018b. Farmland transition and its influences on grain production in China. Land Use Policy, 70: 94–105.

Guo, B., Fang, Y., & Jin, X. (2020). Monitoring the effects of land consolidation on the ecological environmental quality based on remote sensing: A case study of Chaohu Lake Basin, China. Land use policy, 95, 104569.

Humphries, J. (1990). Enclosures, common rights, and women: The proletarianization of families in the late eighteenth and early nineteenth centuries. The Journal of Economic History, 50(1), 17-42.

Jürgenson, E. (2016). Land reform, land fragmentation and perspectives for future land consolidation in Estonia. Land Use Policy, 57, 34-43.

Karaman, S., Gokalp, Z., 2018, Land consolidation practices in Turkey, Current Trends in Natural Sciences, Vol.7(14), 76-80. https://www.natsci.upit.ro/media/1688/paper-9.pdf, Accessed on April 26, 2023.

Kocur-Bera, K., Rapiński, J., Siejka, M., Leń, P., & Małek, A. (2023). Potential of an Area in Terms of Pro-Climate Solutions in a Land Consolidation Project. Sustainability, 15(12), 9306.

Köseoğlu, M., & Gündoğdu, K. S. (2004). Arazi toplulaştırma planlama çalışmalarında uzaktan algılama tekniklerinden yararlanma olanakları. Uludağ Üniversitesi Ziraat Fakültesi Dergisi, 18(1), 45-56.

Li S, Li X, 2017. Global understanding of farmland abandonment: A review and prospects. Journal of Geographical Sciences, 27(9): 1123–1150.

Li X, Yang Y, Liu Y, 2017. Research progress in man-land relationship evolution and its resource-environment base in China. Journal of Geographical Sciences, 27(8): 899–924

Long H, 2014. Land consolidation: An indispensable way of spatial restructuring in rural China. Journal of Geographical Sciences, 24(2): 211–225.

Long H, Ge D, Zhang Y et al., 2018. Changing man-land interrelations in China's farming area under urbanization and its implications for food security. Journal of Environmental Management, 209: 440–451.

Long H, Li Y, Liu Y et al., 2012. Accelerated restructuring in rural China fueled by 'increasing vs. decreasing balance' land-use policy for dealing with hollowed villages. Land Use Policy, 29(1): 11–22.

Long H, Liu Y, Li X et al., 2010. Building new countryside in China: A geographical perspective. Land Use Policy, 27(2): 457–470.

Long H, Qu Y, 2018. Land use transitions and land management: A mutual feedback perspective. Land Use Policy, 74: 111–120.

Long H, Tu S, 2018. Land use transition and rural vitalization. China Land Science, 32(7): 1–6. (in Chinese)

Long, H., Zhang, Y., & Tu, S. (2019). Rural vitalization in China: A perspective of land consolidation. Journal of Geographical Sciences, 29, 517-530.

Qu Y, Long H, 2018. The economic and environmental effects of land use transitions under rapid urbanization and the implications for land use management. Habitat International, 82: 113–121.

Robinson, G. M. (2024). Global sustainable agriculture and land management systems. Geography and Sustainability.

Şahin, D. (2004). Planlama toprak etüdlerinde uzaktan algılama ve coğrafik bilgi sistem tekniklerini uygulama olanakları. Yüksek lisans tezi, Uludağ Üniversitesi Fen Bilimleri Enstitüsü, Bursa.

Toklu, N. (2010). Türkiye'de toprak reformu politikalarının değerlendirilmesi. Yüksek lisans tezi, Selçuk Üniversitesi Fen Bilimleri Enstitüsü, Harita Mühendisliği Ana Bilim Dalı, Konya

Tu S, Long H, 2017. Rural restructuring in China: Theory, approaches and research prospect. Journal of Geographical Sciences, 27(10): 1169–1184.

Uzun, B., & Yomralıoğlu, T. (2005). Doğu Karadeniz Bölgesinde Dağınık Yerleşim Sorunlarının Mülkiyet Açısından İrdelenmesi ve Kırsal Arazi Düzenleme Modeli. Doğu Karadeniz Bölgesi Kalkınma Sempozyumu, 13-14.

Van Dijk, T. (2007). Complications for traditional land consolidation in Central Europe. Geoforum, 38(3), 505-511.

Vitikainen, A. (2004). An overview of land consolidation in Europe. nordic Journal of Surveying and real Estate research, 1(1).

Zhou, Y., Li, Y., & Xu, C. (2020). Land consolidation and rural revitalization in China: Mechanisms and paths. Land Use Policy, 91, 104379.

Chapter 2

STRUCTURE AND PROPERTIES OF GLASS

Betül Demirezen[1]

1 Simav Vocational School of Health Services, Kutahya Health Sciences University, Kutahya,Türkiye

Materials that can change from molten state to solid state without turning into a crystal structure, have high viscosity, are brittle and amorphous are called glass (Vogel, 1985; Shelby, 2005; Rao, 2002). Glass is a fluid material formed by the dissolution of alkali and alkaline earth metal oxides and some other metal oxides that have been cooled suddenly, and its main substance is silicon (SiO_2) (Richet, 2021). Silicon material is irregular in structure and contains crystals smaller than 0.1 μm, as well as short-range (short distance) regular structures can be observed in its structure. The microstructure arrangements of the glasses are given in Figure 1. Blue colored atoms represent silicon and red colored atoms represent oxygen.

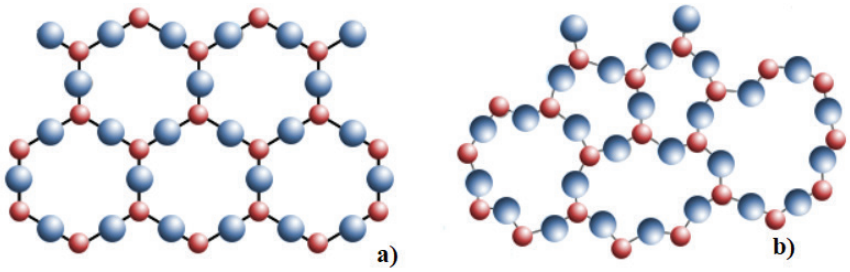

Figure 1 *a) Crystal and b) Amorphous structure of* SiO_2

While the specific gravity of glass varies between 2.2-7.2 g/cm^3 depending on its chemical composition, the density values of window and bottle glass in general use are between 2.3-2.6 g/cm^3 (Taha et al., 2021). Thermal expansion is an important property in determining the resistance of glass to heat-temperature shocks and the stresses that occur in glass between heating and cooling. Thermal expansion, mechanical strength, the dimensions of the glass and the spread of heat in the glass all affect the resistance of the glass to heat. Since thermal resistance is a test method for showing deviations from the normal manufacturing processes of a glass, it is a widely used process control method (Zhao et al., 2023). The thermal conductivity of glass generally increases depending on the proportion of soda, potassium and lead oxide mixtures present in its chemical composition. The heat capacity of glass increases as the temperature of the glass increases. Just as the heat capacity of each type of glass at different temperatures is different, the changes in the heat capacity of glass with temperature may also vary. Glass is a material that has been used in different areas historically and has continuously developed with the advancement of technology. Since glass contains different types of materials, it has gained more functional properties beyond the basic properties of these materials. In this way, both the physical and chemical properties of the glass have improved, making them more resistant to external factors (heat, light, harmful rays, pressure) (Karasu and Sarıcaoğlu, 2018). Glass solidifies

while preserving its amorphous structure. During production, due to rapid cooling, an amorphous structure is formed instead of a crystal structure. This structure gives the glass its strength and transparency.

Glasses are divided into 2 according to their chemical composition and usage areas.

According to chemical components;

Oxide Glasses,

Metallic Glasses,

Halogen Glasses,

Borosilicate Glasses,

Lead Glasses,

Chalcogen Glasses,

Silica Glasses,

Nitrate, Sulfate and Hydrogen Bonded Glasses,

According to areas of use;

Window Glass,

Optical Glass.

90% of the glass produced in the world is soda ash glass. It can be easily melted, it is cheap but it can be used everywhere except for thermal shock resistance and chemical stability. It is used in the production of materials such as normal electric bulbs, fluorescent bulbs, window glass. It has 5% CaO in its structure. Roughly, its content is $Na_2O{\cdot}CaO{\cdot}6SiO_2$, and by adding Al_2O_3, MgO, BaO, K_2O, the melting point is reduced, viscosity is adjusted, strength is increased, and coloring is achieved (Lee, 2021). When PbO replaces lime in soda ash glass, lead glass is obtained. It contains 80% lead oxide in its structure, sometimes more. Lead oxide lowers the melting point of the glass and lowers the softening point below that of CaO glasses. It also provides the glass with the ability to be easily processed, reflect and spread light. Glass types in which the amount of lead oxide exceeds 80% are used to protect against sunlight. Since it is a very expensive glass, barium oxide glasses are used (Schmitz, 1991; Schaeffer, 1995).

Borosilicate glasses have a high softening point. However, they have a large coefficient of expansion, which provides great resistance to thermal shock, very good resistance to water and acids, and superior electrical properties. For these reasons, they are used as laboratory (technical) glass. Kitchenware and large-sized astronomical mirrors are made. Pure borate

glasses are of very limited and low technical importance. The melting temperature of borosilcate glasses is between 800-900 °C (Szumera et al., 2022).

Aluminosilicate glass contains more than 20% alumina, a small amount of boron, some lime and magnesia and very little alkali. However, when there is no alkali, it becomes difficult to melt and process the glass. It is used in the production of thermometers, combustion tubes, and all kinds of parts that will come into direct contact with the flame due to its high softening point and low dilatation coefficient. Its chemical components are 54% SiO_2; 14% Al_2O_3; 23% RO and 8% B_2O_3. Aluminosilicate glasses have a low expansion coefficient and high exchange heat. It also offers high strength and low conductivity properties (Brady et al., 2002).

Silica glass is obtained by melting very pure quartz sand without a solvent. The production and shaping of this glass occurs at very high temperatures (1750 ˚C). Therefore, the shapes and dimensions of the materials to be produced must be limited. It has positive features such as a low coefficient of expansion, a very high softening point and very good UV light permeability. Its dielectric properties are also good. However, due to its high cost, its applications in electrotechnics are limited. It is the glass with the highest resistance to thermal shocks.

Phosphate glasses have very low chemical resistance. Therefore, they are manufactured and used for special purposes. These are heat-protective and colored glasses. Glass is obtained only from P_2O_5. As in silicate glasses, they have high light refraction properties. They are used as laser glass (Brow, 2000).

The internal structure of the glass consists of a complex silicate structure, and the basic components of this structure include SiO_2 (silicon dioxide), CaO (calcium oxide) and Na_2O (sodium oxide). In addition, different components such as boron oxide, aluminum oxide, zinc oxide, lead oxide can be added to improve or change some of the properties of the glass (Esin, 1981).The oxides found in glass can be classified into three main categories according to their functions: vitrifiers, network modifiers and intermediate oxides (Amstock, 1997).

Vitrifiers are oxides that provide the formation of amorphous structure. Glass formers are the substances that form the basic structure of any glass. Generally known as a good glass former is SiO_2. Silica atom is connected to 4 oxygen atoms. Oxygen atom acts as a bridge between silica atoms. Silica atom forms an irregular network when cooled. It is a supercooled liquid that becomes solid with cooling. In addition to SiO_2, which is a glass former, boron oxide (B_2O_3) is also an important glass former. B_2O_3 is rarely used alone; when used with SiO_2, it reduces light,

refraction and expansion, while also increasing chemical resistance. Oxides such as P_2O_5, As_2O_5 and GeO_2 are also used as glass formers; they are generally not preferred in the production of glasses produced in large volumes (Shankhwar et al., 2016).

Intermediate Oxides are components that are added to the existing chain but do not form a new chain. These oxides are added to the mixture to improve the structure of the glass, but they do not change the structure of the chain. The components used as intermediate oxides are Na_2O, K_2O, CaO, MgO and BaO. When Na_2O is added to SiO_2, a chemical reaction occurs between these two substances. The dominant feature of Na_2O here is that it is a melter and it reduces the melting temperature of the mixture, allowing the silica to become fluid at a much lower temperature. With the increase in Na_2O, the melting temperature can fall below 1000°C (Qi et. Al., 2016). When the crystal structure is examined, a hollow structure is seen. Other modifying components can adapt to these hollow spaces within the glassy structure. Another known modifying substance is CaO. When it is desired to increase the resistance of the glass against chemical effects, CaO (lime) is added. Thus, lime gives the glass an indestructible feature. Although MgO is a substance that increases the durability of the glass; it is not as effective as CaO. Other modifying oxides are; K_2O, Li_2O and ZnO. Of these oxides; K_2O and Li_2O; are oxides that have melting properties like Na_2O and are preferred instead of Na_2O. ZnO; is a substance that provides a stable structure to the glass by acting similarly to MgO and CaO.

Oxides such as Al_2O_3 (alumina), TiO_2, ZrO_2, PbO are examples of the intermediate group. The function of intermediate oxides is to reduce the tendency of the glass to crystallize and increase its durability. These oxides participate in the atomic network structure of the glass as a glass former. Intermediate oxides are used to increase the processability of the glass and to provide the glass with the necessary qualities for some application areas.

Network Modifiers are compounds that break the structure of the glass, reduce its viscosity, and provide chemical, optical and economic advantages. These oxides make the glass easier to process and play an important role in the production of glass. Al_2O_3, TiO_2, ZnO, PbO and BeO oxides are used as network modifiers (Hazra, 2013). These substances act as both glass formers and modifiers, affecting the properties of the glass and enriching the atomic network structure of the glass.

Each oxide determines the properties of the glass, enabling the production of suitable glass types for different purposes, and the chemical compositions of glasses commonly used in industry are given in Table 1.

Table 1. *Chemical compositions of some glasses.*

Glass Type	Percentage (%)								
	SiO_2	Na_2O	K_2O	CaO	MgO	BaO	PbO	B_2O_3	Al_2O_3
Fused silicate glass	99.5+								
96% silicate glass	96.3	<0.2	<0.2					2.9	0.4
Window glass	71-73	14-15		8-10	1.5-3.5				0.5-1.5
Flat glass	71-73	12-14		10-12	1-4				0.5-1.5
Glass containers	70-73	13-16 (Na_2O+K_2O)		10-13 (CaO+MgO)					1.5-2.5
Bulb glass	73.6	16	0.6	5.2	3.6				1
Leaded glass—electrical	63	7.6	6	0.3	0.2		21	0.2	0.6
Leaded glass—high lead content	35		7.2				58		
Alumino-borosilicate glass	74.7	6.4	0.5	0.9		2.2		9.6	5.6
Borosilicate glass—low expansion	80.5	3.8	0.4					12.9	2.2
Borosilicate glass—low electrical loss	70		0.5	0.1	0.2			28	1.1
Borosilicate glass—tungsten seal	67.3	4.6	1		0.2			24.6	1.7
Aluminosilicate glass	57	1		5.5	12			4	20.5

In glass production, glass cullet is also used in addition to glass raw materials. There are two sources of glass cullet; the first is broken glass formed in the enterprises, the second is foreign glass cullet (Pavlushkina and Kisilenko, 2011). It is more appropriate to use glass cullet in the production of the same type of glass. If this is not possible, the cullets can be evaluated by making a suitable blend. For example, white glass can be obtained without mixing colored glass with white colored kitchenware glass, bottles, window glass cullets. Glass cullet helps melting. As the glass cullet ratio increases, the melting time decreases.

Chemical properties of glass

It is known that most glasses are chemically quite resistant. For this reason, glasses are widely used to protect chemicals, medicines and food.

Window glass and bottles can also withstand the effects of weather for many years. Silica, the main substance of glass, has a very low solubility in water and acid, but it is damaged by alkaline mixtures and phosphoric acid at high temperatures and by dehydrofluoric acid at all temperature levels. If the glass is produced only from silica and alkali oxides (Na_2O and K_2O), there is a danger of solubility in water and it is called water glass and its area of use is very limited. In this type of glass, alkali oxides can be removed from the surface by acids, which causes a porous silica structure to remain on the surface. Oxides such as CaO, MgO and Al_2O_3 are mandatory compounds in the mixture to make the glass more resistant to chemical effects (Mantell ve diğ., 1958).

Physical properties of glass

One of the most important factors in the shaping of glass is viscosity. Viscosity is a property that varies depending on the chemical properties of the glass as well as the production temperature of the glass. Shaping of glass is a chain of successive processes. It is important that the glass has the desired viscosity at the beginning and end of each process and that it has a high viscosity that can maintain the given shape at the end of the processes. Another important factor in the shaping of glass is surface tension. This property affects the glass's ability to enter and fill very fine pores.

Mechanical properties of glass

The strength of glass is highly dependent on the defects that may be present on its surface. The maximum tensile strength that glass can theoretically withstand can reach 3000 N/mm^2 when tested on freshly produced glass fibers, free of any defects. However, the tensile strength that manufactured glass can have in practice is found as a result of bending tests and corresponds to values between 20 and 200 N/mm^2 depending on the condition of its surface. The strength reaches its highest value immediately after production and as the age of the glass increases, the strength decreases as surface defects increase due to chemical effects or abrasion. Therefore, old glass is more prone to breakage and is more difficult to cut (Taylor, 1983). Glass is an elastic material at normal temperatures. It breaks without plastic deformation, in other words, it is brittle. Another point that draws attention in the response of glass to external loads is that even when a compressive load is applied, the breaking of the glass is due to the tensile component of the stress. Therefore, the behavior of glass under external loads is expressed by its tensile strength (Mantell ve diğ., 1958). The compressive strength of glass varies between 500-900 MPa, and the elasticity modulus varies between 4.5-10 GPa. The Poisson ratio is 0.22. It is also known that glass is quite vulnerable to impact (Baradan, 2003).

Electrical properties of glass

In glass, the electrons in the outer orbits of the atoms are restricted by strong bonds and there are no free electrons as in metals, which causes glasses, unlike metals, to be unable to conduct electric current. Therefore, glasses have high electrical resistance and are also used as insulators in practice. On the other hand, glass is actually a liquid and a large portion of glass contains metallic ions (such as Na+) that can carry current when free. In other words, glass is an insulator only if its viscosity is high enough to keep the metallic ions attached. As a result, as the viscosity of the glass decreases, in other words, as its temperature increases, its electrical resistance decreases. At sufficiently high temperatures, glass can carry a considerable amount of electrical current. As a result of this situation, it is possible to heat the glass by passing current through molten glass. In cases where it is necessary to avoid contamination from fuel, such as in the production of very high quality optical glass, the melting of the materials forming the glass can also be carried out electrically. Borosilicate glass is widely used in electrical products in particular. For example, borosilicate sealing glass is used in the coating of different metals in incandescent lamps and electronic tubes. In addition, although soda-lime glass is used in classic bulbs, low-expansion borosilicate glass is preferred in cases where electrical power will increase or the lamp will be exposed to environmental effects in the open area (Amstock, 1997).

Optical properties of glass

The optical properties of glass are affected by factors such as refractive index, reflectance, light transmittance and chemical composition, and these elements determine the use and performance of the glass.

The *refractive index* of glass affects the speed of light in the glass and usually ranges between 1.45 and 1.90. This property determines how much light is refracted as it hits the glass surface. Reflectance varies depending on the condition of the glass surface, the wavelength of the light, and the angle at which it is incident. Silicate glass reflects an average of 4%, and completely clear glass transmits 92% of the incident light. Reflection losses can be reduced by adding special coatings to the glass surface.

The *light transmittance* of glass describes the ability of glass to transmit light and varies with wavelength. The color of the glass can affect this transmittance. In addition, the chemical composition of the glass can limit the passage of light, especially short wavelengths. The light transmittance of glass can be narrowed or widened by changes in its chemical composition.

The *chemical composition* of glass directly affects the quality of glass. Although chemical analysis can help determine the qualitative and

quantitative properties of glass, these processes can be expensive and time-consuming. Therefore, quality control in glass production is usually done by measuring and observing the physical properties of the glass. The quality of glass varies depending on both its optical properties and its chemical composition (Borchardt and Sowa, 2002; Engelleitner, 1978).

All of these properties determine the suitability of glass for various applications. For example, the high light transmittance of glass makes it preferred in applications such as optical glass and windows, while improving its reflective properties is important to meet energy efficiency requirements.

KAYNAKLAR

Amstock J. S. (1997), Handbook of Glass in Construction, McGraw-Hill, New York, 584p.

Baradan, B. (2003). İnşaat mühendisleri için malzeme bilgisi. *İzmir DEÜ. Müh. Fak. Yayın*, (307), 394.

Borchardt-Ott, W., & Sowa, H. (2002). *Kristallographie* (Vol. 5). Berlin Heidelberg New York: Springer.

Brady G. S., Clauser H. R. ve Vaccari J. A. (2002). Materials Handbook, Fifteenth Edition, McGraw-Hill, New York, 1244p.

Brow, R. K. (2000). The structure of simple phosphate glasses. *Journal of Non-Crystalline Solids*, *263*, 1-28.

Engelleitner, W. H. (1978). Agglomeration in the glass industry. Wıley-VCH.

Esin, A. (1981). *Properties of materials for design* (No. 69). Middle East Technical University.

Hazra, G. (2013). Leaching Study of the some Lead-Iron Phosphate Simulated Nuclear Waste Glasses with Different Modifiers under Soxhlet Condition. *IJAREAS*, *2*(12), 30-47.

Karasu, B., & Sarıcaoğlu, B. (2018). Cam yüzey kaplama teknolojileri. *El-Cezeri*, *5*(2), 475-500.

Lee, H. (2021). *Evaluation of the Hardness of Alkaline Earth Aluminosilicate Glasses* (Doctoral dissertation, New York State College of Ceramics at Alfred University).

Mantell C.L., Salzberg H.W. (1958). Engineering Materials Handbook, Journal of The Electrochemical Society.

Pavlushkina, T. K., & Kisilenko, N. G. (2011). Cullet use in the production of building materials. *Glass and ceramics*, *68*, 162-168.

Qi, S., Porotnikova, N. M., Ananyev, M. V., Kuzmin, A. V., Eremin, V. A., Pankratov, A. A., ... & Zaikov, Y. P. (2016). High-temperature glassy-ceramic sealants SiO_2—Al_2O_3—BaO—MgO and SiO_2—Al_2O_3—ZrO_2—CaO—Na_2O for solid oxide electrochemical devices. *Transactions of Nonferrous Metals Society of China*, *26*(11), 2916-2924.

Rao K. J. (2002), "Structural Chemistry of Glasses", 1. Basım, Elsevier.

Richet, P. (2021). A History of Glass Science. *Encyclopedia of Glass Science, Technology, History, and Culture*, *2*, 1413-1440.

Schaeffer, H. A. (1995). *Allgemeine technologie des glases*. Institut für Werkstoff wissenschaften III (Glas und Keramik), Universität Erlangen-Nürnberg.

Schmitz, W. (1991). W. Borchardt-Ott Kristallographie. Springer Verlag Berlin, 3. überarbeitete Auflage 1990, 265 Seiten, 169 Abbildungen, Literatur-und Sachwortverzeichnis, Aufgaben-und Lösungsteil, Wulffsches Netz, Preis: DM 34,–, ISBN 3-540-52931-4.

Shankhwar, N., Sharma, K., Kothiyal, G. P., & Srinivasan, A. (2016). Bioactive Glass and Glass-Ceramics Containing Iron Oxide: Preparation and Properties. *Trends in Biomaterials*, 1-47.

Shelby J. E. (2005), "Introduction to Glass Science and Technology", 2. Basım, The Royal Society of Chemistry.

Szumera, M., Łagowska, B., Sułowska, J., Jeleń, P., Olejniczak, Z., Lach, R., ... & Kijo-Kleczkowska, A. (2022). Investigating the Crystallization Process of Boron-Bearing Silicate-Phosphate Glasses by Thermal and Spectroscopic Methods. *Molecules*, *27*(3), 867.

Taha, M. A., Youness, R. A., El-Bassyouni, G. T., & Azooz, M. A. (2021). FTIR spectral characterization, mechanical and electrical properties of P_2O_5-Li_2O-CuO glass-ceramics. *Silicon*, *13*, 3075-3084.

Vogel W., (1985), "Glass Chemistry", 2. Basım, Springer-Verlag.

Zhao, X., Li, T., Xie, H., Liu, H., Wang, L., Qu, Y., ... & Hu, L. (2023). A solution-processed radiative cooling glass. *Science*, *382*(6671), 684-691.

Chapter 3

MOFS AND SYNTHESIS METHODS[1]

Halil İbrahim ÇETİNTAŞ[2], Sema SALGIN[3], Uğur SALGIN[4]

1 This chapter is derived from the doctoral dissertation titled "Synthesis, Characterization, and Application of Biological Metal-Organic Frameworks as Drug Delivery Systems," conducted at the Institute of Science of Sivas Cumhuriyet University. The thesis is accessible under thesis number 779746 at the National Thesis Center of the Republic of Turkey.

2 Lect. Dr., Sivas Cumhuriyet University Advanced Technology Research and Application Center, ORCID: 0000-0003-1769-0098

3 Prof. Dr., Sivas Cumhuriyet University Department of Chemical Engineering, ORCID: 0000-0001-6354-3553

4 Prof. Dr., Sivas Cumhuriyet University Department of Chemical Engineering, ORCID: 0000-0002-7587-4402

1. Introduction

Porous materials with high surface area have always been of great importance for industrial processes (Li et al. 1999). Over the past 30 years, various advanced porous materials composed of organic and inorganic materials, such as zeolites, porous organic polymers, covalent organic frameworks (COFs), supramolecular frameworks, and metal organic frameworks (MOFs), have been widely used in many scientific and technological fields. Among them, MOFs have always attracted the attention of scientists for use in various fields due to their distinctive characteristics such as structural tunability, high specific surface area and highly ordered pore structures (Ma et al. 2022).

As of 2016, there are 123,500 MOF structures that may also be termed Coordination Polymers or Networks (almost 10% of all compounds registered in the database based on version 5.45) reported to the Cambridge Structural Database ("Case," n.d.). Although similar materials have been reported before, pioneering studies on MOFs first appeared in the 90s of the last century, and this major scientific breakthrough occurred with the synthesis of MOF-5 ($[Zn_4O(BDC)_3]_n$), which had the highest surface area among the porous materials at that time, with 3000 $m^2 g^{-1}$, by Yaghi and colleagues in 1999 (Figure 1). This work is considered the starting point for MOFs, also known as porous coordination polymers (Bieniek et al. 2021).

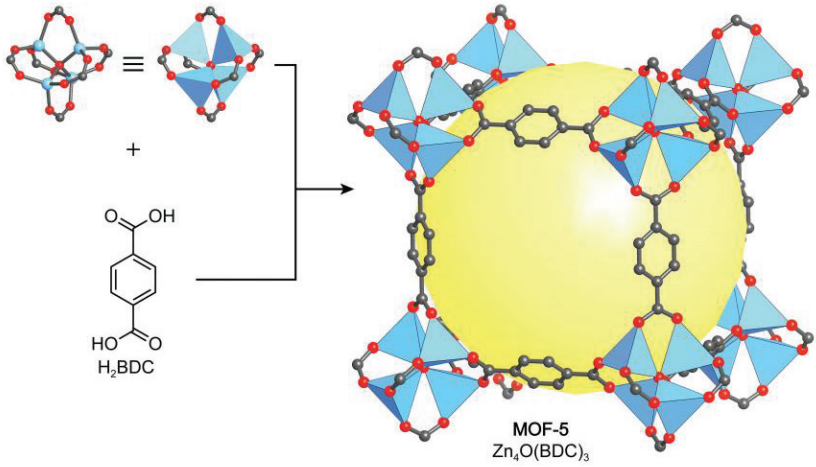

Figure 1. *MOF-5 (Yaghi, Kalmutzki, and Diercks 2019).*

2. Properties of MOFs

To form the structure of MOFs, metal ions or metal clusters self-assemble with organic ligands via coordination bonds and form one, two

or three-dimensional, highly crystalline complex structures (Figure 2) (Silva et al. 2015). Several types of bonds such as electrostatic interactions, hydrogen bonding, metal coordination and π-π stacking can be observed in a MOF crystal (Carne et al. 2011). A wide variety of metal centers and organic linkers can be used to synthesize MOFs under different synthetic conditions, resulting in a unique structural diversity. Here, the type of metal centers and the length, geometry and functional groups of organic linkers are the most important factors determining the structure and properties of MOFs (Mallakpour, Nikkhoo, and Hussain 2022).

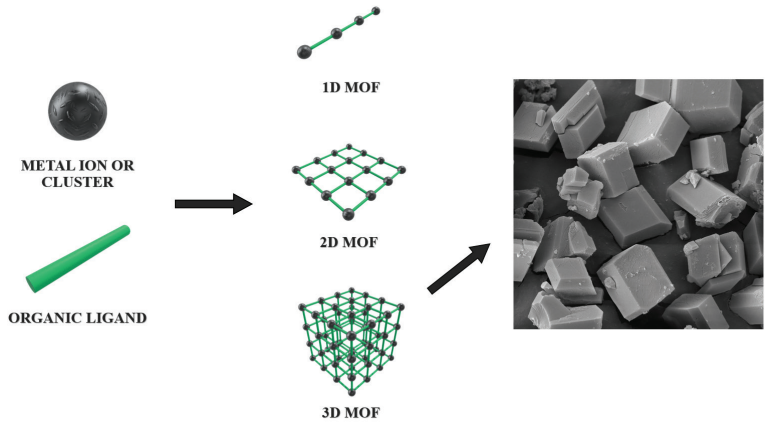

Figure 2. *Schematic representation of MOF geometries and SEM image of a 3D MOF structure synthesized with potassium as metal ion and β-cyclodextrin as ligand.*

Metal ions play an important role in controlling the properties, pores and structures of MOFs. The use of different metal ions can change the bonding patterns of the structural units, while the different coordination geometries of the metal ions can lead to various network structures. While transition metals such as Zn, Cu, Fe, Cr, Co, Ni, V, Sc, Y are the most commonly used elements in the metal nodes forming MOFs; alkali metals such as Li, Na, K; alkaline earth metals such as Mg, Ca, Sr, Ba, Ra; chemically weak metals such as Al, Sn and rare earth elements such as lanthanides are also frequently used in MOF synthesis (Mete 2021; Song et al. 2019).

Organic ligands, also known as organic linkers, play an important role in MOF synthesis. The chemical reactivity and physical properties of organic ligands are one of the main elements that determine the functionality of a MOF (Chen et al. 2014). The use of different ligands affects the morphology of MOFs, controlling the distance between metal ions and the size of the crystal structure. O-donors such as phosphonates, carboxylates, sulfonates

and N-donors such as pyrazines, pyridines, imidazoles, terephthalates are the most commonly used ligand classes (Mete 2021).

MOFs are famous for their flexibility in gaining functionality according to the determined purpose by using a suitable ligand and metal ion/cluster. The most important feature that provides the functionality of MOFs is that they allow a wide variety of structures to be obtained by changing or modifying their building blocks. Many studies have shown us that there are many synthetic strategies to adjust the chemistry, stability, flexibility and dimensions of these structures. In addition, it is possible to change the surface chemistry of MOFs by controlling their crystallographic phases, crystal sizes and morphologies. The tunability of such properties is one of the strongest reasons why MOFs can be used in many different applications (Baumann et al. 2019).

In order for MOF structures to be formed, organic ligands must have two or more functional sites available for binding. Recently developed multifunctional MOFs can easily accommodate more than one functional site on their pore surfaces (Jiao et al. 2019). MOFs can also be functionalized by adding functional groups to their building blocks. This functionalization process is carried out using two different methods: "pre-synthesis modification" and "post-synthesis modification." (Figure 3). In the pre-synthesis modification method, functional groups are attached to the ligands before the MOF structure is formed; in the post-synthesis modification method, functional groups are attached to the structure after the MOF structure is obtained (Şimşek 2021).

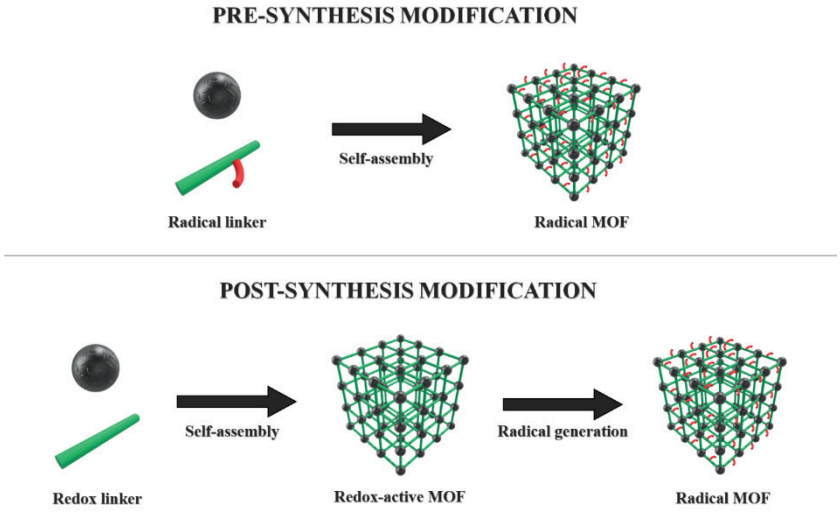

Figure 3. *Functionalization of MOFs.*

The biggest disadvantage of the pre-synthesis modification method is that it is very difficult to ensure that the functional groups attached to the structure are compatible with the coordination sites and to ensure structural stability. In the post-synthesis modification method, the controllability of the functionalization process performed using different functional groups is quite advantageous compared to the pre-synthesis method (Jiang et al. 2021).

The most prominent features of MOFs are their extreme porosity and large specific surface area (Baumann et al. 2019). These features, which can be easily adjusted by changing organic ligands and metal centers, determine the applications in which MOFs can be used. With a theoretical value of 14,600 m^2 g^{-1}, MOFs are unmatched in terms of accessible specific surface areas (Farha et al. 2012). However, it is not very possible to reach the theoretically calculated surface area and pore volume limits experimentally (Hönicke et al. 2018).

Due to their hybrid inorganic-organic structure, MOFs have many attractive properties that are completely absent in either inorganic or organic systems alone. For example, these structures can exhibit higher thermal stability than organic polymers while simultaneously possessing levels of mechanical flexibility that are very difficult to achieve for inorganic materials. Traditional metrics that determine mechanical properties such as Young's modulus and hardness have shown that MOFs have a design diversity that spans the boundaries of both "soft" and "hard" materials. Their extremely strong hybrid nature combined with their permanent porosity make MOFs very attractive materials in terms of their application areas (Burtch et al. 2018).

In general, MOFs exhibit more complex mechanical properties compared to traditional inorganic materials such as zeolites. Their chemical interactions, ranging from strong coordination bonds to weaker dispersion forces and hydrogen bonding interactions, can result in significant structural changes in response to temperature, hydrostatic pressure, or uniaxial stress. For example, some MOFs may undergo reversible or irreversible amorphization when subjected to mechanical stress, while others may exhibit severe compression or phase transitions associated with dramatic bond changes (Li, Henke, and Cheetham 2014).

In addition to all these unique properties, MOFs can be synthesized by a variety of methods. Each method has its own advantages and disadvantages. MOF synthesis methods are examined under nine main headings in this chapter.

3. Synthesis Methods of MOFs

Due to their functional and structural properties, MOFs are considered to be very important porous compounds today. These structures are formed by the combination of metal ions or ion clusters and organic binders that act as a bridge between them. Undoubtedly, the most important criterion in the final structure and properties of MOFs is the selected ligand and ion type. However, along with many other parameters such as temperature, reaction time, pressure, pH and the type of solvent used, the applied synthesis method is also of great importance. These methods used in MOF synthesis are grouped under nine main headings, which can be listed as; vapor diffusion method, solvothermal method, electrochemical method, mechanochemical method, sonochemical method, microwave-assisted method, ionic liquid method, microfluidic method and dry gel method (Dey et al. 2014; Safaei et al. 2019).

Vapor diffusion method

The vapor diffusion method is a simple chemical technique used for MOF synthesis. Compared to other conventional methods used for MOF synthesis, the vapor diffusion method is a cost-effective and easy-to-apply method due to the fact that the synthesis can be carried out at room temperature and low ambient pressure (Han et al. 2018). This method, which allows easy control of reaction parameters, also has a very high crystal yield (Rajkumar et al. 2019).

In this method, the solution containing organic compounds and metal salts is usually placed in an open-mouthed glass tube or container and the substances are expected to dissolve completely. Then, this tube is placed vertically in the middle of a large bottle containing a volatile solvent and the mouth of the bottle is tightly closed. The evaporated organic solvent begins to create vapor pressure on the solution containing the ligand and metal salts. This pressure allows the nucleation of crystalline materials in the solution and MOFs are formed over time (Qin et al. 2015). Chen et al. (2016) reported in their study that the $Zn(INA)_2(H_2O)_4$ complex synthesized by vapor diffusion method achieved rapid crystal growth at low temperature and without energy input thanks to kinetically controlled ammonia diffusion. It was also stated that three-dimensional $Zn(INA)_2$ MOFs exhibited superior properties than other MOFs in terms of ammonia adsorption capacity and structural stability. In another study, Zhang et al. (2023) aimed to develop a recyclable adsorbent that can adsorb dye and heavy metal pollutants in wastewater. For this purpose, they synthesized citric acid modified β-cyclodextrin metal-organic structure (CA-β-CD-MOF) by vapor diffusion method and showed that this structure exhibited high adsorption capacity for Congo red dye and copper ions (Cu^{2+}).

Solvothermal method

Solvothermal reactions are carried out under pressure conditions above the boiling point of the solvent, in closed vessels and without any external intervention. Many starting materials involved in the reaction can undergo unexpected chemical changes, leading to nano-scale morphologies that are generally unattainable through traditional methods. High-boiling organic solvents are often used for solvothermal reactions. The most commonly used organic solvents are dimethyl formamide and diethyl formamide. Sometimes solvent mixtures can be used to overcome solubility problems of different reaction inputs.

Solvothermal reactions can be carried out in different temperature ranges. While glass bottles can be used for reactions at relatively lower temperatures, Teflon-lined autoclaves are required for reactions carried out at temperatures usually higher than 400 K. This method has been successfully used for the synthesis of many inorganic compounds and inorganic-organic hybrid materials. Bhoite et al. (2023) reported the synthesis of binder-free thin Ni-MOF films on a stainless steel substrate by a simple solvothermal method in a glass vial at 90°C using a mixture of N,N-dimethylformamide and ethanol solvents. Their electrochemical characterization studies showed that these Ni-MOF electrodes have the potential to provide high capacity and energy density for supercapacitor applications. Similarly, Wang et al. (2024) synthesized irregular cubic or rod-shaped Cu–Fe metal-organic structure (Cu–Fe-MOF) by a simple one-pot solvothermal method in PTFE-lined autoclaves at 150°C using N,N-dimethylformamide. They reported that pollutants such as phenol, bisphenol A, 2,4-dichlorophenol, methyl blue, rhodamine B, tetracycline and sulfamethoxazole were degraded with over 95% yield within 30 min using these Cu–Fe-MOFs.

Electrochemical method

In the electrochemical synthesis method, the metal ions required for the reaction are not provided by metal salts but directly by oxidation of the electrode. The energy required to oxidize the anode can be provided in amperometric mode, where the voltage is kept constant, or in potentiometric mode, where the current is kept constant. A general advantage of electrochemical synthesis is that it allows synthesis under milder conditions than typical solvothermal methods. At the same time, the time required for synthesis is shorter than many other methods; whereas solvothermal MOF synthesis can take hours or days, electrochemical MOFs can be synthesized in hours or even minutes (Martinez Joaristi et al. 2012). It is also possible to control the thickness and morphology by changing the applied current or voltage in this method. Methods such as

anodic dissolution, reductive electrosynthesis, electrophoretic deposition, and galvanic displacement are among the common electrochemical synthesis methods (Ghoorchian et al. 2020).

Mechanochemical method

In mechanochemical synthesis, a chemical transformation occurs after the mechanical breaking of intramolecular bonds. The mechanochemical synthesis method is an extremely advantageous method, especially because it eliminates the need for organic solvents. Reactions are carried out in a solvent-free environment and at room temperature. In this method, which allows small-sized MOFs to be obtained with high yields in short reaction times of 10-60 minutes, metal oxides are generally preferred as starting materials rather than metal salts; thus, the only by-product that can be formed outside of MOFs is water (Lee, Kim, and Ahn 2013).

Sonochemical method

Ultrasound technology is used for a variety of applications, including medical imaging techniques, solution homogenization, navigation and ranging systems. Also, ultrasounds also serve as a significant energy source for driving chemical reactions. In sonochemical synthesis, ultrasound induces cavitation—a process involving the formation, growth, and implosive collapse of bubbles in a liquid medium (Głowniak et al. 2023). This cavitation generates localized high temperatures and pressures, which initiate and accelerate chemical reactions (Deng et al. 2024). With the sonochemical method, a homogeneous and accelerated nucleation is achieved in MOF synthesis with smaller particle sizes than traditional methods and with a shortened crystallization time. The most important advantages of this method are the low crystal size and short reaction time. Due to the high energy emitted by ultrasonic waves, very fast mixing can be achieved in the reaction medium. Ultrasonic wave frequencies are generally preferred between 20 kHz and 10 MHz. Due to these environmental conditions, the reaction occurs very quickly (Dey et al. 2014).

Microwave-assisted method

Microwave-assisted methods are widely applied for the rapid synthesis of nanoporous MOFs under hydrothermal conditions. This technique has potential advantages such as rapid crystallization, phase selectivity, narrow particle size distribution profile and easy morphology control. In microwave synthesis, a mixture of reaction inputs in a suitable solvent is transferred to a teflon container, the container is tightly closed and placed in the microwave unit and kept under set conditions for a suitable time. Thanks to microwaves, the liquid phase is heated rapidly and nano-sized

crystals are obtained (Lee et al. 2013).

Ionic liquid method

Ionic liquids are organic salts that are non-flammable and have low vapor pressure, generally liquid below 100 °C (Damodaran 2016). Exhibiting outstanding physicochemical properties such as task-specific functionalities, intrinsic structure tunability, and good affinity with target molecules, ionic liquids are an environmentally friendly alternative to toxic solvents (Li et al. 2023). Although this method is similar to the solvothermal method, unlike the solvothermal method, the solvent medium consists of ionic liquids. Ionic liquids can be quite advantageous when used instead of other solvents due to their superior properties such as low volatility, resistance to flame, low vapor pressure, high solvent properties, high electrochemical stability and high thermal stability. The most important advantages of this method are low solvent cost and the solvent not being affected by ambient conditions (Lee et al. 2013; Xu et al. 2019).

Microfluidic method

Microfluidic synthesis method is a method that allows the synthesis of monodisperse nanomaterials with specific properties due to small liquid volumes, fast mass transfer and high mixing efficiency. With this method, the physico-chemical properties of nanomaterials can be changed very precisely (Koryakina et al. 2023). In this method, two different solutions containing organic ligands and metal salts are prepared and these two solutions are sent to a chamber with the help of a pump system. In this chamber, the droplets of the two solutions mix with each other. Then, these droplets pass through a Teflon column immersed in an oil bath or placed in an oven. After the Teflon column, the droplets are transferred to a bath containing a polar solvent with a low boiling point. The solvent is removed from this bath and cage structures are obtained. In addition to shortening the reaction time in this method, nano-sized MOFs with controlled particle size distribution and regular crystal morphologies are also obtained (Faustini et al. 2013).

Dry-gel conversion method

The dry gel conversion method is a widely applied method in the preparation of zeolites and zeolite membranes, and is also among the methods used for MOF synthesis today. This method is divided into two different methods. The first of these is the vapor phase transport method, in which a dry gel is crystallized in volatile amine and water vapor, and the second is the steam-assisted crystallization method, in which a dry gel containing a non-volatile amine is crystallized in vapor. The dry gel conversion method offers several important advantages. Firstly, it

minimizes waste disposal, making the process more environmentally friendly. Secondly, it reduces the reactor size and reaction volume required, which can lower costs and simplify the setup. Lastly, this method efficiently converts the gel into MOFs with a single crystal structure, ensuring high efficiency and consistency in the quality of the produced materials (Das et al. 2016; Lee et al. 2013).

REFERENCES

Baumann, A. E., Burns, D. A., Liu, B., & Thoi, V. S. (2019). Metal-organic framework functionalization and design strategies for advanced electrochemical energy storage devices. *Communications Chemistry*, *2*(1), 86.

Bhoite, A. A., Patil, K. V., Redekar, R. S., Patil, P. S., Sawant, V. A., & Tarwal, N. L. (2023). Solvothermal synthesis of binder free Ni-MOF thin films for supercapacitor electrodes. *Journal of Solid State Chemistry*, *326*, 124192. https://doi.org/10.1016/j.jssc.2023.124192

Bieniek, A., Terzyk, A. P., Wiśniewski, M., Roszek, K., Kowalczyk, P., Sarkisov, L., … Kaneko, K. (2021). MOF materials as therapeutic agents, drug carriers, imaging agents and biosensors in cancer biomedicine: Recent advances and perspectives. *Progress in Materials Science*, *117*, 100743.

Burtch, N. C., Heinen, J., Bennett, T. D., Dubbeldam, D., & Allendorf, M. D. (2018). Mechanical Properties in Metal–Organic Frameworks: Emerging Opportunities and Challenges for Device Functionality and Technological Applications. *Advanced Materials*, *30*(37), 1704124. https://doi.org/10.1002/adma.201704124

Carne, A., Carbonell, C., Imaz, I., & Maspoch, D. (2011). Nanoscale metal–organic materials. *Chemical Society Reviews*, *40*(1), 291–305.

Case: How many MOFs are there in the CSD? - The Cambridge Crystallographic Data Centre (CCDC). (n.d.). Retrieved October 4, 2024, from https://www.ccdc.cam.ac.uk/support-and-resources/support/case/?caseid=46cf9882-92de-ed11-96a2-00505695c114

Chen, T.-H., Popov, I., Kaveevivitchai, W., & Miljanić, O. Š. (2014). Metal–Organic Frameworks: Rise of the Ligands. *Chemistry of Materials*, *26*(15), 4322–4325. https://doi.org/10.1021/cm501657d

Chen, Y., Yang, C., Wang, X., Yang, J., Ouyang, K., & Li, J. (2016). Kinetically controlled ammonia vapor diffusion synthesis of a Zn(II) MOF and its H2O/NH3 adsorption properties. *Journal of Materials Chemistry A*, *4*(26), 10345–10351. https://doi.org/10.1039/C6TA03314H

Damodaran, K. (2016). Chapter Four—Recent NMR Studies of Ionic Liquids. In G. A. Webb (Ed.), *Annual Reports on NMR Spectroscopy* (Vol. 88, pp. 215–244). Academic Press. https://doi.org/10.1016/bs.arnmr.2015.11.002

Das, A. K., Vemuri, R. S., Kutnyakov, I., McGrail, B. P., & Motkuri, R. K. (2016). An Efficient Synthesis Strategy for Metal-Organic Frameworks: Dry-Gel Synthesis of MOF-74 Framework with High Yield and Improved Performance. *Scientific Reports*, *6*(1), 28050. https://doi.org/10.1038/srep28050

Deng, C., Wang, T., Wu, P., Zhu, W., & Dai, S. (2024). High entropy materials for catalysis: A critical review of fundamental concepts and applications. *Nano Energy*, *120*, 109153. https://doi.org/10.1016/j.nanoen.2023.109153

Dey, C., Kundu, T., Biswal, B. P., Mallick, A., & Banerjee, R. (2014). Crystalline metal-organic frameworks (MOFs): Synthesis, structure and function. *Acta Crystallographica Section B: Structural Science, Crystal Engineering and Materials*, *70*(1), 3–10.

Farha, O. K., Eryazici, I., Jeong, N. C., Hauser, B. G., Wilmer, C. E., Sarjeant, A. A., … Hupp, J. T. (2012). Metal–Organic Framework Materials with Ultrahigh Surface Areas: Is the Sky the Limit? *Journal of the American Chemical Society*, *134*(36), 15016–15021. https://doi.org/10.1021/ja3055639

Faustini, M., Kim, J., Jeong, G.-Y., Kim, J. Y., Moon, H. R., Ahn, W.-S., & Kim, D.-P. (2013). Microfluidic Approach toward Continuous and Ultrafast Synthesis of Metal–Organic Framework Crystals and Hetero Structures in Confined Microdroplets. *Journal of the American Chemical Society*, *135*(39), 14619–14626. https://doi.org/10.1021/ja4039642

Ghoorchian, A., Afkhami, A., Madrakian, T., & Ahmadi, M. (2020). Chapter 9—Electrochemical synthesis of MOFs. In M. Mozafari (Ed.), *Metal-Organic Frameworks for Biomedical Applications* (pp. 177–195). Woodhead Publishing. https://doi.org/10.1016/B978-0-12-816984-1.00011-1

Głowniak, S., Szczęśniak, B., Choma, J., & Jaroniec, M. (2023). Recent Developments in Sonochemical Synthesis of Nanoporous Materials. *Molecules*, *28*(6), 2639. https://doi.org/10.3390/molecules28062639

Han, Y., Liu, W., Huang, J., Qiu, S., Zhong, H., Liu, D., & Liu, J. (2018). Cyclodextrin-based metal-organic frameworks (CD-MOFs) in pharmaceutics and biomedicine. *Pharmaceutics*, *10*(4), 271.

Hönicke, I. M., Senkovska, I., Bon, V., Baburin, I. A., Bönisch, N., Raschke, S., … Kaskel, S. (2018). Balancing Mechanical Stability and Ultrahigh Porosity in Crystalline Framework Materials. *Angewandte Chemie International Edition*, *57*(42), 13780–13783. https://doi.org/10.1002/anie.201808240

Jiang, W.-L., Huang, B., Wu, M.-X., Zhu, Y.-K., Zhao, X.-L., Shi, X., & Yang, H.-B. (2021). Post-Synthetic Modification of Metal-Organic Frameworks Bearing Phenazine Radical Cations for aza-Diels-Alder Reactions. *Chemistry – An Asian Journal*, *16*(23), 3985–3992. https://doi.org/10.1002/asia.202100883

Jiao, L., Seow, J. Y. R., Skinner, W. S., Wang, Z. U., & Jiang, H.-L. (2019). Metal–organic frameworks: Structures and functional applications. *Materials Today*, *27*, 43–68.

Koryakina, I. G., Bachinin, S. V., Gerasimova, E. N., Timofeeva, M. V., Shipilovskikh, S. A., Bukatin, A. S., … Zyuzin, M. V. (2023). Microfluidic

synthesis of metal-organic framework crystals with surface defects for enhanced molecular loading. *Chemical Engineering Journal*, *452*, 139450. https://doi.org/10.1016/j.cej.2022.139450

Lee, Y.-R., Kim, J., & Ahn, W.-S. (2013). Synthesis of metal-organic frameworks: A mini review. *Korean Journal of Chemical Engineering*, *30*, 1667–1680.

Li, H., Eddaoudi, M., O'Keeffe, M., & Yaghi, O. M. (1999). Design and synthesis of an exceptionally stable and highly porous metal-organic framework. *Nature*, *402*(6759), 276–279.

Li, W., Henke, S., & Cheetham, A. K. (2014). Research Update: Mechanical properties of metal-organic frameworks–Influence of structure and chemical bonding. *APL Materials*, *2*(12). Retrieved from https://pubs.aip.org/aip/apm/article/2/12/123902/120740

Li, X., Chen, K., Guo, R., & Wei, Z. (2023). Ionic Liquids Functionalized MOFs for Adsorption. *Chemical Reviews*, *123*(16), 10432–10467. https://doi.org/10.1021/acs.chemrev.3c00248

Ma, M., Lu, X., Guo, Y., Wang, L., & Liang, X. (2022). Combination of metal-organic frameworks (MOFs) and covalent organic frameworks (COFs): Recent advances in synthesis and analytical applications of MOF/COF composites. *TrAC Trends in Analytical Chemistry*, *157*, 116741.

Mallakpour, S., Nikkhoo, E., & Hussain, C. M. (2022). Application of MOF materials as drug delivery systems for cancer therapy and dermal treatment. *Coordination Chemistry Reviews*, *451*, 214262.

Martinez Joaristi, A., Juan-Alcañiz, J., Serra-Crespo, P., Kapteijn, F., & Gascon, J. (2012). Electrochemical Synthesis of Some Archetypical Zn^{2+} , Cu^{2+} , and Al^{3+} Metal Organic Frameworks. *Crystal Growth & Design*, *12*(7), 3489–3498. https://doi.org/10.1021/cg300552w

Mete, D. (2021). *Synthesis, characterization and investigation of cytotoxic effects of drug loaded ZIF-8 metal-organic frameworks* PhD Thesis, Izmir Institute of Technology, Turkey.

Qin, Y., Xiao, Y., Huang, P., Zhu, Y., & Yi, M. (2015). The Research Progress on the Synthesis and Application of Microporous Coordination Polymers. *2015 International Symposium on Material, Energy and Environment Engineering*, 5–8. Atlantis Press. Retrieved from https://www.atlantis-press.com/proceedings/ism3e-15/25846125

Rajkumar, T., Kukkar, D., Kim, K.-H., Sohn, J. R., & Deep, A. (2019). Cyclodextrin-metal–organic framework (CD-MOF): From synthesis to applications. *Journal of Industrial and Engineering Chemistry*, *72*, 50–66.

Safaei, M., Foroughi, M. M., Ebrahimpoor, N., Jahani, S., Omidi, A., & Khatami, M. (2019). A review on metal-organic frameworks: Synthesis and applications. *TrAC Trends in Analytical Chemistry*, *118*, 401–425.

Silva, P., Vilela, S. M., Tomé, J. P., & Paz, F. A. A. (2015). Multifunctional metal–organic frameworks: From academia to industrial applications. *Chemical Society Reviews*, *44*(19), 6774–6803.

Song, L., Xue, C., Xia, H., Qiu, S., Sun, L., & Chen, H. (2019). Effects of alkali metal (Li, Na, and K) incorporation in NH2–MIL125 (Ti) on the performance of CO2 adsorption. *Materials*, *12*(6), 844.

Şimşek, U. B. (2021). *Nano/mikro boyutta metal organik kafes yapıların sentezi, karakterizasyonu ve ilaç gideriminde kullanılması.* PhD Thesis, Mersin University, Turkey.

Wang, H., Dai, Y., Wang, Y., & Yin, L. (2024). One-pot solvothermal synthesis of Cu–Fe-MOF for efficiently activating peroxymonosulfate to degrade organic pollutants in water:Effect of electron shuttle. *Chemosphere*, *352*, 141333. https://doi.org/10.1016/j.chemosphere.2024.141333

Xu, Q., Zhang, X., Zeng, S., Bai, L., & Zhang, S. (2019). Ionic Liquid Incorporated Metal Organic Framework for High Ionic Conductivity over Extended Temperature Range. *ACS Sustainable Chemistry & Engineering*, *7*(8), 7892–7899. https://doi.org/10.1021/acssuschemeng.9b00543

Yaghi, O. M., Kalmutzki, M. J., & Diercks, C. S. (2019). *Introduction to reticular chemistry: Metal-organic frameworks and covalent organic frameworks*. John Wiley & Sons.

Zhang, Y., Zhang, L., Wang, N., Feng, C., Zhang, Q., Yu, J., … Chen, J. (2023). Citric acid modified β-cyclodextrin for the synthesis of water-stable and recoverable CD-MOF with enhanced adsorption sites: Efficient removal of Congo red and copper ions from wastewater. *Journal of Environmental Chemical Engineering*, *11*(6), 111413. https://doi.org/10.1016/j.jece.2023.111413

Chapter 4

THE FUTURE OF HYDROGEN: THE ROLE OF GREEN HYDROGEN IN ENERGY, AUTOMOTIVE, AND AVIATION SYSTEMS

Şafak Melih ŞENOCAK[1]

Yasin VAROL[2]

1 Şafak Melih ŞENOCAK, Lecturer, Osmaniye Korkut Ata University, Osmaniye Vocational School, e-mail: mlhsnck@gmail.com, ORCID ID: https://orcid.org/0000-0003-0602-2836

2 Prof. Dr. Yasin VAROL, Firat University, Technology Faculty, Elazig, e-mail: yvarol@gmail.com, ORCID ID: https://orcid.org/0000-0003-2989-7125

1. Introduction

The rapid increase in energy demand, the continuous growth of the global population, and the depletion of fossil fuel resources rank among the most pressing challenges of the 21st century. Fossil fuels such as oil, natural gas, and coal are neither suitable nor sustainable options for the future of energy due to their finite reserves and significant environmental impacts. This situation necessitates a shift towards cleaner, renewable, and long-term energy solutions (Alazemi & Andrews, 2015). Ultimately, any reduction or scarcity in fossil fuel reserves not only leads to fluctuations in oil prices but also poses significant threats to global energy security, potentially causing profound disruptions to the world economy. Such scenarios can trigger instability in energy markets, resulting in increased production costs and a slowdown in economic growth. These risks to energy security underscore the urgent need for alternative and sustainable energy sources to mitigate these challenges and ensure long-term stability in energy systems (Midilli & Dincer, 2007). Automobiles emerge as one of the largest energy consumers in the transportation sector, accounting for approximately 40% of the fossil fuels consumed within this industry (Sulaiman, Hannan, Mohamed, Majlan, & Wan Daud, 2015). Petroleum and natural gas dominate as primary energy sources, collectively accounting for over 84% of global energy production. Specifically, petroleum contributes to 33% of global energy consumption, with approximately 65% of this share being utilized within the transportation sector (Yartys et al., 2021). These figures clearly highlight the significant impact of the transportation sector on energy consumption and carbon emissions. Current trends indicate a gradual transition from fossil fuels to renewable and sustainable energy sources. In this context, hydrogen emerges as one of the most promising candidates to replace fossil fuels in the future. With its environmentally friendly characteristics and broad range of applications, hydrogen is poised to become a cornerstone of the global energy transition (Durbin & Malardier-Jugroot, 2013; Tebibel & Labed, 2014; Yadav & Xu, 2012). Hydrogen, as the most abundant element in the universe, is recognized as a critical resource for clean energy production due to its high energy potential. In terms of thermal combustion energy, hydrogen provides approximately three times the energy of methane and five times that of coal, offering a remarkable advantage in energy efficiency and sustainability (Selvam, 1988; Walker, Fowler, & Ahmadi, 2015). Today, hydrogen is widely utilized in petroleum refining and ammonia production, while also being explored as an alternative fuel. These characteristics highlight hydrogen's potential as a sustainable solution for green energy production (Bennoua, Le Duigou, Quéméré, & Dautremont, 2015; Mayer, 1999). Table 1 presents the fundamental properties of hydrogen alongside those of various alternative fuels.

Table 1. *Comparison of Various Alternative Fuels*

Fuel type	Volumetric energy density [GJ/m³]	LHV [MJ/kg]	Storage pressure [bar]	Storage temperature [°C]
Liquid H_2	8.5	120	1	-253
Compressed H_2	4.5	120	700	25
Liquid NH_3	12.8	18.6	1/10	-35/20
MeOH	15.8	19.9	1	20
LNG	23.4	50	1	-162

According to Table 1, hydrogen demonstrates clear advantages over other fuels in terms of energy density and environmentally friendly storage potential. Both liquid and compressed hydrogen exhibit exceptionally high lower heating values (120 MJ/kg), which are approximately six times greater than alternative fuels like liquid ammonia (18.6 MJ/kg) and methanol (19.9 MJ/kg). This high energy density underscores hydrogen's capacity to carry significant amounts of energy in smaller quantities. Although hydrogen's volumetric energy density is relatively lower compared to other fuels 8.5 GJ/m³ for liquid hydrogen and 4.7 GJ/m³ for compressed hydrogen its environmental advantages outweigh this limitation. Unlike carbon-based fuels, such as liquefied natural gas (LNG), which has a higher volumetric energy density of 23.4 GJ/m³ but emits CO_2 upon combustion, hydrogen produces only water vapor as a byproduct, placing it in a unique position in terms of environmental sustainability. From a storage perspective, hydrogen poses certain logistical challenges. Liquid hydrogen requires extremely low temperatures of -253°C, while compressed hydrogen necessitates high pressures of up to 700 bar. Despite these technical hurdles, hydrogen's role in the clean energy transition is far more significant than that of other fuels. Compared to fuels like liquid ammonia or methanol, hydrogen's superior energy-carrying capacity and zero-carbon emissions make it a central component in future energy systems. These attributes position hydrogen as a unique and compelling alternative in terms of both energy density and environmental compatibility.

In recent years, significant advancements have been made in the automotive industry toward the development of alternative fuel vehicles, driven by goals of environmental sustainability and the need to mitigate the effects of global warming caused by fossil fuels (Jain, 2009; Katikaneni, Al-Muhaish, Harale, & Pham, 2014; Walker et al., 2015). In this context, hydrogen emerges as an innovative energy source. Its ability to provide energy through catalytic combustion or to be converted into electrical energy via a fuel cell positions hydrogen as a viable solution

for the automotive sector (Ball & Weeda, 2015; Dutta, 2014). In internal combustion engines (ICE), hydrogen can be utilized either as a primary fuel entirely or as a supplementary energy source when blended with other fuels (Arat, Baltacioglu, Özcanli, & Aydin, 2016; Baltacioglu, Arat, Özcanli, & Aydin, 2016; Fayaz et al., 2012; Uludamar, Yıldızhan, Aydın, & Özcanlı, 2016). When hydrogen is used as a fuel in internal combustion engines (ICE), the exhaust emissions primarily consist of water vapor, resulting in minimal environmental impact. Conversely, fuel cell electric vehicles (FCEVs) and fuel cell-based plug-in hybrid electric vehicles (FC-PHEVs) stand out as future transportation technologies, offering designs characterized by zero carbon emissions and the elimination of air pollution (Ball & Weeda, 2015). The unique properties of hydrogen offer significant potential for achieving environmental goals within the automotive sector. Additionally, as illustrated in Figure 1, global energy consumption is projected to continue increasing over the next decade (Pareek et al., 2020). This underscores the need for the development of new, clean, and carbon-neutral fuel technologies as a long-term solution to ensure energy sustainability and mitigate the impacts of climate change (Nicoletti, Arcuri, Nicoletti, & Bruno, 2015).

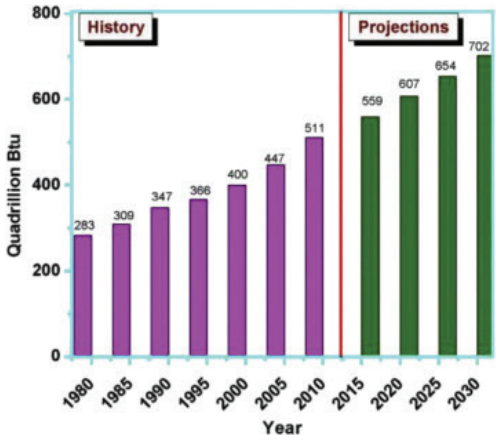

Figure 1. *Energy consumption from 1980 onwards and projections for the near future (Sazali, 2020)*

The broader use of hydrogen in internal combustion engines or fuel cell vehicles necessitates the optimization of storage conditions and the proper segregation of hydrogen based on transportation requirements (Figure 2). Various methods for hydrogen production exist, all of which require energy input derived from renewable or non-renewable sources. This dependency highlights the significant variability in the environmental

and economic impacts of hydrogen production, contingent upon the type of energy source utilized in the process (Alazemi & Andrews, 2015; Hosseini & Wahid, 2016; Yılmaz & Balta, 2017).

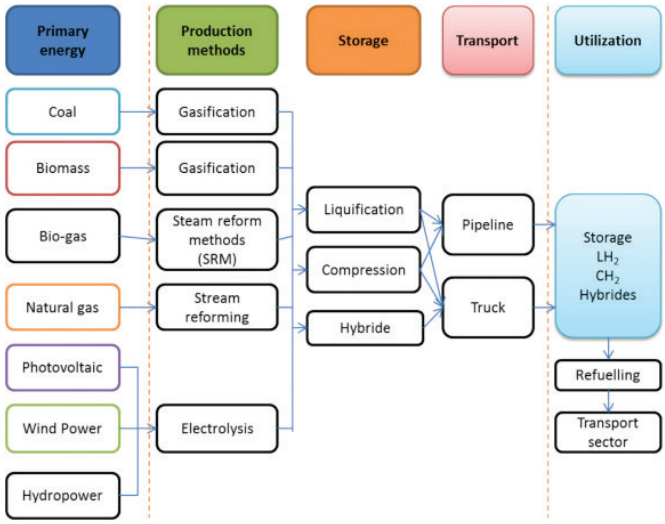

Figure 2. *Required Production and Transportation Systems for Hydrogen (Sinigaglia, Lewiski, Santos Martins, & Mairesse Siluk, 2017)*

Once hydrogen is produced, it must be stored efficiently. This storage can be accomplished using methods like compression, liquefaction, physical storage in hydrides, or chemical storage (Durbin & Malardier-Jugroot, 2013; Tong, Xiao, Cai, Bénard, & Chahine, 2016). The choice of a suitable storage method is influenced by factors such as high volumetric and gravimetric capacity, adherence to safety standards, cost-effectiveness, lightweight design, and the speed and efficiency of the absorption and desorption processes (Dutta, 2014). Despite its widespread potential, the safe storage and transportation of hydrogen continue to be major technical and economic challenges that limit the full adoption of the hydrogen economy. Hydrogen is utilized extensively across diverse industries, including energy, transportation, chemical production, petroleum refining, food processing, space exploration, and aviation. Particularly noteworthy is the growing importance of "green hydrogen" hydrogen produced from renewable energy sources, such as wind energy due to its economic potential and positive impact on environmental sustainability (Likkasit, Maroufmashat, Elkamel, Ku, & Fowler, 2018; Wenguo Liu et al., 2021; Neuwirth, Fleiter, Manz, & Hofmann, 2022; Posdziech, Schwarze, & Brabandt, 2019).

2. Green Hydrogen

For a sustainable future, hydrogen is poised to play a critical role in both energy production and various industrial processes. According to Maggio et al., industrial applications such as chemical synthesis will form the initial major market for green hydrogen, which will subsequently see broader adoption in energy production and the transportation sector (Maggio, Nicita, & Squadrito, 2019). Sgobbi et al. highlight that hydrogen holds significant potential in Europe's energy transition, particularly in transportation and industrial applications (Sgobbi et al., 2016). Currently, most of the hydrogen used is derived from fossil fuels. Hydrogen produced through methods such as steam methane reforming and coal gasification is referred to as "gray" and "brown" hydrogen, respectively. A common drawback of these methods is their significant carbon dioxide (CO2) emissions. Blue hydrogen, on the other hand, is produced by capturing and storing or recycling the CO_2 generated during production processes like steam methane reforming or coal gasification. This approach results in a lower carbon footprint compared to gray and brown hydrogen. However, the widespread adoption of blue hydrogen faces challenges due to the underdeveloped state and high costs of carbon capture and storage technologies. Figure 3 illustrates the feedstocks and key technologies used in hydrogen production.

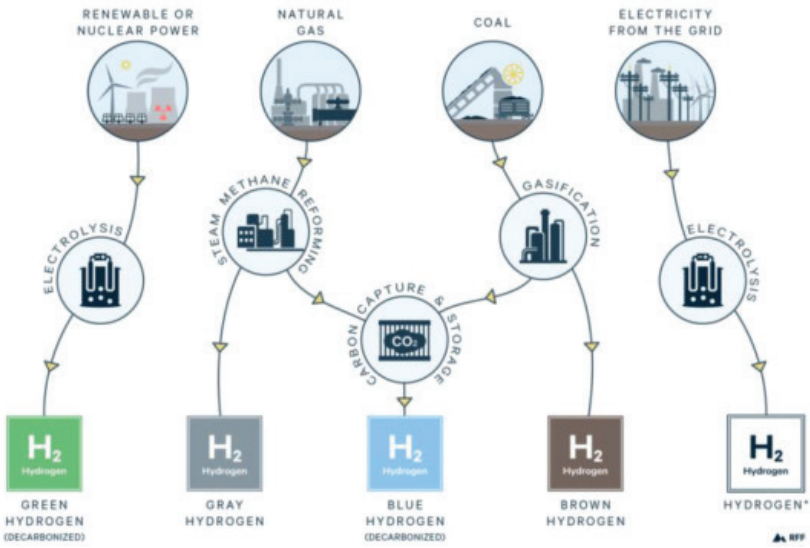

Figure 3. *Types of Hydrogen and Technologies Used İn Production (Panchenko, Daus, Kovalev, Yudaev, & Litti, 2023)*

One of the primary barriers to green hydrogen production today is its significantly higher cost compared to gray and brown hydrogen. Currently,

the cost of green hydrogen is approximately 3 to 6 times higher than that of gray and brown hydrogen. This cost disparity is a major reason why only a small fraction (about 5%) of the total hydrogen produced globally is green hydrogen. Hydrogen production costs are influenced by factors such as the capital cost of electrolyzer systems, electricity prices, and the operating duration of production facilities. Additionally, parameters like system efficiency, fixed operating costs, facility lifespan, interest rates, and the type of feedstock used (e.g., coal or natural gas) play critical roles in determining production costs. Thus, a detailed analysis of hydrogen production costs under varying technological and economic conditions is crucial for developing strategies to transition toward green hydrogen. For hydrogen to compete with other energy carriers, it is essential to reduce energy transmission costs, improve energy efficiency, and optimize the operating hours of production facilities. These challenges are actively being investigated by researchers worldwide.

Green hydrogen production holds significant potential in reducing harmful emissions into the atmosphere. Regions rich in renewable energy resources but lacking fossil fuel reserves could become exporters of this valuable energy source. These regions could also leverage green hydrogen more effectively across industries, the transportation sector, and their broader economies. Plans for the coming years project a staggering increase in green hydrogen production capacity, with estimates suggesting a growth of up to 12 times the current installed capacity (Power, 2019; Rana et al., 2024). This underscores the global interest and high expectations surrounding green hydrogen. Consequently, in the coming decades, scaling up green hydrogen production and expanding its use will become key objectives for the global energy, industrial, and transportation sectors. Achieving these goals will enable countries to transition toward an environmentally sustainable future, reduce their reliance on energy imports, and strengthen energy independence. Green hydrogen is anticipated to play a pivotal role in future energy transitions, contributing significantly to sustainable economic development.

The electricity required for green hydrogen production is primarily sourced from renewable resources such as solar or wind energy. However, the widespread adoption of this method faces several challenges, both from an engineering and economic perspective (van Hulst, 2024). The high energy consumption of the electrolysis process significantly increases production costs. Fortunately, the rapid decline in electricity generation costs from renewable energy sources is making green hydrogen production more economically attractive. Advances in electrolyzer technologies are further expected to reduce production costs, marking a crucial step toward the large-scale adoption of green hydrogen. Projections indicate that the

cost of green hydrogen production could decrease by approximately 70% within the next decade.

3. Hydrogen Storage

In evaluating hydrogen as a fuel source, the concepts of specific energy and energy density emerge as two critical parameters (Zacharia & Rather, 2015). Compared to hydrocarbons, hydrogen possesses a high mass-based energy density but exhibits significantly lower volumetric density (Roes & Patel, 2011). This presents a fundamental challenge in the safe and efficient storage and transportation of hydrogen. Although hydrogen has the highest energy per kilogram among all fuels, its low density results in significantly low volumetric energy density, posing substantial difficulties during the storage process (Chung, Chen, Chen, & Chang, 2015). Overcoming these challenges requires the implementation of high-pressure storage techniques. Additionally, this necessitates the development of solutions aimed at optimizing the storage performance of hydrogen-powered vehicles and enhancing the characteristics of existing energy storage technologies (Jain, 2009; Katikaneni et al., 2014). Building on this foundation, various methods for hydrogen storage have been developed to address the associated challenges effectively (Pollet, Staffell, & Shang, 2012). Among these methods, various options such as liquefaction, compression, metal hydrides, and advanced nanotechnology-based materials stand out. Liquid hydrogen offers high energy density but requires storage at extremely low temperatures of approximately -253 °C, necessitating highly insulated tanks. Moreover, the process of liquefying hydrogen requires almost a quarter of the energy stored in it chemically. Compressed hydrogen, on the other hand, is favored by major electric vehicle manufacturers. For instance, Honda and Nissan operate at 350 bar, while Toyota utilizes 700 bar. However, this method demands significant energy due to hydrogen's low volumetric energy density. Metal hydrides provide a safe storage option but are constrained by their heavy weight and prolonged filling times. Furthermore, metal hydrides typically exhibit low release rates. In contrast, innovative solutions such as metal-organic frameworks (MOFs) and carbon nanotubes (CNTs) represent promising alternatives in hydrogen storage. However, these nanotechnology-driven approaches remain in their nascent stages of development. All these storage methods highlight the critical need for ongoing research and development to optimize hydrogen storage processes and enhance their feasibility. Figure 4 illustrates the volumetric density of hydrogen under various conditions, offering a comparative visual insight into these storage technologies.

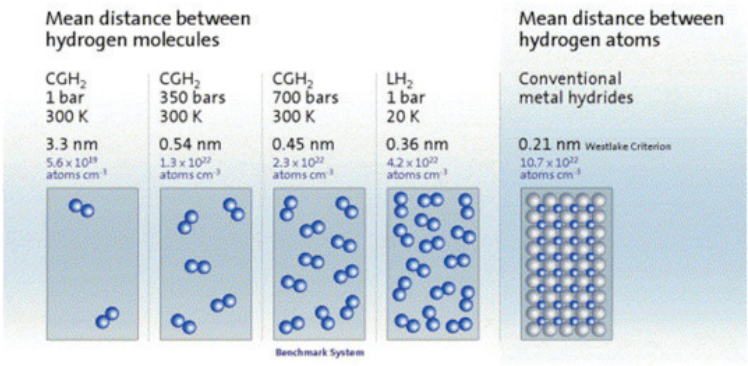

Figure 4. *The volumetric density of hydrogen under various conditions. (von Helmolt & Eberle, 2007)*

Figure 4 illustrates the intermolecular distances and atomic density of hydrogen across various storage methods. For compressed hydrogen (CGH_2), increasing pressure reduces the intermolecular distance and enhances atomic density; for instance, the distance decreases from 3.3 nm at 1 bar to 0.45 nm at 700 bar. Liquid hydrogen (LH_2) achieves a higher density with an intermolecular distance of 0.36 nm at 1 bar and 20 K. In metal hydrides, the distance further decreases to 0.21 nm, achieving the highest density levels. These findings highlight the significant impact of storage methods on hydrogen density.

4. The Use of Hydrogen as a Fuel in Internal Combustion Engines

Interest in dual-fuel engines began to take shape with the pioneering studies of Elliott and Davis in the 1950s. These studies examined how various gaseous fuels, such as natural gas, propane, butane, and hydrogen, influence the combustion efficiency of two-stroke dual-fuel diesel engines. The results revealed that the flammability limits of compressed gas-air mixtures represent a critical parameter for combustion performance in dual-fuel engines. This finding established a foundational understanding necessary for the effective utilization of gaseous fuels in diesel engines (Elliott & Davis, 1951). Hydrogen, despite being a flammable gas, holds significant potential for use in internal combustion vehicles as it produces only environmentally benign emissions, such as water vapor, during combustion. This characteristic makes hydrogen an ideal energy carrier for reducing fossil fuel-related pollution and providing a cleaner alternative for transportation (Fayaz et al., 2012; Sun & Liu, 2010). Table 2 presents a comparison of some properties of hydrogen with those of other fossil fuels and alcohols.

Table 2. *Properties of Hydrogen, Gasoline, and Methane*

Properties	Gasoline	Methane	Hydrogen
Density (kg/m^3)	4.40	0.65	0.084
Diffusion in Air (cm^2/s)	0.05	0.16	0.61
Specific Heat at Constant Pressure (J.g/K)	1.2	2.22	14.89
Ignition Limits in Air (%volume)	1.0-7.6	5.3-15.0	4.0-75.0
Ignition Temperature (°C)	228-471	540	585
Flame Temperature in Air (°C)	2197	1875	2045
Explosion Energy (g.TNT.k/j)	0.25	0.19	0.17
Flame Propagation Speed (%)	34	25	17

Table 2 highlights several distinct properties of hydrogen compared to gasoline and methane. Hydrogen's extremely low density (0.084 kg/m^3) poses unique challenges in transportation and storage, while its high diffusion rate (0.61 cm^2/s) provides an advantage in ensuring rapid mixing during combustion. The notably high specific heat capacity at constant pressure (14.89 J/gK) enhances hydrogen's efficiency in transferring energy. Its broad ignition limits in air (4.0-75.0% by volume) allow for easier ignition under various conditions, supporting its versatility as a fuel. With an ignition temperature of 585°C, higher than gasoline but similar to methane, hydrogen offers a safety advantage. Furthermore, its flame temperature in air at 2045°C reflects its energy-dense nature. Hydrogen's low explosion energy (0.17 g TNT/kJ) and limited flame propagation rate (17%) improve its applicability in controlled combustion processes. These attributes position hydrogen as a compelling choice for clean energy applications and advanced technologies like fuel cells. Particularly for sustainable energy systems, hydrogen emerges as a critical option due to its environmental benefits and high combustion efficiency.

Hydrogen-powered internal combustion engines (H_2-ICE) are known to exhibit lower efficiency compared to gasoline engines. In particular, engines operating on hydrogen using a suction-based pre-mixed strategy, commonly referred to as port fuel injection hydrogen internal combustion engines (PFI-H_2 ICE), demonstrate lower power efficiency than their gasoline or diesel counterparts. To overcome this disadvantage and enhance the performance of hydrogen engines, extensive research has been conducted on engine design and operational parameters. These studies have facilitated significant advancements in improving the efficiency of hydrogen-fueled ICEs and have provided promising developments for the future of this technology (Baltacioglu et al., 2016; Berckmüller et al., 2003; Sebastian Verhelst & Wallner, 2009; WHITE, STEEPER, & LUTZ, 2006). In

this context, several innovative engine concepts that have been developed will be examined as illustrative examples.

The use of hydrogen as a dual fuel offers significant advantages over other fuels in terms of engine efficiency, emissions reduction, and stable operating performance. As illustrated in Figure 5, hydrogen's exceptionally low minimum flammability limit makes it an ideal fuel for lean-burn operating conditions. Moreover, its superior thermodynamic and heat transfer properties enhance engine efficiency by generating high compression temperatures while minimizing energy losses. The fuel's rapid combustion rates and low minimum ignition energy enable hydrogen to perform effectively under challenging engine conditions, such as high-speed operation and cold starts. These attributes position hydrogen as a sustainable and highly efficient energy solution.

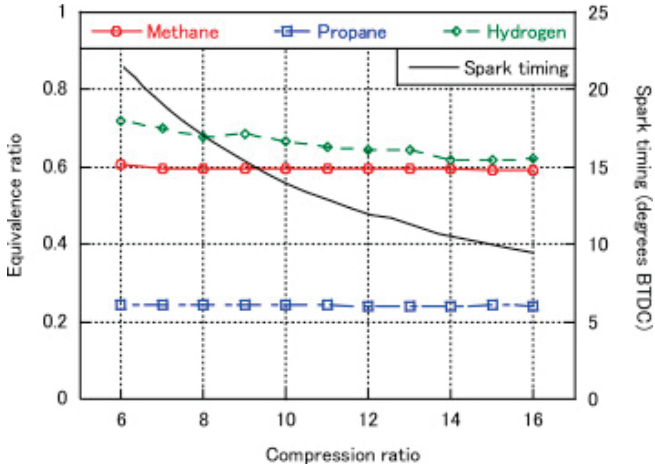

Figure 5. *The variation in lean operating limits of a spark-ignition (SI) engine running at 900 rpm, depending on changes in the compression ratio (CR) for different gaseous fuels, demonstrates significant impacts on engine performance and efficiency (Bade Shrestha, Karim, & Wierzba, 2000)*

Figure 5 illustrates the lean operating limits and ignition timings of a spark-ignition (SI) engine running at 900 rpm for different gaseous fuels (hydrogen, methane, and propane) as a function of compression ratio (CR). The vertical axis on the left represents the equivalence ratios, while the vertical axis on the right indicates the spark timing (BTDC - Before Top Dead Center). The horizontal axis denotes the compression ratio. Hydrogen demonstrates superior performance by significantly extending the lean operating limits as the compression ratio increases. Even at a compression ratio of 6:1, the equivalence ratio observed for hydrogen surpasses that of other fuels, and this trend continues up to a compression ratio of 16:1. This

is attributed to hydrogen's thermophysical properties, such as a high flame propagation speed and low ignition energy.

Compared to methane and propane, hydrogen exhibits earlier ignition timing, indicating its potential to enhance engine efficiency. The graph also shows that while methane and propane maintain relatively constant equivalence ratios with increasing compression ratios, hydrogen's flexible and adaptable operating characteristics make it better suited for lean-burn engine applications. This provides strong scientific support for hydrogen's use as a clean and efficient fuel in internal combustion engines.

4.1. Utilization of Hydrogen in Engines

The utilization of hydrogen in internal combustion engines (ICEs) presents various advantages and challenges through different storage and fueling methods. Pressurized hydrogen ICE configurations enhance volumetric efficiency by increasing intake air and hydrogen pressures, thereby boosting the power density of conventional ICEs. In these systems, hydrogen is optimized for engine performance while employing multi-mode operating strategies to reduce NO_x emissions. For instance, manufacturers such as Ford and BMW have made significant strides in developing these systems, optimizing supercharged and high-pressure engine designs to simultaneously increase power density and lower emission levels.

Liquid hydrogen-fueled ICE (LH_2-ICE) systems require hydrogen to be stored in liquid form, necessitating cryogenic conditions at -253°C and the use of highly insulated tanks. The cooling properties of liquid hydrogen contribute to the formation of a more efficient fuel mixture in the combustion chamber and assist in reducing NO_x emissions. In Europe, research led by BMW has achieved notable progress in improving refueling times and fuel system performance for LH_2-fueled ICEs. These systems demonstrate significant potential for achieving both performance enhancement and environmental sustainability goals due to the high energy concentration of hydrogen and its cooling effect.

Direct injection hydrogen-fueled ICEs (DI-H_2-ICEs) stand out with the use of high-pressure hydrogen injectors. This technology enables the direct injection of hydrogen into the cylinder, significantly improving engine performance and power density. However, challenges such as injector design and achieving homogeneous hydrogen distribution within the combustion chamber remain critical engineering concerns. Dual injection strategies offer enhanced thermal efficiency under low loads and robust performance under high loads. Direct injection systems prevent backfire while enabling stable operation of the engine under high-speed and compression conditions. In conclusion, the use of hydrogen in ICEs through these three distinct storage and fueling methods offers significant

potential for enhancing energy efficiency and reducing emissions. However, the widespread adoption of these systems will depend on technological advancements, cost reductions, and the development of supporting infrastructure.

4.2. Use of Hydrogen in Spark-Ignition Engines

Hydrogen emerges as a powerful alternative fuel that could replace ethanol or gasoline in spark-ignition engines (Jabbr, Vaz, Khairallah, & Koylu, 2016). Due to its superior thermophysical properties, such as high flame propagation speed and low ignition energy, hydrogen has the potential to enhance engine performance while improving its emission profiles (Salvi & Subramanian, 2015). This demonstrates that hydrogen is a sustainable option compared to conventional fuels, offering significant advantages in both environmental and energy efficiency aspects. For hydrogen-powered internal combustion engines (H_2-ICE) to operate effectively, engine modifications are generally required. During the transition from traditional gasoline or diesel engines to H_2-ICE, the physical properties of hydrogen must be carefully considered. Since hydrogen, even in compressed form, is typically in gaseous state compared to liquid gasoline, it necessitates the design of a specialized fueling system. Furthermore, as historical research has shown, the combustion process of hydrogen is highly susceptible to abnormal combustion events such as pre-ignition, backfire, knocking, and auto-ignition. In spark-ignition (SI) engines, pre-ignition occurs when hydrogen, with its low ignition energy, ignites prematurely due to hot spots within the engine cylinders before the appropriate spark timing, typically when the intake valve is closed. Similarly, backfire, also linked to hydrogen's low ignition energy, occurs when the intake valves are open, and the reverse flame propagation may cause damage to the intake manifold. This presents a serious risk of damage to the engine's intake system. To mitigate the risk of backfire, safety measures such as flame arresters, which prevent flame propagation, are integrated into the engine systems. These technological precautions play a critical role in ensuring the reliable and efficient operation of hydrogen-powered engines (Shinagawa, Okumura, Furuno, & Kim, 2004; Sebastian Verhelst & Wallner, 2009). Furthermore, advancements in engine technologies and innovations in injection systems suggest the direct injection of hydrogen into the cylinders to enhance performance and prevent backfires in hydrogen-powered internal combustion engines (H_2-ICE). This approach requires the development of high-pressure, durable hydrogen injectors to ensure a more efficient combustion process. High-pressure injection systems, in particular, play a critical role not only in boosting engine performance but also in ensuring reliability. However, methods such as port fuel injection (PFI) and manifold injection remain popular options due to their low costs, simple installation, and low pressure

requirements (S. Verhelst, 2014). Yamane and colleagues have examined and developed high-pressure hydrogen gas injectors for hydrogen-powered spark-ignition (SI) engines (Lata, Misra, & Medhekar, 2012). The developed design enabled high injection speeds of up to 20 MPa through a common rail actuator system. It was reported that the maximum hydrogen injection amount reached 400 mL per injection at 3000 rpm, which is considered a significant step for hydrogen-powered engines. Additionally, it was found that the proposed gas injectors exhibited a high response rate and showed no leakage during 700 hours of long operating durations (Yamane et al., 2011). These findings clearly demonstrate the future potential of hydrogen injection systems in terms of efficiency and cost-effectiveness

Literature reviews and research studies have shown that hydrogen contributes significantly to improving the performance of spark-ignition (SI) engines in terms of brake thermal efficiency (BTE) and indicated thermal efficiency (ITE). Whether used in its pure form or blended with other fuels, hydrogen enables higher combustion rates to be achieved compared to gasoline (Ji & Wang, 2009). This is largely attributed to hydrogen's inherently high flame speed. Additionally, hydrogen's short quenching distance is another important characteristic that supports more complete and efficient fuel combustion. Another positive effect of hydrogen use on SI engine performance is the observed reduction in fuel and energy consumption in engines running on pure or blended hydrogen. This is made possible by hydrogen's ability to burn effectively even in lean mixtures and its high heating value (Di Iorio, Sementa, & Vaglieco, 2014). Thus, hydrogen not only contributes to the reduction of emissions but also enhances energy savings, offering significant potential for improving the thermal efficiency of SI engines

Du et al (Du et al., 2016); In a study by Du and others, the combustion and emission characteristics of a dual-fuel SI engine combining RON 97 gasoline port fuel injection (PFI) with hydrogen direct injection (DI) systems were examined, with a detailed analysis of the effects of hydrogen on engine performance (Figure 6). The experiments were conducted using hydrogen with a purity of 99.995%, under a fixed engine speed of 1500 rpm, 14% throttle opening, and an injection pressure of 6 MPa. The air-fuel equivalence ratios were set at 1.0, 1.1, 1.2, and 1.5, and mixtures containing hydrogen fractions of up to 11.09% by volume were tested.

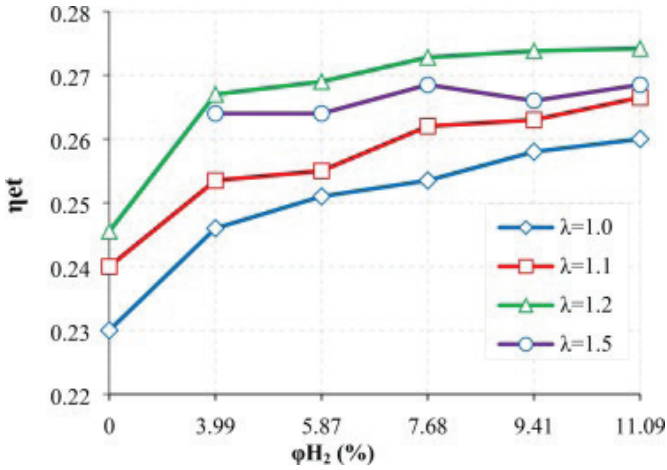

Figure 6. *Effective thermal efficiency as a function of hydrogen addition ratio at different equivalence ratios (Du et al., 2016)*

The results show that the increase in hydrogen fraction leads to a significant improvement in thermal efficiency across all equivalence ratios. Hydrogen's high heating value, fast combustion characteristics, and short quenching distance that supports complete combustion are the primary reasons for this improvement. Notably, at lean mixtures (λ = 1.2), a thermal efficiency of approximately 27% achieved with an 11.09% hydrogen fraction clearly demonstrates the positive impact of hydrogen on combustion efficiency. However, at higher equivalence ratios (λ = 1.5), it was observed that the effect of hydrogen gradually decreased, which could be attributed to the limited impact of low hydrogen content on combustion kinetics. Overall, the potential of hydrogen to enhance thermal efficiency depending on the air-fuel ratio highlights it as a strategic fuel for low-carbon engine technologies and presents significant opportunities for energy savings and emissions reduction.

4.3. Use of Hydrogen in Compression-Ignition Engines

Hydrogen's auto-ignition temperature is 858K, which prevents its use as a sole fuel in compression-ignition engines. As a result, hydrogen cannot be used alone in diesel engines without the integration of a spark plug. However, by blending hydrogen with other fuels in the combustion chamber, it becomes viable to incorporate hydrogen into diesel engine operation (de Morais, Mendes Justino, Valente, Hanriot, & Sodré, 2013). Research has thoroughly explored the impact of hydrogen on diesel engine performance and emissions, revealing several key outcomes: Enriching the fuel with hydrogen can improve thermal efficiency, effective power, mean effective pressure, and specific energy consumption, influenced by factors such as engine speed, load, and the air-fuel ratio. Additionally, incorporating

hydrogen significantly reduces emissions of unburned hydrocarbons, carbon monoxide, carbon dioxide, and particulates, although a rise in NO_x emissions has been noted. These results highlight the considerable potential of using hydrogen as a fuel enhancer in diesel engines, offering benefits in both performance and environmental sustainability (Alrazen, Abu Talib, Adnan, & Ahmad, 2016).

Before applying the dual-fuel operating mode in a conventional diesel engine, it is necessary to evaluate the physicochemical properties of hydrogen. Hydrogen's low density requires more storage capacity, while its high calorific value enables the provision of more energy. However, the high auto-ignition temperature of hydrogen limits its use as a single fuel in diesel engines when the compression ratio is insufficient. Since knocking issues may occur in CI engines running on pure hydrogen, the dual-fuel operating mode is suggested to overcome these challenges by providing an existing ignition source. Öte yandan Deb et al (Deb, Sastry, Bose, & Banerjee, 2015), on a single-cylinder, four-stroke diesel engine running on hydrogen and diesel fuel, they demonstrated that hydrogen enrichment provides a more efficient combustion process, improving brake thermal efficiency (BTE) and specific energy consumption (BSEC). However, in the tests conducted by Karagöz and colleagues with hydrogen-enriched fuel, it was noted that BTE decreased by 6.3-10.9% due to lean combustion processes, resulting in a higher BSFC (Karagöz, Sandalcı, Yüksek, & Dalkılıç, 2015). Lata et al (Lata et al., 2012), conducted on a turbocharged, direct-injection diesel engine operating at 1500 rpm and under different load conditions (Figure 7), they found that the hydrogen-diesel dual-fuel mode increased thermal efficiency under high load conditions. This improvement was attributed to a more effective combustion process due to the shorter ignition delay. These studies demonstrate that the use of hydrogen as an enriching fuel in diesel engines can have both positive and negative effects on engine performance, depending on the load and combustion conditions.

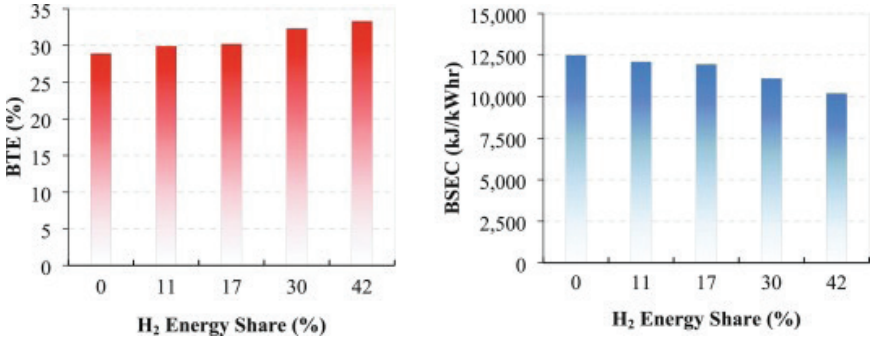

Figure 7. *The Effect of Hydrogen Use on BTE and BSEC (Deb et al., 2015)*

5. Hydrogen-Fueled Fuel Cells as an Electrical Power Source for Electric Vehicles

Fuel cells are devices that generate electricity by converting hydrogen and oxygen into electrical energy through thermochemical reactions. It is essential to emphasize that the hydrogen utilized in fuel cells is a renewable energy source, produced using various methods from energy systems, rather than being directly sourced from natural reserves like fossil fuels. Hydrogen, which constitutes a significant part of the universe's mass, can be produced from both fossil resources and renewable energy sources such as geothermal, solar, and wind energy. However, hydrogen extraction from fossil fuels results in the emission of pollutants that have harmful effects on the environment. As a consequence, new technologies are required to produce hydrogen from sustainable, renewable energy sources.

Fuel cells consist of an electrolyte that is compressed between electrodes on the anode and cathode sides. Fuel cells are classified into various types depending on the electrolyte they use, including polymer electrolyte membrane (PEM), solid oxide, molten carbonate, alkaline, and phosphoric acid fuel cells. Additionally, they are categorized based on their operating temperature: low-temperature (25-100°C), medium-temperature (100-500°C), and high-temperature (500-1000°C) fuel cells. While hydrogen is commonly used to generate electricity in fuel cells, other alternative fuels such as fossil fuels (coal, oil, and natural gas), alcohols like methanol and ethanol, as well as non-hydrocarbon compounds like ammonia and borohydride, along with biomass derived from hydrogen, can also serve as potential fuel sources. The storage and transportation challenges associated with hydrogen have led to the exploration of using waste materials as an alternative fuel source. It is anticipated that in the future, fuel cells will emerge as the primary power source for automobiles, providing clean, high-efficiency energy with reduced energy consumption. Fuel cells are expected to address pressing issues such as environmental sustainability, global warming, the depletion of conventional energy resources, and the geopolitical instability of regions rich in fossil fuels, thereby driving a revolution in the energy sector.

Research on fuel cells as an energy source, especially in the automotive industry, is increasing as part of the broader goal of achieving clean and environmentally friendly transportation solutions. As fuel cell systems are developed, attention must also be paid to the inertia requirements of different system types. According to Sui et al. (2020) and Zore et al. (2021), mechanical components, along with the acceleration, deceleration, and mechanical inertia of these components, must be designed to respond appropriately to the system's demands. In terms of fuel cell usage in automobiles, several companies have made notable advancements.

For example, General Motors has used a 100 kW PEM fuel cell in its "Precept" model, which offers a range of 800 km and accelerates to 100 km/h in 9 seconds. Ford has developed models such as the "P2000" and "FORD FOCUS FCV," while Nissan has created the "Xterra FCV" model. In 2002, Daimler-Chrysler developed a fuel cell bus with a range of 300 km and a maximum speed of 80 km/h. As for future market expectations, numerous companies—including Ford, DaimlerChrysler, PSA/Renault/Nissan, Hyundai, Honda, FIAT,BMW Toyota, and GM/Mitsubishi—are conducting extensive research. Figure 8 illustrates the basic diagram of a fuel cell electric vehicle.

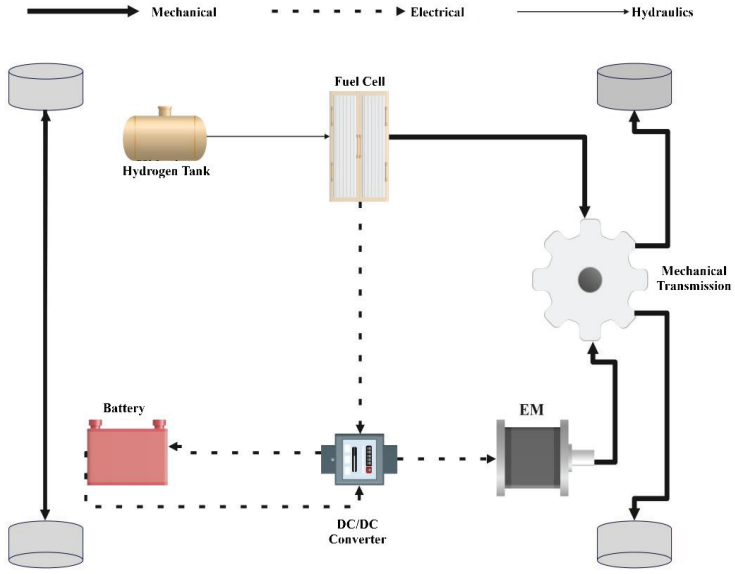

Figure 8. *The Structure of an Electric Vehicle Using Hydrogen Fuel Cells as an Energy Source*

Hydrogen fuel cell vehicles (HFCVs) use an electric motor as the traction motor, generating the necessary electricity through a combination of hydrogen and air in the fuel cell, emitting only water vapor as a byproduct (Kumar & Jain, 2014; *Modern Electric, Hybrid Electric, and Fuel Cell Vehicles, Third Edition*, 2018). In the long term, HFCVs are expected to play a key role in transportation systems due to their potential to reduce dependence on fossil fuels and their environmentally friendly technology (Salvi & Subramanian, 2015). Vehicles using proton exchange membrane fuel cells (PEMFC), in particular, stand out with higher energy efficiency and zero-emission characteristics compared to internal combustion engine vehicles (ICEVs), making them a more effective alternative to ICEVs in the

long term (Ball & Weeda, 2015; Salvi & Subramanian, 2015). The ability of HFCVs to completely eliminate harmful emissions such as greenhouse gases and carbon dioxide makes them an ideal solution in the fight against climate change and urban air pollution (Wei Liu & Christopher, 2015; Mourad, 2014). These vehicles stand out with advantages such as longer range and fast refueling compared to battery electric vehicles (BEVs), while being preferred for their much lower emission levels compared to internal combustion engine vehicles (ICEVs), making them environmentally friendly. In the long term, HFCVs are expected to become widespread as a zero-emission, highly efficient, and sustainable option in transportation systems. Fuel cell electric vehicles (FCEVs) have a highly integrated structure, consisting of key components such as the fuel cell system, electric motor, battery, vehicle control unit, and an intelligent control unit that manages energy between the battery and the fuel cell system (Chan, Bouscayrol, & Chen, 2010; Fernández, Cilleruelo, & Martínez, 2016). The vehicle controller dynamically manages the motor power and energy transfer between the battery and fuel cell system by processing environmental data along with the user's acceleration and braking commands (García, Torreglosa, Fernández, & Jurado, 2013). During acceleration, both the fuel cell and the battery simultaneously provide power to the traction motor, while during braking, the motor acts as a generator, converting braking energy into electrical energy, which is then stored in the battery (Fernández et al., 2016). The control unit optimizes energy management by comparing the fuel cell's nominal output power with the power requested by the vehicle; when the demand is lower than the nominal output power, the battery is charged. In such cases, the high temperatures that arise within the fuel cell (FC) and batteries should also be addressed as a separate issue. Additionally, there are ongoing studies focused on the cooling of such equipment (Faghri & Guo, 2005; Varol, Coşanay, et al., 2025; Varol, Oztop, et al., 2025; Wu et al., 2019). Additionally, the ability of FCEVs to charge their battery without an external power source requires an effective electronic circuit design and energy management strategy for this process (García et al., 2013). These features enhance the energy efficiency of fuel cell vehicles while also strengthening their operational flexibility and environmental sustainability.

6. The Role of Hydrogen in Aviation and Gas Turbines

Gas turbines (GTs) are widely used in the energy sector due to their compact design, high power generation capacity, quick start-up advantages, and their ability to be integrated with other energy generation systems, such as the Rankine cycle (Abrosimov, Baccioli, & Bischi, 2020; JUSTE, 2006). These turbines are typically designed based on the Brayton cycle and consist of three main components: the compressor, combustion chamber, and turbine. The system's performance is largely dependent on

the efficiency and characteristics of the combustion process. The fuel used in the combustion chamber is a key factor that directly determines not only combustion efficiency but also the environmental impact. Fossil fuels, particularly oil and natural gas, have traditionally been the primary fuel sources for these turbines (Maslennikov & Shterenberg, 2011). However, the use of these fuels presents significant environmental sustainability challenges due to high greenhouse gas emissions. To mitigate these negative impacts, the use of eco-friendly alternative fuels such as biofuels and hydrogen in gas turbines (GTs) is being proposed (Devi, S., Vimal, & T.R., 2021). Hydrogen has an exceptionally high energy content of 120 MJ/kg on a mass basis, nearly three times higher than traditional fuels like gasoline (44 MJ/kg). This superior energy density makes hydrogen a promising candidate for clean energy conversion processes. Furthermore, the use of hydrogen in gas turbines (GTs) not only reduces emissions but also provides a more efficient alternative in energy production processes by offering higher thermal efficiency and energy conversion rates. As a result, research on the use of hydrogen in GTs indicates significant potential in terms of both energy efficiency and environmental benefits.

The blending of hydrogen with traditional fuels emerges as a strategic intermediate solution that offers both environmental benefits and facilitates technological transition. Hydrogen's high flame speed and wide flammability range enhance combustion efficiency, enabling the reduction of pollutant emissions, particularly unburned hydrocarbons and CO_2 levels. This approach leverages existing infrastructure and engine technologies, providing a foundation for the gradual integration of hydrogen technologies. In this way, it facilitates a crucial transition phase for the widespread adoption of hydrogen. Specifically, in the aviation sector, a cold-pressurized mixture of hydrogen and natural gas could provide a sustainable solution in the short term (Chae, Kim, Moon, Park, & Lee, 2022; Erdener et al., 2023; Gondal, 2019). This approach combines hydrogen's clean combustion properties with natural gas to reduce emissions, while also allowing for the utilization of natural gas produced during oil extraction, which is typically released into the atmosphere. By burning excess natural gas, greenhouse gas emissions can be controlled. This hybrid fuel strategy not only mitigates environmental impacts but also facilitates the aviation industry's transition to fully hydrogen-powered systems. It enables the optimization of existing infrastructure while significantly reducing the carbon footprint. This can be seen as a critical intermediate step in achieving short-term sustainability goals and accelerating the transition to a hydrogen economy in the long term.

To explore hydrogen's potential and safety as an aviation fuel, numerous aviation companies have developed prototypes and conducted

demonstration projects. These initiatives have involved both limited test flights and ground-based trials. One of the initial milestones was in 1957, when a Martin B-57B aircraft used hydrogen for a brief period in one of its two Wright J65 jet engines. Later, in 1988, the hydrogen-powered Tu-155 prototype successfully completed its inaugural flight. After these pioneering efforts, hydrogen technology gained more focus in electric fuel cell and piston engine propeller systems, rather than in gas turbine engines. Airbus has introduced several hydrogen-powered aircraft concepts utilizing gas turbine engines, and companies such as Pratt & Whitney and CFM International have launched projects focused on hydrogen systems for gas turbines. These efforts contribute to a deeper understanding of hydrogen's potential in aviation and its role in advancing sustainable energy solutions.

7. Conclusion and Recommendations

This study highlights the strategic importance of hydrogen in modern energy systems and its applications across various sectors. In the energy transition process, hydrogen emerges as a key element that enhances environmental sustainability and reduces carbon emissions. The production of hydrogen through electrolysis and renewable energy sources reduces dependence on fossil fuels while enhancing energy security. Successful implementation of hydrogen-powered gas turbine systems in countries like Germany proves the future potential of hydrogen. In the automotive sector, hydrogen fuel cell vehicles offer significant advantages with zero emissions and performance improvements. Findings such as a 7.4% increase in thermal efficiency with an 11.09% hydrogen fraction demonstrate the contribution of hydrogen to combustion processes. In the aviation sector, the use of hydrogen in both gas turbines and electric fuel cells is revolutionary in terms of energy density and environmental impact. Hydrogen-powered prototypes from companies like Airbus and BMW define its role in sectoral transformation. For the widespread applicability of hydrogen, innovative technologies for storage and transportation, efforts to improve the cost-effectiveness of production processes, and acceleration of infrastructure investments are of critical importance. The use of hydrogen blended with fossil fuels in gradual transition strategies can facilitate the integration of hydrogen into energy systems. Furthermore, hydrogen and natural gas mixtures offer a sustainable solution for reducing emissions and utilizing waste natural gas in the aviation sector. The recommendations derived from this context are outlined below.

- Hydrogen's low density reduces efficiency in storage and transportation processes. Next-generation materials, such as carbon nanotubes and metal-organic frameworks (MOFs), can offer higher energy density compared to conventional methods (compressed gas or liquid storage). The Fraunhofer Institute in Germany is conducting successful

studies in this field to optimize hydrogen storage using lightweight composite materials.

- Sector-specific customized solutions are required. Airbus's ZEROe concept has developed prototypes for the use of liquid hydrogen in aviation with a zero-emission goal. In the automotive sector, the Toyota Mirai has demonstrated the viability of hydrogen technology through practical fuel cell applications. These successes necessitate the renewal of infrastructures according to sector-specific needs.

- Japan's FH2R project produces hydrogen using solar energy, helping to balance fluctuations in renewable resources and address large-scale storage issues. Additionally, blending hydrogen into natural gas grids can enhance the use of existing infrastructure while offering hybrid solutions in energy transportation.

- The EU's "Hydrogen Strategy" program, with a budget of 430 billion euros, and the US's "Hydrogen Shot" initiative serve as examples to accelerate the widespread adoption of hydrogen technologies. These types of incentives can lower the costs of hydrogen, increasing its economic viability. For example, the US aims to reduce the cost of clean hydrogen to below 1 dollar per kilogram.

REFERENCES

Abrosimov, K. A., Baccioli, A., & Bischi, A. (2020). Techno-economic analysis of combined inverted Brayton – Organic Rankine cycle for high-temperature waste heat recovery. *Energy Conversion and Management*, 207, 112336. Retrieved from https://doi.org/10.1016/j.enconman.2019.112336

Alazemi, J., & Andrews, J. (2015). Automotive hydrogen fuelling stations: An international review. *Renewable and Sustainable Energy Reviews*, 48, 483–499. Retrieved from https://doi.org/10.1016/j.rser.2015.03.085

Alrazen, H. A., Abu Talib, A. R., Adnan, R., & Ahmad, K. A. (2016). A review of the effect of hydrogen addition on the performance and emissions of the compression – Ignition engine. *Renewable and Sustainable Energy Reviews*, 54, 785–796. Retrieved from https://doi.org/10.1016/j.rser.2015.10.088

Arat, H. T., Baltacioglu, M. K., Özcanli, M., & Aydin, K. (2016). Effect of using Hydroxy – CNG fuel mixtures in a non-modified diesel engine by substitution of diesel fuel. *International Journal of Hydrogen Energy*, 41(19), 8354–8363. Retrieved from https://doi.org/10.1016/j.ijhydene.2015.11.183

Bade Shrestha, S. O., Karim, G. A., & Wierzba, I. (2000). Examination of Operational Limits in Gas Fueled Spark Ignition Engines. Retrieved from https://doi.org/10.4271/2000-01-1944

Ball, M., & Weeda, M. (2015). The hydrogen economy – Vision or reality? 1 1This paper is also published as Chapter 11 'The hydrogen economy – vision or reality?' in Compendium of Hydrogen Energy Volume 4: Hydrogen Use, Safety and the Hydrogen Economy, Edited by Michael Ball, Angelo Ba. *International Journal of Hydrogen Energy*, 40(25), 7903–7919. Retrieved from https://doi.org/10.1016/j.ijhydene.2015.04.032

Baltacioglu, M. K., Arat, H. T., Özcanli, M., & Aydin, K. (2016). Experimental comparison of pure hydrogen and HHO (hydroxy) enriched biodiesel (B10) fuel in a commercial diesel engine. *International Journal of Hydrogen Energy*, 41(19), 8347–8353. Retrieved from https://doi.org/10.1016/j.ijhydene.2015.11.185

Bennoua, S., Le Duigou, A., Quéméré, M.-M., & Dautremont, S. (2015). Role of hydrogen in resolving electricity grid issues. *International Journal of Hydrogen Energy*, 40(23), 7231–7245. Retrieved from https://doi.org/10.1016/j.ijhydene.2015.03.137

Berckmüller, M., Rottengruber, H., Eder, A., Brehm, N., Elsässer, G., Müller-Alander, G., & Schwarz, C. (2003). Potentials of a Charged SI-Hydrogen Engine. Retrieved from https://doi.org/10.4271/2003-01-3210

Chae, M. J., Kim, J. H., Moon, B., Park, S., & Lee, Y. S. (2022). The present condition and outlook for hydrogen-natural gas blending technology. *Korean Journal of Chemical Engineering*, 39(2), 251–262. Retrieved from https://doi.org/10.1007/s11814-021-0960-8

Chan, C. C., Bouscayrol, A., & Chen, K. (2010). Electric, Hybrid, and Fuel-Cell Vehicles: Architectures and Modeling. *IEEE Transactions on Vehicular Technology*, 59(2), 589–598. Retrieved from https://doi.org/10.1109/TVT.2009.2033605

Chung, C. A., Chen, Y.-Z., Chen, Y.-P., & Chang, M.-S. (2015). CFD investigation on performance enhancement of metal hydride hydrogen storage vessels using heat pipes. *Applied Thermal Engineering*, 91, 434–446. Retrieved from https://doi.org/10.1016/j.applthermaleng.2015.08.039

de Morais, A. M., Mendes Justino, M. A., Valente, O. S., Hanriot, S. de M., & Sodré, J. R. (2013). Hydrogen impacts on performance and CO2 emissions from a diesel power generator. *International Journal of Hydrogen Energy*, 38(16), 6857–6864. Retrieved from https://doi.org/10.1016/j.ijhydene.2013.03.119

Deb, M., Sastry, G. R. K., Bose, P. K., & Banerjee, R. (2015). An experimental study on combustion, performance and emission analysis of a single cylinder, 4-stroke DI-diesel engine using hydrogen in dual fuel mode of operation. *International Journal of Hydrogen Energy*, 40(27), 8586–8598. Retrieved from https://doi.org/10.1016/j.ijhydene.2015.04.125

Devi, B., S., V., Vimal, R., & T.R., P. (2021). Influence of high oxygenated biofuels on micro-gas turbine engine for reduced emission. *Aircraft Engineering and Aerospace Technology*, 93(3), 508–513. Retrieved from https://doi.org/10.1108/AEAT-07-2020-0150

Di Iorio, S., Sementa, P., & Vaglieco, B. M. (2014). Experimental investigation on the combustion process in a spark ignition optically accessible engine fueled with methane/hydrogen blends. *International Journal of Hydrogen Energy*, 39(18), 9809–9823. Retrieved from https://doi.org/10.1016/j.ijhydene.2014.04.065

Du, Y., Yu, X., Wang, J., Wu, H., Dong, W., & Gu, J. (2016). Research on combustion and emission characteristics of a lean burn gasoline engine with hydrogen direct-injection. *International Journal of Hydrogen Energy*, 41(4), 3240–3248. Retrieved from https://doi.org/10.1016/j.ijhydene.2015.12.025

Durbin, D. J., & Malardier-Jugroot, C. (2013). Review of hydrogen storage techniques for on board vehicle applications. *International Journal of Hydrogen Energy*, 38(34), 14595–14617. Retrieved from https://doi.org/10.1016/j.ijhydene.2013.07.058

Dutta, S. (2014). A review on production, storage of hydrogen and its utilization as an energy resource. *Journal of Industrial and Engineering Chemistry*, 20(4), 1148–1156. Retrieved from https://doi.org/10.1016/j.jiec.2013.07.037

Elliott, M. A., & Davis, R. F. (1951). Dual-Fuel Combustion in Diesel Engines. *Industrial & Engineering Chemistry*, 43(12), 2854–2864. Retrieved from https://doi.org/10.1021/ie50504a056

Erdener, B. C., Sergi, B., Guerra, O. J., Lazaro Chueca, A., Pambour, K., Brancucci, C., & Hodge, B.-M. (2023). A review of technical and regulatory limits for hydrogen blending in natural gas pipelines. *International Journal of Hydrogen Energy*, 48(14), 5595–5617. Retrieved from https://doi.org/10.1016/j.ijhydene.2022.10.254

Faghri, A., & Guo, Z. (2005). Challenges and opportunities of thermal management issues related to fuel cell technology and modeling. *International Journal of Heat and Mass Transfer*, 48(19–20), 3891–3920. Retrieved from https://doi.org/10.1016/j.ijheatmasstransfer.2005.04.014

Fayaz, H., Saidur, R., Razali, N., Anuar, F. S., Saleman, A. R., & Islam, M. R. (2012). An overview of hydrogen as a vehicle fuel. *Renewable and Sustainable Energy Reviews*, 16(8), 5511–5528. Retrieved from https://doi.org/10.1016/j.rser.2012.06.012

Fernández, R. Á., Cilleruelo, F. B., & Martínez, I. V. (2016). A new approach to battery powered electric vehicles: A hydrogen fuel-cell-based range extender system. *International Journal of Hydrogen Energy*, 41(8), 4808–4819. Retrieved from https://doi.org/10.1016/j.ijhydene.2016.01.035

García, P., Torreglosa, J. P., Fernández, L. M., & Jurado, F. (2013). Control strategies for high-power electric vehicles powered by hydrogen fuel cell, battery and supercapacitor. *Expert Systems with Applications*, 40(12), 4791–4804. Retrieved from https://doi.org/10.1016/j.eswa.2013.02.028

Gondal, I. A. (2019). Hydrogen integration in power-to-gas networks. *International Journal of Hydrogen Energy*, 44(3), 1803–1815. Retrieved from https://doi.org/10.1016/j.ijhydene.2018.11.164

Hosseini, S. E., & Wahid, M. A. (2016). Hydrogen production from renewable and sustainable energy resources: Promising green energy carrier for clean development. *Renewable and Sustainable Energy Reviews*, 57, 850–866. Retrieved from https://doi.org/10.1016/j.rser.2015.12.112

Jabbr, A. I., Vaz, W. S., Khairallah, H. A., & Koylu, U. O. (2016). Multi-objective optimization of operating parameters for hydrogen-fueled spark-ignition engines. *International Journal of Hydrogen Energy*, 41(40), 18291–18299. Retrieved from https://doi.org/10.1016/j.ijhydene.2016.08.016

Jain, I. P. (2009). Hydrogen the fuel for 21st century. *International Journal of Hydrogen Energy*, 34(17), 7368–7378. Retrieved from https://doi.org/10.1016/j.ijhydene.2009.05.093

Ji, C., & Wang, S. (2009). Experimental Study on Combustion and Emissions Characteristics of a Spark Ignition Engine Fueled with Gasoline–

Hydrogen Blends. *Energy & Fuels*, 23(6), 2930–2936. Retrieved from https://doi.org/10.1021/ef900209m

JUSTE, G. (2006). Hydrogen injection as additional fuel in gas turbine combustor. Evaluation of effects. *International Journal of Hydrogen Energy*, 31(14), 2112–2121. Retrieved from https://doi.org/10.1016/j.ijhydene.2006.02.006

Karagöz, Y., Sandalcı, T., Yüksek, L., & Dalkılıç, A. S. (2015). Engine performance and emission effects of diesel burns enriched by hydrogen on different engine loads. *International Journal of Hydrogen Energy*, 40(20), 6702–6713. Retrieved from https://doi.org/10.1016/j.ijhydene.2015.03.141

Katikaneni, S. P., Al-Muhaish, F., Harale, A., & Pham, T. V. (2014). On-site hydrogen production from transportation fuels: An overview and techno-economic assessment. *International Journal of Hydrogen Energy*, 39(9), 4331–4350. Retrieved from https://doi.org/10.1016/j.ijhydene.2013.12.172

Kumar, L., & Jain, S. (2014). Electric propulsion system for electric vehicular technology: A review. *Renewable and Sustainable Energy Reviews*, 29, 924–940. Retrieved from https://doi.org/10.1016/j.rser.2013.09.014

Lata, D. B., Misra, A., & Medhekar, S. (2012). Effect of hydrogen and LPG addition on the efficiency and emissions of a dual fuel diesel engine. *International Journal of Hydrogen Energy*, 37(7), 6084–6096. Retrieved from https://doi.org/10.1016/j.ijhydene.2012.01.014

Likkasit, C., Maroufmashat, A., Elkamel, A., Ku, H., & Fowler, M. (2018). Solar-aided hydrogen production methods for the integration of renewable energies into oil & gas industries. *Energy Conversion and Management*, 168, 395–406. Retrieved from https://doi.org/10.1016/j.enconman.2018.04.057

Liu, Wei, & Christopher, D. M. (2015). Dispersion of hydrogen leaking from a hydrogen fuel cell vehicle. *International Journal of Hydrogen Energy*, 40(46), 16673–16682. Retrieved from https://doi.org/10.1016/j.ijhydene.2015.10.026

Liu, Wenguo, Zuo, H., Wang, J., Xue, Q., Ren, B., & Yang, F. (2021). The production and application of hydrogen in steel industry. *International Journal of Hydrogen Energy*, 46(17), 10548–10569. Retrieved from https://doi.org/10.1016/j.ijhydene.2020.12.123

Maggio, G., Nicita, A., & Squadrito, G. (2019). How the hydrogen production from RES could change energy and fuel markets: A review of recent literature. *International Journal of Hydrogen Energy*, 44(23), 11371–11384. Retrieved from https://doi.org/10.1016/j.ijhydene.2019.03.121

Maslennikov, V. M., & Shterenberg, V. J. (2011). Advanced gas turbine system utilizing partial oxidation technology for ecologically clean power

generation. *International Journal of Low-Carbon Technologies*, 6(1), 55–63. Retrieved from https://doi.org/10.1093/ijlct/ctq043

Mayer, H. (1999). Air pollution in cities. *Atmospheric Environment*, 33(24–25), 4029–4037. Retrieved from https://doi.org/10.1016/S1352-2310(99)00144-2

Midilli, A., & Dincer, I. (2007). Key strategies of hydrogen energy systems for sustainability. *International Journal of Hydrogen Energy*, 32(5), 511–524. Retrieved from https://doi.org/10.1016/j.ijhydene.2006.06.050

Modern Electric, Hybrid Electric, and Fuel Cell Vehicles, Third Edition. (2018). CRC Press. Retrieved from https://doi.org/10.1201/9780429504884

Mourad, M. (2014). A proposed fuel cell vehicle for reducing CO2 emissions and its contribution to reducing greenhouse gas emissions. *International Journal of Engineering & Technology*, 3(2), 252. Retrieved from https://doi.org/10.14419/ijet.v3i2.2349

Neuwirth, M., Fleiter, T., Manz, P., & Hofmann, R. (2022). The future potential hydrogen demand in energy-intensive industries - a site-specific approach applied to Germany. *Energy Conversion and Management*, 252, 115052. Retrieved from https://doi.org/10.1016/j.enconman.2021.115052

Nicoletti, G., Arcuri, N., Nicoletti, G., & Bruno, R. (2015). A technical and environmental comparison between hydrogen and some fossil fuels. *Energy Conversion and Management*, 89, 205–213. Retrieved from https://doi.org/10.1016/j.enconman.2014.09.057

Panchenko, V. A., Daus, Y. V., Kovalev, A. A., Yudaev, I. V., & Litti, Y. V. (2023). Prospects for the production of green hydrogen: Review of countries with high potential. *International Journal of Hydrogen Energy*, 48(12), 4551–4571. Retrieved from https://doi.org/10.1016/j.ijhydene.2022.10.084

Pareek, A., Dom, R., Gupta, J., Chandran, J., Adepu, V., & Borse, P. H. (2020). Insights into renewable hydrogen energy: Recent advances and prospects. *Materials Science for Energy Technologies*, 3, 319–327. Retrieved from https://doi.org/10.1016/j.mset.2019.12.002

Pollet, B. G., Staffell, I., & Shang, J. L. (2012). Current status of hybrid, battery and fuel cell electric vehicles: From electrochemistry to market prospects. *Electrochimica Acta*, 84, 235–249. Retrieved from https://doi.org/10.1016/j.electacta.2012.03.172

Posdziech, O., Schwarze, K., & Brabandt, J. (2019). Efficient hydrogen production for industry and electricity storage via high-temperature electrolysis. *International Journal of Hydrogen Energy*, 44(35), 19089–19101. Retrieved from https://doi.org/10.1016/j.ijhydene.2018.05.169

Power, W. M. (2019). Green hydrogen production: Landscape, projects and costs.

Rana, S., Rana, R., Thapliyal, D., Verma, S., Mehra, A., Kumar Bhargava, C., … Arya, R. K. (2024). Chapter 20 Green hydrogen: challenges and future prospects. In *Sustainable Hydrogen Energy* (pp. 449–486). De Gruyter. Retrieved from https://doi.org/10.1515/9783111246475-020

Roes, A. L., & Patel, M. K. (2011). Ex-ante environmental assessments of novel technologies – Improved caprolactam catalysis and hydrogen storage. *Journal of Cleaner Production*, 19(14), 1659–1667. Retrieved from https://doi.org/10.1016/j.jclepro.2011.05.010

Salvi, B. L., & Subramanian, K. A. (2015). Sustainable development of road transportation sector using hydrogen energy system. *Renewable and Sustainable Energy Reviews*, 51, 1132–1155. Retrieved from https://doi.org/10.1016/j.rser.2015.07.030

Sazali, N. (2020). Emerging technologies by hydrogen: A review. *International Journal of Hydrogen Energy*, 45(38), 18753–18771. Retrieved from https://doi.org/10.1016/j.ijhydene.2020.05.021

Selvam, P. (1988). Studies on the thermal characteristics of hydrides of. *International Journal of Hydrogen Energy*, 13(2), 87–94. Retrieved from https://doi.org/10.1016/0360-3199(88)90045-6

Sgobbi, A., Nijs, W., De Miglio, R., Chiodi, A., Gargiulo, M., & Thiel, C. (2016). How far away is hydrogen? Its role in the medium and long-term decarbonisation of the European energy system. *International Journal of Hydrogen Energy*, 41(1), 19–35. Retrieved from https://doi.org/10.1016/j.ijhydene.2015.09.004

Shinagawa, T., Okumura, T., Furuno, S., & Kim, K.-O. (2004). Effects of Hydrogen Addition to SI Engine on Knock Behavior. Retrieved from https://doi.org/10.4271/2004-01-1851

Sinigaglia, T., Lewiski, F., Santos Martins, M. E., & Mairesse Siluk, J. C. (2017). Production, storage, fuel stations of hydrogen and its utilization in automotive applications-a review. *International Journal of Hydrogen Energy*, 42(39), 24597–24611. Retrieved from https://doi.org/10.1016/j.ijhydene.2017.08.063

Sulaiman, N., Hannan, M. A., Mohamed, A., Majlan, E. H., & Wan Daud, W. R. (2015). A review on energy management system for fuel cell hybrid electric vehicle: Issues and challenges. *Renewable and Sustainable Energy Reviews*, 52, 802–814. Retrieved from https://doi.org/10.1016/j.rser.2015.07.132

Sun, D., & Liu, F. (2010). Research on the Performance and Emission of a Port Fuel Injection Hydrogen Internal Combustion Engine. In *2010 International Conference on Digital Manufacturing & Automation* (pp. 299–302). IEEE. Retrieved from https://doi.org/10.1109/ICDMA.2010.439

Tebibel, H., & Labed, S. (2014). Design and sizing of stand-alone photovoltaic hydrogen system for HCNG production. *International Journal of Hydrogen Energy*, 39(8), 3625–3636. Retrieved from https://doi.org/10.1016/j.ijhydene.2013.12.124

Tong, L., Xiao, J., Cai, Y., Bénard, P., & Chahine, R. (2016). Thermal effect and flow-through cooling of an adsorptive hydrogen delivery tank. *International Journal of Hydrogen Energy*, 41(36), 16094–16100. Retrieved from https://doi.org/10.1016/j.ijhydene.2016.04.242

Uludamar, E., Yıldızhan, Ş., Aydın, K., & Özcanlı, M. (2016). Vibration, noise and exhaust emissions analyses of an unmodified compression ignition engine fuelled with low sulphur diesel and biodiesel blends with hydrogen addition. *International Journal of Hydrogen Energy*, 41(26), 11481–11490. Retrieved from https://doi.org/10.1016/j.ijhydene.2016.03.179

van Hulst, N. (2024). The clean hydrogen future has already begun. *IEA: International Energy Agency*. Retrieved from https://coilink.org/%0A20.500.12592/q5p1nj

Varol, Y., Coşanay, H., Tamdoğan, E., Parlak, M., Şenocak, Ş. M., & Oztop, H. F. (2025). Vapor chamber thermal performance: Partially heated with different heating areas at the center and supported by numerical analysis for the experimental setup. *Applied Thermal Engineering*, 260, 124978. Retrieved from https://doi.org/10.1016/j.applthermaleng.2024.124978

Varol, Y., Oztop, H. F., Tamdoğan, E., Parlak, M., Şenocak, Ş. M., & Coşanay, H. (2025). Thermal Performance Investigation of Vapor Chamber Under Partial Heating and Different Heat Flux Conditions: Effects of Inclination Angle. *ASME Journal of Heat and Mass Transfer*, 147(1). Retrieved from https://doi.org/10.1115/1.4066664

Verhelst, S. (2014). Recent progress in the use of hydrogen as a fuel for internal combustion engines. *International Journal of Hydrogen Energy*, 39(2), 1071–1085. Retrieved from https://doi.org/10.1016/j.ijhydene.2013.10.102

Verhelst, Sebastian, & Wallner, T. (2009). Hydrogen-fueled internal combustion engines. *Progress in Energy and Combustion Science*, 35(6), 490–527. Retrieved from https://doi.org/10.1016/j.pecs.2009.08.001

von Helmolt, R., & Eberle, U. (2007). Fuel cell vehicles: Status 2007. *Journal of Power Sources*, 165(2), 833–843. Retrieved from https://doi.org/10.1016/j.jpowsour.2006.12.073

Walker, S. B., Fowler, M., & Ahmadi, L. (2015). Comparative life cycle assessment of power-to-gas generation of hydrogen with a dynamic emissions factor for fuel cell vehicles. *Journal of Energy Storage*, 4, 62–73. Retrieved from https://doi.org/10.1016/j.est.2015.09.006

WHITE, C., STEEPER, R., & LUTZ, A. (2006). The hydrogen-fueled internal combustion engine: a technical review. *International Journal of Hydrogen Energy*, 31(10), 1292–1305. Retrieved from https://doi.org/10.1016/j.ijhydene.2005.12.001

Wu, W., Wang, S., Wu, W., Chen, K., Hong, S., & Lai, Y. (2019). A critical review of battery thermal performance and liquid based battery thermal management. *Energy Conversion and Management*, 182, 262–281. Retrieved from https://doi.org/10.1016/j.enconman.2018.12.051

Yadav, M., & Xu, Q. (2012). Liquid-phase chemical hydrogen storage materials. *Energy & Environmental Science*, 5(12), 9698. Retrieved from https://doi.org/10.1039/c2ee22937d

Yamane, K., Nogami, M., Umemura, Y., Oikawa, M., Sato, Y., & Goto, Y. (2011). Development of High Pressure H2 Gas Injectors, Capable of Injection at Large Injection Rate and High Response Using a Common-rail Type Actuating System for a 4-cylinder, 4.7-liter Total Displacement, Spark Ignition Hydrogen Engine. Retrieved from https://doi.org/10.4271/2011-01-2005

Yartys, V. A., Lototskyy, M. V., Linkov, V., Pasupathi, S., Davids, M. W., Tolj, I., … Suwarno, S. (2021). HYDRIDE4MOBILITY: An EU HORIZON 2020 project on hydrogen powered fuel cell utility vehicles using metal hydrides in hydrogen storage and refuelling systems. *International Journal of Hydrogen Energy*, 46(72), 35896–35909. Retrieved from https://doi.org/10.1016/j.ijhydene.2021.01.190

Yılmaz, F., & Balta, M. T. (2017). Energy and exergy analyses of hydrogen production step in boron based thermochemical cycle for hydrogen production. *International Journal of Hydrogen Energy*, 42(4), 2485–2491. Retrieved from https://doi.org/10.1016/j.ijhydene.2016.04.017

Zacharia, R., & Rather, S. ullah. (2015). Review of Solid State Hydrogen Storage Methods Adopting Different Kinds of Novel Materials. *Journal of Nanomaterials*, 2015(1). Retrieved from https://doi.org/10.1155/2015/914845

Chapter 5

ULTRASOUND APPLICATIONS IN FOOD SCIENCE AND TECHNOLOGY

Şükrü KURT[1]

Fatma ZENGİN[2]

1 Prof. Dr., ORCID ID: 0000-0002-8695-0810, Faculty of Engineering, Department of Food Engineering, Adıyaman University, Adıyaman, Turkey
2 MSc., ORCID ID: 0009-0006-0722-6645, Faculty of Engineering, Department of Food Engineering, Adana Alparslan Türkeş Bilim ve Teknoloji University, Adana, Turkey

1. Introduction

There are many food products that carry microbiological risks and are not desired to be processed with heat due to their structural-sensory properties. Such thermally sensitive food products may undergo physical, chemical and microbial changes such as aroma, taste, colour and texture changes when subjected to heat treatment. This situation has generated the need for research and development to improve existing technologies and to emerge innovative, effective alternative technologies.

In the food industry, some heat treatment processes are used to extend the shelf life of products and inactivate unwanted microorganisms and enzymes (Güleç, 2006). However, while high heat treatment application positively affects microorganism and enzyme inactivation, it leads to significant losses in the nutritional value of food (Turantas, 2016). Therefore, with the developing and renewed technology, there is an increasing interest and consumer demand for minimum process application, which causes less damage to nutrients and provides longer shelf life. Production with minimum processing but low cost, fast, simple, natural, non-toxic, environmentally friendly, energy-saving and high nutritional value is gaining importance (Şimşekli, 2010; Akdeniz and Akalın, 2017). For this purpose, studies are being conducted on alternative production technologies. Among many alternative technologies, ultrasound technology attracts attention due to its wide area of use and more effective results when combined with other applications (Türken, 2014).

Ultrasound has a significant impact on the rate of various food processes. Food processing with ultrasound can be carried out within seconds or minutes with high reproducibility, reducing the processing costs, simplifying work and providing higher efficiency. In addition, it provides high purity of the final product, eliminates post-treatment to wastewater and saves time and energy needed for traditional processes.

The many features of ultrasound devices, such as low cost, simplicity and portability, make them indispensable elements in research laboratories and food factories. On the other hand, high power (low frequency) ultrasound causes mechanical, physical and chemical/ biochemical changes through cavitation. Thus, it reduces the reaction time by changing the food properties and increases the reaction yield under mild conditions compared to conventional routes (Awad et al., 2012).

In recent years, ultrasonic sound wave applications have become widespread in order to meet market demand and obtain quality products (Ünal, 2012). Studies on the application of this method in food systems are increasing day by day because it is economical, environmentally friendly and can provide energy savings.

2. Ultrasound Technology

The subject of ultrasound technology was first dealt with by Francis Galton, a biologist of the Victorian era. Ultrasound applications were first used in the industry for cleaning purposes in the 1960s. The use of ultrasonic techniques in food systems dates back approximately 60 years (Tuna, 2013). Sound waves are grouped according to their frequency ranges. Figure 1 shows the naming of sound waves according to their frequency ranges. The human ear can perceive the sound range of 20 Hz to 20 kHz. Ultrasound sound waves are sound waves that can pass through solids, liquids and gases, but are not perceived by the human ear (>20 kHz). These waves spread at different vibrations and speeds depending on the environmental conditions (solid, liquid and gas) they are in (Özyurt, 2013). Ultrasound between 20 kHz and 1 MHz is used in the food industry. Frequencies above 1 MHz are used for imaging purposes in medicine (Yılmaz, 2011; Sayın and Tamer, 2014; İşçimen, 2016).

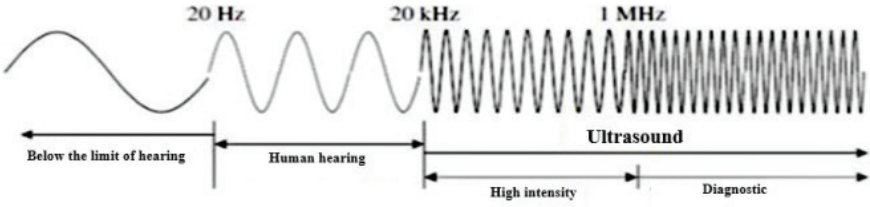

Figure 1. *Naming of sound waves according to frequency range (Yılmaz, 2014a)*

3. Ultrasound Technology Application Methods

Ultrasound applications are classified into two types according to the wavelength used in food processing systems: low intensity and high intensity (Akdeniz and Akalın, 2017). Low intensity ultrasound applications are low intensity (≤ 1 W/ cm2) and high frequency (100 kHz–20 MHz) applications and are generally used in the evaluation of food systems and food quality control for the purpose of observing food products and processes (Yüksel, 2013; Yüksel and Elgün, 2013; Akdeniz and Akalın, 2017). In food applications, high frequencies between 0.1-20 MHz and low energy levels of 100 mW are used (Kırmusaoğlu, 2013; Yüksel, 2013). Figure 2 shows a high frequency low energy ultrasound device diagram. The device consists of signal generator-receiver, amplifier, 2 converters and oscilloscope sections. High-intensity ultrasound applications are relatively low-frequency (20 kHz–100 kHz) and high-intensity applications between 10 and 1000 W/cm2 and cause physical, chemical and mechanical changes in the structure of food (Kırmusaoğlu, 2013; Yüksel, 2013; Yüksel

and Elgün, 2013; Akdeniz and Akalın, 2017). Therefore, this ultrasound method is widely used in inanimate materials and especially in the product processing sector. (Yüksel, 2013; Yüksel and Elgün, 2013). Low-frequency high-energy ultrasound device and its sections are given in Figure 3.

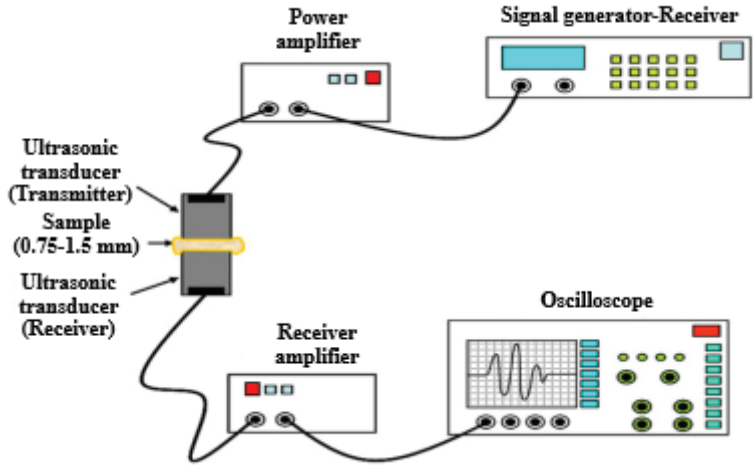

Figure 2. *Diagram of a high frequency low energy ultrasound device (Yüksel, 2013)*

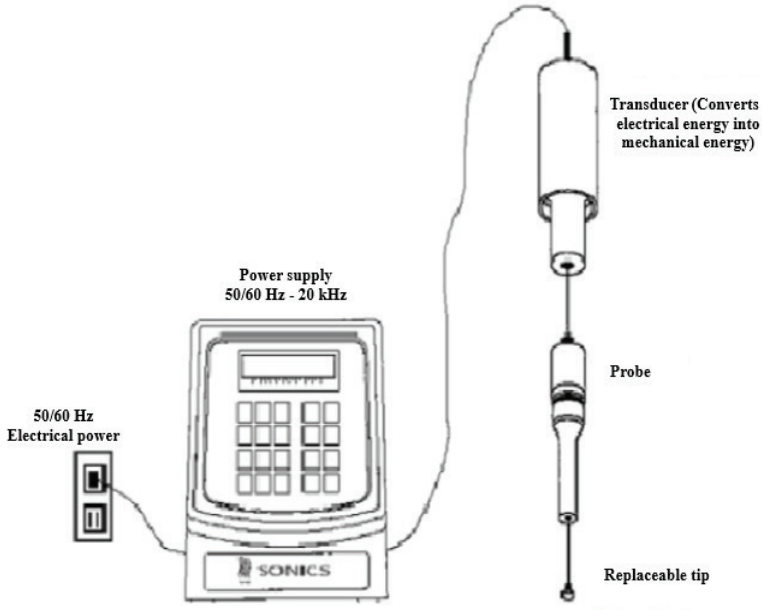

Figure 3. *Probe type low frequency high energy ultrasound device (Yüksel, 2013)*

4. Mechanism of Ultrasound Effect

The basic phenomenon that causes chemical and mechanical effects in ultrasound applications is cavitation (Muhammed Yılmaz, 2014; Akdeniz and Akalın, 2017). The formation of cavitation depends on the ultrasound power (Yılmaz, 2014b). Ultrasound causes a series of compression and expansion waves on the molecules of the medium through which sound waves pass. This phenomenon is called the "sponge effect" because it creates an effect like constantly squeezing and releasing a sponge. This pressure created by the waves creates micro channels, facilitating the release of water inside the cell into the medium (Yılmaz, 2014a).

When ultrasonic sound waves pass through a liquid, they create small bubbles in the liquid (Ercan, 2009; Şengül et al., 2009; Yılmaz, 2014a; Bal, 2016). When these bubbles reach a point where they can no longer absorb energy, they burst. This event is called cavitation (Sayın and Tamer, 2014; Tao and Sun, 2014; Bal, 2016). A large amount of energy is released with the bursting of the bubbles, and as a result, sudden heat and pressure changes occur (Kentish and Feng, 2014; Yılmaz, 2014b; Sayın and Tamer, 2014; Yılmaz, 2015; Bal, 2016). The high temperature and pressure intensity that occurs causes various mechanical and chemical changes in the product (İşçimen, 2016). At the same time, microorganism and enzyme inactivation, cleaning of product surfaces, extraction, filtration, emulsification and crystallization are all based on the cavitation mechanism (Feng et al., 2011; Bal, 2016). The cavitation event and cavitation mechanism are as in Figure 4 and Figure 5.

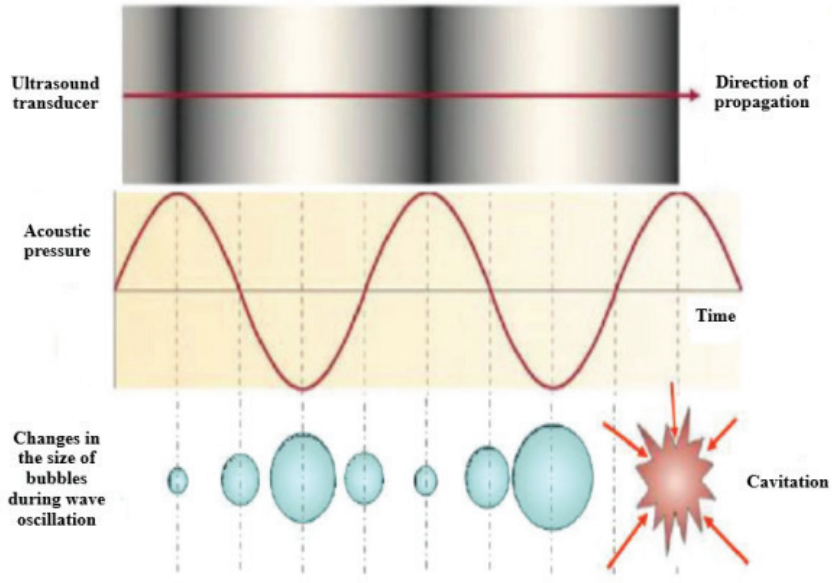

Figure 4. *Cavitation Phenomenon (Er, 2014)*

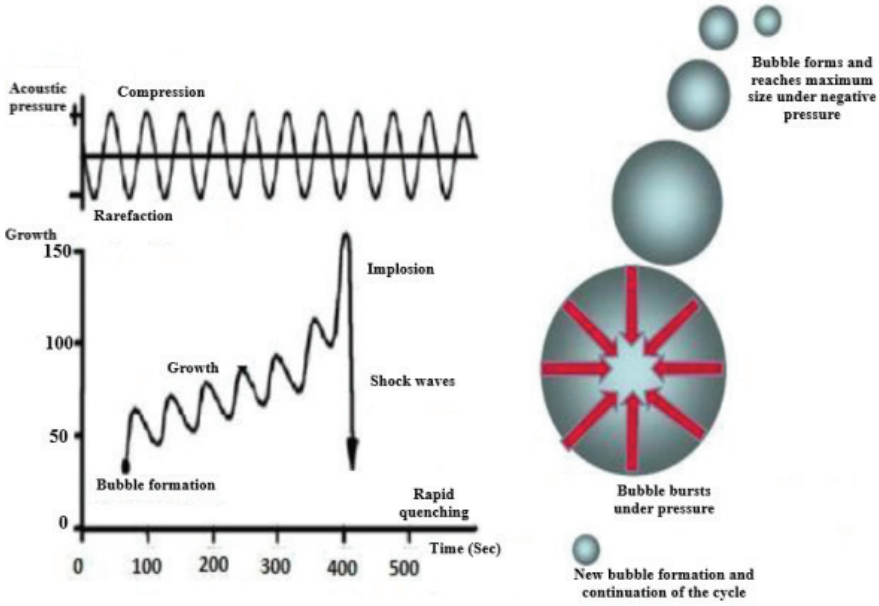

Figure 5. *Cavitation Mechanism (Yılmaz, 2014b)*

5. Potential Applications of Ultrasound In Food Systems

5.1. Ultrasound Applications in Meat Technology

Ultrasound has been used in meat technology since the early 1950s to determine fat and muscle content in live cattle (Dolatowski et al., 2007). In recent years, ultrasound applications have been routinely used in the meat industry (Majid et al., 2015). The most important of these applications are; estimating the quality, flavour and cutting ability of carcasses, grading carcasses, tenderizing meat products, and determining the component properties of meat (Dolatowski et al., 2007; Çilek and Dirican, 2008; Söbeli and Kayaardı, 2014; Majid et al., 2015; Carrillo-Lopez et al., 2017).

One of the most important characteristics affecting consumer satisfaction and the quality of beef is tenderness. Beef tenderness is considered one of the main problems faced by the meat industry. Despite the long-term research interest in obtaining meat with eating quality, it still remains an elusive goal. Tenderness is affected by composition, structural organization and skeletal muscle integrity (Dolatowski et al., 2007). The increasing change in muscle structure during the aging process is closely related to meat tenderness (Carrillo-Lopez et al., 2017). Acoustic cavitation causes disruption of the structure of myofibrillar proteins and collagen macromolecules, and as a result accelerates proteolysis (Chang et al., 2015). It is also possible that ultrasound application affects the amount of ATP

in the muscles in the prerigor phase and increases the aging rate of meat by accelerating the entry into rigor mortis (Carrillo-Lopez et al., 2017). Various experiments have been conducted with ultrasound application to reduce aging time and increase the tenderness of meat without adversely affecting other properties of meat (Dolatowski et al., 2007; Çilek and Dirican, 2008; Carrillo-Lopez et al., 2017; Söbeli and Kayaardı, 2014).

The cavitation, thermal, and mechanical effects of ultrasound are effective on tenderizing of meat products. These effects of ultrasound can change the pressure and temperature of the medium and thereby disrupt intermolecular interactions and destroy the structure of muscle tissue. This change in the muscle can enhance the transfer rate and penetration ability of the medium, thus increasing the tenderness of meat products (Contreras-Lopez et al., 2020). The ultrasound effect can contribute to the increase in meat tenderness by stimulating enzymes and disrupting the muscle fibre structure (Ojha et al., 2018). The mechanical effect of ultrasound destroys the Z-lines in the myofibrillar structure of meat, expanding the space between myofibrils and increasing the water content, causing the muscles to swell, thus improving the tenderness of the meat (Zou et al., 2017). Ultrasound is applied to meat for different purposes other than tenderness, for example, it increases the moisture retention capacity of meat, cooking time and energy efficiency. Therefore, this method can be fast and more energy efficient to improve the quality of cooked meat (Carrillo-Lopez et al., 2017; Zambak and Özkal, 2017). The application of ultrasound in meat curing technology is recommended as an alternative to the traditional application method; its purpose is to accelerate the transfer of salt water, preserve sensory qualities, achieve better distribution and minimize water loss (Sirò et al., 2009; McDonnell et al., 2014; Turantas, 2017). Numerous studies have been conducted to improve the sensory and technological properties of meat and to obtain higher quality meat. However, the results of these studies are not comparable due to the type of muscles used, age of the animal, ultrasonic equipment and efficiency, ultrasound application times and wavelengths. Studies have shown the potential benefits of ultrasound as an alternative technology to change the properties of meat and meat products (Dolatowski et al., 2007; Carrillo-Lopez et al., 2017).

Ultrasound pasteurization of meat products such as sausages provides a homogeneous temperature within the sausages. Compared to the traditional process, it has been shown to extend the shelf life of sausages (up to 20 days or 50% more). In addition to the advantages of ultrasound treatment, such as reducing the time, intensity of heat treatment and energy consumption, no damage was observed in the product, showing the potentiality of ultrasound in post-packaging pasteurization (Cichoski et al., 2015).

Ultrasound affects proteolysis and lipid oxidation in meat products, and promotes the formation of volatile compounds. For example, 3-minute ultrasound treatment (25 kHz, 128 W) results in an increase in threonine, methionine and phenylalanine levels, while 6-minute ultrasound treatment increases glutamic acid and arginine levels during storage. Other compounds associated with lipid oxidation during storage include hexanal, pentanal and hexanol levels were also observed (Alves et al. 2020).

5.2. Ultrasound Applications in Dairy Technology

Due to the consumer demand for healthy, delicious, and minimally processed dairy products, studies on alternative technologies in the development of innovative dairy products are becoming more and more important every day.

The search for such alternative technologies has focused on non-thermal technologies to avoid damaging the flavour or nutritional content of foods during production. One of these is the application of High Intensity Ultrasound (HIU), which is specifically designed for simplicity, economy and energy efficiency.

Ultrasonic applications are among the promising sectors that can provide major improvements in the dairy industry as well as in other food sectors (Carrillo-Lopez et al., 2017). In the dairy industry, ultrasound is used for purposes such as fat removal, whey filtration, cutting of cheese blocks, lactose crystallization, changing the functionality of milk proteins, preventing flavor loss, increasing homogeneity, pasteurization and sterilization (Majid et al., 2015; Özaslan, 2016).

HIU has a positive effect on milk components and curd matrix, especially fat globules in milk. Changes in the physical properties of milk components provide improvement in the physical properties of milk, such as acceleration of gel formation, increase in gel strength and hardness, increase in specific surface area, decrease in curd hardness and particle distribution of fat (Abesinghe et al., 2020; Gregersen et al., 2019; Jo et al., 2019).

The power of ultrasonication reduces the size of fat particles, which is important in pretreatments such as emulsification. The acoustic vibration, together with the size reduction, causes the fat particles to disperse better in the milk by the effect of turbulence. Then, cavitation acts on the breakup of the fat droplets (Leong et al., 2016).

In addition to the power of ultrasonication, its duration is also an important factor for dairy products. It has been reported that times longer than 15 min may increase the release of sulfhydryl groups in whey protein beverages or emulsions, resulting in an increase in free thiols and the

formation of protein crosslinking (Carrillo -Lopez et al., 2021).

Heat treatment is one of the preservation techniques commonly used in the dairy industry to prevent or limit unwanted microorganism and enzyme activity and to extend the shelf life of the product. However, the high temperature applied during heat treatment causes undesirable colour, aroma and nutritional value changes in foods. For this reason, interest in non-thermal preservation methods such as ultrasound and high pressure technology has been increasing recently as an alternative to heat treatment processes (Akdeniz and Akalın, 2017; Şengül et al., 2009).

Ultrasonication alone may not be sufficient for decontamination of milk, so ultrasound must be used in combination with heat to control bacteria. It is more appropriate to use ultrasound together with heat, especially in controlling pathogenic and spoilage microorganisms (Carrillo -Lopez et al., 2021).

Ultrasound is considered as an alternative method to reduce the size of fat globules and is stated to be effectively applied to homogenize milk (Carrillo-Lopez et al., 2017). Homogenization of milk (dispersion of large fat globules) depends on selectivity by cavitation effect. Fat globules of different sizes are broken down by physical forces (turbulence, mixing and shear force) formed during cavitation. Larger fat globules are more affected by the physical forces of ultrasound. As a result of the studies, it was determined that the diameter of fat globules decreased significantly and homogenization efficiency increased depending on the increase in ultrasound exposure times and applied power levels (Ertugay et al., 2004; Şengül et al., 2009; Bosiljkov et al., 2012; Shestakov et al., 2013; Akdeniz and Akalın, 2017). In addition, it was observed that ultrasound increased the viscosity and water retention capacity in fermented milk products (Wu et al., 2000; Sfakianakis et al., 2015).

In addition to its advantages, there are also few disadvantages of applying HIU to milk. For example, it can cause colour differences and slight protein oxidation, and less off-flavours (Carrillo -Lopez et al., 2021). According to Carrillo-Lopez et al. (2021), 20 kHz may be the optimum frequency to be applied in improving the properties of milk and dairy products.

5.3. Ultrasound Applications in Fruit and Vegetable Technology

Increasing consumption of fruits and vegetables worldwide along with the population growth has increased the need to better control the sensory, nutritional and microbiological properties of these foods.

The data obtained by applying ultrasound to fruits and vegetables are somewhat complex and difficult to interpret. Because the voids and

pores found in these products cause the ultrasound to scatter and thus reduce its effect (Mizrach, 2008). The firmness and colour of fresh fruits and vegetables are also affected by ultrasound. The changes in colour are attributed to the effect of ultrasound on phenol oxidase and polyphenol enzymes. Ultrasound has the ability to inhibit browning enzymes by disrupting cellular components. However, sonication also provides an antimicrobial effect, which may result from cavitation and free radical formation (Nicolau-Lapeña et al., 2019).

Ultrasound is used to maintain quality characteristics in fresh fruits and vegetables both before and after harvest (Bozkurt and İçier, 2009; Bal, 2016) (Türken, 2014; Majid et al., 2015; Carrillo-Lopez et al., 2017). In addition, ultrasound is also used for decontamination purposes in the fruit and vegetable industry. Although the most research on the use of ultrasound for this purpose is on lettuce, there are also studies on spinach, chopped carrots, plums, peaches, strawberries, cherries, apples and mushrooms (Turantas, 2016). Ultrasound can be suitable for cleaning fruit and vegetable surfaces when applied together with different methods. Generally, chemical methods, high temperature, high pressure, pulsed electric field and ultraviolet radiation can be applied together with ultrasound for cleaning and disinfection. However, this is not recommended since heat and pressure can damage the fruits and vegetables tissues. For this reason, ultrasound is applied in combination with chemicals such as organic acids, commercial sanitizers and other antimicrobials in fruits and vegetables (Carrillo-Lopez et al., 2017). In addition, ultrasound has the ability to remove pesticide residues from fruits and vegetables, which increases the importance of the technique. Ultrasonic cleaning process significantly reduced fluopyram residues in apples (Słowik-Borowiec and Szpyrka, 2020).

Ultrasound can also be used in extraction processes, improving existing extraction processes and providing new commercial extraction opportunities and processes. It facilitates the isolation of antioxidants, fragrances, carotenoids, phenols, anthocyanins, and natural colours from seeds, fruits, and vegetables (Safwa et al., 2024).

Sonication improves the properties of the product when used in fruit juice production. For example, it has a positive effect on antioxidant capacity, flavonoids, flavanols, total phenolics and ascorbic acid in grapefruit juice (Safwa et al., 2024).

Ultrasound application is also used to inactivate phenolase group enzymes that are found in fruit juices and cause enzymatic browning. This application does not cause a significant change in the nutritional and colour values of the product (Yılmaz, 2014b). However, application of ultrasound

in beverages has improved the healthiness of the product by increasing the levels of antioxidants and bioactive compounds (Jiang et. al., 2015).

Application of ultrasound to fruits and vegetables, especially when combined with an osmotic solution, improves drying kinetics by reducing initial moisture content and modifying tissue structure. The effectiveness of the pre-treatment depends on some factors such as the structure of the sample, the ultrasonic source, the immersion medium, and the acoustic energy parameters (Safwa et al., 2024)

Overall, ultrasound improves fruit and vegetable quality by improving enzyme activity, microbial contamination, and drying properties.

5.4. Ultrasound Applications in Oil Technology

Today, one of the methods used for obtaining oil from seeds is pressurization or solvent extraction or a combination of these two methods, pre-pressure-extraction. Recently, ultrasound-assisted extraction method has been used as an alternative to these methods for obtaining oil from seeds. With ultrasound-assisted extraction, oil can be obtained in a shorter time, with low energy consumption and high yield compared to other methods (Tontul et al., 2018; Acar, 2017; Şimşekli, 2010; Yaman and Kuleaşan, 2016; Li et al., 2013; Teng et al., 2016; Subba Rao et al., 2018; Fuad et al., 2016; İnce, 2011).

Ultrasound can be used as an alternative or in combination with other methods in food processing (Ercan and Soysal, 2013; Yılmaz, 2015). Table 1 summarizes the current applications of ultrasound, its mechanism of action, its advantages and the foods it is applied to.

Table 1. *Current applications of ultrasound, its mechanism of action, advantages and applied foods (Ercan, 2009; Tavman et al., 2009; Adekunte et al., 2010; Mason et al., 2010; Chemat et al., 2011; Çağdaş et al., 2011; Türken, 2014; Yılmaz, 2014b; Kenan Özdoğan, 2015)*

Application	Conventional methods	Advantages	Products
Cooking	Uniform heat transfer	- Less time, - Increasing heat transfer and organoleptic quality, - Increased retention of moisture	Meat products, Fruits and Vegetables

Freezing/ Crystallization	Uniform heat transfer	- Time saving, - Smaller ice crystal formation, - Improved diffusion, - Rapid temperature reduction, - Efficient heat transfer, - Reduced cell damage	Meat products, Fruits and Vegetables, Dairy products, Milk fat, Vegetable oil, Ice cream
Drying	Uniform heat transfer	- Time saving - Increasing organoleptic quality - Improving heat transfer	Fruits and Vegetables
Pickling/Marinating	Increasing mass transfer	- Time saving, - Increasing organoleptic quality, - Product stability, - Reducing product losses, - More crispy product	Vegetables, Meat products, Fish, Cheese
Defoaming/Degassing	Pressure reduction phenomenon, Cavitation phenomenon	- Time saving, - Microbial risk reduction, - Prevention of organoleptic damage	Chocolate, Carbonated drinks, Fermented products (Beer etc.)
Filtration	Vibrations	- Time saving, - Improving filtration	Fruit juices, Edible oils
Demoulding	Vibrations	- Less time, - Reducing product losses	Cooked products (cakes etc.)
Emulsification	Cavitation phenomenon	- Time and energy savings, - Emulsion stability, - Improvement of product shelf life	Emulsions (ketchup, mayonnaise), Fruit juices, Edible oils

Cutting	Cavitation phenomenon	- Time and energy savings, - Reduction of product losses, - Accurate and continuous cutting capability, - Lower maintenance cost, - Reduction of microbial risk, - Better standardization of part weights and dimensions	Cakes, Pastry and Bakery products, Cheese and Sticky oil products, Fresh fruits and vegetables
Depolymerisation	Cavitation phenomenon	- Time and energy savings	Starch, Whey
Extraction	Cavitation phenomenon	- Increase in mass transfer, - More solvent input, - Extraction at lower temperatures and faster, - Ability to work at lower temperatures	Sugar production from sugar beet, Oil extraction from plant seeds, Anthocyanin extraction from fruits
Cleaning and surface decontamination	Uniform and Strong cavitation formation	- Reduction of microbial risk, - Time and cost savings, - Increased shelf life	Cleaning of equipment used in slaughtering poultry, Decontamination of fruits and vegetables, Decontamination of meat products
Microbial inactivation	Cavitation phenomenon	- Time and energy savings, - High inactivation rate at low temperature	Inactivation of pathogenic bacteria from fruit juices, Inactivation of Pichia fermentans in tomato juice
Enzyme inactivation	Cavitation phenomenon	- High inactivation rate at low temperature, - Increased homogeneity and clarity	Inactivation of polyphenoloxidase, peroxidase, pectinmethylesterase and lipoxygenase enzymes

6. Conclusion

Ultrasound is considered a new technology in the processing and preservation of food products. In food technology, many studies have been conducted on ultrasound applications. However, many of these systems cannot be used in the industry. The widespread use of applications developed as alternatives to traditional methods depends on factors such as commerciality, applicability and economy. Current studies show that ultrasound technology provides significant advantages in food systems and that this method can be combined with various methods to increase its advantages.

Efforts on fully automated ultrasound systems are ongoing. Thus, by integrating into food production lines, it will be possible to contribute to energy savings and the production of high value and safe food products. (Awad et al., 2012). More studies are needed to encourage the transition to ultrasound applications.

References

Abesinghe, A.M.N.L., Vidanarachchi, J.K., Islam, N., Prakash, S., Silva, K.F.S.T., Bhandari, B., Karim, M.A. (2020). Effects of ultrasonication on the physicochemical properties of milk fat globules of Bubalus bubalis (water buffalo) under processing conditions: a comparison with shear-homogenization. Innovative Food Science & Emerging Technology, 59: 102237.

Acar, A. (2017). Zeytin Yağı Üretiminde Enzim İlavesi İle Mikrodalga ve Ultrasonikasyon Teknolojileri Bazı Kalite Parametreleri ve Yağ Verimi Üzerine Etkileri, Yüksek Lisans Tezi, Necmettin Erbakan Üniversitesi, Fen Bilimleri Enstitüsü, Konya.

Adekunte, A., Tiwari, B.K., Scannell, A., Cullen, P.J., O'Donnell, C. (2010). Modelling of Yeast Inactivation in Sonicated Tomato Juice, International Journal of Food Microbiology, 137: 116-120.

Akdeniz, V., Akalın, A.S. (2017). Ultrason Uygulamasının Süt Ürünlerinde Homojenizasyon, Jel Yapısı, Viskozite ve Su Tutma Kapasitesi Üzerine Etkisi, Gıda Teknolojisi Derneği Dergisi, 42(6): 743-753.

Alves L.L., Donadel, J.Z., Athayde, D.R., Silva, M.S., Klein, B., Fagundes, M.B., Menezes, C.R., Barin, J.S., Campagnol, P.C.B., Wagner, R., Cichoski, A.J. 2020. Effect of ultrasound on proteolysis and the formation of volatile compounds in dry fermented sausages. Ultrasonics – Sonochemistry, 67: 105161.

Arslan Tontul, S., Mutlu, C., Koç, A., Erbaş, M. (2018). Çiya Tohumundan Ultrason Destekli Yağ Ekstraksiyonunun Optimizasyonu, Gıda Dergisi, 43(3): 393-402.

Awad T.S., Moharram H.A., Shaltout O.E., Asker D., Youssef M.M. (2012). Applications of ultrasound in analysis, processing and quality control of food. Food Research International, 48(2): 410-427.

Bal, E. (2016). Derim Sonrası Santa Rosa Erik Çeşidinde Kalsiyum Klorür İle Ultrasound Uygulamalarının Modifiye Atmosfer Paketler İçerisinde Muhafaza Süresi Ve Meyve Kalitesi Üzerine Etkileri, VII. Bahçe Ürünlerinde Muhafaza ve Pazarlama Sempozyumu, 1(Özel Sayı): 12-18.

Bosiljkov, T., Tripalo, B., Ježek, D., Brnčić, M., Karlović, S., Dujmić, F. (2012). Influence of High İntensity Ultrasound Treatments on Physical Properties of Sheep Milk, Croatian Journal of Food Technology, Biotechnology and Nutrition, 7(Özel Sayı): 44-48.

Bozkurt, H., İçier, F. (2009). UV-C ve Ultrason Önişlemlerinin Çilek Kalitesi Üzerine Etkileri, Gıda Dergisi, 34(5): 279-286.

Carillo-Lopez, L.M., Alarcon-Rojo, A.D., Luna-Rodriguez, L., Reyes-Villagrana, R. (2017). Modification of Food Systems By Ultrasound. Hindawi Journal of Food Quality, Sayı: 2017.

Carrillo-Lopez L.M., Garcia-Galicia I.A., Tirado-Gallegos J.M., Vega R.S., Huerta-Jimenez M., Ashokkumar M., Alarcon-Rojo, A.D. (2021). Recent advances in the application of ultrasound in dairy products: Effect on functional, physical, chemical, microbiological and sensory properties. Ultrasonics Sonochemistry, 73: 105467.

Chang, H.J., Wang, Q., Tang, C.H., Zhou, G.H. (2015). Effects Of Ultrasound Treatment On Connective Tissue Collagen and Meat Quality of Beef Semitendinosusmuscle Journal Of Food Quality, 38(4): 256-267.

Chemat, F., Zill-e-Huma, Khan, M.K. (2011). Applications of Ultrasound in Food Technology: Processing, Preservation and Extraction, Ultrasonics Sonochemistry, 18: 813-835.

Cichoski A.J, Rampelotto C., Silva M.S, Moura H.C, Terra N.N., Wagner R., Menezes C.R., Flores E.M.M., Barin J.S. (2015). Ultrasound-assisted post-packaging pasteurization of sausages. Innovative Food Science & Emerging Technologies, 30: 132-137.

Contreras-Lopez, G., Carnero-Hernandez, A., Huerta-Jimenez, M., Alarcon-Rojo, A. D., Garcia-Galicia, I., & Carrillo-Lopez, ´ L. M. (2020). High-intensity ultrasound applied on cured pork: Sensory and physicochemical characteristics. Food Science & Nutrition, 8(2): 786–795.

Çağdaş, E., Kumcuoğlu, S., Güventürk, S., Tavman, Ş. (2011). Ultrasound-assisted Extraction of Silymarin Components from Milk Thistle Seeds (*Silybum Marianum L.*), Gıda Dergisi, 36(6): 311-318.

Çilek, S., Dirican, S. (2008). Koyun Karkaslarının Derecelendirilmesinde Ultrasonografik Yöntemlerin Kullanımı, Türkiye 10. Gıda Kongresi, 39(4):251-258.

Dolatowski, Z.J., Stadnik, J., Stasiak, D. (2007). Applications of Ultrasound in Food Technology, Acta Scientiarum Polonorum Technologia Alimentaria, 6(3): 89-99.

Er, M. (2014). Ultrasonik Yöntemlerle Ekstrakte Edilen Yaban Mersininin Biyoaktif Özellikleri Ve Kefir Üretiminde Kullanımı, Yüksek Lisans Tezi, Ondokuz Mayıs Üniversitesi, Fen Bilimleri Enstitüsü, Samsun.

Ercan, S.E. (2009). Effect of Ultrasound and Temperature on Tomato Peroxidase, Yüksek Lisans Tezi, Gaziantep Üniversitesi, Fen Bilimleri Enstitüsü, Gaziantep.

Ercan, S.Ş., Soysal, Ç. (2013). Use of ultrasound in food preservation. Natural Science, (5): 5-13.

Ertugay, M. F., Şengül, M., Şengül, M. (2004). Effect of Ultrasound Treatment on Milk Homogenisation and Particle Size Distribution of Fat, Turkish Journal of Veterinary and Animal Sciences, 28: 303-308.

Feng, H., Barbosa-Cánovas, G.V., Weiss, J. (2011). Ultrasound Technologies for Food and Bioprocessing, Springer, s. 65-107.

Gregersen, S.B., Frydenberg, R.P., Hammershøj, M., Dalsgaard, T.K., Andersen, U., Wiking, L. (2019). Application of high intensity ultrasound to accelerate crystallization of anhydrous milk fat and rapeseed oil blends. European Journal of Lipid Science and Technology, 121: 1-9.

Güleç, H.A. (2006). Modern Gıda Muhafazasında Vurgulu Elektrik Alan ve Ultrason Uygulamaları, Türkiye 9. Gıda Kongresi, S.73-76, Bolu.

İnce, A. E. (2011). Usage of Microwave and Ultrasound in the Extraction of Essential Oils and Phenolic Compounds, Yüksek Lisans Tezi, Orta Doğu Teknik Üniversitesi, Fen Bilimleri Enstitüsü, Ankara.

İşçimen, E.M. (2016). Pirinç Kepeğinden Ultrason Destekli Protein Ekstraksiyonun Optimizasyonu: Antioksidan ve Antiproiferatif Özellikler Üzerine Etkiler, Yüksek Lisans Tezi, Erciyes Üniversitesi, Fen Bilimleri Enstitüsü, Kayseri.

Jiang, B., Mantri, N., Hu, Y., Lu, J., Jiang, W., Lu, H. (2015). Evaluation of bioactive compounds of black mulberry juice after thermal, microwave, ultrasonic processing, and storage at different temperatures. Food Science and Technology International, 21 (5): 392–399.

Jo, Y.J., Choi, M.J., Chun, J.Y., Yeon-Ji, J., Mi-Jung, C., Ji-Yeon, C. (2019). Effect of highenergy emulsification on properties of commercial low-temperature pasteurised milk, International Journal Dairy Technology, 72: 357–363.

Kentish, S., Feng, H. (2014). Aplications of Power Ultrasound in Food Processing, The Annual Review of Food Science and Technolgy, 5: 263-284.

Kırmusaoğlu, S. (2013). Elimination of Certain Foodborne Pathogens in Various Fruit Juices by Combination of Ultrasonication and Mustard Seed, Doktora Tezi, Abant İzzet Baysal Üniversitesi, Fen Bilimleri Enstitüsü, Bolu.

Leong, T., Johansson, l., Mawson, R., McArthur, S.L., Manasseh, R., Juliano, P., (2016). Ultrasonically enhanced fractionation of milk fat in a litre-scale prototype vessel. Ultrasonics Sonochemistry, 28: 118–129.

Li, Y., Zhang, Y., Sui, X., Zhang, Y., Feng, H., Jiang, L. (2013). Ultrasound-assisted Aqueous Enzymatic Extraction of Oil From Perilla (*Perilla Frutescens* L.) Seeds, CyTA Journal of Food, 12(1): 16-21.

Majid, I., Nayik, G.A., Nanda, V. (2015). Ultrasonication and Food Technology: A Review, Cogent Food & Agriculture, Sayı: 1.

Mason, T.J., Paniwnyk, L., Chemat, F., Abert Vian, M. (2010). Ultrasonic Processing, Alternatives to Conventional Food Processing, Chapter 10, s. 395-422.

McDonnell, C. K., Lyng, J.G., Arimi, J.M., Allen, P. (2014). The Acceleration of Pork Curing By Power Ultrasound: A Pilot-Scale Production, Innovative Food Science & Emerging Technologies, 26: 191-198.

Mizrach, A. (2008). Ultrasonic technology for quality evaluation of fresh fruit and vegetables in pre-and postharvest processes, Postharvest Biol. Technol. 48 (3): 315–330.

Mohd. Fuad, F., Abd. Karim, K., Mat Don, M. (2016). Ultrasound-assisted Extraction of Oil from *Calophyllum inophyllum* Seeds: Statistical Optimisation using Box-Behnken Design, Journal of Physical Science, 27(2): 103-121.

Nicolau-Lapeña, I., Lafarga, T., Viñas, I., Abadias, M., Bobo, G., Aguiló-Aguayo, I. (2019). Ultrasound processing alone or in combination with other chemical or physical treatments as a safety and quality preservation strategy of fresh and processed fruits and vegetables: a review, Food Bioprocess Technol. 1–20.

Ojha, K. S., Tiwari, B. K., & O'Donnell, C. P. (2018). Effect of ultrasound technology on food and nutritional quality. Advances in Food and Nutrition Research, 84: 207–240.

Özaslan, Z. T. (2016). Effect of Ozonation, Ultrasound Application and Xanthan Gum Adding on the Selected Properties of Rice Starch, Yüksek Lisans Tezi, Gaziantep Üniversitesi, Fen Bilimleri Enstitüsü, Gaziantep.

Özdoğan, K. (2015). Geleneksel ve Ultrasonik Yöntemlerle Krmızı Lahana Antosiyaninlerinin Ekstraksiyon Koşularının Optimizasyonu, Yüksek Lisans Tezi, Tokat Gaziosmanpaşa Üniversitesi, Fen Bilimleri Enstitüsü, Tokat.

Özyurt, V. H. (2013). Fındık Zarı Ve Keçiboynuzu Fenolik Bileşiklerinin ve Diyet Lifinin Ultrasonik ve Klasik Ekstraksiyon Eldelerinin Karşılaştırılması, Yüksek Lisans Tezi, Ege Üniversitesi, Fen Bilimleri Enstitüsü, İzmir.

Safwa, S.M., Ahmed, T., Talukder, S., Sarker, A., Rana, M.R., (2024). Applications of non-thermal technologies in food processing Industries. 18: 100917.

Sayın, L., Tamer, C.E. (2014). Yüksek Hidrostatik Basınç ve Ultrasonun Gıda Koruma Yöntemi Olarak Kullanımı, Uludağ Üniversitesi Ziraat Fakültesi Dergisi, 28(1): 83-94.

Sfakianakis, P., Topakas, E., Tzia, C. (2015). Comparative Study on High – Intensity Ultrasound and Pressure Milk Homogenization: Effect on the

Kinetics of Yogurt Fermentation Process, Food Bioprocess Technol, 8: 548-557.

Shestakov, S., Krasulya, O., Rink, R., Ashokkumar, M. (2013). Sonication of Dairy System, Electronic Journal Technical Acoustics, 7: 1-7.

Słowik-Borowiec, M., Szpyrka, E. (2020). Selected Food Processing Techniques as a Factor for Pesticide Residue Removal in Apple Fruit. Environmental Science and Pollution Research, 27: 2361–2373.

Sir´o, I., V´en, C., Balla, C., J´on´as, G., Zeke, I., Friedrich, L. (2009). Application of An Ultrasonic Assisted Curing Technique For İmproving The Diffusion of Sodium Chloride İn Porcine Meat, Journal of Food Engineering, 91(2): 353–362.

Söbeli, C., Kayaardı, S. (2014). Et Kalitesini Belirlemede Yeni Teknikler, Gıda Dergisi, 39(4): 256-267.

Subba Rao, K. V., Thejasri, V., Kireeti B. R., Sandep, G. D. S., Sivaji, G. (2018). Optimization of Ultrasound-Assisted Extraction of Watermelon Seed Oil Using Response Surface Methodology, The Pharma Innovation Journal, 7(5): 546-549.

Şengül, M., Başlar, M., Erkaya, T., Ertugay, M.F. (2009). Ultrasonik Homojenizasyon İşleminin Yoğurdun Su Tutma Kapasitesi Üzerine Etkisi, Gıda Dergisi, 34(4): 219-222.

Şimşekli, N. (2010). Aspir (*Carthamus Tinctorius* L.) Tohumlarından Ham Yağ Ekstraksiyonu İçin Sokselet Ekstraksiyonuna Alternatif Hızlı Bir Metodun Optimizasyonu: Ultrason Destekli Ekstraksiyon, Yüksek Lisans Tezi, Kahramanmaraş Sütçü İmam Üniversitesi, Fen Bilimleri Enstitüsü, Kahramanmaraş.

Tao, Y., Sun, D-W. (2014). Enhancement of Food Processes by Ultrasound: A Review, Critical Reviews in Food Science and Nutrition.

Tavman, Ş., Kumcuoğlu, S., Akkaya, Z. (2009). Bitkisel Ürünlerin Atıklarından Antioksidan Maddelerin Ultrason Destekli Ekstraksiyonu, Gıda Dergisi, 34(3): 175-182.

Teng, H., Chen, L., Huang, Q., Wang, J., Lin, Q., Liu, M., Lee, W. Y., Song, H. (2016). Ultrasonic-assisted Extraction of Raspberry Seed Oil and Evaluation of Its Physicochemical Properties, Fatty Acid Compositions and Antioxidant Activities, PLOS ONE.

Tuna, Ö. (2013). Kırmızı Biber Salçası Üretimi Artıklarından Ultrason ve Süperkritik Akışkan Ekstraksiyon Yöntemleri İle Antioksidan Eldesi Optimizasyonu, Yüksek Lisans Tezi, Ondokuz Mayıs Üniversitesi, Fen Bilimleri Enstitüsü, Samsun.

Turantaş, F. (2016). Gıda Sanayisinde Ultrason Uygulamalarının Antimikrobiyal Etkileri, Dünya Gıda Dergisi, http://www.dunyagida.com.tr/haber/gida-sanayiinde-ultrason-uygulamarlinin-antimikrobiyal-etkileri-i/5758, Erişim Tarihi: 30.06.2018

Turantaş, F. (2017). Gıda Sanayisinde Ultrason Uygulamalarının Antimikrobiyal Etkileri (2. Kısım), Dünya Gıda Dergisi, http://www.dunyagida.com.tr/haber/gida-sanayiinde-ultrason-uygulamalarinin-antimikrobiyal-etkileri-ii/5917, Erişim Tarihi: 30.06.2018

Türken, T. (2014). Ultrasonikasyonun Vişne Suyunun Bazı Kimyasal ve Mikrobiyolojik Özelliklerine Etkisinin Yüzey Cevap Yöntemi İle Belirlenmesi, Yüksek Lisans Tezi, Abant İzzet Baysal Üniversitesi, Fen Bilimleri Enstitüsü, Bolu.

Ünal, K. (2012). Ekonomik Verim Dönemini Tamamlamış Yumurta Tavuğu Göğüs ve But Etleri Üzerine Ultrasonik Dalgaların Etkileri, Yüksek Lisans Tezi, Selçuk Üniversitesi, Fen Bilimleri Enstitüsü, Konya.

Wu, H., Hulbert, G. J., Mount, J. R. (2000). Effects of Ultrasound on Milk Homogenization and Fermentation with Yogurt Starter, Innovative Food Science & Emerging Technologies, 1(3): 211-218.

Yaman, T., Kuleaşan, Ş. (2016). Uçucu Yağ Elde Etmede Gelişmiş Ekstraksiyon Yöntemleri, Mehmet Akif Ersoy Üniversitesi Fen Bilimleri Enstitüsü Dergisi, Özel Sayı 1: 78-83.

Yılmaz, B. (2014a). Kurutmada Ultrason Kullanımının Ürün Kalitesi ve Kuruma Davranışına Etkileri, Yüksek Lisans Tezi, Ege Üniversitesi, Fen Bilimleri Enstitüsü, İzmir.

Yılmaz, M. (2014b). Ultrasonikasyonun Elma Suyunda Bazı Kimyasal ve Mikrobiyolojik Özelliklere Etkisinin Yüzey Cevap Yöntemi İle Belirlenmesi, Yüksek Lisans Tezi, Abant İzzet Baysal Üniversitesi, Fen Bilimleri Enstitüsü, Bolu.

Yılmaz, T. (2011). Domates İşleme Atıklarından Ultrason Destekli Ekstraksiyonu İşleminin Optimizasyonu, Yüksek Lisans Tezi, Ege Üniversitesi, Fen Bilimleri Enstitüsü, İzmir.

Yılmaz, T. (2015). Bitkisel Ürünlerden Polisakkarit Ekstraksiyonunda Ultrason Kullanımının Optimizasyonu, Doktora Tezi, Celal Bayar Üniversitesi, Fen Bilimleri Enstitüsü, Manisa.

Yüksel, Y. (2013). Buğdaylarda Tavlama İşleminde Ultrason Uygulamasının Öğütme ve Un Kalitesi Üzerine Etkisi, Doktora Tezi, Selçuk Üniversitesi, Fen Bilimleri Enstitüsü, Konya.

Yüksel, Y., Elgün, A. (2013). Buğdayın Islatılması Sırasında Ultrason İşlemi Uygulamanın Tanenin Su Absorbsiyonu Üzerine Etkisi, Balıkesir Üniversitesi Fen Bilimleri Enstitüsü Dergisi, 15(2): 1-14.

Zambak, Ö., Özkal, S.G. (2017). Ultrases Önişlemi Uygulanarak Kurutulan Tavuk Göğüs Etlerinin Rehidrasyon Özellikleri, 4. Uluslararası Beyaz Et Kongresi – Kongre Kitabı, s. 169-174.

Zou, Y. H., Zhang, W. G., Kang, D. C., Zhou, G. H. (2017). Improvement of tenderness and water holding capacity of spiced beef by the application of ultrasound during cooking. International Journal of Food Science & Technology, 53(3): 828–836.

Chapter 6

GLOBAL CLIMATE CHANGE AND CARBON MANAGEMENT: HYBRID SOLUTIONS WITH ANFIS

Didem GULERYUZ[1]

Zennup KARATAŞ [2]

1 Assoc. Prof. Dr., Bayburt University, Faculty of Applied Sciences, Management Information Systems, dguleryuz@bayburt.edu.tr, ORCID: 0000-0003-4198-9997

2 Undergraduate Student (Graduate), Bayburt University, Faculty of Applied Sciences, Management Information Systems, karataszennup1@gmail.com, ORCID: 0009-0006-4962-3569.

1. Introduction

The rapid population growth following the Industrial Revolution and nations' pursuit of economic prosperity led to the establishment of systems that ensured long-term energy consumption. Energy, one of the most critical inputs for social and economic development, plays a vital role in improving living standards and achieving sustainable development. During the Industrial Revolution, while the continuous demand for energy and the systems that met these needs contributed to the development of international trade and the prosperity of nations, emissions from these energy sources became the hidden cost of this system. These emissions led to the planet's rapid warming, evolving into what is known as global warming, which harms climates and ecosystems. In response to global warming, nations have agreed on common international goals to mitigate the increase in global temperatures. Rising global temperatures are causing devastating impacts worldwide, compounding effects on economies and societies. Over the past five years, the average global temperature has been the highest ever recorded. According to the World Meteorological Organization, temperatures are expected to exceed the pre-industrial 1.5°C threshold within the next five years, a limit that must not be crossed to avoid catastrophic impacts. However, the United Nations Emissions Gap Report 2021 revealed that, despite new national commitments and measures, global temperatures will rise by 2.7°C by the end of this century.

CO_2 is the most significant greenhouse gas emitted through human activities, and the effects of the Industrial Revolution have further amplified CO_2 emissions from various operations, leading to an increasingly changing climate. Climate change has brought the world face-to-face with a global climate crisis. Modelling and forecasting CO_2 emissions at the national level is crucial for policymakers. Therefore, a multidimensional determination of the variables influencing emissions is essential to analyze CO_2 emissions in Turkey. Coal, oil, and natural gas consumption contributing significantly to Turkey's CO_2 emissions, have increased yearly. In contrast, using renewable energy sources, which result in lower CO_2 emissions, only began in the 2000s and remains relatively low compared to other sources.

Global climate change stands out as one of human history's most significant environmental and economic threats. The use of fossil fuels, industrial activities, and the rapidly growing energy demand have increased the concentration of greenhouse gases in the atmosphere, leaving long-term impacts on climate systems. In this context, accurately forecasting carbon emissions and developing effective carbon management strategies are critical for combating global climate change and achieving sustainable development goals (Güleryüz&Özden, 2023). This situation necessitates

a meticulous examination of carbon emissions not only at a global level but also at the national level. Each country's economic structure, energy consumption habits, and environmental policies uniquely determine the sources and impacts of carbon emissions. In developing countries, industrialization and rising energy demand have significantly increased per capita greenhouse gas emissions. Thus, understanding past trends in carbon emissions and comparing them to global averages in countries like Turkey provides a critical foundation for the development of both local and global climate policies. Per capita greenhouse gas emissions for Turkey and the global average over the past five years are presented in Figure 1 for comparative analysis.

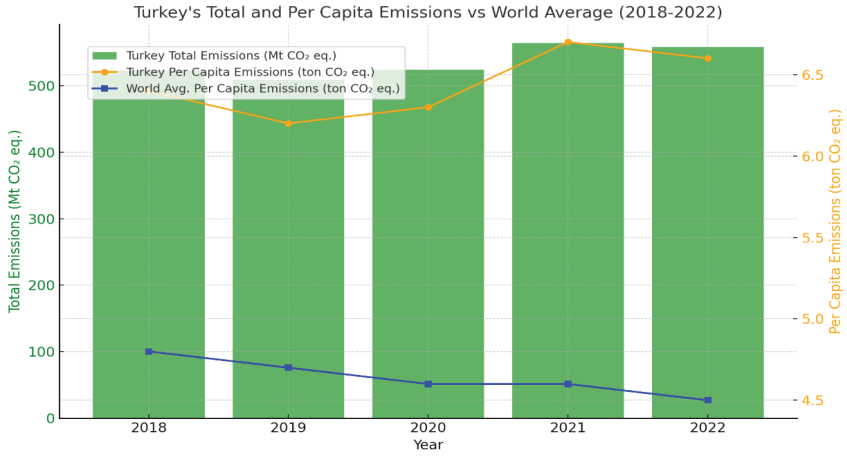

Figure 1. *Greenhouse Gas Emissions: Time Series Comparison of Per Capita Emissions in Turkey and the World (Created by the Author) (TUİK, 2023)*

Between 2018 and 2022, Turkey's per capita greenhouse gas emissions consistently remained higher than the global average. While Turkey's per capita emissions ranged between 6.2 and 6.7 tons of CO_2 equivalent, the global average gradually decreased from 4.8 tons to 4.5 tons of CO_2 equivalent during the same period. This trend reflects international policies' effectiveness in reducing carbon emissions, whereas Turkey's continued reliance on fossil fuels in its energy production and consumption processes remains evident. Turkey's per capita emissions peaked in 2021, which can be attributed to the recovery of economic and industrial activities following the COVID-19 pandemic. In contrast, the global average decline during this period underscores Turkey's lag in meeting international standards for carbon reduction.

Turkey's emission levels, which exceed the global average, can be attributed to its energy-intensive economic structure and challenges in transitioning to renewable energy. The significant reliance on fossil fuels (coal, oil, natural gas) in energy production and rapid urbanization and industrialization are key contributing factors. Meanwhile, many countries worldwide have successfully taken steps to reduce their per capita emissions by increasing renewable energy sources. This trend highlights the need for Turkey to intensify its efforts to reduce greenhouse gas emissions.

In its strategies for reducing emissions, Turkey must prioritize investments in renewable energy, expand energy efficiency policies, and implement low-carbon industrial technologies. Strengthening international collaborations and ensuring active participation in global carbon reduction initiatives are also essential. The global downward trend in emissions demonstrates successful examples of carbon reduction, indicating that Turkey has the potential to achieve progress in this area.

In conclusion, Turkey's current greenhouse gas emission levels present a significant obstacle to achieving sustainable development goals. Restructuring energy policies and accelerating the transition to a low-carbon future are critical necessities. Aligning with the global average is essential for attaining Turkey's national sustainability goals and a strategic imperative for contributing to international efforts to combat climate change. This alignment should be addressed as a priority for ensuring environmental and economic sustainability.

To meet its long-term development goals, accurately predicting and controlling CO_2 emissions will play a critical role in building a sustainable future for Turkey. R&D efforts focused on accelerating industrial transformation, designing more efficient production processes, developing sustainable energy solutions, and adopting innovative production systems will not only support environmental sustainability but also enhance Turkey's global competitiveness (Işık & Kılıç, 2014). Developing accurate prediction models for CO_2 emissions is crucial for determining strategies to reduce emissions, ensuring efficient resource utilization, achieving long-term economic objectives, and promoting environmental sustainability.

Given the nonlinear, complex, and multivariate nature of carbon emission forecasting, traditional methods have demonstrated limited success in this field. Hybrid models combining artificial intelligence and optimization techniques offer a promising alternative for such problems. Hybrid ANFIS-PSO and GA models stand out in carbon emission forecasting due to their ability to model nonlinear relationships and their optimizable structures. ANFIS effectively combines the learning capacity of neural networks with the explainability of fuzzy logic, providing a powerful

solution for modelling complex systems, while metaheuristic algorithms such as PSO and GA optimize model parameters to enhance prediction accuracy. This study explores the application of hybrid ANFIS-PSO and GA models in forecasting carbon emissions and evaluates their comparative performance. It aims to provide new perspectives on practical modeling approaches for carbon management and combating climate change.

Forecasting CO_2 emissions will be a strategic step for accelerating technological progress, fostering innovation, and maintaining competitive advantages. On a global scale, such predictions will support high-quality scientific and technological advancements, contribute to the rapid emergence of discoveries and innovative solutions, and strengthen strategic planning in science and technology-oriented sectors. Accurate CO_2 emission forecasts are critical for developed countries to maintain technological leadership and competitive advantages. These forecasts offer a practical roadmap for economic transformation, local innovation, and global competitiveness in developing countries. For less developed countries, emission forecasts play a key role in sustainable development by addressing basic needs, increasing productivity in key sectors, and focusing on development goals.

In this context, accurate and reliable predictions form the cornerstone of a successful and sustainable strategy. Forecasting CO_2 emissions not only aids in achieving environmental objectives but also supports strategic planning in business, economic development, and competitive advantage.

In emission forecasting processes, the ability of governments to manage CO_2 emissions depends on identifying the main influencing factors and selecting appropriate forecasting models. Most studies rely on traditional statistical methods, which perform well when correlations among variables are strong. However, with advancements in artificial intelligence methods, nonlinear relationships between inputs and outputs can be modeled effectively, and variables uncorrelated with the output variable can also be included in the model. Particularly in recent years, the development of data science and AI-based forecasting models has found widespread applications in many fields (Özbek&Teke, 2024; Özden,2022a; Nassef vd., 2023; Özden,2022b; Efe vd., 2022). Consequently, an AI-based model developed for forecasting CO_2 emissions is expected to yield effective and successful results.

An analysis of previous studies reveals that efforts to forecast CO_2 emissions can be classified into statistical and AI-based methods. Table 1 systematically presents various methods and academic studies conducted in this context. These studies serve as examples of both AI-based models and statistical approaches.

Table 1. *CO_2 Emissions: Topics and Methods*

Study Topic	Methods Used	References
Prediction of CO2 emissions using artificial intelligence	Artificial Neural Networks (FFNN), ANFIS, LSTM, Ensemble Modeling	(Nassef et al., 2023)
CO2 emission prediction using Multivariate Grey Prediction Model	Grey Relation Analysis, Neural-Network-Based Residual Model	(Chiu et al., 2020)
CO2 emission prediction with Biogeography-Based Optimization	Biogeography-Based Optimization (BBO), Gradient Boosting, SHAP, and LIME	(Özkurt, 2024)
CO2 prediction using Regression, Neural Networks, and Support Vector Machines	Regression, Neural Network, SVM	(Liu, 2024)
Machine learning for vehicle emission prediction	Multivariate Polynomial Regression, Decision Tree, Random Forest	(Manvitha et al., 2023)
CO2 emission prediction for the post-COVID-19 period	SARIMA, SARIMAX Modeling	(Meng & Noman, 2022)
Prediction of greenhouse gas emissions in agricultural soils	LSTM, Random Forest, SVM	(Hamrani et al., 2020)
Vehicle emission prediction using the CO2MPAS model under actual traffic conditions	CO2MPAS Model, EMEP/EEA Guide Method	(Mogno et al., 2020)
Vehicle emission prediction using machine learning with Grid Search Optimization	Grid Search Optimization, Random Forest, SVR	(Sidana, 2024)
CO_2 emission prediction using Wavelet-based Extreme Learning Machine	Wavelet Transform, Extreme Learning Machine (W-EELM), Noise Removal	(Alomar et al., 2023)

Evaluating the applications of studies conducted on CO_2 emissions provides an in-depth perspective on forecasting carbon emissions. Summaries of several studies from the literature are presented below. Forecasting carbon emissions is critical in combating global warming and climate change. In this context, artificial intelligence and machine learning methods offer innovative approaches for modelling emissions more accurately and effectively. Studies in the literature demonstrate the applicability and effectiveness of these methods across various sectors and application areas, contributing significantly to achieving sustainable development goals. Numerous studies have been conducted on predicting

and reducing CO_2 emissions using multiple modeling approaches and technologies.

Nassef et al. (2023) employed artificial intelligence tools to forecast annual CO_2 emissions in Saudi Arabia. The study utilized artificial neural networks (FFNN), adaptive neuro-fuzzy inference systems (ANFIS), and long short-term memory (LSTM) models. These models predicted future emission values based on historical data. Among the models, the LSTM model outperformed others with higher accuracy and lower error rates. The findings of this study projected a decrease in emissions by 2030 and emphasized the importance of these results for the development of sustainable environmental policies.

Similarly, the multivariate grey prediction model (MGPM) developed by Chiu et al. (2020) provided an effective method for data with missing values and those that do not conform to statistical assumptions. Combining grey relational analysis with neural network-based residual models, this approach demonstrated strong performance in CO_2 emissions forecasting. The study proposed a framework for the development of energy policies. Özkurt (2024) focused on forecasting CO_2 emissions using the Biogeography-Based Optimization (BBO) algorithm and Gradient Boosting methods. Using explainable AI tools such as SHAP and LIME improved the interpretability of model outcomes. The study analyzed key determinants of emissions and contributed to environmental management processes. Liu (2024) compared various machine learning methods, including regression, artificial neural networks, and support vector machines (SVM), for CO_2 emissions prediction. The research highlighted the effectiveness of these models from different perspectives and encouraged the application of machine learning in environmental analyses. Manvitha et al. (2023) applied machine learning models to predict vehicle-related CO2 emissions. Variables such as engine size, fuel type, cylinder count, and vehicle class significantly impacted predictive performance. Models like multivariate polynomial regression and decision trees successfully enhanced prediction accuracy. Meng and Noman (2022) investigated the impact of COVID-19 on CO2 emissions using SARIMA and SARIMAX models, which provided forecasts specific to the pandemic period. These models offered insights into post-pandemic emission levels and contributed to developing emission reduction strategies. Hamrani et al. (2020) employed long short-term memory (LSTM) models and other machine learning approaches to estimate greenhouse gas (GHG) emissions from agricultural soils. LSTM models demonstrated superior performance in forecasting seasonal CO_2 and N_2O fluxes variations.

Mogno et al. (2020) examined vehicle emissions under actual traffic conditions using the CO2MPAS model. This model proved to be valuable

for both certification processes and traffic simulations. Sidana (2024) utilized grid search optimization, random forest (RF), and support vector regression (SVR) models for predicting vehicle-related CO_2 emissions. The study achieved high accuracy rates in emission forecasts and highlighted the applicability of these results to environmental policymaking. Finally, Alomar et al. (2023) employed the Wavelet-Enhanced Extreme Learning Machine (W-EELM) model to predict CO_2 emissions across different time scales. The use of noise reduction techniques and wavelet transforms enhanced model accuracy. This model emerged as a valuable tool for the development of environmental strategies.

Forecasting Turkey's CO_2 emissions is vital for achieving sustainable development goals and minimizing environmental impacts. However, studies in the literature remain limited, particularly in the application of AI-based models in this domain. This study aims to introduce an innovation by optimizing the Adaptive Neuro-Fuzzy Inference System (ANFIS) model using Genetic Algorithm (GA) and Particle Swarm Optimization (PSO) to forecast Turkey's CO_2 emissions. The use of these methods offers significant advantages in modeling nonlinear relationships and improving forecast accuracy.

Studies on the applicability of hybrid ANFIS models to environmental problems such as carbon emission forecasting are notably scarce in the literature. Specifically, there are evident research gaps in the comparative analysis of the performance of different metaheuristic algorithms (e.g., PSO and GA) and their effective application to small datasets. This study aims to address these gaps by comprehensively evaluating PSO- and GA-based ANFIS models, thereby making a significant contribution to the literature. Thus, this research seeks to provide new perspectives on both the theoretical and practical aspects of modeling and forecasting carbon emissions.

The input variables used in this research comprehensively reflect Turkey's energy and urbanization dynamics. These variables include alternative and nuclear energy use, electricity generation from renewable resources, electricity generation from fossil fuels (coal, oil, natural gas), renewable energy consumption, and urban population. These variables significantly influence CO_2 emissions and are frequently used indicators in sustainability and environmental analyses in the literature. The comprehensive selection of input variables aims to enhance the accuracy and reliability of the forecasting model. The study aims to improve forecast performance by optimizing the ANFIS model with Genetic Algorithm (GA-ANFIS) and Particle Swarm Optimization (PSO-ANFIS). The developed models were comparatively analyzed, and the performance of the algorithms was evaluated. The study's findings are expected to provide

a data-driven foundation for restructuring Turkey's energy policies and supporting strategic decision-making processes for environmental sustainability. Furthermore, the performance evaluations of the optimized ANFIS models aim to provide a methodological framework for developing AI-based ecological forecasting models, contributing to policy design at the local level and grounding global environmental sustainability strategies in scientific evidence.

This study is structured into four main sections. The second section elaborates on the methods and materials used in the research, detailing the Genetic Algorithm (GA) and Particle Swarm Optimization (PSO) techniques applied to the ANFIS model and presenting the metrics used to evaluate model performance. The third section analytically examines the results obtained from the ANFIS, GA-ANFIS, and PSO-ANFIS models and assesses their forecasting performance from a comparative perspective. Finally, the fourth section discusses the implications of the findings in light of the study's objectives, highlighting the potential contributions of this approach to forecasting Turkey's CO_2 emissions and informing sustainable energy policies. This systematic framework enables a comprehensive understanding of the study's methodology, findings, and strategic conclusions.

2. Material and Methods

2.1. Data Collection Process

The inputs used in this study encompass various indicators related to Turkey's energy use and demographic structure. Alternative and nuclear energy represent their share in total energy consumption, enabling an assessment of the use of these sources alongside traditional fossil fuels in energy production. Electricity generation from renewable sources reflects the proportion of renewable energy sources (e.g., wind, solar, hydroelectric) in total electricity generation, serving as a critical indicator for environmental sustainability. Electricity generation from oil, gas, and coal sources highlights the share of fossil fuels in electricity production, providing an essential metric for evaluating the environmental impact of carbon-intensive production processes. Renewable energy consumption represents the proportion of renewable energy in total final energy consumption and is utilized to assess the sustainability of energy resources. Urban population ratio indicates the percentage of individuals residing in urban areas relative to the total population, serving as a vital variable in analyzing the impact of urban energy demand. Finally, CO_2 emissions, considered the output variable in the model, constitute a critical indicator for environmental sustainability and are evaluated as a fundamental metric in the policy development processes aimed at reducing emissions.

The dataset utilized in the study spans the years 1990-2015, with the first 18 years allocated for training the model and the final 8 years designated for testing purposes. The selection of 2015 as an analytical reference year is based on its critical importance in the national and international context concerning energy policies and environmental sustainability. This year marked a turning point in shaping energy and environmental policies, witnessing significant developments on both global and regional scales.

Notably, 2015 was a pivotal year for reinforcing global commitments to reducing carbon emissions. In this context, the Paris Climate Agreement, adopted in 2015, was a milestone in setting and reporting carbon reduction targets for countries. The agreement aimed to limit global temperature rise to below 2°C while emphasizing the necessity for countries to transform their energy production and consumption patterns. Many countries, including Turkey, undertook policy changes under the agreement to reduce emissions and increase the use of renewable energy sources (ÇŞİDB, 2023).

Table 2 provides a detailed presentation of the abbreviations, units, and sources of the variables used in the study. These inputs have been integrated into the model to comprehensively analyze the energy and socio-economic factors affecting Turkey's CO_2 emissions.

Table 2. *Variable Abbreviations, Units, and Sources*

Variables	**Unit**	**Abbr.**	**Source**
Alternative and Nuclear Energy	(% of total energy use)	ANE	World Bank (2023)
Renewable Energy Electricity Production	(% of total)	YKE	World Bank (2023)
Electricity Production from Oil, Gas, and Coal	(% of total)	PGK	World Bank (2023)
Renewable Energy Consumption	(% of total final energy consumption)	YET	World Bank (2023)
Urban Population	(% of total population)	KN	World Bank (2023)
CO2 Emissions	(metric tons per capita)	CO2	TUIK (2023)

The increase in renewable energy use shapes Turkey's energy production and consumption profile, reliance on fossil fuels, and urbanization dynamics, all of which directly impact greenhouse gas emissions. In this context, increasing the share of renewable resources in energy supply and reducing emissions from fossil fuels are critical for achieving sustainable development goals. Figures 2 and 3 provide comprehensive visualizations of the trends in the utilization rates of various energy sources in Turkey's energy production, the progression of renewable energy consumption, urbanization rates, and per capita carbon emissions between 1990 and 2015.

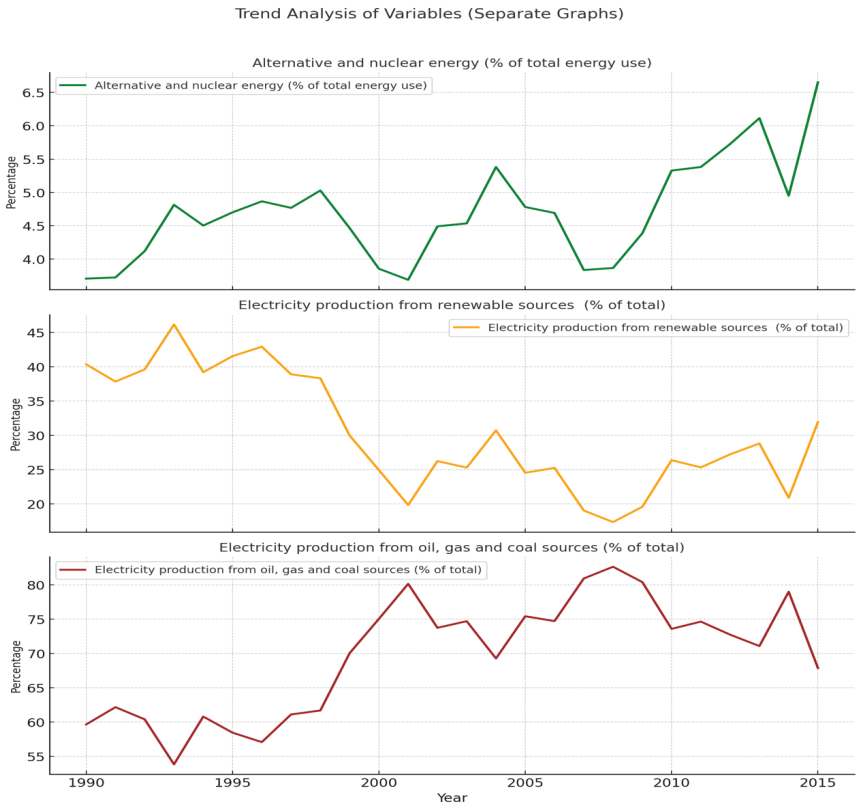

Figure 2. *Trends in Alternative and Nuclear Energy, Electricity Generation from Renewable Sources, and Electricity Generation from Oil, Gas, and Coal Sources*

Alternative and Nuclear Energy (%): A general upward trend in using alternative and nuclear energy is observed between 1990 and 2015. While the share of these energy types was relatively low in the 1990s, the pace of growth accelerated, particularly in the late 2000s, reaching its highest level in 2015. This trend indicates an increasing interest in alternative energy sources and the growing integration of nuclear energy into the energy production mix.

Electricity Generation from Renewable Sources (%): The proportion of electricity generated from renewable sources started at a relatively higher level in the early 1990s but experienced fluctuations over time, ultimately showing a general downward trend. This decline can be associated with a preference for fossil fuels and other energy sources over renewable energy production. However, a partial recovery in these ratios is noticeable in the 2010s, suggesting a renewed focus on renewable energy sources.

Electricity Generation from Oil, Gas, and Coal Sources (%): The share of fossil fuels in electricity production was around 60% in the 1990s, increasing steadily to approximately 80% by the early 2000s. However, since 2005, this proportion has shown a fluctuating decline, continuing its downward trend until 2015. This reduction can be attributed to implementing clean energy policies and increased investments in renewable energy sources.

When these three trends are considered together, it becomes evident that there is a shift toward alternative energy sources and a gradual move away from fossil fuels in energy production. However, the electricity production from renewable sources has yet to reach the desired levels, indicating that further efforts are needed to enhance the role of renewables in Turkey's energy mix.

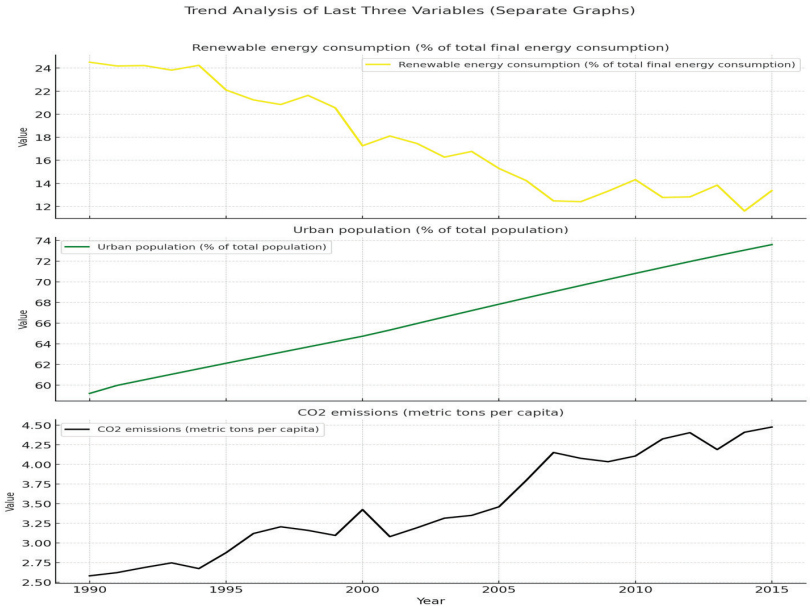

Figure 3. *Trends in Renewable Energy Consumption, Urbanization Rate, and CO_2 Emissions*

Renewable Energy Consumption (%): Renewable energy consumption was approximately 24% in 1990 but began to decline from the mid-1990s onward. By the early 2000s, this share had dropped to around 17%, further decreasing after 2005 to about 13% in 2015. However, a slight recovery was observed in 2015. This trend indicates a diminishing share of renewable energy in total energy consumption over time, reflecting the dominance

of fossil fuels in energy production and the slow transition to renewables.

Urbanization Rate (%): The urbanization rate increased steadily from 59% in 1990 to 73% in 2015. This consistent rise demonstrates the accelerating urbanization process and the growing proportion of the population living in cities. Urbanization is a significant factor in energy consumption and carbon emissions, and this trend highlights its critical role in shaping energy demand and consumption patterns.

CO_2 Emissions (Metric Tons/Capita): Per capita CO_2 emissions increased from approximately 2.58 metric tons in 1990 to over 4 metric tons by 2007. Following a slight decline due to the 2008 economic crisis, emissions resumed upward after 2010, reaching around 4.48 metric tons per capita in 2015. This rise clearly illustrates the impact of the high share of fossil fuels in energy production and the environmental consequences of growing energy demand.

These findings underscore the need for Turkey to accelerate its sustainable energy policies, promote the transition to renewable energy, and reduce its reliance on fossil fuels. Advancing energy transformation is crucial not only for reducing carbon emissions but also for achieving sustainable development goals. Policymakers must prioritize innovative energy solutions and develop integrated strategies to support environmental sustainability. This analysis provides valuable insights into the future direction of Turkey's energy policies. Table 3 presents the descriptive statistics and key statistical measures for the input and output variables used in the study.

Table 3. *Descriptive Statistics*

	Ort	Std	Min	25%	50%	75%	Max	Kurtosis	Skewness
ANE	4,71	0,75	3,69	4,18	4,70	5,01	6,65	-1,20	0,00
YKE	30,32	8,47	17,35	25,02	28,03	38,77	46,18	0,22	0,67
PGK	69,64	8,45	53,82	61,23	71,89	74,94	82,61	-1,19	0,25
YET	17,68	4,48	11,61	13,49	17,02	21,54	24,51	-1,19	-0,25
KN	66,41	4,42	59,20	62,78	66,29	70,09	73,61	-1,43	0,26
CO2	3,48	0,63	2,58	3,08	3,33	4,10	4,48	-1,23	0,04

The descriptive statistics of the variables in the dataset reveal significant relationships between energy production, consumption trends, and environmental impacts. The average percentage of Alternative and Nuclear Energy stands at approximately 4.7%, with a standard deviation of only 0.75%, indicating a relatively stable increase over the years. Electricity Generation from Renewable Sources averages around 30%

but varies significantly between 17% and 46%, reflecting fluctuating investments in renewable energy across years. Electricity Generation from Oil, Gas, and Coal Sources has a dominant share in energy production, with an average of 69.6% and a standard deviation of 8.44%, suggesting a gradual decline in the reliance on fossil fuels over time. Renewable Energy Consumption averages 17.7%, with a minimum value of 11.6%, indicating its limited representation in total energy consumption. This demonstrates that renewable energy has yet to integrate significantly into the overall energy mix. The Urbanization Rate shows a consistent upward trend with an average of 66.4%, emerging as a key factor driving increased energy demand. Urbanization significantly impacts energy consumption patterns and CO_2 emissions. CO_2 Emissions, with an average of 3.48 metric tons per capita, peaked at 4.47 metric tons, clearly reflecting the environmental costs of fossil fuel-based energy production. When skewness and kurtosis values are examined, most variables exhibit asymmetric distributions, with some showing positive or negative skewness. For instance, CO_2 Emissions indicate a positively skewed distribution, reflecting an increasing trend. Overall, the statistics highlight challenges in transitioning to renewable energy, the impact of urbanization and rising energy demand on increased reliance on fossil fuels, and the rise in CO_2 emissions. However, increasing investments in renewable energy holds the potential to facilitate a transition toward sustainable energy production.

Data preprocessing is a fundamental step in the development of AI-based models. In this phase, the raw data was transformed into a format suitable for computational processing. Differences in the scales of variables were addressed through normalization, bringing all variables to a standard scale and eliminating inconsistencies. This allowed the AI model to be trained more effectively. Specifically, all values in the dataset were normalized using the min-max normalization method to ensure consistency across variables of different units. The dataset was split into two subsets, with 70% allocated for training and 30% for testing, enabling effective model development and evaluation.

2.2. Adaptive Neuro-Fuzzy Inference System (ANFIS)

Hybrid models that combine different methods have proven effective and successful solutions for solving complex problems. These hybrid structures are designed by considering the strengths and weaknesses of each method and leveraging their complementary features. Hybrid intelligent systems developed in this context are widely used in solving complex problems. The Adaptive Neuro-Fuzzy Inference System (ANFIS), first introduced by Jang in 1991, is a notable example of such hybrid systems. ANFIS is a hybrid artificial intelligence technique that integrates Artificial Neural Networks (ANN) learning capability with the expert

knowledge provision and flexible computation features of Fuzzy Inference Systems (FIS).

Due to their rule-based structure, fuzzy systems lack robust learning capabilities and cannot directly learn complex relationships between inputs and outputs. However, the rule-based nature of these systems facilitates the modelling of linguistic information, enabling better interpretability of models (Teke, 2022; Efe&Efe, 2023). On the other hand, artificial neural networks are highly effective in solving nonlinear problems. ANFIS combines the ability of neural networks to address nonlinear problems with the capacity of fuzzy logic systems to process linguistic expressions. With this structure, ANFIS offers a flexible and interpretable hybrid model (Guleryuz, 2021).

2.3. Particle Swarm Optimization

Particle Swarm Optimization (PSO) is a population-based optimization algorithm developed in 1995 by psychologist James Kennedy and electrical engineer Russell Eberhart. Inspired by the social behaviours of living organisms such as birds, ants, fish, and bees, PSO models the collective behavior of individuals within a swarm. Each moves toward the optimal solution by sharing information and updating their velocity and position based on the best solution observed within the swarm. This mechanism emulates the process of individuals following each other and collectively progressing toward a goal (Guleryuz, 2021).

2.4. Genetic Algorithm

The Genetic Algorithm (GA), classified under evolutionary algorithms, is an optimization method inspired by biological evolution processes. The term "Genetic Algorithm" was first introduced by Bagley in 1967, and its principles were formally defined and applied by John Holland in 1975 (Battle and Vose, 1991; Mitchell, 1998). GA simulates the process of inheritance, natural selection, and mutation observed in biological life. This algorithm iteratively improves solutions by applying evolutionary operations such as crossover and mutation to the genetic codes (chromosomes) representing the solution set.

GA operates through a predefined number of generations until a target fitness value is achieved. In each iteration, genes, the fundamental components of genetic algorithms, are modified through evolutionary operations, and the fitness function is calculated for each solution. The process continues with the selection of suitable solutions and the generation of new populations (Guleryuz, 2021). This method has proven effective in solving nonlinear problems and optimization issues with large search spaces.

2.5. Hybrid PSO-ANFIS and GA-ANFIS Models

Hybrid models are effective tools for improving accuracy in modelling and forecasting processes for complex and nonlinear problems. Hybrid PSO-ANFIS and GA-ANFIS models are innovative approaches that combine the flexibility and interpretability of the Adaptive Neuro-Fuzzy Inference System (ANFIS) with the strengths of optimization algorithms. By integrating the advantages of different methods, these models achieve more efficient results in solving nonlinear problems.

Critical parameters within the ANFIS structure are optimized to enhance hybrid models' performance. These parameters include membership function parameters, fuzzy rules, threshold values, and learning rates related to the training process. Membership function parameters define the shape and boundaries of functions for input variables, while fuzzy rules establish the rule base linking inputs and outputs. Threshold values improve the model's predictive accuracy, and learning rates regulate the adaptation speed during the training process. Optimizing these parameters enhances the accuracy and generalizability of the ANFIS model, leading to more reliable results. Hybrid PSO-ANFIS and GA-ANFIS models offer robust alternatives for solving complex, nonlinear problems and hold significant potential for applications across various disciplines (Basser et al., 2015).

2.5.1. PSO-ANFIS Model

The Particle Swarm Optimization (PSO) algorithm is a population-based technique used to optimize the aforementioned parameters of the ANFIS model. Inspired by the social behaviour of birds and fish, PSO can quickly reach global optima. By updating the velocity and position for each parameter, PSO determines the optimal values for these parameters. The PSO-ANFIS model enhances model accuracy through this optimization process, enabling more effective predictive outcomes.

2.5.2. GA-ANFIS Model

The Genetic Algorithm (GA), inspired by biological evolution, is another optimization method used to optimize the parameters of the ANFIS model. GA iteratively improves parameters using natural selection, crossover, and mutation mechanisms. The GA-ANFIS model leverages GA's global search capabilities to optimize ANFIS parameters, thereby improving accuracy performance. In addition, hybrid PSO-ANFIS and GA-ANFIS models, with their optimized parameters, enhance both accuracy and generalization performance, making them effective solutions for modelling complex systems. The PSO-ANFIS model utilizes the rapid global optimization capabilities of Particle Swarm Optimization,

delivering high-performance solutions with shorter computational times. This feature makes PSO-ANFIS a crucial option, particularly in time-constrained scenarios.

Conversely, the GA-ANFIS model employs the extensive search capabilities of the Genetic Algorithm, offering a robust method for solving complex problems. This model excels in handling large datasets and addressing nonlinear issues. The distinct strengths of both models enable selecting the most appropriate hybrid approach based on the problem type and specific requirements.

3. Findings and Performance Comparisons

The forecasting of CO_2 emissions was examined using the Adaptive Neuro-Fuzzy Inference System (ANFIS) and its optimized versions utilizing Particle Swarm Optimization (PSO) and Genetic Algorithm (GA) approaches. The performance of the developed models was evaluated by visualizing the alignment between actual and predicted values. ANFIS, PSO-ANFIS, and GA-ANFIS models were compared to analyze each model's accuracy and generalization capacities. This study aims to identify methods that provide higher accuracy in CO_2 emission forecasting and offer reliable prediction tools for policymakers.

The ANFIS model generally demonstrates a reasonable alignment between actual and predicted values, although some deviations are observed in its forecasts on test data. In particular, the model's performance in predicting higher CO_2 emissions appears to decline slightly, indicating limitations in capturing the whole variance of the data. This may be attributed to the unoptimized parameters of the ANFIS model, which prevent it from fully realizing its accuracy potential. Nevertheless, the model provides a practical foundational approach for capturing the overall trends in CO_2 emissions. The PSO-ANFIS model demonstrates a more substantial alignment between actual and predicted values, outperforming the ANFIS model in accuracy. The model has successfully predicted CO_2 emissions on the test data, mainly providing more consistent results at medium and high emission levels. This performance highlights the effectiveness of PSO optimization in enhancing the ANFIS parameters, thereby improving the model's accuracy and generalization capability. The model's predictive performance closely parallels the actual values for most data points, showcasing its reliability and robustness. The GA-ANFIS model demonstrates the most substantial alignment between actual and predicted values, achieving the best performance among all the models evaluated. On test data, the model consistently exhibited high accuracy, even at extreme levels of CO_2 emissions. This exceptional performance is attributed to the effective optimization of model parameters through Genetic Algorithm

(GA), which significantly enhanced its predictive capabilities. As a result, the GA-ANFIS model stands out due to its low error rates and superior explanatory power, establishing it as a reliable solution for forecasting CO_2 emissions. Two key evaluation metrics were utilised to assess the model's performance: Mean Squared Error (MSE) and R-squared (R^2). MSE measures the average squared difference between predicted and actual values, with lower MSE values, indicating higher predictive accuracy (Teke vd., 2023; Şen vd., 2023) . On the other hand, R^2 evaluates the proportion of variance in the dependent variable that the model can explain, ranging from 0 (no explanatory power) to 1 (perfect explanatory power). While MSE provides an error-centered perspective, R^2 highlights the model's capacity to explain the variability in the data. Together, these metrics comprehensively evaluate the model's accuracy and explanatory strength. The predictive efficiency of the models is fundamentally dependent on accurately capturing the relationships between inputs and outputs during the training phase. This accurate representation ensures that the model performs satisfactorily during the testing phase. This study allocated 30% of the dataset for testing to evaluate overall model performance. By analyzing the results, the GA-ANFIS model demonstrated its effectiveness in forecasting CO_2 emissions, confirming its potential as a robust and reliable predictive tool. Table 4 provides detailed evaluation metrics for the developed models, presenting their predictive capabilities during both the training and testing phases. These metrics highlight the comparative strengths of the models in forecasting CO_2 emissions.

Table 4. *Performance Metrics of Developed Models for CO_2 Emission Forecasting*

Model	Metrics	Training	Testing
ANFIS	**MSE**	0,01104	0,0526
	R^2	0,97167	0,8489
PSO_ANFIS	**MSE**	0,0062	0,0296
	R^2	0,9841	0,9148
GA_ANFIS	**MSE**	0,00907	0,0205
	R^2	0,97674	0,941

The performance metrics of the three developed models reveal that each model exhibits distinct characteristics and strengths. The ANFIS (Adaptive Neuro-Fuzzy Inference System) model, serving as a baseline approach, demonstrated satisfactory performance in the training and testing phases without optimization. During the training phase, the model achieved an MSE of 0.01104 and an R^2 of 0.97167, indicating its substantial

ability to explain the training data. However, in the testing phase, the MSE increased to 0.05257, and the R^2 decreased to 0.84890, highlighting the model's limited generalization capability compared to the optimized models.

The PSO-ANFIS model (ANFIS optimized using Particle Swarm Optimization) displayed significantly improved performance in both the training and testing phases. During the training phase, the MSE decreased to 0.00620, and the R^2 increased to 0.98410, surpassing the explanatory power of the baseline ANFIS model. In the testing phase, the MSE further decreased to 0.02963, and the R^2 increased to 0.91483. These results demonstrate the effectiveness of the PSO algorithm in optimizing ANFIS model hyperparameters, reducing error rates, and enhancing the model's generalization ability.

The GA-ANFIS model (ANFIS optimized using Genetic Algorithm) emerged as the best-performing model, particularly in the testing phase. The MSE was measured at 0.00907 during training, and the R^2 was 0.97674. In the testing phase, the model achieved the lowest MSE of 0.02054 and the highest R^2 of 0.94097 among all models, indicating its superior explanatory power. These findings underscore the capability of the GA method to optimize hyperparameters effectively, resulting in low error rates and high generalization capacity. Although the GA-ANFIS model showed slightly lower performance during training than the PSO-ANFIS model, its exceptional performance during testing established it as the best overall model.

In conclusion, the GA-ANFIS model is considered the most suitable model due to its superior generalization capability in the testing phase. However, the PSO-ANFIS model, which exhibited strong results during training, can serve as a robust alternative for specific applications. The ANFIS model, while functional as an unoptimized baseline, generally underperformed compared to the optimized models. These analyses demonstrate the critical role of hyperparameter optimization in enhancing the performance of ANFIS models. Visualizing the error rates provides a more straightforward depiction of the models' performance. Accordingly, the error rates are illustrated in Figure 4.

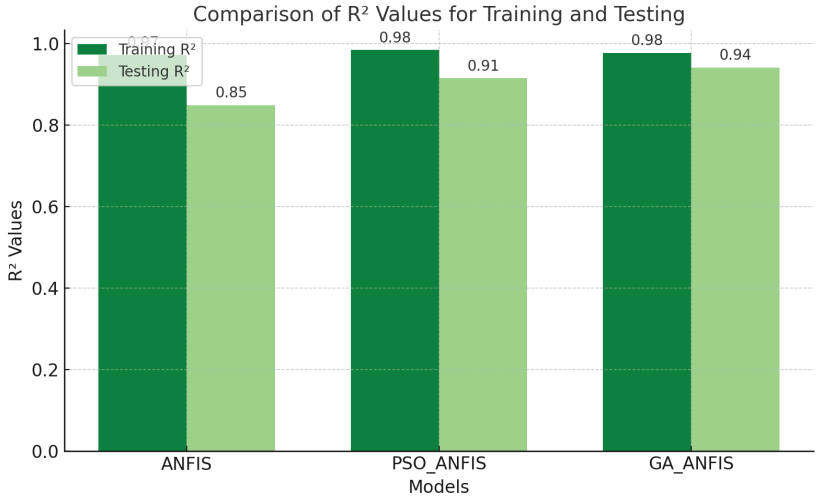

Figure 4. *Comparison of R² Values Among Models*

The graphical comparison indicates that the optimized models (PSO-ANFIS and GA-ANFIS) outperformed the baseline ANFIS model. Among these, the GA-ANFIS model demonstrated the highest generalization capability during the testing phase, achieving the lowest MSE (0.02054) and the highest R^2 (0.94097). The PSO-ANFIS model, while excelling in training phase performance, also exhibited substantial improvements compared to the baseline model. The baseline ANFIS model, due to the lack of optimization, delivered limited success in both phases. Overall, the GA-ANFIS model is the most effective, while the PSO-ANFIS model presents itself as a strong alternative.

4. Conclusion

The findings of this study provide significant insights into the applicability of hybrid approaches in fields such as energy management, financial analysis, and environmental modelling. ANFIS and optimization methods (such as PSO and GA) are widely used in modelling complex and nonlinear systems. These approaches demonstrate high accuracy and generalization capacity, delivering effective results in energy consumption forecasting, financial market analysis, medical diagnostic systems, agricultural yield prediction, and environmental modelling. The performance improvements achieved by hybrid models (PSO-ANFIS and GA-ANFIS) compared to the baseline ANFIS model enable more reliable predictions and analyses through parameter optimization.

This study showed that optimized hybrid models achieved significant

improvements in both the training and testing phases compared to the baseline ANFIS model. Among the models analyzed, GA-ANFIS emerged as the most effective model, with its low error rate and superior generalization capacity. These findings underscore the substantial potential of hybrid approaches in solving complex real-world problems. Future studies could focus on improving the performance of these models on larger datasets and integrating them with advanced techniques such as artificial neural networks or deep learning methods. Specifically, ANFIS models combined with deep learning techniques are expected to handle high-dimensional and complex datasets more effectively. Additionally, alternative metaheuristic algorithms, such as artificial bee colony optimization, genetic programming, or quantum algorithms, could introduce new solutions to tackle more complex problems. Furthermore, integrating cloud computing and AI-driven automation technologies could enhance the scalability and applicability of these models to large-scale datasets and make them accessible to a broader user base.

In conclusion, hybrid PSO-ANFIS and GA-ANFIS models are robust methods for addressing theoretical and practical problems. In the future, focusing on comparing different optimization techniques, enhancing model performance on big data, and integrating hybrid AI approaches will contribute to advancing research in this promising field.

Acknowledgements

We thank the TÜBİTAK 2209-A University Students Research Projects Support Program for their support under Application No: 1919B012205909.

References

AlOmar, M. K., Hameed, M. M., Al-Ansari, N., Mohd Razali, S. F., & AlSaadi, M. A. (2023). Short-, Medium-,and Long-Term Prediction of Carbon Dioxide Emissions using Wavelet-Enhanced Extreme Learning Machine. In Civil Engineering Journal (Vol. 9, Issue 4, pp. 815–834). Ital Publication. https://doi.org/10.28991/cej-2023-09-04-04

Basser, H., Karami, H., Shamshirband, S., Akib, S., Amirmojahedi, M., Ahmad, R., Jahangirzadeh, A., & Javidnia, H. (2015). Hybrid ANFIS–PSO approach for predicting optimum parameters of a protective spur dike. In Applied Soft Computing (Vol. 30, pp. 642–649). Elsevier BV. https://doi.org/10.1016/j.asoc.2015.02.011

Battle, D. L., & Vose, M. D. (1991). Isomorphisms Of Genetic Algorithms. In Foundations of Genetic Algorithms (pp. 242–251). Elsevier. https://doi.org/10.1016/b978-0-08-050684-5.50018-5

Chiu, Y.-J., Hu, Y.-C., Jiang, P., Xie, J., & Ken, Y.-W. (2020). A Multivariate Grey Prediction Model Using Neural Networks with Application to Carbon Dioxide Emissions Forecasting. In T. Balezentis (Ed.), Mathematical Problems in Engineering (Vol. 2020, pp. 1–10). Hindawi Limited. https://doi.org/10.1155/2020/8829948

ÇŞİDB (Türkiye Cumhuriyeti Çevre Şehircilik ve İklim Değişikliği Bakanlığı) (2023). Güncellenmiş birinci ulusal katkı beyanı. *Güncellenmiş Birinci Ulusal Katkı Beyanı*. https://iklim.gov.tr/db/turkce/dokumanlar/turkiye-cumhuriyeti--8230-102-20230512125223.pdf

Efe, B., & Efe, Ö. F. (2023). Fine-Kinney method based on fuzzy logic for natural gas pipeline project risk assessment. *Soft Computing, 27*(8), 16465–16482. https://doi.org/10.1007/s00500-023-09108-6

Efe, B., Efe, Ö. F., & Ishizaka, A. (2022). A model proposal to examine the effects of ships to marine pollution in terms of internal and external factors. *Soft Computing, 26*(4), 2121–2134. https://doi.org/10.1007/s00500-021-06626-z

Güleryüz, D. (2021). Determination of industrial energy demand in Turkey using MLR, ANFIS and PSO-ANFIS. *Advances in Intelligent Systems, 3*, 16–34. https://doi.org/10.33969/AIS.2021.31002

Güleryüz, D., & Özden, E. (2023). Tarımsal veriler ışığında sürdürülebilir su yönetimi: Makine öğrenmesi tahmin modelleri. In İ. Cengizler & S. Duman (Eds.), *Sürdürülebilirlik ve Su Yönetimi* (pp. 135–153). Duvar Yayınları. https://doi.org/978-625-6585-92-8

Hamrani, A., Akbarzadeh, A., & Madramootoo, C. A. (2020). Machine learning for predicting greenhouse gas emissions from agricultural soils. In Science

of The Total Environment (Vol. 741, p. 140338). Elsevier BV. https://doi.org/10.1016/j.scitotenv.2020.140338

Işık, N., & Kılıç, E. (2014). Ulaştırma sektöründe CO_2 emisyonu ve enerji Ar-Ge harcamaları ilişkisi. Sosyoekonomi Dergisi, 21(1), 45-58

Liu,X. (2024).CO2 emissions prediction based on regression, neural network and SVM.Applied and Computational Engineering,54,98-103

Manvitha, M. S., Vani Pujitha, M., Prasad, N. H., & Yashitha Anju, B. (2023). A Predictive Analysis on CO2 Emissions in Automobiles using Machine Learning Techniques. In 2023 International Conference on Intelligent Data Communication Technologies and Internet of Things (IDCIoT) (pp. 394–401). https://doi.org/10.1109/idciot56793.2023.10053539

Meng, Y., & Noman, H. (2022). Predicting CO_2 Emission Footprint Using AI through Machine Learning. *Atmosphere*, *13*(11), 1871. https://doi.org/10.3390/atmos13111871

Mitchell, M. (1998). *An introduction to genetic algorithms.* MIT Press.

Mogno, C., Fontaras, G., Arcidiacono, V., Komnos, D., Pavlovic, J., Ciuffo, B., Makridis, M., & Valverde, V. (2022). The application of the CO2MPAS model for vehicle CO2 emissions estimation over real traffic conditions. In Transport Policy (Vol. 124, pp. 152–159). Elsevier BV. https://doi.org/10.1016/j.tranpol.2020.01.005 Nassef, A. M., Olabi, A. G., Rezk, H., & Abdelkareem, M. A. (2023). Application of Artificial Intelligence to Predict CO2 Emissions: Critical Step towards Sustainable Environment. Sustainability, 15(9), 7648. https://doi.org/10.3390/su15097648

Özbek, A., & Teke, Ç. (2024). Prediction of Turkey's cotton sock exports to Germany using deep learning approach. Tekstil Ve Mühendis, 31(135), 174-181. https://doi.org/10.7216/teksmuh.1486577

Özden, E. (2022a). Forecasting of export volume using artificial intelligence based algorithms. *Bitlis Eren Üniversitesi Fen Bilimleri Dergisi, 11*(2), 715–726. https://doi.org/10.17798/bitlisfen.1107311

Özden, E. (2022b). The Dynamics Affecting the Export-Import Ratio in Turkey: A Hybrid Model Proposal with Econometrics and Machine Learning Approach. *Journal of Economic Policy Researches*, *9*(2), 265-291. https://doi.org/10.26650/JEPR1088322

Özkurt, C. (2024). Environmental Sustainability through AI: A Case Study on CO2 Emission Prediction. *ADBA Computer Science*, *1*(1), 19-25.

Sidana, S. (2024). Grid Search Optimized Machine Learning based Modeling of CO2 Emissions Prediction from Cars for Sustainable Environment. In

International Journal of Current Science Research and Review (Vol. 07, Issue 09). Everant Journals. https://doi.org/10.47191/ijcsrr/v7-i9-37

Şen, H., Efe, Ö. F., & Efe, B. (2023). Estimation Of Occupational Accidents In Turkey Until 2030. *Natural Resources and Technology*, *17*(1), 26–32.

Teke, Ç. (2022). Bireylerin Koroner Arter Hastalığı Risk Seviyesinin Bulanık Uzman Sistem Yaklaşımı İle Belirlenmesi. Journal of Intelligent Systems: Theory and Applications, 5(2), 153-160. https://doi.org/10.38016/jista.1144535

Teke, Ç., Akkurt, I., Arslankaya, S., Ekmekci, I., & Gunoglu, K. (2023). Prediction of gamma ray spectrum for 22Na source by feed forward back propagation ANN model. In Radiation Physics and Chemistry (Vol. 202, p. 110558). Elsevier BV. https://doi.org/10.1016/j.radphyschem.2022.110558

TÜİK. (2023). *Sera gazı emisyonları: Türkiye ve dünya kişi başına düşen emisyon oranlarının karşılaştırılması (2018-2022)* [Grafik]. Veri kaynağı: https://data.tuik.gov.tr/Bulten/Index?p=Sera-Gazi-Emisyon-Istatistikleri-1990-2022-53701

Wordbank (2023)., Data Bank, https://databank.worldbank.org/

Chapter 7

AI-ENHANCED BIOMECHANICS: ADVANCING FINITE ELEMENT ANALYSIS FOR SIMULATION AND OPTIMIZATION

Hamid Zamanlou[1]

Filiz KARABUDAK[2]

1 Dr., Ataturk University, Faculty of Engineering, Departmant of Mechanichal engineering, ORCID: 0000-0002-9780-8924

2 Associate professor, Gumushane University, Faculty of Engineering and Natural Science, Departmant of Mechanichal Engineering, ORCID: 0000-0002-7365-0333

1. Introduction

Biomechanics is an interdisciplinary field that applies principles of mechanical engineering, physics, and biology in the study of forces and motions within living organisms. The ultimate goal of biomechanics is to understand the mechanical behavior of bio-logical tissues, organs, and systems, and to apply this knowledge in solving real-world problems in medicine, sports science, and rehabilitation. From designing prosthetics to understanding the mechanism of musculoskeletal injuries, to optimizing the rehabilitation protocols, biomechanics plays an important role in improving human health. The field has grown leaps and bounds during the past few decades due to its amalgamation with computational method advancements, improved imaging technology, and enhanced material science. The most widely used computa-tional tool applied in biomechanics is Finite Element Analysis (FEA), allowing for the detailed simulation of mechanical behavior in bio-logical systems.

FEA is a numerical method that splits a complex structure into a finite number of smaller elements, each of which can be ana-lyzed independently to solve the governing equations of motion or deformation. By assembling the results from each element, FEA provides an approximate solution for the entire system. In biomechanics, FEA is widely applied to model a wide variety of biological systems, such as bones, cartilage, muscles, ten-dons, ligaments, and implants. For example, FEA is often utilized to simulate deformation and stress distribution in bones and joints for a variety of load conditions. These are very useful in optimizing implant design and interpreting the mechanisms of degeneration in joints. Similarly, FEA can model soft tissue behav-ior, such as the stretching and compression of muscles and liga-ments, providing insights into their mechanical properties and response to physical forces (Mononen etal., 2024).

While FEA has revolutionized the field of biomechanics, there are significant challenges associated with its application, particu-larly when it comes to the complexity and heterogeneity of bio-logical tissues. Biological tissues exhibit highly nonlinear, time-dependent, and often anisotropic material properties, making it difficult to accurately model their behavior using traditional FEA approaches. Moreover, creating accurate FEA models re-quires detailed geometrical and anatomical data, which are often difficult to obtain. For instance, detailed 3D models of organs and tissues require advanced imaging techniques like MRI, CT scans, or ultrasound, and their interpretation for simulation purposes can be a source of delays and mistakes. Moreover, the computational cost of solving large-scale FEA problems may be prohibitively high, especially when sensitivity analyses or optimizations are carried out that require the running of several simulations.

Artificial Intelligence, and more precisely Machine Learning and Deep Learning, are promising solutions to these challenges, enhancing and augmenting traditional FEA techniques. AI refers to algorithms and models that can enable machines to perform tasks that normally require human intelligence, such as learning from data, recognizing patterns, and making predictions. In a biomechanical context, AI can be used to enhance FEA simulations in various ways: from accelerating the creation of anatomical models from imaging data to the optimization of biomechanical designs and the forecast of outcomes based on historical data. Machine learn-ing algorithms can help in identifying material properties and creating predictive models for tissue behavior, while deep learn-ing techniques can extract complex features from medical imag-es, allowing for automatic segmentation and modeling of ana-tomical structures. Furthermore, AI-driven surrogate models can approximate the output of FEA simulations, reducing computa-tional time and cost while maintaining accuracy (Zhao etal., 2024).

The integration of AI into biomechanics, especially in combination with FEA, has enormous potential to change the face of this field. Machine learning techniques can contribute to the improvement of material models for biological tissues by learning directly from experimental data and providing more accurate and patient-specific predictions of tissue behavior. Furthermore, deep learning algorithms have significantly revolutionized image analysis and segmentation by accelerating the creation of 3D anatomical models from medical scans that can be used directly in FEA simulations. AI-based optimization algorithms will be able to find for them the best designs of implants, prosthetics, or surgical interventions that offer optimal clinical outcomes. This can consider a vast range of design variables that it would otherwise be computationally expensive to analyze manually.

Perhaps one of the most exciting things about AI in the field of biomechanics has to do with real-time simulations and personalized healthcare. Traditional FEA simulations are very computationally expensive and require much time; thus, their application in real-time applications is limited. In contrast, AI-enhanced simulations-especially by using surrogate models-can be executed much faster, and therefore real-time analysis for personalized medical applications can be made possible. For instance, AI may allow for on-the-fly biomechanical simulations to help surgeons make better decisions during operations on how to place an implant or manipulate tissue in real time. Moreover, AI can play a key role in the design of personalized implants and prosthetics, using patient-specific data to create optimized devices that more closely match the biomechanical properties of individual patients, thus leading to better functional outcomes.

Despite the enormous promise of AI for enhancing biomechanics, significant challenges remain. One of the main challenges is the requirement for high-quality, diverse datasets that truly reflect the complexity and variability of biological systems. In biomechanics, data acquisition is often expensive, time-consuming, and limited in scope, especially regarding medi-cal imaging and biomechanical testing. Moreover, the variability between individuals concerning anatomical structures, tissue properties, and mechanical response adds another layer of com-plexity to developing AI models. Another challenge is interpretability and explainability of AI models, especially deep learning-based models. Though highly accurate, their "black-box" nature makes it difficult sometimes for the clinicians and researchers to understand how they reached their conclusions, hence limiting their adoption in real-world medical applications. In addition, ethical issues arise when AI is integrated into clinical practice: data privacy, algorithmic bias, and the over-reliance on automated systems.

This paper explores the intersection of AI and biomechanics, focusing on the ways in which AI can enhance and optimize FEA for biomechanical simulations. We will review key AI techniques, including machine learning, deep learning, and reinforcement learning, and discuss their applications in the de-velopment of biomechanical models, optimization of designs, and prediction of outcomes. We will illustrate, by case studies and examples, how AI is already being applied in areas such as implant design, soft tissue modeling, and injury prevention, and highlight challenges and future directions of AI in bio-mechanics. We will also present the implications of AI-enhanced biomechanics in view of the future of personalized medi-cine, rehabilitation, and clinical practice.

In summary, AI-enhanced biomechanics represents a paradigm shift in how we approach the modeling, simulation, and optimi-zation of biological systems. It has the potential to increase the accuracy, efficiency, and personalization of biomechanical analyses by incorporating the power of ma-chine learning, deep learning, and computational modeling into AI. This, in turn, will contribute to improved medical outcomes, optimized implants, and better treatment strategies. However, for AI to fully realize its potential in biomechanics, efforts must be directed at surmounting challenges related to data quality, model interpretability, and ethical considerations, with a view to integrating AI solutions in a manner that benefits both patients and healthcare professionals.

2. Role of Finite Element Analysis in Biomechanics

FEA is a computational technique that has been widely used to simulate the mechanical behavior of biological systems, such as bones, soft tissues, and implants. FEA divides a structure into a finite number of small-

er elements, solves the governing equations of motion or deformation for each element, and then assembles the results to obtain a global solution for the entire system.

In biomechanics, a wide range of me-chanical behaviors has been simulated with FEA: from stress and strain distributions to material properties and deformations of tissues and implants. Some examples include bone deformations in various loading conditions, through which optimal implant performance may be designed. Similarly, FEA can be performed to simulate the behavior of soft tissues under physiological loads, thereby enabling insight into tissue response to external forces.

Traditional FEA approaches have a number of challenges in biomechanics despite their widespread use. First, the major problem is that the biological system usually possesses nonlinear material properties, time-dependent behaviors, and large deformations. Besides, detailed anatomical data is required to accurately model the biological structure, which is not always available. Finally, solving large-scale FEA problems can be computationally expensive, especially when multiple simulations are needed for optimization purposes.

These challenges can potentially be addressed by AI through enhancing FEA with data-driven approaches, improving model accuracy, and reducing computational cost. In the following sec-tions, we discuss how AI techniques can be applied to enhance FEA in biomechanics.

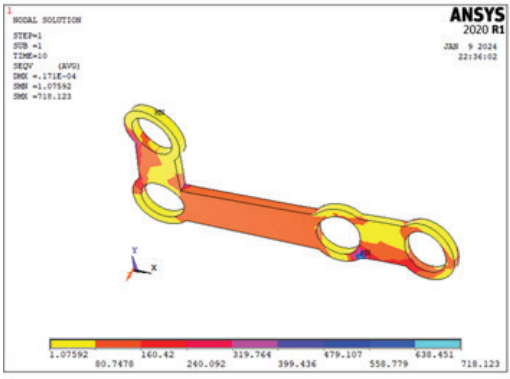

Figure 1. *FEM Analysis of Patient-Specific Biomechanical Implants*

3. AI Techniques in Biomechanics

AI techniques, especially ML and DL, have proven to be effective in enhancing both the accuracy and efficiency of biomechanical simulations (Molavian, 2023). Applications range from model creation, parameter estimation, to simulation optimisation in an FEA process.

3.1. Machine Learning for Model Development

Machine learning algorithms have the potential to improve the development of biomechanical models by learning knowledge from experimental data. Traditional FEA usually determines material properties by predefined mathematical models or experimental data from literature (Bishop, 2013). However, material properties of biological tissues such as bones, tendons, and cartilage vary significantly among individual people, which makes it difficult to simulate these tissues accurately.

ML algorithms, including regression models, support vector machines, and random forests, can learn the material properties of biological tissues from experimental data. For example, ML models trained on mechanical test data, such as stress-strain curves, can predict the behavior of tis-sues under various loading conditions. This approach allows for the development of more accurate and personalized models that can be incorporated into FEA simulations.

3.2. Deep Learning for Image-Based Modeling

Deep learning approaches, especially convolutional neural networks (CNNs), have proven their power in the feature extraction of medical images such as MRI and CT for biomechanical model development. These medical images contain rich information regarding anatomy and geometry that forms a critical basis for making authentic FEA models (Hu etal., 2018).

Automatic medical image segmentation with identification of bones, muscles, and other key anatomical structures can be done by training CNNs. The automatic segmentation significantly reduces the time and effort needed to create FEA models from medical images. More importantly, direct prediction of tis-sue properties and mechanical behavior directly from imaging data is also possible using CNNs, increasing the accuracy of biomechanical simula-tions.

3.3. Surrogate Models for Simulation Acceleration

One of the key challenges of FEA in biomechanics is the compu-tational cost of solving large-scale simulations, particularly when optimization or sensitivity analysis is required. Running multiple simulations to explore different design configurations or loading conditions can be prohibitively expensive. AI techniques, such as surrogate models and neural networks, can be used to approxi-mate FEA results, significantly reducing the computational cost (Tresidder etal., 2012).

Simplified models, often referred to as surrogate models, provide approximations for a given complex simulation model's output. Such models

might be trained from data at a limited number of FEA solutions and subsequently utilized in prediction at several other needed values, without requiring any new solving of the governing equations. GPR, RBF, and DNNs are some of the techniques that can be used to generate surro-gate models of biomechanical systems. These surrogate models can be utilized within optimization algorithms for the fast exploration of design spaces and to find optimal solutions.

3.4. Reinforcement Learning for Optimization

Reinforcement learning is a paradigm of machine learning concerned with learning optimal actions through trial and error. In the context of biomechanics, reinforcement learning can be used to optimize designs such as implant shapes or prosthetics by interacting with a simulation environment. The RL agent explores different design configurations and receives feedback based on the performance of the design in biomechanical simulations.

It may, for instance, apply RL in geometry optimization of an orthopedic implant to ensure peak performance for any particular loading scenario, whether that be minimization of stress concentration or maximization of mechanical stability. RL can also be used to optimize surgical procedures, such as the placement of implants or joint alignment, by learning the most effective strategies from biomechanical simulations (Powell etal., 2020).

3.5. Hybrid AI-Driven Optimization

AI techniques can further be combined with traditional optimization algorithms to enhance the design and optimization of biomechanical systems. For example, genetic algorithms and particle swarm optimization are most commonly implemented with machine learning models to sweep through large design spaces to come up with the most optimal solution. AI-powered optimization can be used within a wide range of applications in biomechanics to arrive at an optimal solution for prosthetic limbs, implants, and surgical procedures (Patil, 2023).

4. Case Studies in AI-Enhanced Biomechanics

4.1. Implant Design and Optimization

One of the most prominent applications of AI in biomechanics is in the design and optimization of implants, such as orthopedic and dental implants. FEA simulations are commonly used to assess the mechanical performance of implants under physiologi-cal loads. However, the complexity of biological systems and the need for personalized designs often make traditional FEA ap-proaches time-consuming and computationally expensive.

AI-augmented FEA techniques have the potential to greatly enhance the im-plant design process. For instance, machine learning algorithms can be employed to forecast the material properties at the bone-implant interfaces, whereas deep learning models can automatically segment CT or MRI scans to generate personalized 3D models of pa-tients' anatomy. Reinforcement learning can then be applied to optimize the implant geometry for the best mechanical performance.

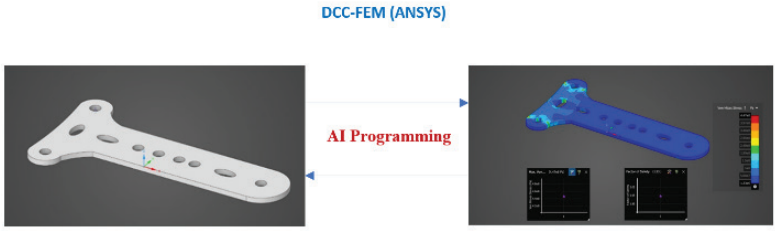

Figure 2. *Schematic view of AI usage in biomechanical analysis*

4.2. Soft Tissue Modeling

Modeling soft tissue is a very special challenge in biomechanics due to the highly nonlinear and time-dependent behavior of tissuessuch as muscles, tendons, and ligaments. Traditional FEA models for soft tissues often rely on simplifying assumptions about material properties, which may not accurately reflect the true behavior of these tissues (Tang, 2023).

The use of AI techniques allows the identification of tissue properties from experimental data in order to enhance the accuracy of soft tissue models. Machine learning algorithms, including support vector machines or neural networks, can be trained on data from mechanical tests to predict the behavior that soft tissues will exhibit given different loading condi-tions. On the other hand, deep learning models can also be employed for the segmentation and identification of key soft tissue struc-tures from medical images, hence enhancing the accuracy of FEA simulations.

4.3. Injury Prediction and Prevention

AI-enhanced biomechanics can also play an important role in injury prediction and prevention. By analyzing data from biomechanical simulations, AI models are able to identify risk factors for injury, such as abnormal joint mechanics or excessive stress on tissues. Such insights can be used in order to design personalized injury prevention strategies, including custom orthotics or targeted exercises.

Reinforcement learning can optimize rehabilitation protocols by learning the most effective strategies for recovering from injury. AI models can also be utilized to analyze real-time biomechanical data coming from wearable devices, which can provide feedback on movement patterns and injury risk to athletes and patients (Herasevich etal., 2024).

5. Challenges and Future Directions

Despite the huge promise of AI-enhanced biomechanics, several challenges remain. One of the most important problems is the need for high-quality and diverse datasets to train machine learning mod-els. In biomechanics, experimental data is often hard to obtain due to the complexity of biological systems and variability among individuals.

Other challenges include interpretability of AI models, especially deep learning models. Although these models provide accurate predictions, understanding how they reach their conclusions is often hard. This can limit the application of AI in clinical settings where transparency and trust are required.

Ethical considerations also dominate in AI-enhanced biomechanics, especially in those cases applied to medical fields: ensuring patient privacy, avoiding bias in models, and considering the implications of AI decision-making. Some key areas that need consideration.

6. Conclusion

The integration of AI into biomechanics, especially through the enhancement of FEA, holds transformative potential to advance our understanding of biological systems and improve a wide range of medical applications. The adoption of AI-driven methods in biomechanics has already started to revolutionize traditional computational techniques by providing more efficient, accurate, and personalized simulations. These advances are improving the design of prosthetics, implants, and medical devices, and at the same time promoting better clinical decision-making, strategies for injury prevention, and rehabilitation protocols.

Standing at the heart of these revolutionary changes are AI techniques-ML, DL, and RL-which basically complement and optimize the process of FEA. Machine learning algorithms have been able to enhance the accuracy of biomechanical models by learning from experimental data directly, thus avoiding the need for highly simplifying assumptions or generalized material models. Similarly, deep learning models, especially convolutional neural networks, are drastically improving speed and accuracy in image-based segmentation, which in turn permits the efficient creation of personalized 3D models from medical imaging data. This enables real-time biomechanical simulations that are personalized to the specific

needs and anatomy of individual patients, which is important for personalized medicine. The recent rapid developments in AI have also enabled the creation of surrogate models, which significantly reduce the computational cost of running large-scale FEA simulations, thus accelerating the optimization of designs and allowing near real-time decision-making.

Beyond this, AI-driven optimization algorithms, for example, reinforcement learning (RL), improve the state of the art in designing biomimetic devices and structures. In applications ranging from implant design to orthopedic prosthetics and even surgical procedures, AI-based optimization methods can investigate much larger design spaces and can identify superior configurations that might have been prohibitively costly computationally with traditional FEA methods. These algorithms can help determine the most efficient and biomechanically sound solutions by continuously learning from previous simulations and providing real-time adjustments in designs. This is an important advance because it enables the clinicians and engineers to customize medical devices and interventions according to unique anatomical and mechanical properties of each particular patient, thus improving the functional outcomes and reducing the risks of complications.

AI's role in biomechanics extends beyond the engineering of devices to include critical areas of clinical application. For in-stance, AI-enhanced biomechanics can be used to predict mus-culoskeletal injuries by analyzing motion data and biomechanical simulations to identify abnormal stress distributions or move-ment patterns that could lead to injury. With the aid of real-time AI-based models, clinicians can offer personalized injury preven-tion strategies for athletes or patients recovering from surgeries. These AI-driven models not only provide insight into the me-chanical conditions that lead to injury but also allow for the de-sign of tailored rehabilitation protocols, making sure patients are guided through recovery with optimized evidence-based treat-ment plans.

Despite the obvious advantages that AI brings to biomechanics, challenges persist which must be overcome if the full potential of AI-enhanced biomechanics is to be achieved. The first major challenge is the demand for high-quality, varied, and large datasets. AI models, mainly deep learning algorithms, heavily rely on data. This variability in biological systems-either in terms of tissue properties, anatomical structure, or mechanical response-presents one of the major challenges of dataset acquisition that are truly representative of real-world variability. Most critically, these datasets need to reflect many different age groups, genders, and ethnicities so as not to bias the algorithms of AI models, yield incorrect results, and propagate health disparities. Although vast improvements have been made for medical imaging data, bio-mechanical testing, and patient outcomes, getting

high-quality and sufficient data stands out as one of the most important challenges in further scaling AI-driven biomechanics.

Another challenge arises in the interpretability and explainability of AI models. Deep learning models, though achieving high levels of accuracy, are usually "black-box" and hardly understandable by researchers, clinicians, and patients for the decision-making process behind the model outputs. In biomechanics, where safety and clinical outcomes are paramount, interpretability and the ability to explain how a model arrives at a particular conclusion are key in the adoption and trust of these AI-based tools. This lack of interpretability can limit the widespread use of AI in clinical settings, as healthcare professionals must have con-fidence in the recommendations made by these models. Therefore, future research will need to concentrate not only on enhancing the performance of AI models but also on developing methods for improving the transparency and interpretability of models without sacrificing accuracy.

Besides this, ethical issues using AI in biomechanics have to be discussed. In fact, with the clinical practice of integrating AI, critical issues related to the privacy of patients, the security of data, and possible biased decision-making should be of great concern. The sensitive nature of medical data requires compliance with strict privacy regulations and security measures to ensure the confidentiality of patients. In addition, AI models may result in suboptimal predictions or unfair ones due to biases learned from the dataset on which they were trained, especially when the variety in training datasets is at a minimum. As such, it is important, as AI models are utilized in medical applications, to prioritize the mitigation of bias and fairness in predictions and decisions. Moreover, the role that AI plays in healthcare decisions should always be seen as complementary and not the replacement of human expertise. AI should be used in augmenting the decision capabilities of healthcare professionals by offering data-driven insights to enhance the care of patients, not making decisions on their own.

The future of AI applications in biomechanics likely will expand into new territories as the field continues evolving. Integration of AI with the latest technologies, such as 3D printing, wearable sensors, and augmented reality, could create more sophisticated systems for designing and testing bio-mechanical devices. For example, AI-driven simulations could be combined with 3D printing for personalized im-plants and prosthetics, optimized in real time for a given individual's specific anatomical and biomechanical properties. Similarly, wearable sensors could continuously collect data on a patient's biomechanical movements, feeding that data back into AI models to provide real-time feedback and adjustments to rehabilitation protocols or injury prevention strategies. The future of AI-enhanced biomechanics is bright, with the potential to create highly personalized

and adaptive healthcare solutions that cater to the unique needs of each individual.

In summary, AI-enhanced biomechanics represents a quantum leap in our capabilities to simulate, optimize, and understand the mechanical behavior of biological systems. By incorporating machine learning, deep learning, and other AI techniques into more traditional biomechanical approaches such as FEA, we are entering a new frontier of personalized medicine and medical device optimization. However, it might also improve how AI operates in the sphere of accu-racy and efficiency with regard to biomechanical modeling of injury occurrence, clinical decision-making, prevention, and rehabilitation. Further research is needed for resolving other big challenges: the quality of data, explainability of the models, ethical concerns. Nevertheless, due to continued development in related technologies, AI will radically enhance outcomes for patients through further biomedical innovations. As AI continues to be integrated into both biomechanical research and clinical settings, it will drive innova-tions that will lead, in turn, to effective treatments, better surgical outcomes, and a more personalized way of caring for patients.

References

Mononen, M. E., Turunen, M. J., Stenroth, L., Saarakkala, S., & Boesen, M. (2024). Biomechanical modeling and imaging for knee osteoarthritis–is there a role for AI?. Osteoarthritis Imaging, 4(2), 100182.

Zhao, Z., & Xing, X. (2024). Design of an AI-Enhanced Medical Research-Informed Multi-Sensor-Based Online Physical Education Motion Capture System.

Rawlings, G., Montalvo, F., Thai, P., Stephens, P., Guillén, I., & Mehta, Y. (2024, August). Leveraging AI to Improve Task-specific Biomechanical Safety Instructions. In Proceedings of the Human Factors and Ergonomics Society Annual Meeting (p. 10711813241275939). Sage CA: Los Angeles, CA: SAGE Publications.

Molavian, Rozhin, et al. "Artificial intelligence approach in biomechanics of gait and sport: a systematic literature review." Journal of Biomedical Physics & Engineering 13.5 (2023): 383.

Bishop, C. M. (2013). Model-based machine learning. Philosophical Transactions of the Royal Society A: Mathematical, Physical and Engineering Sciences, 371(1984), 20120222.

Hu, Z., Tang, J., Wang, Z., Zhang, K., Zhang, L., & Sun, Q. (2018). Deep learning for image-based cancer detection and diagnosis– A survey. Pattern Recognition, 83, 134-149.

Tresidder, E., Zhang, Y., & Forrester, A. I. (2012). Acceleration of building design optimisation through the use of kriging surrogate models. Proceedings of building simulation and optimization, 2012, 1-8.

Powell, K. M., Machalek, D., & Quah, T. (2020). Real-time optimization using reinforcement learning. Computers & Chemical Engineering, 143, 107077.

Patil, K., & Desai, B. (2023). AI-Driven Adaptive Network Capacity Planning for Hybrid Cloud Architecture. MZ Computing Journal, 4(2).

Tang, Y., Liu, S., Deng, Y., Zhang, Y., Yin, L., & Zheng, W. (2021). An improved method for soft tissue modeling. Biomedical signal processing and control, 65, 102367.

Herasevich, S., Schulte, P. J., Hogan, W. J., Alkhateeb, H., Zhang, Z., White, B. A., ... & Yadav, H. (2024). Lung injury prediction model in bone marrow transplantation: a multicenter cohort study. American journal of respiratory and critical care medicine, 209(5), 543-552.

Chapter 8

OPTUNA AND TABNET APPROACH TO FETAL HEALTH CLASSIFICATION

Naciye Nur ARSLAN[1]

1 Res. Asst., naciye.arslan@dpu.edu.tr

INTRODUCTION

Monitoring fetal health is critical to protecting maternal and fetal health. Cardiotocogram (CTG) data assesses fetal condition by recording fetal heart rate, uterine activity, and other vital parameters. Analysis of this data is critical to detect possible prenatal complications and provide timely interventions. This study aims to classify fetal health into three main classes using CTG data: normal, suspicious, and pathological. The TabNet model, which is particularly effective on tabular data, was preferred for classification. TabNet is a model that combines the learning capabilities of decision trees using deep learning techniques. These features provide advantages in understanding complex dataset relationships and exhibiting high performance in various classification tasks.

The imbalance problem in the dataset was addressed by the Random OverSampling method. An imbalanced data distribution is characterized by some classes being overrepresented compared to others, which can negatively affect the model's performance. Random OverSampling provides a balanced representation for each class during the model's learning process by expanding the dataset with more examples of minority classes. Thus, the model could learn various classes better and make accurate predictions.

The model's hyperparameter optimization was performed using the Optuna library. Optuna allows users to define hyperparameter search spaces and uses advanced Bayesian optimization techniques to maximize performance. This process increased the overall performance of the model by determining the best hyperparameter combinations of the model.

The study applied a 5-fold stratified cross-validation method to ensure the model's validity. This method preserves the class distribution of the data set in each fold, allowing the model to provide more reliable and generalizable results. Cross-validation is essential for optimizing the model's training and testing processes. The results show that CTG data can be effectively classified with this approach.

The findings reveal that TabNet and Optuna provide an effective solution for monitoring fetal health and early detection of possible health problems. Thus, this study aims to contribute to developing fetal health monitoring processes and protecting maternal and infant health.

1. Deep Learning Based Fetal Health Classification

Every day in 2020, nearly 800 women died from preventable causes related to pregnancy and childbirth. Maternal death occurred almost every two minutes in 2020, and almost 95% of all maternal deaths occurred in low- and lower-middle-income countries (World Health Organization, 2020). These deaths, many of which are preventable, require the development

of more effective methods for monitoring maternal and child health. In this context, CTG devices offer an effective and economical solution for evaluating fetal health. CTG collects fetal heart rate, movements, and uterine contractions using ultrasound waves, providing essential clues about maternal and fetal health (Rahmayanti et al., 2021). This study aims to classify fetal health status and detect possible anomalies using CTG data. However, CTG data usually have a high-dimensional and complex structure, which makes it difficult to perform accurate classification and evaluation. In addition, unbalanced data distribution can negatively affect the performance of classification models due to some classes being less represented than others. For example, normal cases may be in the majority, while pathological cases may have few examples. This may prevent the model from learning minority classes correctly.

The effectiveness of methods developed to assess fetal health is critical to protecting the health of the mother and baby. Therefore, developing an effective classification model helps healthcare professionals provide accurate information and ensures early detection of situations requiring intervention. In this context, accurate classification methods and hyperparameter optimization techniques are essential. Current studies use various machine learning and deep learning methods to classify CTG data (Dang et al., 2023; Kannan et al., 2021; Mehbodniya et al., 2022). In particular, traditional methods such as decision trees and support vector machines are widely preferred. However, these methods need more success in complex data sets. In recent years, deep learning-based models, especially structures such as TabNet developed for tabular data analysis, have been more successful in overcoming these problems (Jin et al., 2023).

This study used the TabNet model to classify fetal health as normal, suspicious, and pathological. The Random OverSampling method was applied to eliminate the imbalance in the dataset. In addition, the Optuna library was used for hyperparameter optimization of the model to determine the most appropriate parameters. In this process, 5-fold stratified cross-validation was applied to increase the model's validity. In conclusion, this study shows that TabNet and Optuna effectively evaluate fetal health and contribute to the existing literature in this field.

2. Material and Methods

2.1. Dataset

The dataset used in this study consists of 2126 CTG records (Ayres-de-campos et al., 2000). The dataset consists of 22 columns, each row representing a sample (refer to Table 1). The last column in the dataset, fetal_health (fetal health status), is a categorical variable that is the classification target and classifies the health status of the fetus as "normal," "suspicious,"

and "pathological." The other 21 columns contain various cardiac and uterine measurements. This study created a model that classifies fetal health status using these features.

Table 1. *Features in the dataset*

Feature name	Description
baseline value	The baseline value of fetal heart rate (FHR)
accelerations	The number of accelerations in FHR
fetal_movement	The number of fetal movements
uterine_contractions	The number of uterine contractions
light_decelerations	The number of mild decelerations
severe_decelerations	The number of severe decelerations
prolongued_decelerations	The number of prolonged decelerations
abnormal_short_term_ variability	Abnormal short-term variability (STV)
mean_value_of_short_term_ variability	The mean value of STV
percentage_of_time_with_ abnormal_long_term_variability	The percentage of time spent with abnormal long-term variability (LTV)
mean_value_of_long_term_ variability	The mean value of LTV
histogram_width	The width of the histogram
histogram_min	The minimum value of the histogram
histogram_max	Maximum value of the histogram
histogram_number_of_peaks	Number of peaks in the histogram
histogram_number_of_zeroes	Number of zero values in the histogram
histogram_mode	Mode of the histogram
histogram_mean	Average of the histogram
histogram_median	Median of the histogram
histogram_variance	Variance of the histogram
histogram_tendency	Trend of the histogram (positive/negative)
fetal_health	Target variable; 1- Normal, 2- Suspicious, 3- Pathological

2.2. **Data Preprocessing**

As a result of the analysis performed on the dataset, it was noticed that the target variable, the fetal_health class, was unbalanced. The number of samples among the three classes is not equal; the "normal" class contains more samples, while the "suspicious" and "pathological" classes contain fewer samples (see Figure 1). This imbalance may cause certain classes (predominantly minority classes) to be underrepresented during the model's training process and may cause the model to perform unbalanced

classification. To solve this problem, the Random OverSampling method is implemented. This method randomly resamples the data samples in minority classes so that all classes have a balanced distribution.

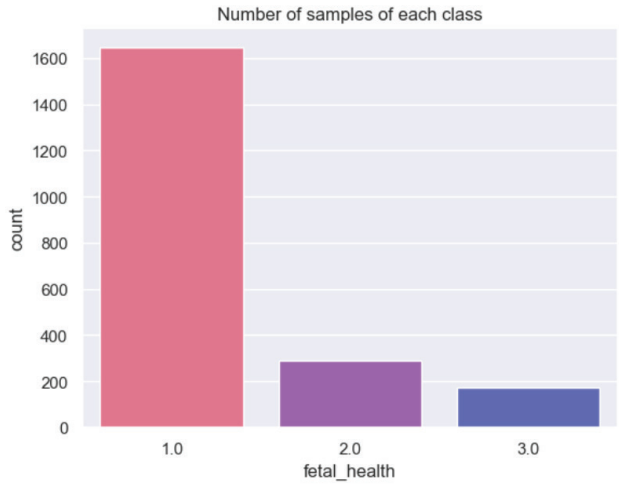

Figure 1. *Number of samples of each class*

As a result of this process, an equal number of data samples were obtained from each class for model training (see Figure 2). This allows the model to pay equal attention to all three classes and better represent the "suspicious" and "pathological" classes, which are particularly sparsely populated. *Random OverSampling* is an effective method used in imbalanced classification problems and was preferred in this study to balance the fetal health status classes. It played an essential role in improving the model's performance because, in imbalanced data sets, the model usually tends to learn the majority class, which can reduce the accuracy in minority classes. With this method, the model was able to learn each class better. After applying this method, the TabNet model was trained, and the results obtained were more reliable with a model that eliminated data imbalance.

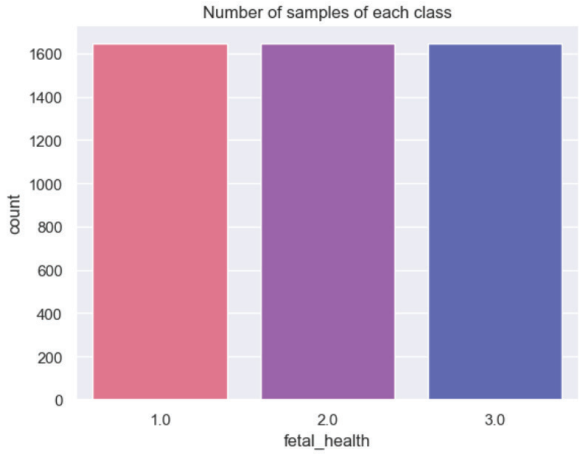

Figure 2. *Number of samples of each class with Random OverSampling*

2.3. **TabNet**

The TabNet model was used to classify CTG data. TabNet is a model that enables the effective use of deep learning methods, especially on tabular data (structured data). The model selects important features using the attention mechanism, which facilitates the interpretation of the data. TabNet consists of various interconnected components, each of which performs a different operation on the data to reach the final decision.

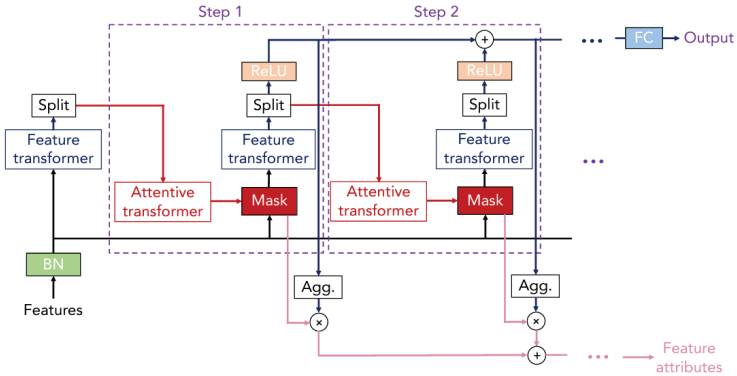

(a) TabNet encoder architecture

Figure 3. *TabNet Encoder Architecture (Arik and Pfister, 2021)*

The "encoder" part of the TabNet model is a component whose primary function is to transform the data and select important features (see Figure 3). At this stage, the data is processed in a certain way, and the features are subjected to different attention mechanisms throughout the decision steps (Joseph et al., 2022).

• Feature Transformer: This block transforms the data and makes it more meaningful. The feature transformer ensures the data is transformed into different dimensions at each step. At each step, specific layers are used in decision-making, while others can continue the functionality of the attention mechanism.

• Attentive Transformer: At each step, the attention mechanism learns that certain features are more important and selects these features. The attention mechanism increases the interpretability of the model by focusing only on important parts of the data.

• Feature Masking: A masking process is performed at each step of the model to determine which features will be used. This masking lets us see which features the model pays attention to and which features it selects. In this way, more information is obtained about the decision mechanism of the model. Collecting feature masks makes it possible to determine which features are more important globally.

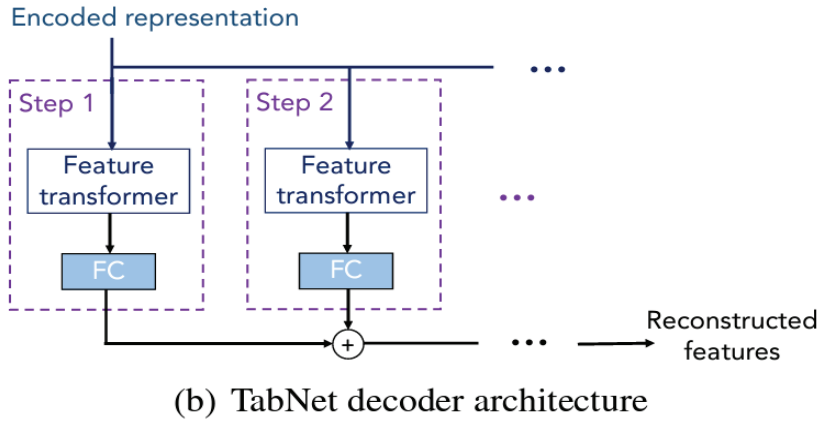

Figure 4. *TabNet Decoder Architecture (Arik and Pfister, 2021)*

The "decoder" part of TabNet is used in the training phase of the model and contributes to the learning process by reconstructing the data (see Figure 4). The information received from the encoder helps reconstruct the decoder's features (Yan et al., 2021). The decoder includes a feature transformer block at each step. • Feature Transformer Block: This block, which is also included in the decoder, allows the transformed data in the encoder to gain meaning again. It reconstructs the features used by the model in decision-making.

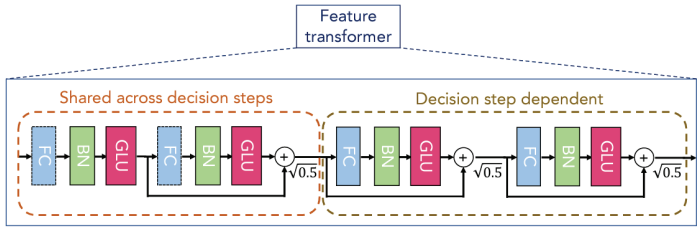

Figure 5. *Feature transformer block (Arik and Pfister, 2021)*

Feature transformer blocks are one of the main components on the encoder and decoder side (see Figure 5). This block is used to transform features at different stages. For example, the first two layers of the data are commonly used in all decision steps, while the following two are designed to be specific to each decision step.

• Layers (Fully Connected Layers): Each feature converter block contains fully connected (FC) layers. These layers allow the data to be reduced to different dimensions and made meaningful.

• Batch Normalization (BN): Batch Normalization is applied to each model layer, balancing the gradients during training and ensuring the model learns more stably.

• Gated Linear Unit (GLU) Nonlinearity: A Gated Linear Unit is a mechanism that allows the data to undergo a nonlinear transformation. In this way, the model can learn more flexible and complex relationships.

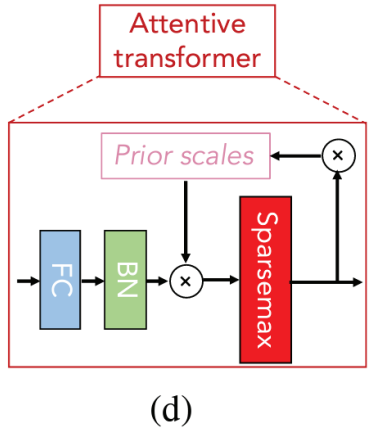

Figure 6. *Attentive Transformer Block (Arik and Pfister, 2021)*

Attentive Transformer block, where the attention mechanism is applied, determines which data features will be used (see Figure 6). At this stage, information is collected about which features were used in previous decision steps, and a new decision is made based on this information. With this scale information showing how many features are used, the attention mechanism assigns different importance to each feature.

• Sparsemax: At the end of the attention mechanism, a sparse structure is created in the selection of features by using the sparsemax function. Sparsemax selects only the most important features and ensures that the model is only interested in the most remarkable ones (Zhang et al., 2024). This contributes to the model being more efficient and interpretable.

2.4. **Hyper-parameter Optimization with Optuna**

Optuna is a powerful library used for hyperparameter optimization (Akiba et al., 2019). It helps determine the optimal values of hyperparameters to improve the performance of machine learning and deep learning models. Hyperparameters are settings that affect the training process and performance of the model (Hassanali et al., 2024). Finding the best combination of these settings is often critical to improving the model's accuracy.

The objective(trial) function defines the hyperparameters that Optuna will optimize. Within this function, various hyperparameters that determine the model's performance are determined (Chen et al., 2024; Mo et al., 2024).

The selected hyperparameters in the study are as follows:

n_d: Number of hidden units (an integer between 8 and 64).

n_a: Attention mechanism units (an integer between 8 and 64).

learning_rate: Learning rate (a value between 0.0001 and 0.01 on a logarithmic scale).

batch_size: Batch size to be used during training (an integer between 16 and 128).

virtual_batch_size: Virtual batch size (an integer between 8 and batch_size).

max_epochs: Maximum training time of the model (an integer between 100 and 300).

patience: Early stopping patience (an integer between 10 and 30).

A TabNetClassifier model was created with the defined hyperparameters. Adam optimization algorithm was used for model optimization. The model

was trained on training data (X_train, y_train). A validation set (X_val, y_val) was used to check the validity of the training. The trained model made predictions with test data (X_test), and the accuracy score was calculated. This accuracy is returned as the output of the target function. The Optuna study was started, and 50 different trials were performed. Different hyperparameter combinations were tried in each trial.

Optuna returns the best hyperparameter combination obtained from the trials. Thanks to this structure, the best hyperparameters are found for the TabNet model; thus, the model's overall performance can be increased. In the hyperparameter optimization process performed with Optuna, the hyperparameters determined to provide the best performance of the model are as follows:

• n_d (Number of Hidden Units): 28

This parameter expresses the number of units in the hidden layer of the model. In this way, the model can better learn the complexity of the data.

• n_a (Attention Mechanism Units): 18

Attention mechanism units determine which features the model will focus on carefully. In this way, the model provides better learning by emphasizing important features.

• lr (Learning Rate): 0.0091

The learning rate determines the step size in the model's learning process. This parameter controls how much the model will be updated in each iteration. A suitable learning rate allows the model to learn quickly and effectively.

• batch_size: 78

Batch size determines how many examples the model will process at once in each iteration. Larger batch sizes provide a more stable learning process, while smaller sizes provide more opportunities for updates.

• virtual_batch_size: 59

Virtual batch size indicates how many examples the model is processing virtually. This increases memory efficiency and allows for working with larger data sets.

• max_epochs: 213

This parameter determines the maximum number of iterations the model will undergo during training. Increasing this number allows the model to learn more but also carries the risk of overfitting.

• patience: 17

Early stopping ensures that the training is terminated when the model does not improve after a certain number of iterations. This helps prevent the model from overlearning.

These hyperparameters were determined for the optimal performance of the TabNet model and played an important role in the classification of fetal health. These parameters obtained with Optuna increased the model's overall accuracy, providing a more effective classification process.

2.5. **Workflow of Study**

Optuna's best hyperparameters were the basis for training the TabNet model. The model was trained on the training data with these best settings, and a 5-fold stratified cross-validation method was used in the learning process. Stratified K-Fold reduced the negative effects of imbalanced data sets by ensuring that the class distribution in each fold remained the same as the original data set. During the training process, the model's learning rate and other hyperparameters were adjusted to increase the model's accuracy, and overfitting was prevented with the early stopping strategy. Training and testing were performed for each fold, and the overall success of the model was measured using test data. The results obtained showed that the model's ability to effectively distinguish normal, suspicious and pathological classes of fetal health.

2.6. **Evaluation Metrics**

The number of accurate positive class predictions the classifier made is shown by True Positive (TP). When the classifier correctly recognizes the negative class as negative, it is said to be True Negative (TN). The number of inaccurate predictions in which the classifier incorrectly classifies the negative class as positive is known as False Positives (FP). The number of incorrect predictions where the classifier incorrectly classifies a positive class as negative is known as False Negative (FN) [32]. Formulas in Equation (1), Equation (2), Equation (3), and Equation (4) determine accuracy, recall, precision, and F1-score values based on TP, FP, TN, and FN values.

Accuracy value is the ratio of correctly predicted samples to total samples.

$$\text{Accuracy}=(TP+TN)/(TP+FN+TN+FP) \quad (1)$$

Sensitivity (recall) calculates how many of the samples that should be predicted as Positive are predicted as positive.

$$\text{Recall}=TP/(TP+FN) \quad (2)$$

Precision is the metric that reveals the proportion of true positives among all positive predictions.

$$\text{Precision}=TP/(TP+FP) \quad (3)$$

The F1 Score is the harmonic mean of the Precision and Recall values.

$$\text{F1 Score}=2\times(\text{Presicion}\times\text{Recall})/(\text{Precision}+\text{Recall}) \quad (4)$$

3. Experimental Results

The 5-fold cross-validation results were calculated to evaluate the model's overall performance, and the accuracy rates in each layer are presented in Table 2. The obtained accuracy rates reveal the model's performance on different data subsets. The accuracy rates in layers from Fold-1 to Fold-4 were recorded as 93%, 95%, 98%, and 96%, respectively. These results show that the model achieves high accuracy rates and consistently performs. However, the accuracy rate dropped to 88% in Fold-5, and there was a significant performance loss compared to other layers. This decrease suggests that the model may have limited learning capacity on specific data subsets. While the highest accuracy rate in Fold-3 was 98%, the lowest accuracy rate of 88% in Fold-5 indicates that the model performs well, but its generalization ability may decrease in some data groups.

Table 2. *5-fold cross validation Accuracy rates*

Fold-1	Fold-2	Fold-3	Fold-4	Fold-5
0.93	0.95	0.98	0.96	0.88

The classification performance of the third layer of 5-fold cross-validation is shown in detail in Table 3. This table includes the model's accuracy measures (precision, recall, F1 score) for each class (normal, suspicious, and pathological) and the number of examples in the classes (support). The classification results in the third layer are generally quite strong.

For Class 1 (Normal), precision, recall, and F1 scores were calculated as 99%. This shows that the model classified the data in the normal class with high accuracy and was quite successful in both capturing true positives (recall) and avoiding false positives (precision). The model was able to identify 329 normal examples with very high success.

For Class 2 (Suspicious), precision was 97%, recall was 96%, and F1 score was 96%. Although the performance in the suspicious class was slightly lower than the other classes, the model also produced a strong and balanced result in this class. The F1 score of 96% shows that the model maintains both accuracy and sensitivity in classifying suspicious cases.

For Class 3 (Pathological), the precision, recall, and F1 scores were determined to be 98%. The model also classified the data in the pathological class with high accuracy. Very consistent results were obtained with an F1 score of 98% by working on 330 pathological samples.

As seen in the Support column, each class is represented by 329-330 samples, which shows that the data set is balanced. The high F1 scores of the model reveal that it exhibits consistent and successful performance between classes.

As a result, the model's performance in the third layer is quite high and balanced. While almost perfect results are obtained for the normal and pathological classes, the performance in the suspicious class is slightly lower but still satisfactory. These results show that the model can successfully distinguish different fetal health classes.

Table 3. *Classification Report*

Classes	Precision	Recall	F1 Score	Support
1.0	0.99	0.99	0.99	329
2.0	0.97	0.96	0.96	329
3.0	0.98	0.98	0.98	330

The confusion matrix shows the accuracy and error distribution in the model's classification performance (see Figure 7). For the normal class (1.0), 326 samples were correctly classified, while only three samples were incorrectly assigned to the suspicious class, and no samples were incorrectly classified to the pathological class. For the suspicious class (2.0), 317 samples were correctly classified, but four samples were incorrectly assigned to the normal class, and eight samples were incorrectly assigned to the pathological class. For the pathological class (3.0), 322 samples were correctly classified, while eight samples were incorrectly assigned to the suspicious class, and no errors were made to the normal class. As a result, the model made the most errors between the suspicious and pathological classes and was quite successful in correctly classifying the normal class.

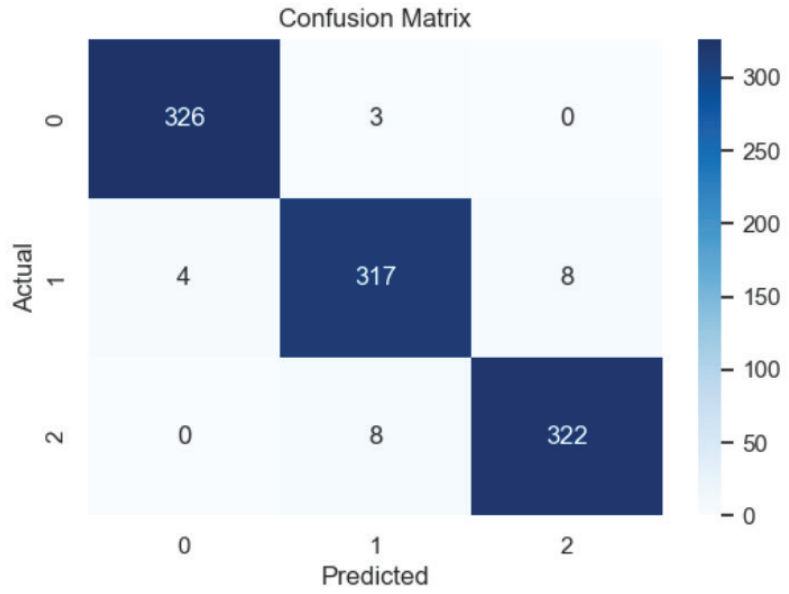

Figure 7. *Confusion Matrix*

4. Results

This study presents a deep learning-based approach for classifying fetal health as normal, suspicious, and pathological using CTG data. In particular, the application of the TabNet model enabled the efficient processing of complex and high-dimensional CTG data. Overcoming the unbalanced data distribution with the Random OverSampling method enabled the model to learn minority classes better and increased the classification performance. The hyperparameter optimization performed through the Optuna library enabled the model to work with the most appropriate parameters and improve its overall performance. The 5-fold stratified cross-validation increased the model's validity and helped to obtain reliable results.

In conclusion, using TabNet and Optuna provides an effective solution for assessing fetal health conditions and significantly contributes to the existing literature. The findings obtained play a critical role in the early detection of situations that require intervention by allowing more accurate and timely information to be provided to healthcare professionals. Future studies may further improve fetal health assessment processes by comparing different deep-learning methods and testing CTG data on larger datasets.

REFERENCES

Akiba, T., Sano, S., Yanase, T., Ohta, T., & Koyama, M. (2019). *Optuna: A Next-generation Hyperparameter Optimization Framework*. http://arxiv.org/abs/1907.10902

Ayres-de-campos, D., Bernardes, J., Garrido, A., Marques-de-sá, J., & Pereira-leite, L. (2000). SisPorto 2.0: A Program for Automated Analysis of Cardiotocograms. *Journal of Maternal-Fetal and Neonatal Medicine*, *9*(5), 311–318. https://doi.org/10.3109/14767050009053454

Chen, C. H., Lin, Y. L., & Pai, P. F. (2024). Forecasting Flower Prices by Long Short-Term Memory Model with Optuna. *Electronics (Switzerland)*, *13*(18). https://doi.org/10.3390/electronics13183646

Dang, T. H., Thi, H. T., & Do Van, D. (2023). Improve Classification Quality of Fetal Status from Cardiotocogram Data by Using Machine Learning. *2023 1st International Conference on Health Science and Technology, ICHST 2023*. https://doi.org/10.1109/ICHST59286.2023.10565357

Hassanali, M., Soltanaghaei, M., Javdani Gandomani, T., & Zamani Boroujeni, F. (2024). Software development effort estimation using boosting algorithms and automatic tuning of hyperparameters with Optuna. *Journal of Software: Evolution and Process*. https://doi.org/10.1002/smr.2665

Jin, Y., Ren, Z., Wang, W., Zhang, Y., Zhou, L., Yao, X., & Wu, T. (2023). Classification of Alzheimer's disease using robust TabNet neural networks on genetic data. *Mathematical Biosciences and Engineering*, *20*(5), 8358–8374. https://doi.org/10.3934/mbe.2023366

Joseph, L. P., Joseph, E. A., & Prasad, R. (2022). Explainable diabetes classification using hybrid Bayesian-optimized TabNet architecture. *Computers in Biology and Medicine*, *151*. https://doi.org/10.1016/j.compbiomed.2022.106178

Kannan, E., Ravikumar, S., Anitha, A., Kumar, S. A. P., & Vijayasarathy, M. (2021). Analyzing uncertainty in cardiotocogram data for the prediction of fetal risks based on machine learning techniques using rough set. *Journal of Ambient Intelligence and Humanized Computing*. https://doi.org/10.1007/s12652-020-02803-4

Mehbodniya, A., Lazar, A. J. P., Webber, J., Sharma, D. K., Jayagopalan, S., Kousalya, K., Singh, P., Rajan, R., Pandya, S., & Sengan, S. (2022). Fetal health classification from cardiotocographic data using machine learning. *Expert Systems*, *39*(6). https://doi.org/10.1111/exsy.12899

Mo, K., Tang, Y., Zhu, Y., Li, X., Li, J., Peng, X., Liao, P., & Zou, P. (2024). Fresh Meat Classification Using Laser-Induced Breakdown Spectroscopy

Assisted by LightGBM and Optuna. *Foods*, *13*(13). https://doi.org/10.3390/foods13132028

Rahmayanti, N., Pradani, H., Pahlawan, M., & Vinarti, R. (2021). Comparison of machine learning algorithms to classify fetal health using cardiotocogram data. *Procedia Computer Science*, *197*, 162–171. https://doi.org/10.1016/j.procs.2021.12.130

Arık, S. Ö., & Pfister, T. (2021). TabNet: Attentive Interpretable Tabular Learning. www.aaai.org

World Health Organization (2020), Maternal mortality.

Yan, J., Xu, T., Yu, Y., & Xu, H. (2021). Rainfall forecast model based on the tabnet model. *Water (Switzerland)*, *13*(9). https://doi.org/10.3390/w13091272

Zhang, H., Wu, Y., Zhang, W., & Zhang, Y. (2024). FFNN–TabNet: An Enhanced Stellar Age Determination Method Based on TabNet. *Applied Sciences (Switzerland)*, *14*(3). https://doi.org/10.3390/app14031203

Chapter 9

INVESTIGATION OF THE EFFECT OF CURRENT VALUE ON REAL ESTATE VALUE USING MACHINE LEARNING ALGORITHMS

Tansu ALKAN[1],[2]

Murat KARAKOYUN[3]

Süleyman Savaş DURDURAN[4]

1 Niğde Ömer Halisdemir University, Department of Geomatics Engineering, Niğde, ORCID: 0000-0001-8293-2765

2 Necmettin Erbakan University, Institute of Science, Konya

3 Necmettin Erbakan University, Department of Computer Engineering, Konya, ORCID: 0000-0002-0677-9313

4 Necmettin Erbakan University, Department of Geomatics Engineering, Konya, ORCID: 0000-0003-0509-4037

1. Introduction

Real estate encompasses physical and economic assets, including plots, land, buildings, and other permanent structures. Real estate valuation is a systematic process aimed at determining the characteristics of these assets, such as their market value, utility, or investment potential. By analyzing specific attributes and statistical data, real estate valuation establishes the true value of properties (Demirel, Yelek, Alağaş, & Eren, 2018). The importance of this field in the world of real estate is increasing day by day and therefore the scientific studies in this field are also increasing exponentially. (Erdem, 2018). This discipline holds a pivotal role in the real estate sector, serving as a critical reference point for financing, insurance, taxation, and legal procedures, in addition to informing investment decisions.

The valuation of real estate with a range of values according to different purposes of use gives rise to a complex structure in the valuation process. The application of concepts such as current value, market value, expropriation value and tax base value gives rise to disparate outcomes, thereby engendering transparency and reliability issues in the real estate market. Furthermore, the situation is compounded by an inadequate application of standards in the valuation process, an absence of rigorous analysis of market dynamics, and a dearth of objective criteria. Nevertheless, it is essential that a real estate asset should have a single value over a defined period (Bozdağ & Ertunç, 2020). It is anticipated that valuations conducted in accordance with internationally recognized standards will yield comparable outcomes, irrespective of the specific characteristics and intended use of the real estate in question.

In the current context, the process of real estate valuation requires a high level of detail due to the complex and diverse nature of the legislation that applies in the real estate market, the methods used, and the criteria evaluated (Hazer, Bozdağ, & Atasever, 2024). As a result of the shortcomings of traditional methodologies and the benefits conferred by contemporary techniques, this process has become more intricate and interdisciplinary. Given that traditional methods are typically founded upon a narrow set of criteria, they may lack the requisite objectivity in determining the value of properties. Conversely, modern and hybrid methodologies provide an approach based on quantitative analysis, multi-criteria decision-making processes and data analytics technologies, thereby facilitating the attainment of more consistent and reliable results in simultaneous and collective valuation processes (Şişman & Aydınoğlu, 2023). These methods are preferred in the management of large-scale real estate portfolios, public projects and expropriation processes due to their time and cost efficiency.

In the mass valuation of real estate, machine learning algorithms offer

an innovative tool for fast, accurate and objective analysis of large data sets. While traditional valuation methods based on limited criteria are insufficient for simultaneous and mass valuation of real estate, machine learning algorithms produce more consistent and scientifically based results by analyzing many variables simultaneously. They offer a significant advantage in understanding the complex relationships between factors affecting real estate values and predicting future market trends. These algorithms can create value estimation models by considering the market values of real estate and the physical, spatial, environmental and legal characteristics that affect the value of real estate. Thus, while the valuation processes save both time and cost, more reliable results are obtained for investors and public institutions.

In the literature, there are studies in which machine learning methods such as decision tree (Burhan, 2023; Özsoy & Şahin, 2009; Park & Bae, 2015; Sarı, Bedirhan, & Sel, 2024; Yücebaş, Doğan, & Genç, 2022), k-nearest neighborhood (Alkan, Dokuz, Ecemiş, Bozdağ, & Durduran, 2023; Borde, Rane, Shende, & Shetty, 2017; Choy & Ho, 2023; Hu et al., 2019; Sevgen & Tanrivermiş, 2024; Yıldırım, 2019), artificial neural networks (Chou, Fleshman, & Truong, 2022; Deaconu, Buiga, & Tothăzan, 2022; Sammour et al., 2024; Xu & Zhang, 2022, 2024; Yılmazel, Afşar, & Yılmazel, 2018), random forest (Guo, Chiang, Liu, Yang, & Gou, 2020; Hong, Choi, & Kim, 2020; Huang & Lai, 2023; Kim, Lee, Lee, & Hong, 2022; Mora-Garcia, Cespedes-Lopez, & Perez-Sanchez, 2022; Zhang, Rahman, & Miller, 2023).

In this study, data obtained from 685 real estate in Konya province was employed to estimate the value of real estate using four different algorithms: Decision Tree (DT), k-Nearest Neighbor (k-NN), Neural Networks (NN) and Random Forest (RF). In addition to the structural characteristics of the real estates, neighborhood-based average current value was included in the study as a spatial feature and its effect on the real estate value was investigated. The efficacy of the employed methodologies was evaluated, and the random forest algorithm was identified as the most successful in value estimation. The results demonstrate that the average current value has a significant impact on the value of the real estate.

2. Material and Method

2.1. Data Sets

Konya is the largest province of Turkey in terms of surface area. It consists of 31 districts, including the central districts of Selçuklu, Meram and Karatay. Its population is 2.320.241 as of the end of 2023. In this study, data were collected from the central districts of Konya province (**Figure 1**).

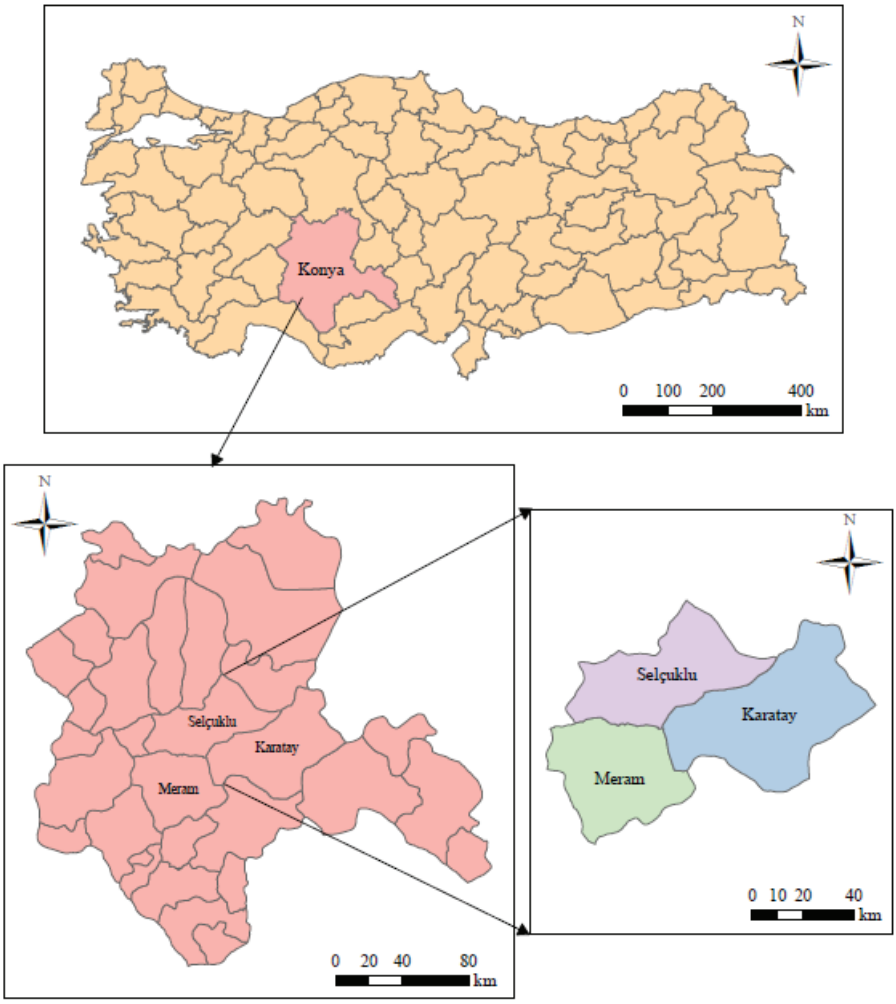

Figure 1. *Konya city study area*

In this study, data on the criteria affecting the value of 685 real estate was obtained using online property websites. The information collected includes the area, number of rooms, age of the building, floor, heating type, number of bathrooms, balcony status, site status, location and Market Value (MV). Data was collected following the Kahramanmaraş earthquakes in Turkey on 6th February 2023. Konya is a province with low earthquake risk. After the disaster, there was migration to Konya province, causing fluctuations in the real estate market. **Table 1** presents a sample dataset for the data.

Table 1. *Sample data set*

Area (m^2)	Number of Rooms	Age of the building	Floor	Heating Type	Number of Bath	Balcony Status	Site Status	Location	Market value (TL)
55	1+1	2	4	Centre heating (pay meter)	1	Yes	Yes	Karatay/ Akabe	975000
80	1+1	5-10	1	Natural gas (Combi boiler)	1	Yes	Yes	Meram/Aşkan	1060000
95	2+1	0	5	Floor heating	2	Yes	No	Selçuklu/ Aydınlıkevler	1750000
100	2+1	21-25	4	Natural gas (Combi boiler)	1	Yes	No	Selçuklu/ Feritpaşa	975000
145	3+1	0	3	Natural gas (Combi boiler)	1	Yes	Yes	Selçuklu/ Hocacihan	3250000
140	3+1	11-15	3	Stove	1	Yes	No	Karatay/ Ulubatlıhasan	1000000
150	3+1	4	Ground floor	Natural gas (Combi boiler)	1	Yes	Yes	Karatay/ Ulubatlıhasan	1380000
140	3.5+1	26-30	4	Floor calorifier	1	Yes	No	Selçuklu/ Ferhuniye	850000
200	4+1	4	2	Natural gas (Combi boiler)	2	Yes	No	Meram/ Osmangazi	3200000
175	4+1	5-10	4	Centre heating (pay meter)	2	Yes	Yes	Karatay/ Hacıveyiszade	2250000

To estimate real estate values using machine learning algorithms with the data set of real estate characteristics provided in **Table 1**, the data were digitized. According to the descriptions given below, the data has been digitized, considering its impact on the value of the real estate and prepared for use in machine learning algorithms.

Area: No changes have been made regarding the area criterion.

Number of Rooms: The criterion for the number of rooms is quantified by the total count. For instance, 1+1 rooms would be quantified as 2, while 2+1 rooms would be quantified as 3.

Age of the building: The age of the building was determined by assigning a score between 1 and 8, as outlined in **Table 2**.

Table 2. *Numerical values for the age of building*

Age of the building	0	1-4	5-10	11-15	16-20	21-25	26-30	31+
Numerical values	8	7	6	5	4	3	2	1

Floor: The criterion for the floor was quantified by scoring on a scale of 1-8, as shown in **Table 3**.

Table 3. *Numerical values for the floor*

Floor	Basement	Attic, Ground, High Entrance Floor	1-3	4-6	7-9	10-12	13-15	16-18
Numerical values	1	2	3	4	5	6	7	8

Heating Type: The heating type criterion was scored on a scale of 1-7 (Doğan, Bande, Genç, & Koç, 2023), as shown in **Table 4**.

Table 4. *Numerical values for the heating type*

Heating Type	Stove	Floor calorifier	Natural gas (Stove)	Floor heating	Centre heating	Centre heating (pay meter)	Natural gas (Combi boiler)
Numerical values	1	2	3	4	5	6	7

Number of Bathrooms: No changes have been made regarding the number of bathrooms criterion.

Balcony Status: The dataset was created by indicating 'Yes' for real estate with a balcony and 'No' for those without (as shown in Table 1). The criterion for balcony status was quantified by assigning a value of 1 for 'Yes' and 0 for 'No'.

Site Status: The dataset was created by indicating 'Yes' if the real estate is within the site and 'No' if it is not (as shown in Table 1). The criterion for site status was quantified by assigning a value of 2 for 'Yes' and 1 for 'No'.

Location: The location criterion comprises information on the district and neighborhood where the real estate is situated. The location criterion was quantified by calculating the average current value for each neighborhood, based on the street-based land current values shared by Selçuklu, Meram, and Karatay district municipalities, while considering the district and neighborhood information. No changes have been made in the values obtained.

Market Value: No changes have been made regarding the market value.

Table 5 presents the digitized version of the sample data set provided in Table 1.

Tablo 5. *Digitized version of the sample data set*

Area (m^2)	Number of Rooms	Age of the building	Floor	Heating Type	Number of Bath	Balcony Status	Site Status	Average Current Value (TL)	Market value (TL)
55	2	7	4	6	1	1	2	458,11	975000
80	2	6	3	7	1	1	2	517,36	1060000
95	3	8	4	4	2	1	1	950,86	1750000
100	3	3	4	7	1	1	1	1527,7	975000
145	4	8	3	7	1	1	2	645,09	3250000
140	4	5	3	1	1	1	1	618,19	1000000
150	4	7	2	7	1	1	2	618,19	1380000
140	4.5	2	4	2	1	1	1	1620,86	850000
200	5	7	3	7	2	1	1	232,3	3200000
175	5	6	4	6	2	1	2	464,82	2250000

Area, number of rooms, age of the building, floor, heating type, number of bathrooms, balcony status and site status are the structural characteristics of the real estate. The average current value based on the neighborhood is the spatial characteristic of the real estate. For machine learning algorithms, data on the structural characteristics, spatial characteristics, and market value of 685 real estates were digitized and made ready for use.

2.2. Machine Learning Algorithms

2.2.1. Decision Tree (DT)

Decision tree algorithm is a widely used supervised learning algorithm in the literature (Louati, Lahyani, Aldaej, Aldumaykhi, & Otai, 2022), primarily for classification or estimation purposes (Onan, 2015). The structure of a DT comprises three fundamental elements: nodes, branches, and leaves. The data set variables are referred to as attributes, and all nodes in the tree structure, including the root, are composed of attributes. The root is at the top, the leaves at the bottom, and the branches in between. A tree structure includes a root node with data, internal nodes (branches), and terminal nodes (leaves) (Kavzoğlu & Çölkesen, 2010).

2.2.2. k Nearest Neighbors (k-NN)

k-nearest neighbors algorithm was developed by Cover and Hart in 1967 (Cover & Hart, 1967). It is a supervised learning algorithm and is considered one of the easiest algorithms to use in machine learning (Bansal, Goyal, & Choudhary, 2022). It is used for classification and regression. The k-NN algorithm is particularly effective on small datasets and when there is a clear distinction between classes (Hacıbeyoglu, Çelik, & Erdaş Çiçek, 2023). In the k-NN algorithm, the class or value of a data point is predicted based on the information of its k nearest neighbors. The k-NN algorithm commonly employs a variety of distance metrics, including Euclidean, Chebyshev, Manhattan, and Mahalanobis, to quantify the proximity of the data (Çelik, 2023).

2.2.3. Neural Network (NN)

Neural network is a sophisticated and effective machine learning algorithm that draws inspiration from the functional mechanisms of the human brain. The objective of developing and utilizing neural networks is to establish relationships between data, solve optimization problems, perform identification and categorization, and make predictions about future outcomes (Ertaylan, Aktaş, & Doğan, 2021). A neural network cell is comprised of five fundamental components: inputs, weights, a combining function, an activation function and an output (Kuşkapan, Çodur, & Çodur, 2022). Inputs represent the information coming to the neural cell from the external environment, while weights indicate the importance of this information. The inputs received from the external environment are transmitted to the cell together with their weights and the net input value obtained from here is processed through the activation function and the output value is calculated. Neural network consists of three main layers: input, hidden, and output, and each layer is made up of neurons that form a network structure through connections with each other (Kara, 2024).

2.2.4. Random Forest (RF)

Random forest algorithm was developed by Breiman in 2001 (Breiman, 2001). In this algorithm, each tree is constructed using a randomly selected subset of the training data and a random selection of features, which serves to increase diversity and improve generalization. In the algorithm, the number of samples to be used at each node and the total number of trees to be constructed must be determined, while the classification process is carried out using a decision forest composed of K trees specified by the user (Karakoyun & Hacıbeyoğlu, 2014). The algorithm can be used as a decision tree method in categorical, continuous and both data sets, as well as in large or small data sets (Parlak & Kayri, 2022).

2.3. Performance Metrics

Machine learning algorithms were used to estimate the value of real estate, and the success of these algorithms was analyzed using performance metrics. In this study, the success of the algorithms was tested using commonly used metrics such as the coefficient of determination (R^2), Mean Absolute Error (MAE), and Root Mean Square Error (RMSE). R^2 represents the relationship between the market values and the estimated values and is calculated using Equation (1). The value of R^2 ranges from 0 to 1, with a value close to 1 indicating good model performance (Sevinç & Kaya, 2021). MAE represents the mean of the absolute differences between the market and estimated values and is calculated using Equation (2) (Utku & Can, 2022). RMSE measures the amount of error between market and estimated values and is calculated using Equation (3)(Türkan, Bozdağ, Karkınlı, & Ulucan, 2023).

$$R^2 = 1 - \frac{\sum_{i=1}^{n}(y_i - \hat{y}_i)^2}{\sum_{i=1}^{n}(y_i - \bar{y})^2} \quad (1)$$

$$MAE = \frac{1}{n}\sum_{i=1}^{n}|y_i - \hat{y}_i| \quad (2)$$

$$RMSE = \sqrt{\frac{1}{n}\sum_{i=1}^{n}(y_i - \hat{y}_i)^2} \quad (3)$$

The equations use 'y_i' to represent the market values, '$\hat{y}_i$' to represent the estimated values, '$\bar{y}$' to represent the average value, and 'n' to represent the numbers of data.

Additionally, the coefficient of dispersion (COD) and price-related differential (PRD) metrics as defined by the International Association of Assessing Officers (IAAO) were used for the success of the algorithms. COD is calculated using Equation (4) and a relative statistic that measures the degree of dispersion of the ratio between the estimated value and the market value (Zhao, Shen, Ma, & Yu, 2023). PRD is calculated by equation (5) as the mean valuation ratio divided by the weighted mean ratio (Bourassa & Hoesli, 2022). According to the Standard on Ratio Studies, the acceptable range for COD is 5 to 15, while the acceptable range for PRD is 0.98 to 1.03, and the PRD value should be close to 1 (IAAO, 2013).

$$COD = \frac{100}{n}\frac{\sum_{i=1}^{n}\left|\frac{EV_i}{MV_i} - Median\left(\frac{EV_i}{MV_i}\right)\right|}{Median\left(\frac{EV_i}{MV_i}\right)} \quad (4)$$

$$PRD = \frac{Mean\left(\frac{EV_i}{MV_i}\right)}{\sum_{i=1}^{n} EV_i / \sum_{i=1}^{n} MV_i} \quad (5)$$

The equations use 'MV_i' to represent the market values, 'EV_i' to represent the estimated values, and 'n' to represent the numbers of data.

3. Results

In this study, DT, k-NN, NN and RF methods from machine learning algorithms were used to estimate the real estate value. The application was carried out in two stages.

The first stage was parameter analysis. It was determined on which parameters the machine learning algorithms performed best.

The second stage was the estimation of the value of real estate by means of machine learning algorithms. This stage consists of two steps. In the first step, the value of the real estate was estimated using the criteria of structural characteristics such as area, number of rooms, age of the building, floor, heating type, number of bathrooms, balcony status and site status. In the second step, the value of the real estate was estimated by including the neighborhood-based average current value criterion as a spatial characteristic. Thus, the effect of the market value on the value of real estate has been investigated.

3.1. Parameter Analysis

In the DT algorithm, the minimum tree subsets and minimum instances in leaves parameters were analyzed (**Table 6**). At the same value of the minimum instances in leaves parameter, all values of the minimum tree subsets parameter gave the same result. The best result was obtained when the minimum instances in leaves parameter was 25 and this parameter was used in the application.

Table 6. *DT parameter analysis*

Min Tree Subsets	Min Instances in Leaves				
	5	10	15	20	25
2	0,375	0,419	0,449	0,456	**0,481**
3	0,375	0,419	0,449	0,456	**0,481**
4	0,375	0,419	0,449	0,456	**0,481**
5	0,375	0,419	0,449	0,456	**0,481**

In the k-NN algorithm, k and distance metric parameters were analyzed (**Table 7**). The best result was obtained when the k parameter was 7 and

the distance metric parameter was Mahalanobis and these parameters were used in the application.

Table 7. *k-NN parameter analysis*

k	Distance Metrics			
	Euclidean	Manhattan	Chebyshev	Mahalanobis
3	0,339	0,425	0,236	0,499
5	0,381	0,438	0,298	0,499
7	0,395	0,429	0,333	**0,502**
9	0,372	0,441	0,327	0,500

In the NN algorithm, the number of neurons and activation function parameters were analyzed (**Table 8**). The identity function was found to be more successful than the logistic and tanh functions. It produced the same result for all neuron number values. Therefore, the identity function was used in the application as it gave the best result.

Table 8. *NN parameter analysis*

Neuron Number	Activation Function		
	Identity	Logistic	Tanh
8	**0,513**	0,241	0,317
16	**0,513**	0,292	0,255
24	**0,513**	0,232	0,227
32	**0,513**	0,316	0,225

In the RF algorithm, minimum tree subsets and trees parameters were analyzed (**Table 9**). The best results were obtained when the minimum tree subsets parameter to 4 and the trees parameter to 10, and these parameters were used in the application.

Table 9. *RF parameter analysis*

Min Tree Subsets	Trees			
	5	10	15	20
2	0,471	0,511	0,536	0,527
3	0,487	0,548	0,526	0,527
4	0,510	**0,553**	0,516	0,549
5	0,495	0,52	0,517	0,537

3.2. Experimental Results

Disregarding the average current value, the structural characteristics of the real estate were used to estimate the value with the DT, k-NN, NN and RF algorithms. The success of these algorithms was analyzed using performance metrics. The R^2, MAE, RMSE, COD and PRD values for each algorithm are presented in **Table 10**.

Table 10. *Performance metrics of the algorithms (without average current value)*

	DT	k-NN	NN	RF
R^2	0,481	0,502	0,513	**0,523**
MAE	681109	645411	749992	**628159**
RMSE	1304050	1277767	1263605	**1250302**
COD	27,663	25,651	35,600	24,988
PRD	1,010	0,989	0,980	**1,008**

Upon analysis of Table 10, it can be concluded that the RF algorithm is the most successful based on the R^2 metric. Following this, the k-NN, NN, and DT algorithms respectively demonstrate decreasing levels of success. The acceptable range for COD is between 5 and 15, and no algorithm is within the acceptable range. The acceptable range for PRD is between 0.98 and 1.03 and all algorithms are within this range. Since the number of data is large, for the clarity of the graph, the graph comparing the market value with the estimated values obtained using algorithms of 200 real estate is given in **Figure 2**.

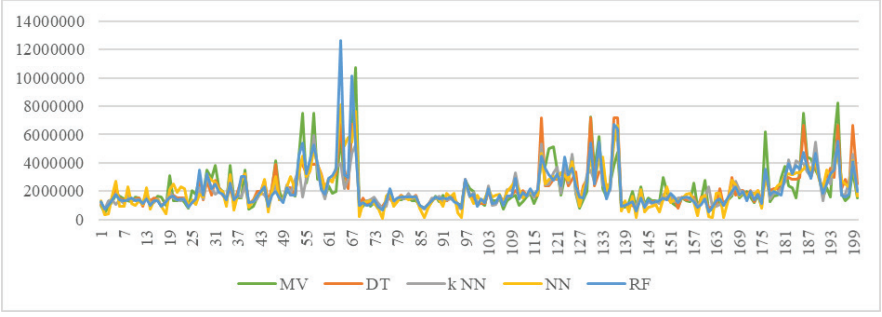

Figure 2. *Comparison of market value and estimated values (without average current value)*

Using the structural characteristics and the average current value criterion as a spatial characteristic, the value of the real estate was estimated by DT, k-NN, NN and RF algorithms. **Table 11** presents the performance metrics used to analyze the success of these algorithms.

Table 11. *Performance metrics of the algorithms (with average current value)*

	DT	k-NN	NN	RF
R^2	0,576	0,546	0,534	**0,607**
MAE	603659	591266	707925	**552982**
RMSE	1179385	1220189	1235469	**1135265**
COD	27,269	24,393	33,882	22,517
PRD	1,012	0,977	1,333	**1,005**

Upon analysis Table 11, it becomes apparent that the R^2 values of all algorithms have improved with the inclusion of the average current value criterion. According to the R^2 metric, the RF algorithm is the most successful, followed by DT, k-NN, and NN. COD values also improved, but none of the algorithms are within the acceptable range. PRD values are acceptable for all algorithms except NN. The graph comparing the estimated values and the market value is given in **Figure 3**.

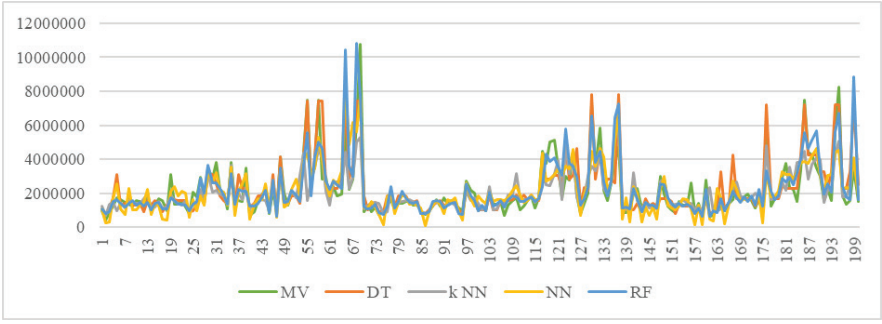

Figure 3. *Comparison of market value and estimated values (with average current value)*

Upon analysis Figures 2 and 3, it becomes clear that the RF algorithm aligns more closely with market values. Figure 3 demonstrates that incorporating the average current value into the application leads to more successful results.

4. Conclusion

Real estate valuation is a significant process for both individual and institutional decision-making mechanisms. An accurate and objective valuation process serves to prevent legal disputes, ensure the efficient use of economic resources and increase the trust between the parties by providing buyers and investors with information regarding market conditions. It is therefore evident that the valuation of real estate is significant, not only in economic terms but also in terms of its social and legal implications.

The value of real estate is affected by several criteria, and it is therefore essential to identify these correctly to ensure the most comprehensive valuation process. In addition to the physical, spatial, environmental and legal factors, the economic situation, market conditions and the future use potential of real estate are the criteria that affect the value of the real estate. Following the earthquakes that struck the Kahramanmaraş region of Turkey on 6 February, there has been a notable increase in demand for real estate in provinces with a relatively low risk of seismic activity. This has led to fluctuations in the real estate market and a corresponding rise in real estate values.

In this study, data on 685 properties in Konya province were collected from online property websites. The data set comprised several structural criteria, including area, number of rooms, building age, floor, heating type, number of bathrooms, balcony status and site status information. In addition, district and neighborhood information was included to provide a spatial context for the real estate data. The structural criteria were assigned a score, while the spatial criteria were digitized by calculating the average current value at the neighborhood level. The impact of the average current value on real estate value was investigated through the utilization of machine learning algorithms.

In this study, real estate valuation is performed using DT, k-NN, NN, and RF algorithms. Initially, a parameter analysis was conducted. The most successful results were obtained when the minimum instances in leaves parameter was 25 of the DT algorithm, k parameter was 7 and the distance metric was Mahalanobis of the k-NN algorithm, activation function was identity of the NN algorithm, and minimum tree subsets 4 and trees parameter was 10 of the RF algorithm. To ascertain the value, a valuation application was conducted, encompassing both the inclusion and exclusion of the average current value. The success of the algorithms was evaluated with performance metrics. In the application without the average current value, the R^2 value for DT, k-NN, NN and RF algorithms was calculated as 0.481, 0.502, 0.513 and 0.523, respectively. In the application with the average current value, the R^2 value for DT, k-NN, NN and RF algorithms was calculated as 0.576, 0.546, 0.534 and 0.607, respectively. The RF algorithm proved to be the most efficacious in determining the value of real estate. The addition of the average market value as a criterion resulted in more successful outcomes for all algorithms.

Economic conditions, financial crises and natural disasters are critical factors that can alter market demand, purchasing power and regional attractiveness by directly affecting the value of real estate. To conduct real estate valuation in an objective and scientific manner, it is essential to express the criteria influencing the value of the real estate in numerical terms and to analyze these criteria using mathematical methods. Consequently, the influence of subjective interpretations is diminished, thereby facilitating the attainment of more precise, transparent, and reliable outcomes.

References

Alkan, T., Dokuz, Y., Ecemiş, A., Bozdağ, A., & Durduran, S. S. (2023). Using machine learning algorithms for predicting real estate values in tourism centers. *Soft Computing*, *27*(5), 2601–2613. https://doi.org/10.1007/S00500-022-07579-7

Bansal, M., Goyal, A., & Choudhary, A. (2022). A comparative analysis of K-Nearest Neighbor, Genetic, Support Vector Machine, Decision Tree, and Long Short Term Memory algorithms in machine learning. *Decision Analytics Journal*, *3*, 100071. https://doi.org/10.1016/j.dajour.2022.100071

Borde, S., Rane, A., Shende, G., & Shetty, S. (2017). Real estate investment advising using machine learning. *International Research Journal of Engineering and Technology (IRJET)*, *4*(3), 1821–1825.

Bourassa, S. C., & Hoesli, M. (2022). Hedonic, residual, and matching methods for residential land valuation. *Journal of Housing Economics*, *58*, 101870. https://doi.org/10.1016/j.jhe.2022.101870

Bozdağ, A., & Ertunç, E. (2020). CBS ve AHP Yöntemi Yardımıyla Niğde Kenti Örneğinde Taşınmaz Değerleme. *Geomatik*, *5*(3), 228–240. https://doi.org/10.29128/geomatik.648900

Breiman, L. (2001). Random forests. *Machine Learning*, *45*, 5–32. https://doi.org/10.1023/A:1010933404324

Burhan, H. A. (2023). Konut Fiyatları Tahmininde Makine Öğrenmesi Sınıflandırma Algoritmalarının Kullanılması: Kütahya Kent Merkezi Örneği. *Dumlupınar Üniversitesi Sosyal Bilimler Dergisi*, (76), 221–237. https://doi.org/10.51290/dpusbe.1249461

Çelik, A. (2023). Determination of the Classification Success of KNN Algorithm Distance Metric Methods on Wheat Seeds Dataset. *Afyon Kocatepe Üniversitesi Fen ve Mühendislik Bilimleri Dergisi*, *23*(5), 1142–1149. https://doi.org/10.35414/akufemubid.1263900

Chou, J. S., Fleshman, D. B., & Truong, D. N. (2022). Comparison of machine learning models to provide preliminary forecasts of real estate prices. *Journal of Housing and the Built Environment*, *37*(4), 2079–2114. https://doi.org/10.1007/S10901-022-09937-1

Choy, L. H. T., & Ho, W. K. O. (2023). The Use of Machine Learning in Real Estate Research. *Land*, *12*(4), 740. https://doi.org/10.3390/land12040740

Cover, T. M., & Hart, P. E. (1967). Nearest Neighbor Pattern Classification. *IEEE Transactions on Information Theory*, *13*(1), 21–27. https://doi.org/10.1109/TIT.1967.1053964

Deaconu, A., Buiga, A., & Tothăzan, H. (2022). Real estate valuation models performance in price prediction. *International Journal of Strategic Property Management*, *26*(2), 86–105. https://doi.org/10.3846/ijspm.2022.15962

Demirel, B., Yelek, A., Alağaş, H. M., & Eren, T. (2018). Taşınmaz değerleme kriterlerinin belirlenmesi ve kriterlerin önem derecelerinin çok ölçütlü karar verme yöntemi ile hesaplanması. *Kırıkkale University Journal of Social Sciences*, *8*(2), 665–682.

Doğan, O., Bande, N., Genç, Y., & Koç, F. (2023). Yapay Sinir Ağları Metodu ile Konut Özellikleri Yeniden Sayısallaştırılarak Rayiç Değerinin Tahmin Edilmesi: Keçiören/Ankara Örneği. *Turkish Journal of Land Management*, *5*(1), 9–19. https://doi.org/10.51765/tayod.1219413

Erdem, N. (2018). Türkiye Taşınmaz Değerleme Sisteminin Yeniden Yapılandırılmasına Yönelik Bilimsel Çalışma ve Öneriler Üzerine Bir Değerlendirme. *Niğde Ömer Halisdemir Üniversitesi Mühendislik Bilimleri Dergisi*, *7*(1), 159–170. https://doi.org/10.28948/ngumuh.386408

Ertaylan, A., Aktaş, Ö., & Doğan, Y. (2021). Yapay Sinir Ağları ile Piyasa Takas Fiyatı Tahminlemesi. *Dokuz Eylül Üniversitesi Mühendislik Fakültesi Fen ve Mühendislik Dergisi*, *23*(67), 93–105. https://doi.org/10.21205/deufmd.2021236708

Guo, J. Q., Chiang, S. H., Liu, M., Yang, C. C., & Gou, K. Y. (2020). Can machine learning algorithms associated with text mining from internet data improve housing price prediction performance? *International Journal of Strategic Property Management*, *24*(5), 300–312. https://doi.org/10.3846/ijspm.2020.12742

Hacıbeyoglu, M., Çelik, M., & Erdaş Çiçek, Ö. (2023). K En Yakın Komşu Algoritması ile Binalarda Enerji Verimliliği Tahmini. *Necmettin Erbakan Üniversitesi Fen ve Mühendislik Bilimleri Dergisi*, *5*(2), 65–74. https://doi.org/10.47112/neufmbd.2023.10

Hazer, A., Bozdağ, A., & Atasever, Ü. H. (2024). Hiper-optimize edilmiş makine öğrenim teknikleri ile taşınmaz değerlemesi, Yozgat Kenti örneği. *Geomatik*, *9*(3), 299–312. https://doi.org/10.29128/geomatik.1454915

Hong, J., Choi, H., & Kim, W. (2020). A house price valuation based on the random forest approach: the mass appraisal of residential property in South Korea. *International Journal of Strategic Property Management*, *24*(3), 140–152. https://doi.org/10.3846/ijspm.2020.11544

Hu, L., He, S., Han, Z., Xiao, H., Su, S., Weng, M., & Cai, Z. (2019). Monitoring housing rental prices based on social media:An integrated approach of machine-learning algorithms and hedonic modeling to inform equitable housing policies. *Land Use Policy*, *82*, 657–673. https://doi.org/10.1016/j.landusepol.2018.12.030

Huang, Z., & Lai, G. (2023). A House Price Prediction Model Based on K-means Clustering and Random Forest in Guangzhou. *Frontiers in Business,*

Economics and Management, *10*(2), 377–381. https://doi.org/10.54097/fbem.v10i2.11077

IAAO. (2013). Standard on Ratio Studies. Retrieved September 25, 2024, from https://www.iaao.org/wp-content/uploads/Standard_on_Ratio_Studies.pdf

Kara, M. A. (2024). Fındık Fiyatlarının Yapay Sinir Ağları ile Tahminlenmesi: Türkiye Örneği. *Batman Üniversitesi Yaşam Bilimleri Dergisi*, *14*(1), 31–42. https://doi.org/10.55024/buyasambid.1394033

Karakoyun, M., & Hacıbeyoğlu, M. (2014). Biyomedikal Veri Kümeleri ile Makine Öğrenmesi Sınıflandırma Algoritmalarının İstatistiksel Olarak Karşılaştırılması. *Dokuz Eylül Üniversitesi Mühendislik Fakültesi Fen ve Mühendislik Dergisi*, *16*(48), 30–42.

Kavzoğlu, T., & Çölkesen, İ. (2010). Karar Ağaçları ile Uydu Görüntülerinin Sınıflandırılması: Kocaeli Örneği. *Harita Teknolojileri Elektronik Dergisi*, *2*(1), 36–45.

Kim, J., Lee, Y., Lee, M. H., & Hong, S. Y. (2022). A Comparative Study of Machine Learning and Spatial Interpolation Methods for Predicting House Prices. *Sustainability*, *14*(15), 9056. https://doi.org/10.3390/su14159056

Kuşkapan, E., Çodur, M. K., & Çodur, M. Y. (2022). Türkiye'deki Demiryolu Enerji Tüketiminin Yapay Sinir Ağları ile Tahmin Edilmesi. *Konya Journal of Engineering Sciences*, *10*(1), 72–84. https://doi.org/10.36306/konjes.935621

Louati, A., Lahyani, R., Aldaej, A., Aldumaykhi, A., & Otai, S. (2022). Price forecasting for real estate using machine learning: A case study on Riyadh city. *Concurrency and Computation: Practice and Experience*, *34*(6), e6748. https://doi.org/10.1002/cpe.6748

Mora-Garcia, R. T., Cespedes-Lopez, M. F., & Perez-Sanchez, V. R. (2022). Housing Price Prediction Using Machine Learning Algorithms in COVID-19 Times. *Land*, *11*(11), 2100. https://doi.org/10.3390/land11112100

Onan, A. (2015). Şirket İflaslarının Tahminlenmesinde Karar Ağacı Algoritmalarının Karşılaştırmalı Başarım Analizi. *Bilişim Teknolojileri Dergisi*, *8*(1).

Özsoy, O., & Şahin, H. (2009). Housing price determinants in Istanbul, Turkey: An application of the classification and regression tree model. *International Journal of Housing Markets and Analysis*, *2*(2), 167–178. https://doi.org/10.1108/17538270910963090

Park, B., & Bae, J. K. (2015). Using machine learning algorithms for housing price prediction: The case of Fairfax County, Virginia housing data. *Expert Systems with Applications*, *42*(6), 2928–2934. https://doi.org/10.1016/j.eswa.2014.11.040

Parlak, M. S., & Kayri, M. (2022). Öğretmenlerin E-Öğrenme Hazırbulunuşluk Düzeylerini Etkileyen Faktörlerin Rastgele Orman Algoritması Yöntemi ile İncelenmesi. *Van Yüzüncü Yıl Üniversitesi Eğitim Fakültesi Dergisi*, *19*(3), 670–696. https://doi.org/10.33711/yyuefd.1117068

Sammour, F., Alkailani, H., Sweis, G. J., Sweis, R. J., Maaitah, W., & Alashkar, A. (2024). Forecasting demand in the residential construction industry using machine learning algorithms in Jordan. *Construction Innovation*, *24*(5), 1228–1254. https://doi.org/10.1108/CI-10-2022-0279

Sarı, P., Bedirhan, İ. D., & Sel, Ç. (2024). Comparing the Practical Differences Between Decision Tree and Random Forest Algorithms in Estimating Housing Prices. *Current Trends in Computing*, *1*(2), 149–157.

Sevgen, S. C., & Tanrivermiş, Y. (2024). Comparison of Machine Learning Algorithms for Mass Appraisal of Real Estate Data. *Real Estate Management and Valuation*, *32*(2), 100–111. https://doi.org/10.2478/remav-2024-0019

Sevinç, A., & Kaya, B. (2021). Derin Öğrenme ve İstatistiksel Modelleme Yöntemiyle Sıcaklık Tahmini ve Karşılaştırılması. *Avrupa Bilim ve Teknoloji Dergisi*, (28), 1222–1228. https://doi.org/10.31590/ejosat.1014106

Şişman, S., & Aydınoğlu, A. Ç. (2023). Toplu Taşınmaz Değerlemesi için Coğrafi Verinin İşlenmesi ve Rastgele Orman Makine Öğrenmesi Tekniğiyle Tahmin Modelinin Geliştirilmesi. *Harita Dergisi*, *169*, 13–27.

Türkan, M., Bozdağ, A., Karkınlı, A. E., & Ulucan, A. G. (2023). Kent Ölçeğinde Konutlara İlişkin Toplu Değer Değişiminin Makine Öğrenim Algoritmaları ile Analizi. *Türkiye Arazi Yönetimi Dergisi*, *5*(2), 66–77. https://doi.org/10.51765/tayod.1275671

Utku, A., & Can, Ü. (2022). Covid-19 Aşılama Sürecinin Tahminine Yönelik Derin Öğrenme Tabanlı Bir Model. *International Journal of Pure and Applied Sciences*, *8*(2), 367–379. https://doi.org/10.29132/ijpas.1125729

Xu, X., & Zhang, Y. (2022). Second-hand house price index forecasting with neural networks. *Journal of Property Research*, *39*(3), 215–236. https://doi.org/10.1080/09599916.2021.1996446

Xu, X., & Zhang, Y. (2024). Office property price index forecasting using neural networks. *Journal of Financial Management of Property and Construction*, *29*(1), 52–82. https://doi.org/10.1108/JFMPC-08-2022-0041

Yıldırım, H. (2019). Property value assessment using artificial neural networks, hedonic regression and nearest neighbors regression methods. *Selçuk Üniversitesi Mühendislik, Bilim ve Teknoloji Dergisi*, *7*(2), 387–404. https://doi.org/10.15317/Scitech.2019.207

Yılmazel, Ö., Afşar, A., & Yılmazel, S. (2018). Konut Fiyat Tahmininde Yapay Sinir Ağları Yönteminin Kullanılması. *Uluslararası İktisadi ve İdari İncelemeler Dergisi*, (20), 285–300. https://doi.org/10.18092/ulikidince.341584

Yücebaş, S., Doğan, M., & Genç, L. (2022). A C4. 5–Cart Decision Tree Model for Real Estate Price Prediction and The Analysis of The Underlying Features. *Konya Journal of Engineering Sciences*, *10*(1), 147–161. https://doi.org/10.36306/konjes.1013833

Zhang, Y., Rahman, A., & Miller, E. (2023). Longitudinal modelling of housing prices with machine learning and temporal regression. *International Journal of Housing Markets and Analysis*, *16*(4), 693–715. https://doi.org/10.1108/IJHMA-02-2022-0033/FULL/PDF

Zhao, Y., Shen, X., Ma, J., & Yu, M. (2023). Path selection of spatial econometric model for mass appraisal of real estate: evidence from Yinchuan, China. *International Journal of Strategic Property Management*, *27*(5), 304–316. https://doi.org/10.3846/ijspm.2023.20376

Chapter 10

THE USE OF EXPANDED CLAY AGGREGATE IN THE CONSTRUCTION INDUSTRY IN TÜRKİYE

Nil Yapıcı[1]

Ercüment Bilger[2]

1 Asst. Prof., Çukurova University, Institute of Science and Technology, Department of Mining Engineering, Adana/Türkiye

nyapici@cu.edu.tr, 05336421904

ORCID ID: 0000-0001-9761-9122

2 Inst. Çukurova University, Institute of Science and Technology, Department of Mining Engineering, Adana/Türkiye, ebilger@cu.edu.tr, ORCID ID: 0000-0002-8557-0576

1. Introduction

In parallel with the rapid development of technology, various research topics have emerged in the construction sector. Undoubtedly, the most well-known and widely applied of these areas is the use of lightweight structural elements.

In terms of concrete building materials used in the construction industry, clay, shale, and slate stand out as types of lightweight aggregates obtained from natural materials used in concrete. For the production of lightweight building materials and aggregates used worldwide, expanded clay has become an indispensable primary resource for the construction sector, especially in developed countries like those in Europe. Despite its significance, expanded clay aggregate resources in our country have yet to be fully recognized due to insufficient research. Identifying and utilizing these resources would provide an important contribution to our national economy. However, our country has significant potential in terms of expandable clay reserves. Therefore, it is essential to identify these expandable clay reserves and conduct detailed tests on them to determine their properties for industrial use.

Clay, clayey shale, and shales that undergo a rapid sintering process and experience a certain volume increase at temperatures between 1100-1300˚C are referred to as expandable clays. These clay groups are mineralogically composed of layered silicates such as illite, sericite, and montmorillonite. Three main parameters that affect the expansion of clays are clay particle size, aggregate particle size, and the initial temperature encountered by the aggregate in the furnace.

When considered as a building material within the scope of its technomechanical properties, expanded clay is known for its high strength. This mechanism occurs very rapidly as part of the sintering process, which is the thermal treatment used to bond the particles together. As a result of chemical reactions at temperatures between 1100-1300˚C, a significant volume increase occurs in the expandable clay material. The production process is carried out in special rotary kiln (Figure 1).

Figure 1. Rotary kiln

When examined in terms of their areas of use, clays classified as lightweight aggregates are most notable for their application in lightweight concrete production. Evaluating the physical and mechanical properties of expanded lightweight clays, we observe that they have low unit weight, water-repellent characteristics, and are highly resistant to thermal insulation due to their porous structure. Additionally, they exhibit high compressive strength and bond well with cement. All of these properties make expanded clays a sought-after raw material in civil engineering projects.

When examining the formation mechanisms of expandable clay deposits in Europe, it is observed that clays found on the seabed, brackish water clays, loess clays formed by wind erosion, Jurassic clays, and Devonian-aged clayey shales and shifertons are particularly suitable due to their structural properties.

Globally, especially in developed countries, expanded clay production efforts are notable.

Norway: High-rise buildings constructed with lightweight concrete using expanded clay aggregate, resulting in lighter structures, reduced foundation loads, and improved earthquake resistance.

Germany: Bridge piers made with expanded clay aggregate concrete, reducing structural weight and shortening construction time due to lighter materials.

Sweden: Expanded clay aggregate used as road embankment material, enhancing ground stability and preventing settlement due to its light-

weight and excellent drainage capacity.

UK: Residential projects utilizing expanded clay aggregate concrete blocks to enhance thermal insulation and improve energy efficiency.

USA: Expanded clay pebbles used as drainage and root protection layers in green roofs, increasing water retention and supporting plant growth.

These examples highlight the diverse applications of expanded clay aggregate in engineering projects, showcasing its benefits like lightness, durability, thermal and sound insulation, and moisture control.

In Turkey, however, these studies are quite new, with a primary focus on research and development.

2. Definıition of Clay

Clays are layered aluminum silicates containing water (H_2O) within their crystal lattice. They typically crystallize in a hexagonal system. Depending on the presence of ions such as Fe, Mg, K, Ca, and Na, along with H_2O or OH^- between the layers, they are classified into basic clay mineral groups.

In terms of particle size, clays are sediments composed of particles smaller than 0.02 mm. They are earthy minerals with high alumina and silica content, which increase in plasticity when combined with certain amounts of water.

2.1.Types of Clay Mineral Groups and Crystal Lattice Structures

Due to their complex mineralogical structure, the presence of foreign elements, and the differences in the location where their formation mechanisms occur, clay minerals can be classified in a broad sense.

They generally form by the stacking of two types of layers in a specific arrangement, resembling the pages of a notebook. These sheets consist of SiO_2 (silicon tetrahedra) and Al_2O_3 (aluminum octahedra) (Figure 2).

Kaolinite (Kaolin) Group Clays:

Chemical Formula: Al2O3•2SiO2•2H2O

Illite Group Clays:

Chemical Formula: KAl2(OH)2(AlSi3(O•OH)10), these clays are rich in K (potassium).

Smectite-Montmorillonite Group Clays:

Chemical Formula: 2Al2O3.8SiO2.2H2O.nH2O, these clays are rich in Mg (magnesium). This group of clays can swell when absorbing water and shrink when releasing it.

Chlorite Group Clays:

Chemical Formula: Mg5(Al,Fe)(OH8)(AlSi4)O10, these clays are rich in Fe (iron).

When considering the classification criteria for clays with expansion properties, illite or mica groups stand out with more than 40% silica content. Among clay groups, it is preferable for kaolinite content to be low.

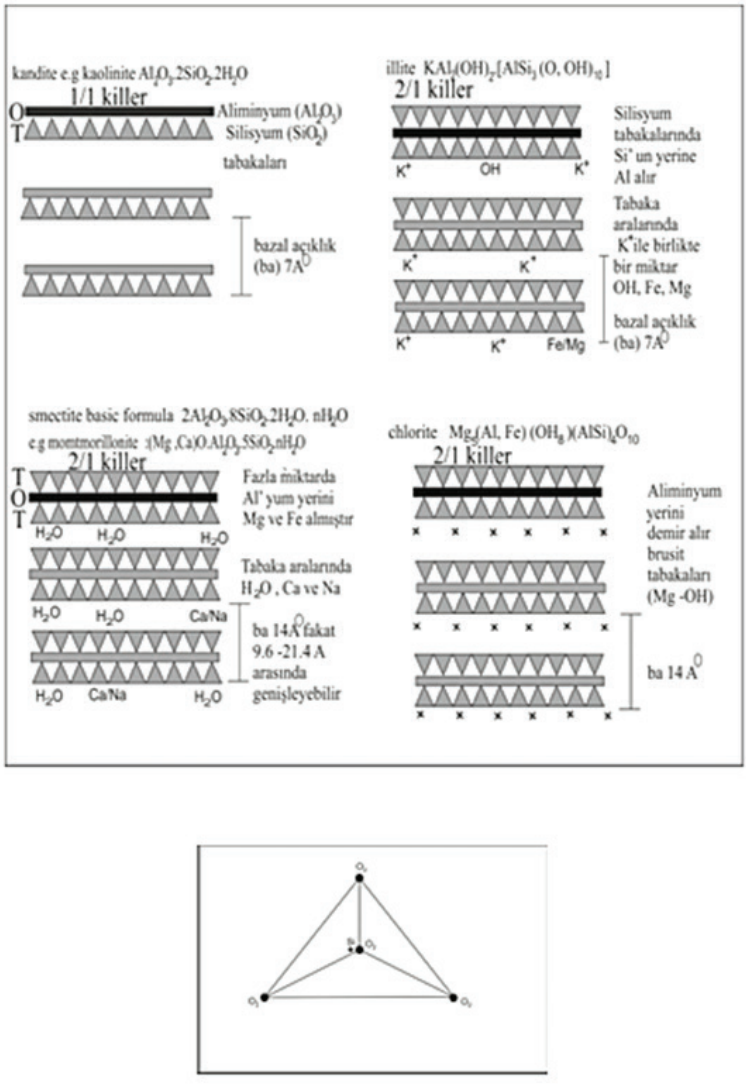

Figure 2. *Clay Groups According to Their Crystal Structures*

1.2. Properties of Expanding Clays

The raw materials most commonly used in lightweight aggregate production technology are clays and shales, which are products of the weathering of sedimentary rocks, magmatic minerals (feldspar), and metamorphic rocks (Purbrick 1991; Özgüven 2019). The main components of these rocks include mica, illite, kaolinite, smectite, and various amounts of quartz, feldspar, carbonates, iron oxides and hydroxides, as well as small amounts of sulfur and organic compounds. The fluxing agents in the composition are $CaO+MgO+Na_2O+K_2O+Fe_2O_3$ (Riley 1951; Özgüven 2019). The presence of these fluxing agents can affect the melting temperature chemically, and thus may also be effective in expansion (de'Gennaro et al., 2004; Özgüven 2019).

When considering the chemical properties and mineralogical composition that affect the expandability of clays:

1. The material should have high plastic properties and fine grain size (the proportion of particles smaller than 2 μm should be greater than 35%). The critical characteristic for structural clay, especially for nodular shale, is the particle size.

2. The material should have a high proportion of layered silicates. Considering the classification criteria of clays, illite or mica groups stand out with more than 40% silicate content. The kaolinite content within the clay groups should preferably be low.

3. Although materials containing calcite ($CaCO_3$) or dolomite [$CaMg(CO_3)_2$] show a decrease in expansion time, the presence of lime in lumps should be avoided, as it can lead to later fragmentation.

4. In terms of chemical composition:

- a) The Al_2O_3 value should be between 12-25%,
- b) The SiO_2 value should be between 50-78%,
- c) The fluxing agents (Na_2O, K_2O, CaO, MgO, Fe_2O_3, FeO) should be between 8-25%, Table 1).
- d) The organic carbon (C) content should be between 0.6-2.5%,
- e) The FeS_2 content should be fine-grained (with SO_3 content around 1-1.5%),
- f) The material intended for expansion should have a high Fe_2O_3 content (as the development of expansion characteristics is believed to depend on this, ideally between 5-10% or higher),

- g) Another important feature is that the sintering and melting point values should be very close to each other, and the temperature should be below 1200 °C,
- h) If the clay particles exhibit pyroplastic softening during gas formation, the ideal expansion ratio will be achieved.

Table 1. *Chemical analysis results (Ankara/Kalecik clays)*

Component	%
Al_2O_3	19,40
SiO_2	51,60
CaO	3,68
TiO_2	1,36
MgO	2,13
Fe_2O_3	10,71
CuO	0,05
Na_2O	0,91
SO_3	0,80
K_2O	4,23

Expanded aggregates, which show expansion after exposure to high temperatures, undergo rapid firing (Figure 3).

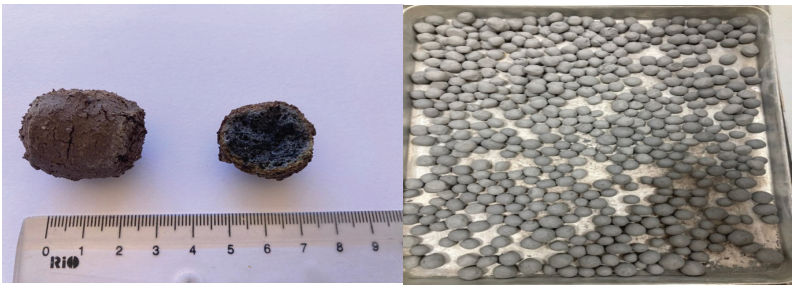

Before Expansion *A*fter Expansion

Figure 3. *Porous Internal Structure and Sintered Shell of Expanding Clay Samples from the Ankara Region*

In order for expansion to occur, a sintered shell must form on the surface of the material. The formation of this sintered shell is possible through the creation of a viscous structure. To form the viscous structure, the following conditions must be met:

1. The SiO_2/Eutectic ratio should be 4 or lower.
2. The $Na_2O + MgO + K_2O + Fe_2O_3$ / CaO ratio should be 4 or higher.

The viscous structure in the SEM images is shown in Figure 4.

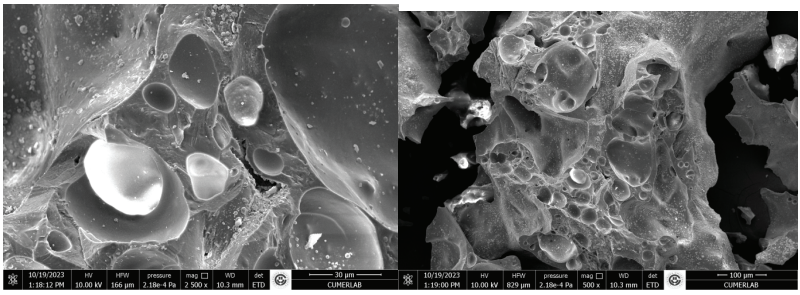

Figure 4. *SEM Image of Expanded Clay from the Ankara/Kalecik Region*

In the studies conducted by Çandır (2018), expansion was evaluated based solely on the major oxides SiO_2, Al_2O_3, and $Na_2O + MgO + K_2O + Fe_2O_3 + CaO$ values, and it was suggested that the values should remain within a shaded area on a diagram.

According to Riley, a high Al_2O_3 content increases heat resistance and consequently reduces expansion. Çandır (2018) suggested that, for proper expansion, the Al_2O_3 value should be less than 25%. This facilitates vesiculation, or the formation of bubbles inside the fired material, at a lower rate.

One of the most common areas where expanded clay aggregates are used is in the production of lightweight concrete. In civil engineering, the main applications are related to geotechnical studies and the use of lightweight concrete as fill material. When evaluated in terms of thermal insulation and unit volume weight, lightweight concrete offers many advantages and has become quite widespread today. One of the biggest structural problems in reinforced concrete buildings is the weight of the structure, and various materials have been tested over time to reduce this weight. The lightweight material considered for use should have high strength, be resistant to temperature, and provide good thermal insulation (Figure 5).

Since the material is a manufactured product, its properties (particle weight density, diameter, shell thickness) may vary depending on the desired characteristics for its final use.

According to experimental results conducted by researchers, for different cement contents, a concrete with a density of 1.7 g/cm³ and a compressive strength of 41.7 MPa, which includes expanded clay, has been stated to be suitable for use as structural concrete in reinforced concrete construction. This would reduce the overall weight of the building, there-

by decreasing the potential damage the structure may sustain during an earthquake (Subaşı, 2009).

Figure 5. *Construction Material Block Produced from Expanded Clay Aggregate (masterwarm.techinfus.com)*

In the study by Gündüz (2020), detailed field and laboratory work was carried out on the Ankara-Kalecik clay field to introduce it to industry. As a result of expansion experiments without any additives, it was found that it is possible to produce high-quality expanded clay aggregate with a unit volume weight of 291 kg/m^3 and an expansion rate of 6.3.

3. Development of Expanding Clays in Turkey

The existence of expanding clays worldwide has been known since the 1850s. However, in Turkey, the failure to consider the expanding characteristics of clay deposits and potentialities in terms of their chemical and mineralogical properties has delayed the production phase of this material.

In the United States, expanding clay is produced in 27 states. These clay aggregates are available in approximately 15 market products, such as Solite, Basalite, Buildex, Lite-Wate, Rocklite, etc.

In Europe, the production of expanded clay aggregates began in Denmark, which has rich clay potential but lacks natural pumice or furnace slag, and the rotary kiln method known as "LECA" was developed there. In Eastern Bloc countries such as Russia, Poland, and Czechoslovakia, expanding clays are referred to as "Keramsite."

In Turkey, studies on the potential of clays that could have expanding properties began in the 2000s by MTA (Mineral Research and Exploration General Directorate). Some clay potentials found in the Ankara/

Kalecik, Zonguldak, and Bartın regions expanded at 1150°C (Can, 2020). From 2000-2001, potential clay exploration was carried out by the institution, and this project revealed the richness of Turkey's expanding clay resources. The working regions in the project were: Ankara-Chankırı region (Kalecik, Beypazarı, Nallıhan, Gölbaşı, Çayırhan-Orta, Sakarcaören), İzmir-Manisa region (Bornova, Cumaovası, Karaburun, Mordoğan-Muradiye), Aydın-Muğla region (Kavaklıdere-Yatağan-Bafa Lake), Afyon-Kütahya region (Kızıldağ, Efeköy, Isıklar, Üyücek, Ovacık), Konya region (Kızılören, Hatunsaray, Kadınhanı, Ilgın), Bolu-Düzce-Sakarya region (Kaynaşlı, Yığılca, Ferizli), Zonguldak-Bartın-Karabük-Kastamonu (Ereğli, Çaycuma, Ulus, Kumluca Ömerli, Tekesin-Büyükköy, Devrakani), and Sivas region (Çetinkaya-Divriği-Mursal). Additionally, according to the Eighth Five-Year Development Plan (2001), it was stated that potential clay deposits are widespread in areas such as Feke-Saimbeyli/Adana, Istanbul-Zonguldak-Kastamonu, and Ankara-Kalecik, and it was determined that the tertiary clays in the Bolu-Göynük region also expand. However, it was noted that no reserve studies were conducted in any of these areas.

Until today, academic studies have focused more on conducting various experiments on samples taken from well-known clay formations, such as the Ankara/Kalecik region, rather than discovering new potential reserves. These studies have demonstrated that the clays from these regions yield positive results. It is clear that there are expanding clay deposits in Turkey, and the identification of their reserves needs to be done urgently.

Expanded clay production is carried out in over 20 countries, including Denmark, Finland, Norway, Portugal, Germany, Italy, and Iran, under the name "Leca." In Italy, it is known as "Laterlite," in Spain as "Liapour," in France as "Argex," in Russia as "Keramzit," and in South Africa as "Aglite."

In Turkey, it is called "Lecat." Lecat is primarily produced from clays found in the Bilecik/Söğüt district and is primarily sold in the domestic market. The material began production in early 2019. Each day, 2000 tons of clay are transported from regional clay reserves to the raw material preparation unit (Figure 6). 500 tons of aggregate are produced per day.

Figure 6. *General view of the clay pit and the aggregate produced*

The main advantages of using LECAT® (the Turkish version of Leca) in construction are as follows:

- The notable features of Expanded Clay Beads include excellent sound and heat insulation, which are further enhanced in blocks, resulting in reduced insulation costs.
- The "breathing" feature, which can be lost over time in other blocks when exposed to water, is retained in LECAT blocks, helping eliminate humidity.
- LECAT blocks maintain this feature because all the chambers in the expanded clay beads structure are independent of each other, and they have a low water retention capacity.
- Low cost.
- Reduction in building weight, which decreases the usage of materials like concrete and steel, ultimately lowering overall costs.
- Being lightweight, LECAT simplifies labor and internal building installations, and its strong structure holds anchors and fasteners better than other wall elements.
- Environmentally friendly in terms of gas emissions.

Aggregate produced between 0-8 mm in our country is supplied to the construction sector.

The use of expanded clay in the production of building materials is directly linked to the discovery of raw material reserves and the widespread production of expanded clay aggregates. Currently, potential areas that have not undergone reserve studies but show promise need to be developed for mining. While clay aggregates are more commonly used in agricultural activities in Turkey, their development in the construction sector has not yet reached the desired level.

Concrete, granule, screed, mortar and wall block products are used in the construction industry. Concrete products; lightweight structural concrete,/prefabricast concrete-C30/37 and above.

It seems like you're referring to engineering examples using expanded clay aggregate concrete and construction materials, as listed in Table 2.

Table 2. Engineering Examples from Around the World

Italy- Mont Blanc Tunnel	Fınland- Nurmijarvi Munıcıpalıty Buıldıng
Italy- The Zara Expo Road (Sound Barrıer)	Italy - Trıennale Desıgn Museum
Italy - Pıazza Cıttà Lıbera	Italy - Twın-Set Headquarters
Norway - Sørlandssenteret	Italy - Unıcredıt Tower
Portugal - Braamcamp Freıre School	Norway- Gjoklep Secondary School
Netherlands - Maasstad Hospıtal	Italy - Cıtylıfe Resıdentıal Project
England- Brıdgewater Place	Italy - Gallerıa Vıttorıo Emanuele (Mall)
England- Londra Metropolıtan Municıpality Buildıng	Italy - Mallero Brıdge
Austrıa- Salzburg Postareal	Italy - Mose Project (Experimental Electromechanical Module)
Fınland- Asunto Mestarınkatu	Italy - Sesta Porta Bus Termınal
Fınland - Nurmijarvi Munıcıpalıty Buıldıng	Norway - Eidsvoll Bridg
Italy- Malpensa Airport	
Fınland- Asunto Mestarınkatu	

Conclusion

Clay with expansion properties is classified as a lightweight aggregate. These aggregates are produced by heating the material to 1200°C in rotary kilns. During the heating process, the formation of gas occurs within the material. As the gas escapes, the volume of the clay can expand up to 5-6 times its original size. This process results in the creation of thousands of small bubbles, which significantly contribute to the expansion of the clay. Due to the rotational movement of the rotary kiln, expanded clay generally takes on a round or curved shape in varying sizes and unit weights.

The importance of clay in Türkiye increases due to the wide area coverage of clay beds and the high reserve rates in the regions where they are found. Increasing research on the expansion properties of clay beds with significant potential and identifying expanded clay beds with superior characteristics compared to alternatives would be beneficial.

Before conducting expansion experiments for expanded clay aggregate production, it would be useful to carry out chemical and mineralogical analyses of suitable clays, shales, slates, etc., as this could provide valuable insight into predicting the expansion process.

In Turkey, expanded clay aggregates are sold and used under the LECAT® patent. In 2013, Türkiye's first expanded clay aggregate production facility was established under the brand name Lecat. Globally, this product is known by various names such as Hydroton, Keramzit, Light Expanded Clay, Exclay, Blaehton, Haydite, Expanded Clay, Hydroponic Pebbles, Hydroton, Clay Pellets, and Clay Balls.

The porous structure of expanded clay aggregate offers benefits such as lightness, thermal and sound insulation, and water and air retention. Its thick shell structure enhances durability and longevity, while the high-temperature firing process improves its hygienic properties and binding capabilities.

While these aggregates are used in the agricultural sector, their usage in the construction industry has not yet reached the desired level.

References

Can, R. (2020). *Genleştirilmiş kil agregaları ile hazırlanan kompozit malzemelerin geoteknik uygulamalarda kullanılabilirliği*, Yüksek Lisans Tezi, Konya.

Çandır, İ. (2018). *Bentonitlerden Genleştirilmiş Kil Agregası Üretimi ve Karakterizasyonu*, Doktora Tezi, Adana.

de'Gennaro, R., Cappelletti, P., Cerri, G., de'Gennaro, M., Dondi, M., Langella, A. (2004). Zeolitic tuffs as raw materials for lightweight aggregates. *Applied Clay Science, 25*, 71-81.

Purbrick, J. (1991). Lightweight aggregates-manufacture and applications. *Exploration, Mining and Uses of Ceramic Raw Materials*, Proceedings of the 23rd Annual Symposium of the African Ceramic Society, pp. 45-49.

Subaşı, S. (2009). Genleştirilmiş kil agregası ile taşıyıcı hafif beton üretimi. *Gazi Üniversitesi Mühendislik ve Mimarlık Fakültesi Dergisi*, 24(3), 559-567.

Özgüven, A. (2019). Killerde genleşmenin üçgen diyagram ile tahmini. *MTA Dergisi*, 158, 303-315.

Riley, C.M. (1951). Relation of chemical properties to the bloating of clays. *Journal of the American Ceramic Society*, 34(4), 121-128.

https://lecat.com.tr/

Chapter 11

GEOLOGY, MORPHOLOGY AND FORMATION MECHANISM OF THE ÇANDIR YAREN SINKHOLE (SELÇUKLU, KONYA)

Yaşar EREN[1]

Şeyda PARLAR[2]

Berkant COŞKUNER[3]

1 Prof. Dr., Konya Technical University, Faculty of Engineering and Natural Sciences, Department of Geological Engineering, ORCID: ID/0000-0002-7899-8507
2 Asst. Prof. Dr., Konya Technical University, Faculty of Engineering and Natural Sciences, Department of Geological Engineering, ORCID:ID/0000-0003-1048-0100
3 Res Asst. Dr. Konya Technical University, Faculty of Engineering and Natural Sciences, Department of Geological Engineering, ORCID: ID/0000-0002-9798-8793

1. INTRODUCTION

Konya (Central Anatolia, Türkiye) region contains many sinkholes of different features and sizes (Erinç, 1960, Eroskay, 1976; Eroskay and Günay 1979; Güldalı and Şaroğlu, 1983; Canik and Çörekçioğlu 1986; Erol 1991; Bayari et al., 2009; Doğan and Yılmaz 2011; Göçmez 2011; Günay et al., 2010; Özdemir, 2015a, 2015b; Orhan et al., 2020; Eren et al, 2024). Especially in recent years, this region has attracted attention with its widespread sinkhole formations. One of the most well-known sinkhole areas in the Konya region is the Karapınar region. In this region called the Sinkhole Plateau, there are many sinkholes, each of which is a natural monument, with a diameter of 1 km and a depth of 150 meters. Most of these sinkholes are old formations, but there are also many recent sinkholes that have formed especially in the last 25 years.

The formation of sinkholes (doline, Williams, 2004, Waltham et al., 2005; Cvijic, 1893) or, in the local language, opan is basically a karstic event, and soluble rocks such as limestone, dolomite, gypsum, etc., groundwater and the fractures of the earth's crust play a major role in their formation. Carbon dioxide-rich waters circulating in the fractures within the soluble rocks dissolve these rocks over time and lead to the formation of underground cavities and cave systems.

There are several reasons for sinkhole formation. However, the main reason for sinkhole formation is the collapse of the ceilings of underground cavities (karst cavities) in soluble rocks (evaporitic rocks such as limestone, dolomite, gypsum and anhydrite). The chemical reactions related to the dissolution of limestones are as follows;

• Underground water combines with carbon dioxide to form carbonic acid

– $H_2O + CO_2 \rightarrow H_2CO_3$ (carbonic acid)

• (CO_2 gas usually originates from young volcanic rocks in areas where sinkholes are formed).

– Carbonic acidic waters affect the limestone in which it is located to form calcium bicarbonate

– $CaCO_3 + H_2CO_3 \rightarrow Ca(HCO_3)_2$

– Thus, limestones are dissolved

Due to the widespread presence of limestones in Turkey, sinkholes are generally observed in such rocks.

Through this mechanism, underground cavities and caves are formed when carbonic acid-rich waters circulating along fractures and faults dis-

solve limestones. The rocks above these cave systems dissolve towards the surface over time and the ceiling collapses, resulting in the formation of sinkholes. Sinkholes have formation mechanisms such as dissolution, collapse, etc. and can be divided into 6 main groups as solution sinkhole, collapse sinkhole, caprock sinkhole, dropout sinkhole, suffosion sinkhole and buried sinkhole (Waltham et al, 2005) (Fig. 1).

In addition to these, collapse of underground mining galleries, excessive withdrawal of clastic material together with water from underground by drilling, surface deformations due to excessive withdrawal of underground water, etc. may also lead to sinkhole formation.

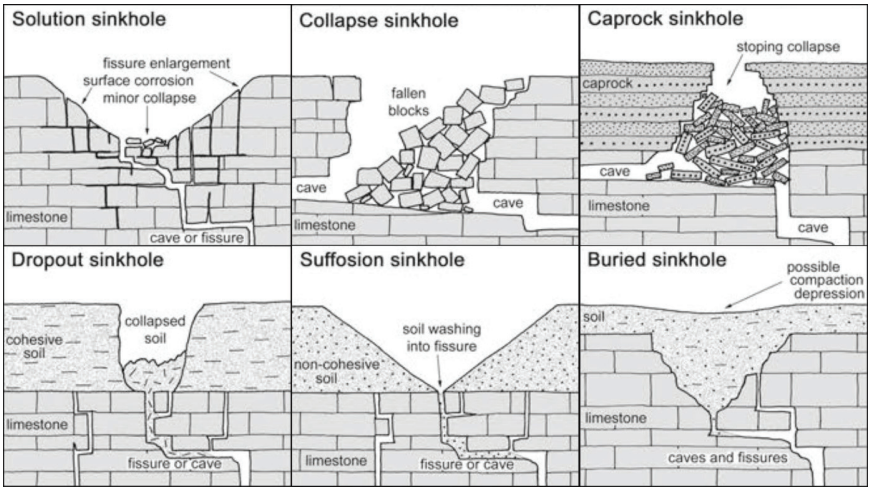

Fig. 1. Sinkhole types (taken from Waltham et al. 2005).

In the Konya region, sinkholes are commonly encountered in the elevations where settlement is very scarce and in the basins between these elevations. Yaren Sinkhole (Fig. 2), located 30 km northeast of Konya city center, is a collapse sinkhole that developed within the Mesozoic marbles and dolomite marbles in the mountain range called Bozdağlar. In this study, the geological and morphological features of the Yaren Sinkhole will be explained and its formation model will be revealed.

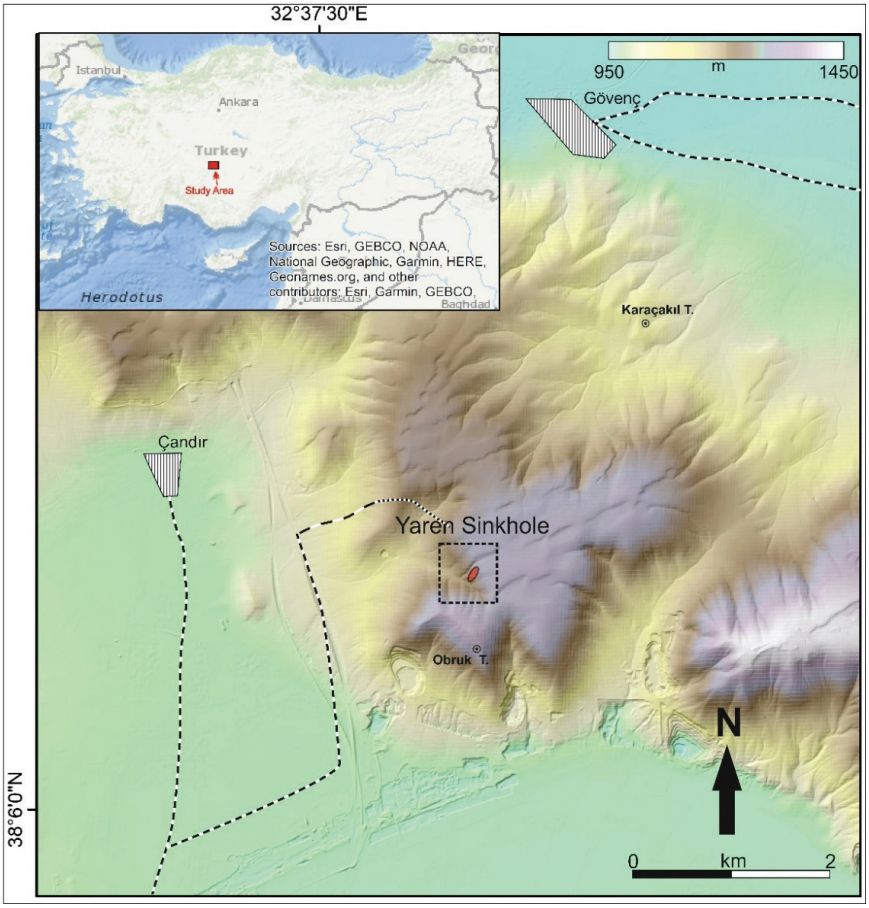

Fig. 2. Location map of the study area

2. GEOLOGY

The study area is located in the north of Konya Province, within a group called Bozdağlar Massif, which contains Paleozoic and Mesozoic rocks and has been affected by pre-Alpine, Alpine and late tectonic movements (Kaaden, 1966; Wiesner 1968; Göger and Kıral 1969; Eren 1993, 1996a, 1996b, 2003a, Eren et al., 2004; Özcan et al. 1988, 1990; Kurt 1996, 1997, Kurt & Arslan 1999; Ulu et al.,1994). The main morphological structures of the region are formed by east-west and northwest-southeast trending elevations and the basins located between them. The elevations contain Paleozoic and Mesozoic metamorphic rocks, rocks of oceanic origin and Miocene-Pliocene lacustrine, continental and volcanic rocks. The basins located between these elevations and bounded by faults contain Pliocene-Quaternary aged lacustrine-alluvial and young volcanic formations (Keller, 1974; Besang et al. 1977; Eren, 1996a, 2001, 2003b; Eren 2011; Eren et al. 2024; Koç et al. 2012; Hüseyinca and Eren 2007; Aksoy 2019; Asan et al.

2021; Friedrichs et al. 2020; Gençoğlu et al. 2022).

Paleozoic-Mesozoic rocks were affected by pre-Alpine and Alpine movements were folded, metamorphosed and gained nappe, thrust and fractures (Eren 1996 and 2001). In the young tectonic period, block faulting formed north-south and east-west trending depression basins in the region and the basement rocks were fractured and uplifted again.

2.1. Stratigraphy

In the study area, from oldest to youngest; Triassic-Jurassic Kızılören formation, Jurassic-Cretaceous Lorasdağı formation, Cretaceous Midostepe formation, Upper Miocene-Pliocene Ulumuhsine formation, Pliocene-Quaternary Topraklı formation and Quaternary Konya formation were identified (Fig. 3).

2.1.1. Kızılören Formation

The unit, which is predominantly composed of dark-colored metacarbonates and was first named by Göğer and Kıral (1969), crops out in a wide area around Karaçakıl Hill and in a few narrow areas northwest of Çandır in the study area (Fig. 3).The unit is generally composed of dark gray and black colored dolomite and dolomitic marbles with medium and thick layers and brecciated. The unit that forms the base in the study area is overlain by the Lorasdağı formation with a lateral-vertical transition conformably. The age of the unit is accepted as Triassic-Jurassic (Göğer and Kıral, 1969; Eren, 1993).

2.1.2. Lorasdağı Formation

The unit, which originally consists of shallow marine metacarbonates, was first named by Göğer and Kıral (1969). It crops out over a very wide area from northwest to southeast in the study area (Fig. 3). Metacarbonates with gray, blue, white and cream colors also contain metachert and metaquartzite interlayers parallel to the bedding. Karstic cave and sinkhole formations are also present in the unit. Çandır Yaren Sinkhole, which is the main subject of this study, is also within the Lorasdağı formation. Midostepe formation is conformably rest on the Lorasdağı formation with lateral-vertical transition (Fig. 3). The age of the unit is Late Triassic-Early Cretaceous (Göğer and Kıral 1969; Özcan et al. 1988 and Eren 1993).

2.1.3. Midostepe Formation

Midostepe formation (Göğer and Kıral 1969), which is originally formed by the alternation of pelagic metacarbonate, metachert and metaclastics, crops out in a narrow area in the east of Çandır in the study area (Fig. 3). The lithology of the unit is mostly composed of light gray, gray, beige and pink-white colored metacarbonates with very thin layering. Among these

metacarbonates, thin and medium layered metachert and metaquartzites are observed, while in the upper levels of the unit, yellow, gray, pink and purple colored phyllites and calcphyllites are observed. Topraklı formation is on the Midostepe formation with an angular unconformity (Fig. 3).

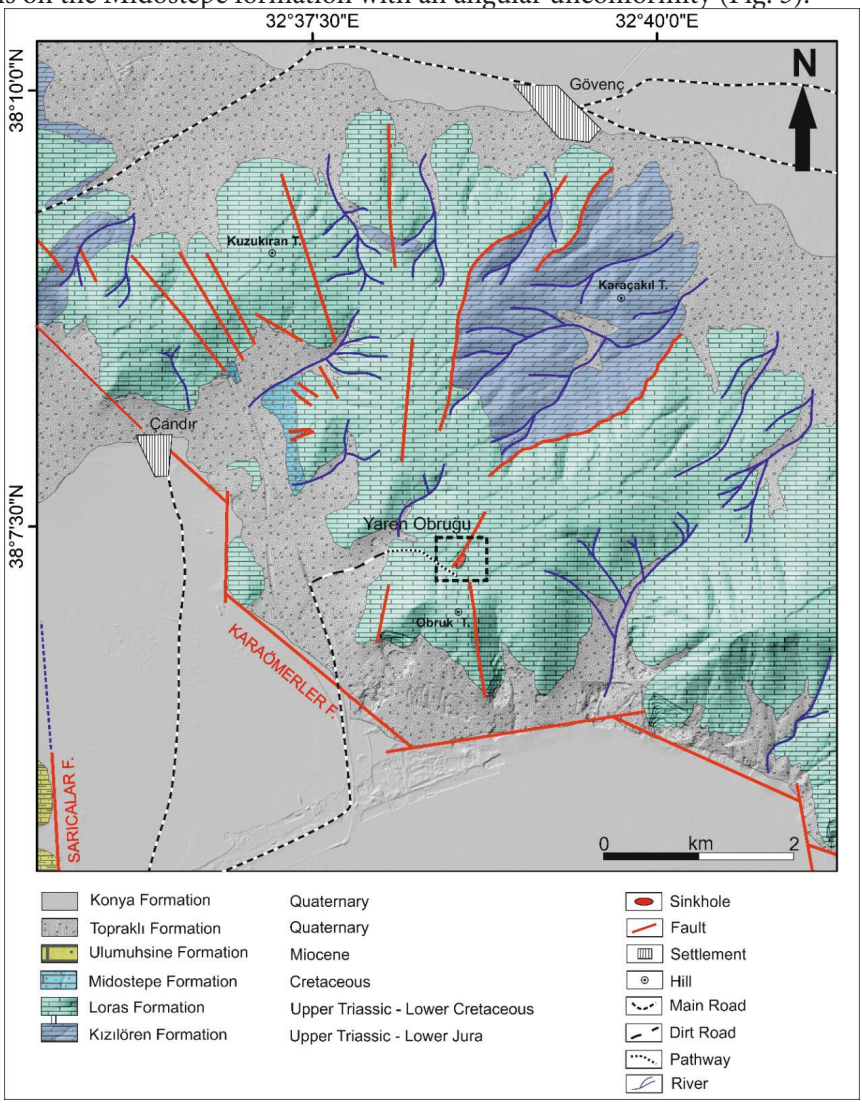

Fig. 3. Geological map of the study area

2.1.4. Ulumuhsine Formation

The Ulumuhsine formation (Göğer and Kıral 1969 and Eren 1993), which consists of lacustrine limestone, clayey limestone, marl, mud, conglomerate and sandstone, crops out in a narrow area in the southwest of

the study area (Fig. 3). The thin-thick layered limestones of the formation have white, yellow, cream, beige and gray colors and contain distinctly oncolithic and stromatolithic structures, freshwater gastropod and bivalve fossils. In addition, clayey limestones and marls with white, yellowish, green and gray colors are also observed. The conglomerates in the lower levels of the unit are matrix-bounded and have the shape of lensoidal and erosional channels. Gradations, parallel and cross laminations are observed in the conglomerates and sandstones in the upper levels. In the eastern part, seismites are also observed in the Ulumuhsine Formation which is in contact with the Konya Formation along the Sarıcalar fault. The Ulumuhsine formation is overlain by the Topraklı and Konya formations with an angular unconformity (Fig. 3). The age of the unit is Late Miocene-Early Pliocene (Göğer and Kıral 1969 and Eren 1993).

2.1.5. Topraklı Formation

Topraklı Formation (Doğan 1975) consists of red, brown and gray conglomerate, mud, sand, clay, and caliche. The unit is observed as alluvial fan deposits in the transitions from elevations to plains in the study area and crops out in very large areas (Fig. 3). The conglomerates with clay, sand and mud successions are matrix-binded and their constituents are mostly massif-derived clastics. They are polygenic and heterogeneous. In some parts of the unit, there are 3-5 cm thick caliche nodules and levels in dirty white and light yellow colors. Topraklı formation covers the older units with an angular unconformity and according to Eren (1993), it is Late Pliocene-Quaternary in age.

2.1.6. Konya Formation

The deposits of streams, swamps and temporary lakes in the large basins on both sides of the elevations formed by the older units in the study area are considered as Konya Formation. The unit outcrops in the south and north of the northwest-southeast trending elevations in the study area (Fig. 3). Konya Formation consists of mostly unconsolidated gravel, sand, clay and mud. This unit is Quaternary aged and has a nearly horizontal dip and covers all the older units in the region with angular unconformity.

2.2. Structural Geology

Mesozoic aged rocks in the study area were deformed, folded and fractured by Alpine events. In these rocks, outcrop-scale folds, generally small-scale strike-slip faults and fractures in variable directions are observed in the Alpine stage. During the Miocene-Pliocene period, these rocks were uplifted as a horst by block faulting. Depending on the basin formation, the edges of the elevations are bounded by normal faults. Karaömerler and Sarıcalar faults are examples of these faults in the study

area. Karaömerler Fault, which delimits the elevations in the study area from the southwest, is oriented NW-SSE and is connected with transfer faults of different orientations and is 10 km long (Fig. 3). The south side of the southwest-trending normal fault has been subsided and the north side has been uplifted. It generally forms the boundary between Konya and Toprakli formations.

The Sarıcalar fault is a north-south trending east- dipping normal fault that forms the boundary between the Ulumuhsine and the Konya formations in the southwestern part of the study area. It is an active fault and produced an earthquake with a magnitude of Mw: 5.0 in 2023 according to Kandilli observatory data.

In addition to these, widespread fractures are encountered in the basement rocks. In the south of the Güvenç District, the Kiziloren Formation was raised as a horst by two normal faults extending north-northeast between the Lorasdagi Formation.There are many northwest-southeast trending faults parallel to the Sarıcalar and Karaömerler Faults within the Mesozoic aged units in the northwest of the study area. There are also aragonite veins parallel to the northeast-southwest and north-south trending faults. These aragonite veins are 1-2 metres wide and up to 100 metres long. Numerous dissolution structures formed as a result of external karstification are commonly observed along the fractures. Yaren sinkhole, which is the subject of this study, developed parallel to such a fractured structure.

3. MORPHOLOGICAL FEATURES OF THE YAREN SINKHOLE

Located northeast of Konya, Yaren Sinkhole is 30 km horizontally and 37 km by road from the city centre (Fig. 2). Located on a small-scale slope (Fig. 4a), the Yaren sinkhole is immediately recognisable in satellite images with its teardrop-like appearance (Fig. 4b, 4c, 5a, 5b). Yaren Sinkhole is located 3.385 km southeast of Çandır Quarter, 4.755 km northeast of Güvenç Quarter and 4.815 km northeast of Sarıcalar Quarter. Obruk is located on the border of Güvenç and Çandır neighbourhoods. Since it is located on the northeastern slope of a stream running west-northwest and east-southeast and surrounded by higher areas, it is not visible from a distance and does not attract attention. For this reason, it is not well known except for the people in the surrounding neighbourhoods. It can be reached by walking 1.5 km from Sarıcalar Quarter on a stabilised road parallel to the high speed railway on the way to the quarries (Fig. 2).

The sinkhole was formed within the highly fractured and jointed marbles of the Lorasdagi Formation. The sinkhole developed parallel to a

northeast-southwest trending fracture, apparently about 600 metres long (Fig. 4d, 4e). In this study, the cavity was divided into 3 sections; body (b), tail (t) and roofed section (r) (Fig. 5c, 5d). The main section (body) with collapsed roof is located on the southwest side of the fracture (Fig. 4f), the narrow and deep tail section with less depth is located on the northeast side of the fracture (Fig. 4g), and the section with uncollapsed roof (roof) continues horizontally for 20 metres (Fig. 5c). In the satellite view, the length of the sinkhole (including the tail) ($L_s = L_t+L_b+L_r$) is 107 metres, the surface length of the sinkhole excluding the tail (L_b+L_r) is 61 metres and the width of the sinkhole (W_s) is 33 metres at the widest part of the sinkhole. It also continues 20 metres to the southwest under the uncollapsed roof (L_r) except for the surface view (Fig. 5d).Above this uncollapsed roof, there is a window up to 3 metres deep opening into the subsurface through which the sinkhole can be observed (Fig. 4h). The deepest part of the sinkhole ($d_s=d_b$) was measured to be 25 metres. The maximum depth of the tail section (d_t) was measured as 11 metres.

Fig. 4. Views from the Yaren Sinkhole; (a) Google Earth satellite image, (b, c) remote view from west to east, (d, e) close-up view from southwest to northeast, (f) large section with collapsed roof (g) close-up view of the tail section from south-west, (h) Small window opening into the sinkhole from the section without collapsed roof

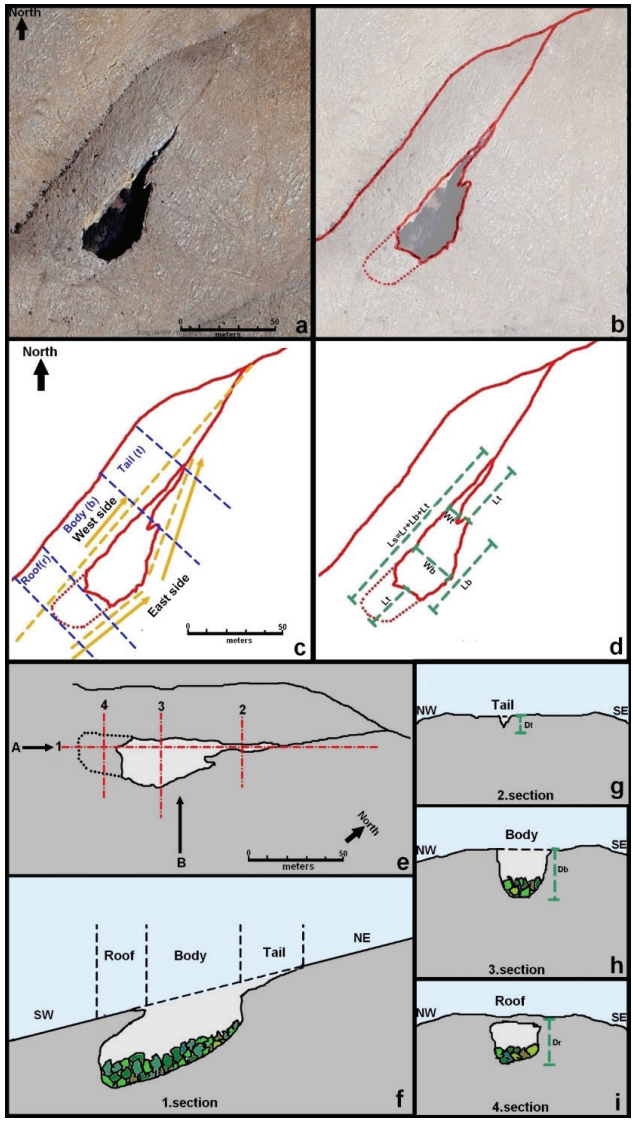

Fig. 5. (a) Satellite image of the Yaren Sinkhole (b) Schematic drawing superimposed on the satellite view (c) Subdivision of the sinkhole and the orientation of its sides with respect to the fracture to the northwest (d) Morphological components of the sinkhole (e) Bird's-eye view showing profile section locations (f) 1st cross-section along the long axis in view direction A (g) 2nd cross section showing the tail in view direction B, (h) 3rd cross section showing the body, (i) 4th cross section showing the roof (A, B: view directions; 1, 2, 3, 4: section directions; SW, NE, NW, SE: section directions, L: length, W: width, d: depth)

The length of the tail section is L_t=36 metres and its width varies between W_t=0-5 metres (Fig. 5d). There are aragonite veins parallel to the course of the tail in this section. The depth of this section varies between d_t=0-11 metres. The hollow opening in the tail is up to 1.5 metres (Fig. 6a-6e).

The width of the main sinkhole varies between W_s=W_b=7-33 metres. The section parallel to the tail on the west side has a straight course (Fig. 6f) and changes direction towards the west at the end. In other words, most of this section is parallel to the fracture forming the sinkhole (Fig. 6g, 6h). The eastern cut is also parallel to the fracture in a northwest-southeast direction and changes its direction to northeast-southwest in the central part (Fig. 5c). In order to reveal the shape of the sinkhole, profile sections were taken through the sinkhole (Fig. 5e). The sections prepared along the long axis (Fig. 5f) and perpendicular to the long axis from the tail (Fig. 5g), body (Fig. 5h) and roof (Fig. 5i) show the in-depth shape of the sinkhole.

It is filled with trees of various sizes (Fig. 7a, 7b and 7c). Located on a completely bare land, the sinkhole looks like an "oasis in the middle of the desert". The sinkhole expands downwards after a depth of 20 metres in the eastern section and the trees continue until this section. In the western section, the trees start at a depth of 5 metres and continue downwards as a sloping surface into the sinkhole.

In the sinkhole which has at least 4 fracture sets in the map view, two of the fracture sets are perpendicular to each other and the other two sets make an acute angle with the long axis trending northeast-southwest. On the walls of the sinkhole, there are two sets of low inclined fractures and a third set of steeper inclined fractures cut by them (Fig. 7d and 7e). On the walls parallel to the short axis, there is another set of nearly vertical fractures filled with aragonite veins.

The shape of the uncollapsed dome section (roof) (Fig. 7f, 7g and 7h) is controlled by two low-angle fracture systems. Above the roof itself there are smaller windows, up to 2 metres long and 1 metre wide, opening into the sinkhole. As the collapse of the edges of this section continues, it is foreseen that these smaller windows may merge with the larger one in the future. The length of the covered section is approximately 20 metres and its width is 18 metres, and its depth decreases in an arc downwards and ends.

4. FORMATION MODEL

According to the geometry of the sinkhole and the characteristics of the surrounding fracture systems, it is seen that the sinkhole started to form parallel to the northeast-southwest trending fractures and its morphology is controlled by these fracture systems.

The Mesozoic aged marble and dolomite marbles in which the sinkhole is located were deformed and folded by the Alpine mountain-building events in the late Cretaceous (Fig. 8a, 8b). During the last phase of these orogenic events, the rocks again became fractured in the form of low-angle shear fractures due to horizontal shortening (Fig. 8c).

Fig. 6. (a) Cross section view of the tail section from south inside the sinkhole, (b) View of the tail section from northeast to southwest (c) V-shaped section view of the tail section, (d) Aragonite veins in the tail section, (e) View of the end of the tail section from southwest to northeast (f) Close-up view of the wall of the western section of the sinkhole (g, h) View of the sinkhole from north to south

Fig. 7 (a) View of the boundary of the main sinkhole with the unroofed section. (b, c) top view of the trees inside the sinkhole, (d, e) view of the broken systems on the eastern walls of the sinkhole, (f, g, h) views of the unroofed section from north to south

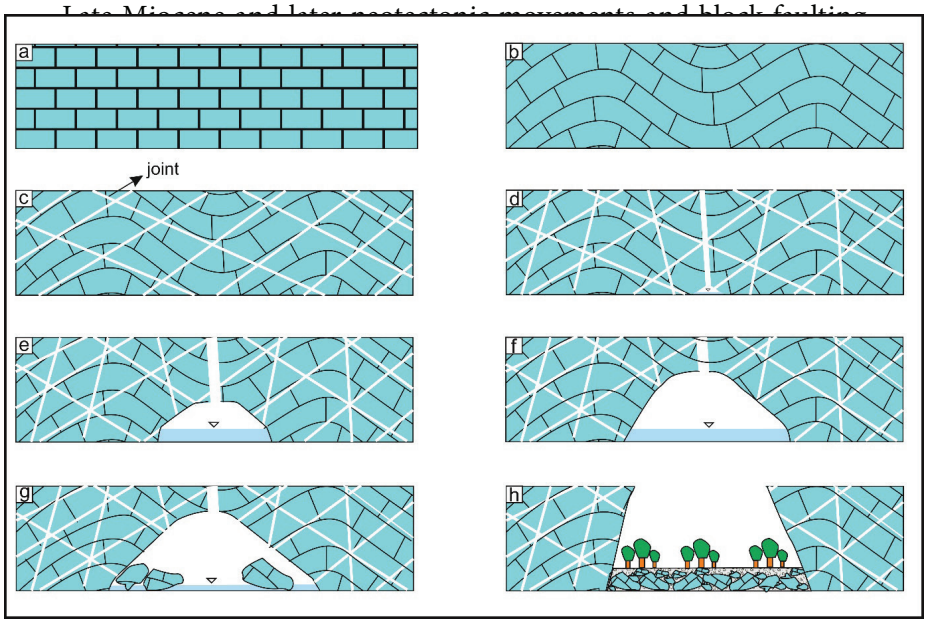

Fig. 8. Formation model of the Yaren Sinkhole (a) The state of the bedrock in which the sinkhole is located before deformation (b) deformation and folding (c) formation of a fractured structure in the form of low-angle shear fractures (d) formation of steeper inclined shear and tensile fractures (e) initiation of karstic dissolution (f) upward rise of the void with karstic dissolution (g) increase in the size of the void with collapses (h) formation of the sinkhole with the collapse of the roof

5. THE SIGNIFICANCE IN TERMS OF GEOTOURISM

Like Karapınar plateau sinkholes, the Yaren sinkhole is an important geological formation in terms of geotourism. The sinkhole, which contains different types of trees, creates the appearance of an "oasis in the desert" on a bare land without vegetation. With this attractive appearance, it resembles the Cennet Obruk in Mersin. Both its shape and the fact that it is an interesting and rare geological formation and that it is worthy of study by researchers working in different branches of science other than geology increase the value of the sinkhole even more. In addition, its proximity to Konya city centre and easy accessibility increases the importance of this sinkhole.

6. CONCLUSIONS AND SUGGESTION

The Yaren Sinkhole formed as a result of karstification within the marbles of the Mesozoic aged Lorasdağı Formation is a collapse sinkhole.

The long axis of Yaren Sinkhole developed parallel to a KKD-GGB trending fracture in the region and its formation and morphological shape were shaped by dense fracture sets. There are hundreds of trees of various sizes and species in the WNW-ESE trending depression, which forms a unique habitat in an elevation that can be considered completely devoid of vegetation, and serves as a shelter centre for wild birds. With its proximity to Konya city centre and its interesting structure, the Yaren sinkhole is an important natural wonder in terms of geotourism. In order to protect this natural wonder and bring it to tourism, the following measures are proposed.

1. The perimeter should be equipped with fences, warning signs, barriers and similar safety equipment,

2. Installation of lifts or similar mechanisms to provide descent to the parts where there is no risk of collapse,

3. The part of the roof that has not yet collapsed is to be prevented from being walked on or entered,

4. Construction of a vehicular or pedestrian road that will provide access to the stream at the bottom of the sinkhole.

These proposals will make it possible for this structure to be reached and seen by a large number of people. In this way, a suitable place alternative will be created for social activities such as walking and photography. Such geological structures are rare structures that can be formed in thousands or millions of years. Damage, destruction or destruction of this structure would be an irreversible loss

7. REFERENCES

Aksoy, R. (2019). Extensional neotectonic regime in west-southwest Konya, Central Anatolia, Turkey. International Geology Review, 61 (14), 1803-1821.

Asan, K., Kurt, H., Gündüz, M., Gençoğlu Korkmaz, G. and Morgan, G. (2021). Geology, geochronology and geochemistry of the Miocene Sulutas volcanic complex, Konya-Central Anatolia: genesis of orogenic and anorogenic rock associations in an extensional geodynamic setting. International Geology Review, 63 (2), 161-192.

Bayarı, C. S., Pekkan, E., Ozyurt, N. N., (2008). Obruks, as giant collapse dolines caused by hypogenic karstification in Central Anatolia, Turkey: analysis of likely formation processes. Hydrogeology Journal, 17, 327–345. https://doi.org/10.1007/s10040-008-0351-9

Besang, C., Eckhardt, FJ, Harre, W., Kreuzer, H. and Müller, P. (1977). Radiometrische-Altersbestimmungen An Neogenen Eruptivgesteinen Der Türkei. Geol. Jb., B25, 3-36.

Canik, B., Çörekçioğlu, İ., (1986). The Formation Of Sinkholes (Obruk) Between Karapınar and Kızören – Konya. IAHS-AISH publication, 161, 193-205.

Cvijić, J., 1893. Das Karstphanomen. Versuch einer morphologischen Monographie. Geographischen Abhandlung, 3, 218-329.

Doğan, U., Yılmaz, M. (2011). Natural and induced sinkholes of the Obruk Plateau and Karapınar-Hotamış Plain, Turkey. J. Asian Earth Sci., 40, 496–508. doi: 10.1016/j.jseaes.2010.09.014.

Eren, Y., Parlar, Ş., Coşkuner, B. Arslan, Ş. (2024). Geological and Morphological Features of the Karapınar Sinkholes (Konya, Central Anatolia, Türkiye). J. Earth Sci. 35, 1654–1668 (2024). https://doi.org/10.1007/s12583-023-1853-z.

Eren, Y. (1993). Stratigraphy of autochthonous and cover units of the Bozdağlar massif NW Konya. Geological Bulletin of Turkey, 36, 7-23.

Eren, Y. (1996). Structural features of the Bozdağlar massif to the south of Ilgın and Sarayönü (Konya). Geological Bulletin of Turkey, 39 (2), 49-64.

Eren, Y. (1996b) Stratigraphy and geological evolution of the Bozdağlar Massif in the south of Ilgın and Sarayönü (Konya). In: Korkmaz, S., Akçay, M. (Eds) Karadeniz Technical University Department of Geology 30th Year Symposium, Proceedings, II: 694–707 (in Turkish, English abstr.).

Eren, Y. (1996c). Pre-Alpine overthrusts in the north of Sille-Tatköy (Bozdağlar Massif-Konya). Bull Geol. Congr. Turkey 11, 163–169 (in Turkish, English abstr.).

Eren, Y. (2001). Polyphase Alpine deformation at the northern edge of the Menderes-Taurus block, North Konya, Central Turkey. J. of Asian Earth Sci., 19 (6), 737-749.

Eren, Y. (2003a). Konya bölgesinin depremselliği. Türkiye Petrol Jeologları Derneği Özel Sayı, 5, 85-98.

Eren, Y. (2003b). Yazır Fayı'nın (Konya) Neo-Tektonik Özellikleri. Pamukkale Üniversitesi Mühendislik Bilimleri Dergisi, 9 (2), 237-244.

Eren, Y. (2011). Konya'nın jeolojisi, Neo-tektonik yapısı ve depremselliği. I. Konya Kent Sempozyumu, 111-120.

Eren, Y., Kurt, H., François, R., Stampfli, G.M. (2004). Palaeozoic deformation and magmatism in the northern area of the Anatolide block (Konya), witness of the Palaeotethys active margin. Eclogae Geologicae Helvetiae, 97(2), 293-306. https://doi.org/10.1007/s00015-003 -1131-8

Erinç, S. (1960) Karst forms in the Konya Section and the Inner Taurus ranges. Turkish Journal of Geograph, 20, 83-106 (in Turkish).

Erol, O. (1991). The relationship between the phases of the development of the Konya-Karapinar obruks and the Pleistocene Tuz Gölü and Konya pluvial lakes, Turkey. Journal of Istanbul University Institute of Marine Sciences and Geography, 7, 5-49 (in Turkish).

Eroskay, O., Gunay, G. (1979). Tectonic classification and hydrogeological properties of the karst regions in Turkey. In: Gunay G eds. International Seminar on Karst Hydrogeology, 1–41.

Eroskay, S. O. (1976). The factors influencing the Konya Obruks and their groundwater potentials evaluation. İstanbul Üniv., Fen. Fak. Mec. Seri. B, 41 (1-4), 5-14.

Friedrichs, B., Atıcı, G., Danišík, M., Atakay, E., Çobankaya, M., Harvey, J. C., Yurteri, E. and Schmitt, A. K. (2020). Late Pleistocene eruptive recurrence in the post-collisional Mt. Hasan stratovolcanic complex (Central Anatolia) revealed by zircon double-dating. J. of Volcanology and Geothermal Res., 404, 107007.

Gençoğlu, K. G., Kurt, H., Asan, K. and Leybourne, M. (2022). Ar-Ar Geochronology and Sr-Nd-Pb-O Isotopic Systematics of the Post-collisional Volcanic Rocks from the Karapınar-Karacadağ Area (Central Anatolia, Turkey): An Alternative Model for Orogenic Geochemical Signature in Sodic Alkali Basalts. Journal of Geosciences, 1, 53 – 69. http://doi.org/10.3190/jgeosci.343.

Göçmez, G. (2011). Sinkholes and Travertine Cones in Konya Province. Proceedings of I. Konya City Symposium, 459-464 (in Turkish).

Göğer, E., Kıral, K. (1969) Geology of the Kızılören region. Min. Res. Expl. Rep. 5204 (in Turkish)

Güldalı, N., Şaroğlu, F. (1983). Sinkholes of Konya region. T.J.K. Yeryuvarı ve İnsan, 7(4), 44-55 (in Turkish).

Günay, G., Çörekçioğlu, İ., Eroskay, S., Övül, G. (2010). Konya Karapınar Obruks (Sinkholes) of Turkey. In: B. Andreo et al. (ed) Advances in Research in Karst. Media, Springer, 367-372. https://doi.org/10.1007/978-3-642-12486-0.

Hüseyinca, M. Y., Eren, Y. (2007). Ilgın (Konya) Kuzeyinin Stratigrafisi ve Tektonik Evrimi. Selçuk Üniv. Müh., Bil.ve Tekn. Derg., 22 (1), 83-96.

Kaaden, W.G. (1966). The significance and distribution of glaucophane rocks in Turkey. MTA Bull. 67, 36–67

Keller, J., 1974. Quaternary maar volcanism near Karapinar in Central Anatolia. Bulletin Volcanologique, 38, 378-396.

Koç, A., Kaymakci, N., Hinsbergen, D.J.J. VanKuiper, K.F., Vissers, R.L.M. (2012). Tectono sedimentary evolution and geochronology of the middle Miocene Altınapa Basin, and implications for the late Cenozoic uplift history of the Taurides, southern Turkey. Tectonophysics, 532 (535), 134-155.

Kurt, H., Arslan, M. (1999). Geochemistry and petrogenesis of Kadınhanı (Konya) K-rich metatrachyandesite: The evolution of Devonian (?) volcanism. Geol. Bull. Turkey 42(1), 57-69

Kurt, H. (1996). Geochemical characteristics of the meta-igneous rocks near Kadınhanı (Konya), Turkey. Geosound 28, 1–22.

Kurt, H. (1997), Geochemistry of metasedimentary rocks of the Kadınhanı (Konya) area, Turkey. Geosound, 31, 1–21.

Orhan, O., Yakar, Y., Ekercin, S. (2020). An application on sinkhole susceptibility mapping by integrating remote sensing and geographic information system. Arabian Journal of Geosciences, 13, 1-17. https://doi.org/10.1007/s12517-020-05841-6.

Özcan, A., Göncüoğlu, M.C., Turhan, N., Uysal, S., Şentürk, K., Işık, A. (1988) Late Palaeozoic evolution of the Kütahya-Bolkardağı belt. METU J. Pure Appl. Sci., 21 (1/3), 211–220.

Özdemir, A. (2015a). Sinkhole Susceptibility Mapping Using a Frequency Ratio Method and GIS Technology Near Karapınar, Konya-Turkey. Procedia

Earth and Planetary Science, 15, 502-506. https://doi.org/10.1016/j.proeps.2015.08.059.

Özdemir, A. (2015b). Investigation of sinkholes spatial distribution using the weights of evidence method and GIS in the vicinity of Karapinar (Konya, Turkey). Geomorphology, 245, 40-50. http://dx.doi.org/10.1016/j.geomorph.2015.04.034.

Ulu, Ü., Öcal, H., Bulduk, A.K., Karaka, M., Arbaş, A., Saçlı, L., Taşkıran, M.A., Ekmekçi, E., Adır, M., Sözeri, Ş. and Karabıyıkoğlu. M. (1994). Güneybatı İç Anadolu'nun stratigrafisi ve yapısal evrimi. Proceedings, 9th Turkish Geology Symposium, 171-182.

Waltham, T., Bell, F., Culshaw, M. (2005). Sinkholes and subsidence: karst and cavernous rocks in engineering and construction. Berlin. 300, https://doi.org/10.1007/b138363.

Wiesner, K. (1968). Konya civa yataklari ve bunlar üzerindeki etüdler, M,T. A. Ens. Dergisi, 70, 178-213.

Williams, P. W. (2004). Dolines. In: Gunn J (ed.) Encyclopedia of Caves and Karst Science, Fitzroy Dearnorn, New York, 304 – 310.

Chapter 12

ENHANCEMENT OF PHASE CHANGE MATERIALS WITH NANOPARTICLES: THERMAL PERFORMANCE AND ENERGY APPLICATIONS

Şafak Melih ŞENOCAK[1]

Yasin VAROL[2]

1 Şafak Melih ŞENOCAK, Lecturer, Osmaniye Korkut Ata University, Osmaniye Vocational School, e-mail: mlhsnck@gmail.com, ORCID ID: https://orcid.org/0000-0003-0602-2836

2 Prof. Dr. Yasin VAROL, Firat University, Technology Faculty, Elazig, e-mail: yvarol@gmail.com, ORCID ID: https://orcid.org/0000-0003-2989-7125

1. Introduction

Over the past few years, global energy demand has witnessed a substantial rise, fueled by interrelated factors such as rapid population growth and the intensifying impacts of globalization. This trend underscores the increasing pressure on energy systems to meet the demands of expanding urbanization and industrial activities. According to the International Energy Agency (IEA), primary energy consumption has surged by 48% over the past two decades, with a corresponding 42% increase in carbon dioxide (CO_2) emissions, further exacerbating global environmental challenges. Moreover, projections indicate that the demand for cooling an essential component of modern infrastructure is expected to triple between 2010 and 2050, driven by factors such as rising living standards, urban heat island effects, and climate change. Within this context, passive cooling strategies have emerged as a critical focus of research due to their energy efficiency and sustainability. In particular, innovative methods utilizing nanofluids, vapor chambers, and phase change materials (PCM) have garnered significant attention in the literature, offering promising solutions for enhanced thermal management in a variety of applications, including building systems, electronics cooling, and renewable energy technologies (Hussain, Ertam, Ben Hamida, Oztop, & Abu-Hamdeh, 2023; J. Li, Zhang, Xu, & Yuan, 2021; Varol, Coşanay, et al., 2025; Varol, Oztop, et al., 2025). In recent years, researchers have focused on enhancing the latent thermal energy storage capabilities of phase change materials (PCM) across various fields, including building thermal comfort (Kean, 2019; Sidik, Nor Azwadi Che & M'hamed Beriache, 2020), electronics cooling (Krishna, Kishore, & Solomon, 2017) and solar energy technologies (Mao, Chen, & Yang, 2019) A key advantage of PCMs lies in their ability to store thermal energy either as latent or sensible heat, or through chemical reactions, making them versatile for different applications. The suitability of a storage medium depends on several critical factors, including its specific size or weight, the energy storage capacity, and the temperature range required for a particular application. These parameters play a pivotal role in optimizing the material's performance for energy management solutions (Chandrasekaran, Cheralathan, Kumaresan, & Velraj, 2014; Shank et al., 2022; Shank & Tiari, 2023; Tofani & Tiari, 2021). Recent studies have also highlighted the importance of tailoring PCM properties to align with specific use cases, further driving innovations in material design and application efficiency. Thermal energy storage (TES) technology enables the alignment of supply and demand by addressing the time gap between energy generation and consumption. This capability allows for the reduction or even elimination of peak electricity loads in buildings, improving energy efficiency and grid stability. TES systems are particularly

effective in low-temperature applications such as milk preservation, food transportation, and cold storage. In recent years, researchers have focused on integrating the TES concept into various low-temperature systems with enhanced thermal performance, aiming to optimize energy use in these applications. Phase change materials (PCM) play a pivotal role in TES systems due to their ability to absorb and release latent heat during phase transitions, making them efficient energy storage solutions. Such latent heat storage methods are especially favored for their ability to provide high energy storage capacity over a broad range of operating temperatures, making them indispensable for diverse thermal management applications. (Tofani & Tiari, 2021; Trelles & Dufly, 2003). Phase transitions can occur through various phase combinations; however, for PCM applications, the most efficient phase changes are those involving liquid-to-solid (solidification) and solid-to-liquid (melting) transitions (Bruno, Belusko, Liu, & Tay, 2015). In other words, the solidification process in PCMs allows the release of latent heat, while the melting process facilitates its storage. Figure 1 illustrates latent heat, representing the energy required to induce a phase change in liquids and materials without any change in temperature.

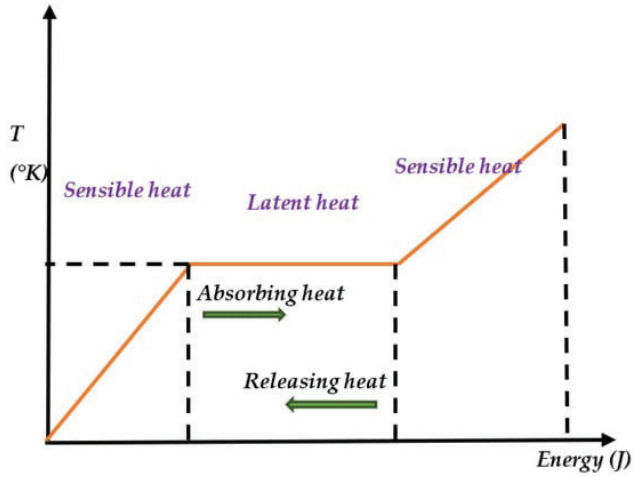

Figure 1. *Definition of latent and sensible heat alteration (Skovajsa, Koláček, & Zálešák, 2017)*

2. Classification of PCMs

PCMs (Jesumathy, Udayakumar, & Suresh, 2012; Kolokotsa, Santamouris, Synnefa, & Karlessi, 2012), are compounds capable of storing or releasing sufficient amounts of energy under specific conditions to create an optimal environment. This characteristic holds significant potential, particularly in heat storage and temperature regulation systems. (Kushwah,

Kumar Gaur, & Kumar Pandit, 2020; Swathykrishnan, Sreelakshmi, Duggal, & Tomar, 2020; Tariq, Ali, Akram, Janjua, & Ahmadlouydarab, 2020). In this context, investigating the role of phase change materials in thermal storage systems emerges as a critically important subject (Hassan, Shakeel Laghari, & Rashid, 2016; Rathore & Shukla, 2019). As shown in Figure 2, PCMs include organic, inorganic, and eutectic components. However, due to their safety, non-corrosive nature, availability, and low cost, paraffins, particularly paraffin wax, are among the most commonly used types of PCMs (Ayala, Enghardt, & Horton, 1997).

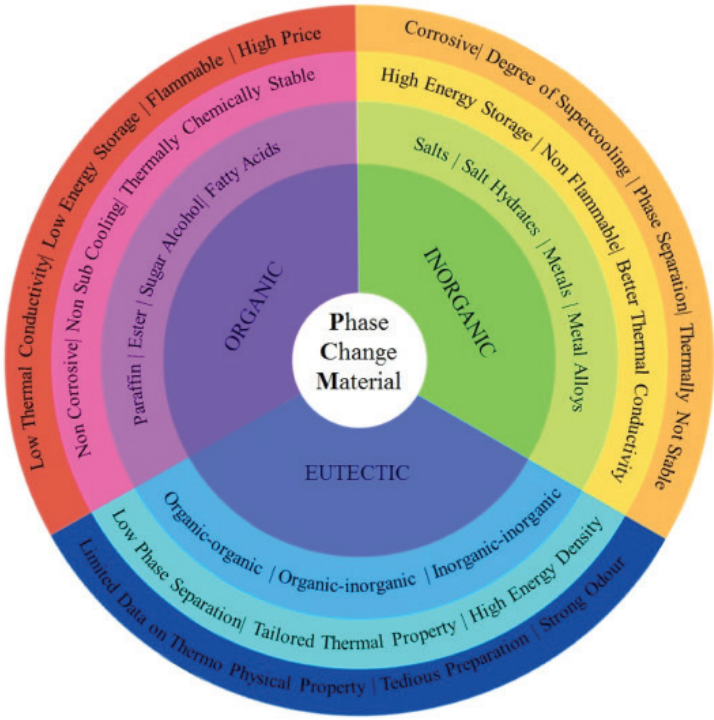

Figure 2. *Nano-enhanced phase change materials: Fundamentals and applications (Said et al., 2024)*

PCMs can be classified according to the phase transitions they undergo, such as solid-to-solid, solid-to-liquid, solid-to-gas, liquid-to-gas, and their reverse transformations. Among these, the solid-to-liquid transition is particularly prominent due to its versatility in energy storage and thermal management applications. This prominence stems from its unique advantages, including substantial energy storage capacity, a broad spectrum of phase change temperatures, and minimal volume fluctuation during phase transitions (Kalidasan, Pandey, Saidur, Samykano, & Tyagi, 2023; Yadav, Samykano, Pandey, Kareri, & Kalidasan, 2024). Solid-to-liquid

PCMs can be further grouped into two distinct categories: low molecular compounds and polymers. Low molecular compounds encompass a wide range of substances, including organic materials such as paraffins, esters, sugar alcohols, glycols, fatty acids, and alcohols; inorganic materials like salt hydrates and metallic compounds; and eutectic mixtures that can combine organic, inorganic, or hybrid components. Polymers, on the other hand, are distinguished by their molecular weight distribution, with examples like polyethylene glycol offering phase transition temperatures that vary depending on their molecular structure and application requirements (Yadav et al., 2024). In addition to their classification by phase transitions, PCMs can also be categorized based on specific criteria such as their chemical composition, intended application, or physical properties. These classifications allow for the precise selection of materials tailored to specific needs, ensuring optimal performance in applications ranging from energy storage systems to thermal regulation solutions. By aligning material properties with their functional demands, PCM technology continues to advance across diverse fields.

2.1. Classification Based on Physical Properties

PCMs can be broadly categorized into two main groups based on their physical structure: organic and inorganic. Organic PCMs typically consist of compounds such as paraffins, fatty acids, and esters. These materials are characterized by their ability to undergo phase transitions within specific temperature ranges, enabling efficient energy storage and release. Known for their high latent heat storage capacities, organic PCMs are highly efficient in thermal energy management systems. They are composed of molecules containing carbon, hydrogen, and oxygen atoms, which are further classified into categories such as fatty acids, alkanes, and alcohols. During phase transitions, organic PCMs can store large amounts of energy and release it when needed, making them suitable for various energy management applications.

In contrast, inorganic PCMs are primarily composed of metals, salts, and eutectic mixtures. These materials are distinguished from their organic counterparts by their higher thermal conductivity and density. Inorganic PCMs are particularly notable for their ability to withstand high temperatures and their superior thermal conductivity, making them advantageous in applications that require durability and high-temperature resistance. Due to their stable structure, inorganic PCMs are often used in demanding conditions where systems are exposed to significant temperature fluctuations. Their robustness and excellent thermal conductivity make them especially valuable in applications where precise temperature control is critical.

2.2. Classification Based on Chemical Properties

Phase change materials (PCMs) can be broadly categorized into three primary groups based on their chemical composition: salt hydrates, paraffins, and esters. Salt hydrates, a type of inorganic PCM, are formed by combining salts with water molecules. These materials are highly efficient in storing latent heat, owing to the strong ion-dipole interactions between the salt and water molecules. Widely used examples include calcium chloride hexahydrate, magnesium sulfate heptahydrate, and sodium sulfate decahydrate. Despite their high energy storage capacity, salt hydrates face challenges such as supercooling, corrosive behavior, and phase separation during repeated use. Popular salts like sodium sulfate (Na_2SO_4), magnesium sulfate ($MgSO_4$), and calcium chloride ($CaCl_2$) remain critical components in many thermal storage systems, as researchers continue to mitigate these limitations. (Dixit et al., 2022).

Paraffins, on the other hand, represent a class of organic PCMs that are widely utilized in thermal energy storage applications. These materials excel in transitioning between solid and liquid phases, during which they absorb or release significant amounts of latent heat. Chemically stable and composed of saturated hydrocarbons (alkanes) with the general formula C_nH_{2n+2}, paraffins can withstand multiple phase change cycles without degradation. Commonly used examples include alkanes such as octadecane (Cl_8H_{38}) and eicosane ($C_{20}H_{42}$), which vary in molecular chain length and phase transition properties. Their reliability and efficiency make paraffins a preferred choice for systems requiring consistent thermal performance over time. (Hagelstein & Gschwander, 2017).

Another type of PCM includes fatty acids and esters, which are organic compounds that absorb or release latent heat during phase transitions between liquid and solid states. Their molecular structure, defined by hydrocarbon chains and functional groups, significantly influences their phase change behavior. Fatty acids consist of hydrocarbon chains with a carboxyl group (–COOH) and can be either saturated or unsaturated. They are typically biodegradable, environmentally friendly, and derived from renewable sources. Esters, on the other hand, are organic compounds formed through reactions between carboxylic acids and alcohols. They are often considered safer due to their low toxicity levels. These characteristics make fatty acids and esters ideal candidates for applications requiring efficient thermal energy management.

2.3. Classification Based on Melting Temperature

Phase change materials (PCMs) can be classified based on their melting point into three distinct categories: low-temperature, medium-temperature, and high-temperature PCMs. Low-temperature PCMs,

with phase change temperatures below standard room temperature, are primarily utilized in cold storage and refrigeration systems to maintain low temperatures efficiently. Medium-temperature PCMs operate within a phase change range spanning from room temperature to approximately 100°C, making them ideal for applications such as cooling electronic devices and enhancing the thermal performance of building materials. In contrast, high-temperature PCMs are engineered to handle phase transitions above 100°C, catering to systems that require heat storage at elevated temperatures, such as in industrial processes. Typical examples of high-temperature PCMs include molten salts and metal alloys, both known for their exceptional thermal storage capabilities under extreme conditions.

3. Nano-Enhanced PCMs

The solidification process of PCMs begins when the liquid phase transitions into a solid phase, resulting in an increase in the solid phase's volume. Before solidification starts, there is typically little to no solid nucleus present within the PCM. For nucleation to occur, the system must release latent heat and reduce its energy level by freezing at the surface of the liquid phase. Once the nucleus grows to a sufficient size, the solidification process begins, indicating the presence of energy barriers that must be overcome. In some cases, solidification can occur under supercooled conditions, at temperatures significantly below the freezing point. Consequently, nucleation is classified into two types: homogeneous nucleation, which is initiated solely by the PCM, and heterogeneous nucleation, which occurs due to an external source outside the PCM (Sundaram & Kalaisselvane, 2022). Heterogeneous nucleation is typically triggered by factors such as additives introduced into the PCM, impurities, or cracks in the container walls. To prevent supercooling in the PCM, specialized additives known as nucleators can be employed to initiate heterogeneous nucleation.

The addition of nanoparticles has emerged as an effective method for enhancing heat transfer properties. The process of suspending nanoparticles to optimize the performance of storage materials, specifically the base PCM (phase change material), is commonly referred to as NEPCM (Nano-Enhanced PCM). In this approach, additives or surfactants are utilized to improve nucleation and dispersion within the base PCM, leading to the development of NFPCM (Nanofluid PCM) (Kumar, Kumaresan, & Velraj, 2016; Kumaresan, Velraj, & Das, 2012). During the freezing process, heat transfer between the PCM and nanomaterials during nucleation is largely dependent on the thermophysical properties of the PCM.

The widespread adoption of NEPCM in latent heat storage technologies, replacing traditional PCM, is primarily attributed to the

presence of dispersed nanoparticles such as copper (Cu), copper oxide (CuO), aluminum oxide (Al_2O_3), and carbon nanotubes (CNT). These nanoparticles significantly influence the phase change behavior of NEPCM due to their high thermal conductivity. Figure 3 illustrates that increasing the volume fraction of Cu nanoparticles from 0% to 20%, and from 0% to 5% in a ring-shaped NEPCM, enhances thermal conductivity and heat transfer rates, thereby reducing the overall solidification time. Elbahjaoui et al. (Elbahjaoui & El Qarnia, 2017), observed an improvement in the solidification rate of rectangular NEPCM plates containing 0-8% Cu volume fractions. Kashani et al. (Kashani, Ranjbar, Madani, Mastiani, & Jalaly, 2013), reported that during the solidification process of square NEPCM, an increase in Cu volume fraction from 0% to 8% resulted in a larger solidified region, facilitated by lower wall temperatures as the volume fraction increased. Sharma et al. (Sharma, Ganesan, Sahu, Metselaar, & Mahlia, 2014), they observed that the solidification time of Cu-based NEPCM decreased as the volume fraction increased from 0% to 20%. Li et al. (Z. Li, Sheikholeslami, Jafaryar, & Shafee, 2019) they simulated the performance of NEPCM in a channel and reported that an increase in nanoparticle fraction enhanced the solidification rate.

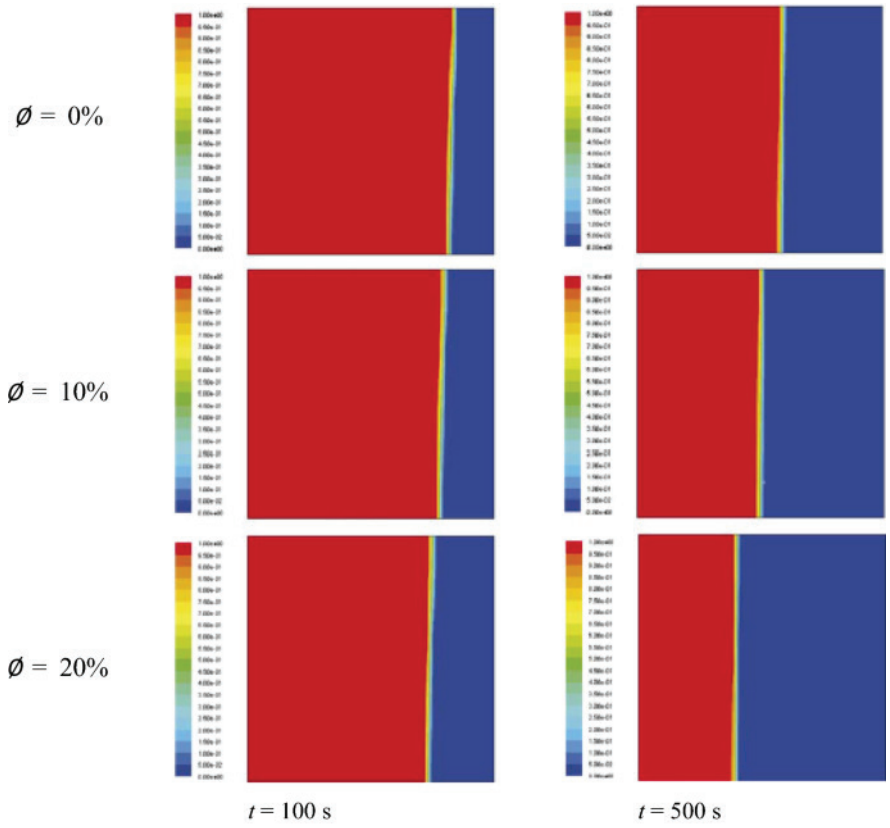

Figure 3. *The comparison of liquid fractions during NePCM solidification at different time intervals (t = 100 s and 500 s) was conducted for Cu volume fractions of Ø = 0%, 10%, and 20%. In this analysis, the red color represents the liquid region, while the blue color indicates the solid region (Khodadadi & Hosseinizadeh, 2007).*

As shown in Table 1, the use of these fluids has led to significant improvements in heat transfer, providing data that highlights the enhancement of thermo-physical properties when incorporated into PCMs.

Table 1. *The effect of nanoparticles on heat transfer (Mebarek-Oudina & Chabani, 2023).*

Nanoparticles	Observations
SiO_2 , TiO_2, Al_2O_3	The introduction of nanoparticles generally results in a 45% increase in thermal efficiency.
Cu ve TiO_2	The high thermal conductivity of nanoparticles enables better utilization of the thermal configuration.
TiO_2	Thermal efficiency is directly associated with the increased presence of nanoparticles.
Al_2O_3 ve CuO	The type and thermo-physical properties of nanoparticles determine the rate and circulation of heat absorption.
Fe_2O_3 , ZnO, Ag, SiO_2	Nanoparticles can alter and enhance the thermal conductivity of the base fluid.
MgO , CuO, Al_2O_3, TiO_2	The thermo-physical properties of nanoparticles make them excellent candidates for heat exchange, cooling, and heating systems.
MWCNT and Al_2O_3	Nanofluids can absorb heat for prolonged periods, thus altering the performance of heat exchangers.

From an economic perspective, the cost of integrating nanoparticles and phase change materials into systems is relatively low compared to the significant thermal performance enhancements they provide. These materials can be acquired at affordable prices, depending on their types, sizes, purity levels, and thermo-physical properties.

3.1. The Effect of Nanoparticles on the Thermal Conductivity of PCM

Incorporating nanoparticles into PCMs requires a thorough analysis of how their thermo-physical properties impact the behavior and performance of the base materials. Adjustments in the nanoparticle volume fraction play a key role in altering the characteristics of nano-enhanced PCMs (NePCM). For instance, a study examining the thermal conductivity of pure paraffin PCM and paraffin PCM infused with CuO nanoparticles at varying temperatures highlighted a significant increase in thermal conductivity for the nanoparticle-enhanced PCM. The data, as illustrated in Figure 3, demonstrated that the inclusion of CuO nanoparticles markedly improved the material's ability to conduct heat. Additionally, increasing the concentration of nanoparticles further enhanced the thermal conductivity, indicating a direct correlation between nanoparticle volume fraction and heat transfer performance. These observations underline the importance of nanoparticle integration in optimizing PCM efficiency.

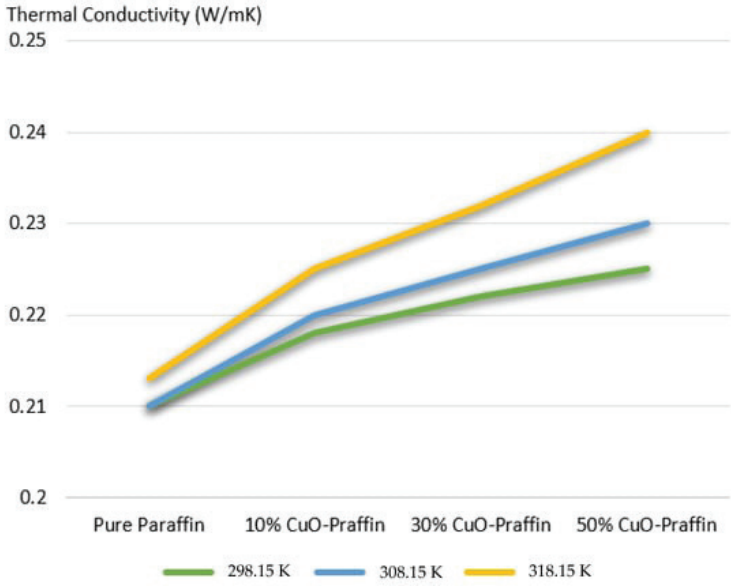

Figure 4. *Thermal Conductivity of PCM and Nano-PCM at Different Temperatures (Mebarek-Oudina & Chabani, 2023).*

Figure 4 compares the thermal conductivities of pure paraffin PCM and CuO-based nano-PCM at different temperatures and CuO concentrations. A significant improvement in thermal conductivity is observed with an increase in the volume fraction of CuO nanoparticles. Compared to pure paraffin, nano-PCMs containing 10%, 30%, and 50% CuO exhibit noticeably higher thermal conductivities across all temperatures. As the temperature increases, the thermal conductivity of the nano-PCMs also rises, with the highest values recorded at the maximum temperature. This suggests that elevated temperatures positively influence the energy transfer between nanoparticles and the base PCM, potentially accelerating phase change processes.

The study highlights that nanoparticles with high thermal conductivity, such as CuO, optimize the thermal performance of PCMs, enhancing energy transfer efficiency. Notably, when the CuO concentration is increased to 50%, the thermal conductivity reaches its peak, confirming the positive impact of nanoparticle presence on the thermal properties of PCM. Overall, the graph demonstrates that nano-PCMs offer superior performance compared to conventional PCMs in thermal management applications, particularly at high temperatures, by improving energy storage and transfer efficiency.

4. Applications of NePCM

In recent years, nano-enhanced phase change materials (NePCM) have become a focal point of interest due to their wide range of applications across various industries. NePCM stand out for their ability to store and release significant amounts of thermal energy during phase change processes. The inclusion of nanoparticles in PCMs not only enhances their thermal conductivity and heat transfer rates but also significantly improves their energy storage capacity. These attributes make NePCM an ideal choice for numerous applications, ranging from photovoltaic/thermal (PV/T) systems and battery thermal management solutions to building insulation applications, HVAC systems, solar cookers, textiles, and the food industry.

Figure 5 provides an overview of these applications, detailing the thermal regulation mechanisms involved. PCMs integrated into thermal energy storage (TES) systems offer substantial advantages in temperature regulation and energy efficiency. The success of such integrations depends on factors such as material compatibility, the effectiveness of heat transfer mechanisms, and the optimization of system design. Selecting the appropriate methods and materials can significantly enhance system performance and energy savings.

One of the most commonly used methods for integrating PCMs into TES systems is the direct incorporation of PCMs into the storage medium. This is typically achieved through two approaches: encapsulating PCMs in microcapsules or impregnating them into porous structures. In the microencapsulation method, PCMs are enclosed within a polymeric shell, and these capsules are uniformly distributed throughout the storage medium. This technique enhances the efficiency of energy storage and release processes during phase change, improves heat transfer, prevents phase separation, and increases the long-term stability of the PCM. These features enable PCM-based systems to have broader applications in thermal management solutions.

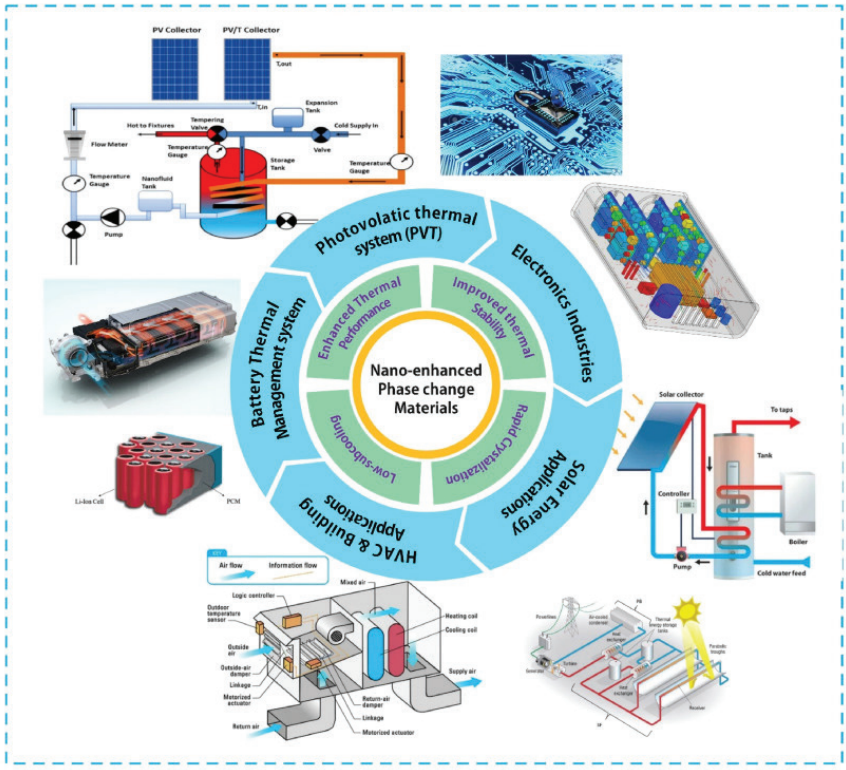

Figure 5. *Thermal Method Implementation for NePCM (Said et al., 2024)*

Figure 5 illustrates the diverse applications and key advantages of nano-enhanced phase change materials (NePCM) across various industries. The central circle highlights the benefits of NePCM, including enhanced thermal performance, improved thermal stability, better phase crystallization, and reduced subcooling. Surrounding segments detail the application areas, emphasizing solutions provided by NePCM in photovoltaic/thermal (PV/T) systems, the electronics industry, HVAC applications, solar-powered systems, and battery thermal management.

Technical diagrams around the visual provide concrete examples of how NePCM are integrated into these applications, detailing scenarios such as energy management in buildings, thermal control in batteries, and their use in solar energy systems. This visual effectively demonstrates the potential of NePCM' in thermal management and the broad scope of their applications.

4.1. Thermal Method Application for NePCM

The Battery Thermal Management System (BTMS) aims to ensure safe and long-lasting performance by effectively managing the heat generated

during battery operation. By maintaining a balanced battery temperature, BTMS eliminates the risk of thermal runaway and minimizes capacity loss. It is designed to provide long cycle life for battery modules, efficient operation at low cost, and safe discharge at the desired voltage. While current batteries generally operate within a temperature range of 40°C to 60°C (Jiang, Li, Qu, & Zhang, 2022), researchers consider the ideal range to be between 20°C and 45°C. However, when the battery temperature exceeds 80°C, severe consequences such as thermal runaway may occur. Additionally, temperature imbalances within the battery can adversely affect its lifespan; even a 5°C temperature difference can lead to a 1% to 2% reduction in battery capacity (Feng et al., 2018). Therefore, designing an effective BTMS is crucial to improving the adaptability of batteries across various applications.

Cooling strategies in BTMS, such as PCM-based methods, provide notable benefits including efficient heat storage, user-friendly application, long-term reliability, and seamless integration with battery systems. However, one major challenge limiting their broader application is the inherently low thermal conductivity of PCMs. Recent advancements suggest that this issue can be effectively mitigated through the inclusion of nanoparticles (NPs) (Xiong, Zheng, & Shah, 2020). Significant research efforts are focused on boosting the thermal conductivity of PCMs by incorporating various types of nanoparticles, including carbon-based, metal-based, and hybrid materials. Concurrently, different preparation methods are being refined to maximize nanoparticle efficiency. While these enhancements improve heat transfer performance, they can also introduce challenges such as imbalances in the additive ratio, reduced latent heat capacity, or changes in the melting point and structural stability of composite PCMs.

This section delves into the formulation of nano-enhanced PCMs (NePCM), analyzing their impact on the thermal and physical properties of PCMs, the design parameters of NePCM-based battery systems, and the efficiency of thermal management systems employing carbon-based, metal-based, and hybrid nanoparticles.

To optimize BTMS performance, NePCMs must meet specific requirements. The melting point of NePCMs should align with ambient conditions and the operational temperature range of batteries, typically between 25°C and 50°C. The selected temperature should exceed ambient levels while remaining within safe operational limits. High thermal conductivity is vital for effective heat absorption and distribution, especially during rapid charge-discharge cycles. Additionally, NePCMs should maintain substantial latent and specific heat capacities to efficiently store the thermal energy generated by battery operations. Furthermore,

thermal stability is another key criterion to ensure uniform temperature distribution during application and to minimize energy loss. To maintain reliability over long-term use, the NePCM must retain its chemical and physical properties during multiple heating and cooling cycles without degradation.

From a safety perspective, NePCM should be non-flammable and free from corrosive properties to prevent reactions with the battery electrodes. To simplify integration into battery modules, the NePCM must possess low density, minimizing complications during system design and reducing the risk of leakage during melting. Form stability is equally crucial to ensure the NePCM retains its structure during phase transitions. Phenomena such as supercooling can negatively impact NePCM performance, making it essential for the material to exhibit suitable crystallization rates and low supercooling tendencies. Additionally, cost-effectiveness is vital for the commercial viability of BTMS, ensuring the NePCM is readily available in the market and offering economic efficiency to shorten the payback period during integration. This balance of technical and economic factors can significantly improve the performance and reliability of battery systems with a well-designed BTMS. The low thermal conductivity of PCM is a major limitation in its application to BTMS. During high heat accumulation and rapid charge-discharge cycles, the PCM alone is insufficient for effective heat transfer. To address this, the addition of NP to PCM is necessary to enhance thermal conductivity, resulting in the development of NePCM. Two primary methods are employed for NePCM preparation: the one-step method and the two-step method. In the one-step method, the preparation of nanoparticles NPs and their dispersion within the PCM are carried out simultaneously. However, the two-step method is more commonly preferred. In the two-step method, NPs are first synthesized or obtained and then combined with the base PCM. This approach involves various techniques such as mixing and sonication, vapor impregnation, autoclaving, ultrasonication, kneading mixing, and coating with a varnish layer (Reji Kumar, Samykano, Pandey, Kadirgama, & Tyagi, 2020). The techniques employed in the preparation of NePCM have a direct impact on the thermo-physical properties of the material, depending on factors such as the size, weight percentage, and distribution of the nanoparticles. For instance, incorporating nanoparticles with high thermal conductivity, such as graphene, significantly enhances the thermal conductivity of the material. Similarly, porous materials like expanded graphite (EG) not only improve thermal conductivity but also enhance shape stability (Chaudhuri, Chaudhuri, & Joydhar, 2022; Singh et al., 2022). Similarly, support materials such as epoxy resin play an effective role in enhancing mechanical strength. However, the addition of nanoparticles may reduce

the latent heat capacity of NePCM. Therefore, it is crucial to design NePCM in a way that not only improves thermal conductivity but also maintains shape stability and flexibility.

An appropriate NePCM design for BTMS applications should not only deliver high thermal performance but also ensure a form-stable structure to prevent leakage and support flexibility. In this context, NePCM preparation methods represent a significant area of research, focusing on enhancing the long-term performance and widespread commercial applicability of these materials.

5. Conslusions

This study explored the effects of nano-enhanced phase change materials (NePCM) and their performance and potential applications in thermal management systems. NePCM offer significant advantages over traditional PCMs due to their improved thermal conductivity and accelerated phase change processes. The findings indicate that the addition of nanoparticles enhances both heat transfer rates and thermal stability, although certain limitations exist in properties such as shape stability and latent heat. The integration of additives like graphene, CuO, Al2O3, and expanded graphite into PCMs has increased the energy efficiency of thermal management systems and resulted in more uniform temperature distribution.

The literature extensively examines the impact of various preparation techniques and nanoparticle ratios on the performance of NePCM. However, the need for cost-effective, sustainable, and long-lasting system designs remains a key focus. Overall, this study highlights the applicability of NePCM not only in battery thermal management but also in a wide range of areas, including energy savings in buildings, electronics cooling, food preservation, and solar energy applications.

In light of all these findings, the following suggestions can be offered to guide future studies:

· Additives such as graphene, expanded graphite, carbon nanotubes (CNT), CuO, and Al_2O_3 can be used at varying concentrations to examine changes in thermal conductivity, latent heat, and specific heat values. For instance, the effects of nanoparticle ratios ranging from 0.5% to 5% can be evaluated.

· The physical and chemical stability of NePCM should be investigated over multiple heating and cooling cycles. Thermal fatigue tests can be used to evaluate material performance degradation.

· Research should focus on additives capable of functioning across wide temperature ranges while minimizing the effects of supercooling. For example, support materials like epoxy resin, known for enhancing mechanical strength, could be tested in various systems.

· Computational Fluid Dynamics (CFD) analyses can be utilized to model the phase change behavior, temperature distribution, and heat transfer mechanisms of NePCM. Models such as the enthalpy-porosity method are particularly suitable.

· Optimization methods like the Taguchi method or genetic algorithms can be applied to understand the impact of nanoparticle distribution on thermal performance. These approaches can identify the ideal combinations of additive ratios and preparation techniques.

· Numerical models incorporating parameters such as phase change temperatures, nanoparticle concentration, and PCM density should be developed to predict the performance of energy storage systems under real operating conditions.

· Hybrid combinations of carbon-based and metal oxide-based nanoparticles could yield better results in terms of thermal conductivity and shape stability. Experiments could, for instance, focus on graphene-CuO or CNT-Al_2O_3 combinations.

· The compatibility of PCMs with nanoparticles derived from natural fibers or biological materials could be explored.

· Methods that enhance thermal conductivity while preserving latent heat capacity should be investigated. For instance, the porous structure of expanded graphite could simultaneously improve heat transfer and shape stability.

· The effects of nucleating additives that eliminate supercooling should be tested.

· The recyclability and environmental impact of NePCM should be assessed, prioritizing sustainability.

These recommendations, through the combined use of experimental and numerical approaches, will enhance the energy efficiency of NePCM, optimize their performance across various applications, and support their commercial viability.

REFERENCES

Ayala, E., Enghardt, M. H., & Horton, M. (1997). Cost Effective, Environmentally Safe Tissue Processing Method With Paraffin Oil. *Journal of Histotechnology*, 20(2), 133–137. Retrieved from https://doi.org/10.1179/his.1997.20.2.133

Bruno, F., Belusko, M., Liu, M., & Tay, N. H. S. (2015). Using solid-liquid phase change materials (PCMs) in thermal energy storage systems. In *Advances in Thermal Energy Storage Systems* (pp. 201–246). Elsevier. Retrieved from https://doi.org/10.1533/9781782420965.2.201

Chandrasekaran, P., Cheralathan, M., Kumaresan, V., & Velraj, R. (2014). Enhanced heat transfer characteristics of water based copper oxide nanofluid PCM (phase change material) in a spherical capsule during solidification for energy efficient cool thermal storage system. *Energy*, 72, 636–642. Retrieved from https://doi.org/10.1016/j.energy.2014.05.089

Chaudhuri, A., Chaudhuri, A., & Joydhar, A. (2022). Graphene nanocomposites and applications in electrochemical energy storage materials. *Materials Today: Proceedings*, 64, 1569–1581. Retrieved from https://doi.org/10.1016/j.matpr.2022.02.226

Dixit, P., Reddy, V. J., Parvate, S., Balwani, A., Singh, J., Maiti, T. K., … Chattopadhyay, S. (2022). Salt hydrate phase change materials: Current state of art and the road ahead. *Journal of Energy Storage*, 51, 104360. Retrieved from https://doi.org/10.1016/j.est.2022.104360

Elbahjaoui, R., & El Qarnia, H. (2017). Thermal analysis of nanoparticle-enhanced phase change material solidification in a rectangular latent heat storage unit including natural convection. *Energy and Buildings*, 153, 1–17. Retrieved from https://doi.org/10.1016/j.enbuild.2017.08.003

Feng, X., Xu, C., He, X., Wang, L., Zhang, G., & Ouyang, M. (2018). Mechanisms for the evolution of cell variations within a LiNixCoyMnzO2/graphite lithium-ion battery pack caused by temperature non-uniformity. *Journal of Cleaner Production*, 205, 447–462. Retrieved from https://doi.org/10.1016/j.jclepro.2018.09.003

Hagelstein, G., & Gschwander, S. (2017). Reduction of supercooling in paraffin phase change slurry by polyvinyl alcohol. *International Journal of Refrigeration*, 84, 67–75. Retrieved from https://doi.org/10.1016/j.ijrefrig.2017.08.016

Hassan, A., Shakeel Laghari, M., & Rashid, Y. (2016). Micro-Encapsulated Phase Change Materials: A Review of Encapsulation, Safety and Thermal Characteristics. *Sustainability*, 8(10), 1046. Retrieved from https://doi.org/10.3390/su8101046

Hussain, S., Ertam, F., Ben Hamida, M. B., Oztop, H. F., & Abu-Hamdeh, N. H. (2023). Passive control of, energy storage of NePCM, heat and mass transfer with gamma-shaped baffle in a thermo-bioconvection system using CFD and artificial intelligence. *International Communications in Heat and Mass Transfer*, 144, 106764. Retrieved from https://doi.org/10.1016/j.icheatmasstransfer.2023.106764

Jesumathy, S., Udayakumar, M., & Suresh, S. (2012). Experimental study of enhanced heat transfer by addition of CuO nanoparticle. *Heat and Mass Transfer*, 48(6), 965–978. Retrieved from https://doi.org/10.1007/s00231-011-0945-y

Jiang, Z. Y., Li, H. B., Qu, Z. G., & Zhang, J. F. (2022). Recent progress in lithium-ion battery thermal management for a wide range of temperature and abuse conditions. *International Journal of Hydrogen Energy*, 47(15), 9428–9459. Retrieved from https://doi.org/10.1016/j.ijhydene.2022.01.008

Kalidasan, B., Pandey, A. K., Saidur, R., Samykano, M., & Tyagi, V. V. (2023). Nano additive enhanced salt hydrate phase change materials for thermal energy storage. *International Materials Reviews*, 68(2), 140–183. Retrieved from https://doi.org/10.1080/09506608.2022.2053774

Kashani, S., Ranjbar, A. A., Madani, M. M., Mastiani, M., & Jalaly, H. (2013). Numerical study of solidification of a nano-enhanced phase change material (NEPCM) in a thermal storage system. *Journal of Applied Mechanics and Technical Physics*, 54(5), 702–712. Retrieved from https://doi.org/10.1134/S0021894413050027

Kean, T. H. (2019). Thermal Performance Analysis of Nanoparticles Enhanced Phase Change Material (NEPCM) in Cold Thermal Energy Storage (CTES). *CFD Letters*, 11(Vol. 11 No. 4: CFD Letters,April(2019)). Retrieved from https://www.akademiabaru.com/index.php/archives/article/view/207

Khodadadi, J. M., & Hosseinizadeh, S. F. (2007). Nanoparticle-enhanced phase change materials (NEPCM) with great potential for improved thermal energy storage. *International Communications in Heat and Mass Transfer*, 34(5), 534–543. Retrieved from https://doi.org/10.1016/j.icheatmasstransfer.2007.02.005

Kolokotsa, D., Santamouris, M., Synnefa, A., & Karlessi, T. (2012). 3.19-passive solar architecture. *In Comprehensive Renewable Energy.*

Krishna, J., Kishore, P. S., & Solomon, A. B. (2017). Heat pipe with nano enhanced-PCM for electronic cooling application. *Experimental Thermal and Fluid Science*, 81, 84–92. Retrieved from https://doi.org/10.1016/j.expthermflusci.2016.10.014

Kumar, P. G., Kumaresan, V., & Velraj, R. (2016). Experimental investigation on thermophysical properties of solar glycol dispersed with multi-walled carbon nanotubes. *Fullerenes, Nanotubes and Carbon*

Nanostructures, 24(10), 641–652. Retrieved from https://doi.org/10.1080/1536383X.2016.1219852

Kumaresan, V., Velraj, R., & Das, S. K. (2012). The effect of carbon nanotubes in enhancing the thermal transport properties of PCM during solidification. *Heat and Mass Transfer*, 48(8), 1345–1355. Retrieved from https://doi.org/10.1007/s00231-012-0980-3

Kushwah, A., Kumar Gaur, M., & Kumar Pandit, R. (2020). The Role of Phase Change Materials for Lifetime Heating of Buildings in Cold Climatic Conditions. *International Journal of Built Environment and Sustainability*, 7(3), 81–96. Retrieved from https://doi.org/10.11113/ijbes.v7.n3.600

Li, J., Zhang, X., Xu, B., & Yuan, M. (2021). Nanofluid research and applications: A review. *International Communications in Heat and Mass Transfer*, 127, 105543. Retrieved from https://doi.org/10.1016/j.icheatmasstransfer.2021.105543

Li, Z., Sheikholeslami, M., Jafaryar, M., & Shafee, A. (2019). Time-dependent heat transfer simulation for NEPCM solidification inside a channel. *Journal of Thermal Analysis and Calorimetry*, 138(1), 721–726. Retrieved from https://doi.org/10.1007/s10973-019-08140-9

Mao, Q., Chen, H., & Yang, Y. (2019). Energy Storage Performance of a PCM in the Solar Storage Tank. *Journal of Thermal Science*, 28(2), 195–203. Retrieved from https://doi.org/10.1007/s11630-019-1076-x

Mebarek-Oudina, F., & Chabani, I. (2023). Review on Nano Enhanced PCMs: Insight on nePCM Application in Thermal Management/Storage Systems. *Energies*, 16(3), 1066. Retrieved from https://doi.org/10.3390/en16031066

Rathore, P. K. S., & Shukla, S. K. (2019). Potential of macroencapsulated PCM for thermal energy storage in buildings: A comprehensive review. *Construction and Building Materials*, 225, 723–744. Retrieved from https://doi.org/10.1016/j.conbuildmat.2019.07.221

Reji Kumar, R., Samykano, M., Pandey, A. K., Kadirgama, K., & Tyagi, V. V. (2020). Phase change materials and nano-enhanced phase change materials for thermal energy storage in photovoltaic thermal systems: A futuristic approach and its technical challenges. *Renewable and Sustainable Energy Reviews*, 133, 110341. Retrieved from https://doi.org/10.1016/j.rser.2020.110341

Said, Z., Pandey, A. K., Tiwari, A. K., Kalidasan, B., Jamil, F., Thakur, A. K., … Ali, H. M. (2024). Nano-enhanced phase change materials: Fundamentals and applications. *Progress in Energy and Combustion Science*, 104, 101162. Retrieved from https://doi.org/10.1016/j.pecs.2024.101162

Shank, K., Bernat, J., Regal, E., Leise, J., Ji, X., & Tiari, S. (2022). Experimental Study of Varying Heat Transfer Fluid Parameters within a Latent Heat

Thermal Energy Storage System Enhanced by Fins. *Sustainability*, 14(14), 8920. Retrieved from https://doi.org/10.3390/su14148920

Shank, K., & Tiari, S. (2023). A Review on Active Heat Transfer Enhancement Techniques within Latent Heat Thermal Energy Storage Systems. *Energies*, 16(10), 4165. Retrieved from https://doi.org/10.3390/en16104165

Sharma, R. K., Ganesan, P., Sahu, J. N., Metselaar, H. S. C., & Mahlia, T. M. I. (2014). Numerical study for enhancement of solidification of phase change materials using trapezoidal cavity. *Powder Technology*, 268, 38–47. Retrieved from https://doi.org/10.1016/j.powtec.2014.08.009

Sidik, Nor Azwadi Che, A. T. M., & M'hamed Beriache. (2020). Thermo Physical Enhancement of Advanced Nano-Composite Phase Change Material. *Journal of Advanced Research in Applied Mechanics*, 54(Vol. 54 No. 1: February (2019)), 1–8. Retrieved from https://www.akademiabaru.com/submit/index.php/aram/article/view/1831

Singh, P., Sharma, R. K., Khalid, M., Goyal, R., Sarı, A., & Tyagi, V. V. (2022). Evaluation of carbon based-supporting materials for developing form-stable organic phase change materials for thermal energy storage: A review. *Solar Energy Materials and Solar Cells*, 246, 111896. Retrieved from https://doi.org/10.1016/j.solmat.2022.111896

Skovajsa, J., Koláček, M., & Zálešák, M. (2017). Phase Change Material Based Accumulation Panels in Combination with Renewable Energy Sources and Thermoelectric Cooling. *Energies*, 10(2), 152. Retrieved from https://doi.org/10.3390/en10020152

Sundaram, P., & Kalaisselvane, A. (2022). Effect of different additives on freezing characteristics and stability of GnP-aqueous-based PCM for cold thermal storage. *Journal of Thermal Analysis and Calorimetry*, 147(14), 8033–8045. Retrieved from https://doi.org/10.1007/s10973-021-11056-y

Swathykrishnan, B., Sreelakshmi, C., Duggal, P., & Tomar, R. K. (2020). Application Of Phase Change Materials In Buildings. In *2020 International Conference on Intelligent Engineering and Management (ICIEM)* (pp. 203–206). IEEE. Retrieved from https://doi.org/10.1109/ICIEM48762.2020.9160323

Tariq, S. L., Ali, H. M., Akram, M. A., Janjua, M. M., & Ahmadlouydarab, M. (2020). Nanoparticles enhanced phase change materials (NePCMs)-A recent review. *Applied Thermal Engineering*, 176, 115305. Retrieved from https://doi.org/10.1016/j.applthermaleng.2020.115305

Tofani, K., & Tiari, S. (2021). Nano-Enhanced Phase Change Materials in Latent Heat Thermal Energy Storage Systems: A Review. *Energies*, 14(13), 3821. Retrieved from https://doi.org/10.3390/en14133821

Trelles, J. P., & Dufly, J. J. (2003). Numerical simulation of porous latent heat thermal energy storage for thermoelectric cooling. *Applied Thermal Engineering*, 23(13), 1647–1664. Retrieved from https://doi.org/10.1016/S1359-4311(03)00108-X

Valan, A., Sasmito, A., & Mujumdar, A. (2013). Numerical performance study of paraffin wax dispersed with alumina in a concentric pipe latent heat storage system. *Thermal Science*, 17(2), 419–430. Retrieved from https://doi.org/10.2298/TSCI110417004A

Varol, Y., Coşanay, H., Tamdoğan, E., Parlak, M., Şenocak, Ş. M., & Oztop, H. F. (2025). Vapor chamber thermal performance: Partially heated with different heating areas at the center and supported by numerical analysis for the experimental setup. *Applied Thermal Engineering*, 260, 124978. Retrieved from https://doi.org/10.1016/j.applthermaleng.2024.124978

Varol, Y., Oztop, H. F., Tamdoğan, E., Parlak, M., Şenocak, Ş. M., & Coşanay, H. (2025). Thermal Performance Investigation of Vapor Chamber Under Partial Heating and Different Heat Flux Conditions: Effects of Inclination Angle. *ASME Journal of Heat and Mass Transfer*, 147(1). Retrieved from https://doi.org/10.1115/1.4066664

Xiong, T., Zheng, L., & Shah, K. W. (2020). Nano-enhanced phase change materials (NePCMs): A review of numerical simulations. *Applied Thermal Engineering*, 178, 115492. Retrieved from https://doi.org/10.1016/j.applthermaleng.2020.115492

Yadav, A., Samykano, M., Pandey, A., Kareri, T., & Kalidasan, B. (2024). Optimizing thermal properties and heat transfer in 3D biochar-embedded organic phase change materials for thermal energy storage. *Materials Today Communications*, 38, 108114. Retrieved from https://doi.org/10.1016/j.mtcomm.2024.108114

Chapter 13

LAND CONSOLIDATION PARCEL SHAPE ANALYSIS: KARAMAN KAZIMKARABEKIR ÖZYURT EXAMPLE

Ömer ACAR[1]

1 Lecturer, Kahramanmaraş Sütçü İmam University, Göksun Vocational School, Department of Architecture and Urban Planning, oacar@ksu.edu.tr, Orcid No: 0000-0002-2382-8594

INTRODUCTION

Along with population growth, economic development, rapid urbanization, and industrialization, sufficient land resources are the basis of human life and the most valuable natural resource for a country (Guo et al., 2015). Land resources are finite and non-reproducible consumption resources that are financial security transferred as wealth across generations (Niroula & Thapa, 2005). Agricultural production areas are also where land resources are used intensively (Dengiz et al., 2007; Karamatov & Sadykova, 2018). Agricultural production areas are fragmented due to reasons such as inheritance/transfer, expropriation processes (Küsek, 2014; Boztoprak, 2015), agricultural population density, land use, and distribution pattern (Küsek, 2014; Demirtaş & Sarı, 2016). Excessive fragmentation of land owned by agricultural enterprises negatively affects the income obtained from agricultural production (Latruffe & Piet, 2014; Janus & Markuszewska, 2017; Acar & Bengin, 2018; Bengin & Acar, 2018; Postek, 2018; Tezcan et al., 2020; Stręk et al., 2021). Many studies have concluded that the economic consequences of land fragmentation not only have adverse effects on agricultural production but also food security (Shaw, 1963; Tan et al., 2006; Orea et al., 2015; Hiironen & Riekkinen, 2016; Knippenberg et al., 2020; Ntihinyurwa & Vries, 2021; Tran & Van Vu, 2021; Kangethe, 2024; Mayele et al., 2024; Su et al., 2024). Land fragmentation also impacts agricultural land degradation (Janus & Markuszewska, 2017; Jiang et al., 2022; Acar & Akdeniz, 2023). Many countries widely use land consolidation projects to eliminate the adverse effects of land fragmentation (Vitikainen, 2004; Thapa & Niroula, 2008; Orea et al., 2015; Akdeniz & Acar, 2023). The benefits obtained from land consolidation studies have a positive effect in many ways. Because it not only increases the economic efficiency of agricultural production areas but is an important tool used to support the multifunctional development of rural areas (Janus & Markuszewska, 2017). Land consolidation is expressed as a practice with multiple vital functions, such as organizing rural areas, ensuring food security, coordinating rural and regional development, ensuring sustainable and efficient use of resources, and improving the living conditions of farmers (Li et al., 2018; Long et al., 2019). According to the Food and Agriculture Organization of the United Nations, land consolidation is expressed as "a highly effective land management tool that allows for the improvement of the structure of agricultural enterprises and farms, increases their economic and social efficiency, and benefits both the beneficiaries and society in general" (FAO, 2020). Land consolidation emerged in Germany in 1343 (Demetriou et al., 2012; Kocur-Bera et al., 2023). Historically, land consolidation projects have shifted from economic efficiency to environmental and social sustainability. While initially carried out to increase agricultural production, it has evolved

into a multidimensional structure through rural development, natural resource management, and adaptation to modern technologies. Depending on economic, political, and technological developments, it has been shaped with different purposes.

A separate law on land consolidation has not been established in Turkey. The establishment law of the institution performing the consolidation has been implemented and continues to be implemented with statutes and regulations (Cengiz, 2021). Today, it is carried out by the Land Consolidation and On-Farm Development Services Implementation Regulation, which entered into force on February 7, 2019. In this regulation, land consolidation is defined as "preventing the degradation and fragmentation of agricultural lands due to natural and artificial effects, combining multiple land plots in fragmented lands by taking into account their natural characteristics, usage integrity, and property rights, creating new parcels that are economical, ecological and more functional, determining the usage patterns of these parcels by evaluating their land characteristics and areas, and providing land development services." Consolidation works, which started in 1961 in Turkey, were completed in a total area of 9.20 million hectares by 2023, and it is estimated that they will be completed in an area of 11.70 million hectares by the end of 2028 (12th Development Plan, 2023).

MATERIAL METHOD

This study used the numerical and attribute data of the Özyurt Village land consolidation study included in the Karaman 3rd Section Land Consolidation and In-Farm Development Services Project (Figure 1). The data of the project area was obtained from the 4th Regional Directorate of the General Directorate of State Hydraulic Works. The study used LiCAD, LiTOP 7, ArcMap 10.5, and NetCAD 8.5 software to calculate parcel area and perimeter length, determine parcel shapes, calculate index values, and create thematic maps.

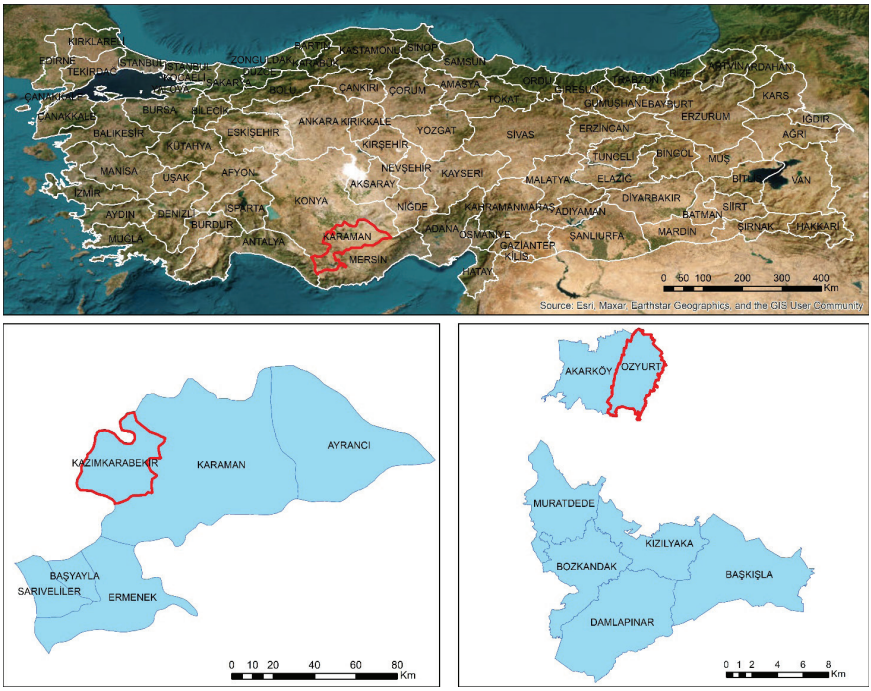

Figure 1. Özyurt Village Location Map

Total parcel area, number of parcels, average parcel size, deduction rate, and consolidation ratio information belonging to Özyurt Village land consolidation and on-farm development services project were evaluated. Geometric shape analysis of parcels before and after consolidation was performed, and a shape index was used to determine and evaluate parcel shape changes (1). "Shape Index (SI)" is used to evaluate parcel shape changes in land consolidation and on-farm development services projects (McGarical & Marks, 1995). SI value takes values in the range of $1 \leq SI \leq \infty$. Values where the SI value is 1 and close to 1 indicate that parcel shapes are close to regular geometric shapes such as squares and rectangles (approximately 1/4 to 1/6 aspect ratio). The SI value indicates irregular and shapeless parcels as it moves away from 1 (Demetriou et al., 2013; Kirmikil & Arici, 2013; Shi et al., 2018; Arslan et al., 2021).

SI: Shape Index

S_{ij}: Parcel Perimeter

F_{ij}: Parcel Area

The effect of parcel geometric shapes and fragmentation on the arable area was examined. The effect of consolidation on the arable area was

evaluated by calculating the arable area before and after consolidation. It is known that machines cannot plant 50 cm wide at the parcel border in agricultural areas. These areas where difficulties occur are called lost areas. The arable area can be calculated by subtracting the lost area from the parcel area (Akdeniz & Temizel, 2018; Seyyar, 2019). In all parcels included in the project, agriculturally arable areas were created by creating a 0.5 meter lost area along the parcel perimeters, and their areas were calculated. The total arable area was calculated before and after consolidation.

FINDINGS

There are 480 enterprises within the scope of the Özyurt village consolidation project. A total of 1616.39 hectares of parcel area was regulated before the project. A total of 1567.90 hectares of parcel area was created after the project. 2.64 hectares of this area belongs to the Village Legal Entity. No deductions were made from the parcels owned by the Village Legal Entity in the project area. The total number of parcels belonging to the enterprises before consolidation was 1392; the total number of parcels after consolidation decreased to 1091, and the consolidation rate was 21.62%. The project area's average parcel size was 11.61 before consolidation and 14.37 after consolidation. Within the regulation works, a participation share rate of 2.97% was calculated for newly opened roads, irrigation, drainage systems, and shared facilities. (Table 1).

Table 1. Özyurt Village Project Summary

	Before the Project	**After the Project**
Parcel Area (ha)	1616.39	1567.90
Number of Parcels	1392	1091
Average Parcel Size (da)	11.61	14.37
Dedication Rate (%)	2.97	
Consolidation Rate (%)	21.62	

While parcel geometry is among the criteria affecting agricultural mechanization, the appropriate parcel geometry for agricultural production should be rectangular, with an aspect ratio between 1/3 and 1/7. The most appropriate geometric shape for agricultural production is rectangular. In the order of parcel shape suitability, trapezoid, amorphous, and triangular took their place in the literature after rectangle. (Acar and Akdeniz, 2023). In the parcel shape analysis conducted in the study area, there has been a significant change between rectangular and trapezoid-shaped parcels. While trapezoid-shaped parcels were the majority before the project, rectangular-shaped parcels were the majority after the project. The number

of rectangular parcels increased from approximately 34% to 61%; a 27% increase is observed. The number of trapezoidal parcels decreased from approximately 44% to 28%; a 16% decrease is observed. The number of triangular-shaped parcels decreased by approximately 5%, and the number of amorphous parcels decreased by approximately 6% (Table 2). It has been determined that there has been a significant change according to the geometric shapes of the parcels.

Table 2. Özyurt Village Parcel Shapes

Parcel Shape	Before Project		After Project	
	Pieces	%	Pieces	%
Triangle	105	7.54	35	3.21
Square	14	1.01	24	2.20
Rectangle	471	33.84	660	60.50
Trapezoid	616	44.25	301	27.59
Shapeless	186	13.36	71	6.51
Total	**1392**	**100.00**	**1091**	**100.00**

The shape index analyzes the parcel shape over the existing area-perimeter relationship of the parcel. According to the calculations, it takes values in the range of $1 \leq SI \leq \infty$ according to the perimeter and area value of the parcel. The value of the shape index approaching 1 indicates that the parcel shapes are suitable for mechanized agriculture and have regular shapes. If the width/height ratio of the parcel increases, the shape index value moves away from 1 and reveals that the geometric shape of the parcels is unsuitable for agriculture (Arslan et al., 2021). The shape index statistical results before and after consolidation in the study area are given in Table 3. The shape index pre-project status is given in Figure 2, and the post-project status is given in Figure 3. According to the shape index statistical results, it was determined that there was an increase in the mean and median values and a decrease in the standard deviation and variance values. The decrease in the standard deviation indicates less diversity in the shape index among the parcels after consolidation. The decrease in variance confirms that the shape index values are squeezed into a narrower range after aggregation, and the parcels show more similar characteristics. According to the statistical data, there is an improvement in the parcel geometry.

Table 3. Özyurt Village Shape Index Statistical Results

	Land Consolidation	
	Before	**After**
Minimum	1.09533	1.10609
Maximum	4.12198	3.14933
Mean	1.51205	1.54215
Median	1.36074	1.43398
Standard Deviation	0.43475	0.39074
Variance	0.18901	0.15268

Figure 2. Pre-Consolidation Shape Index Map

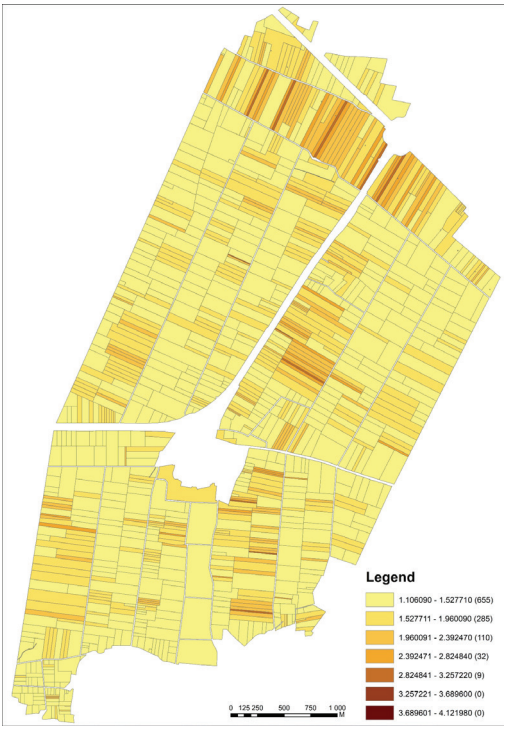

Figure 3. Post-Consolidation Shape Index Map

According to the shape index value, the parcel density is between 1 and 1.5 before and after consolidation. When the proportional distribution is examined according to the shape index values after consolidation, it is seen that there is a decrease of approximately 5% in the range of 1-1.5, while there is an increase of 5% in the range of 1.5-1.9. It has been determined that parcel shapes with values of 3.2 and above have transformed into more suitable forms (Table 4).

Table 4. Özyurt Village Shape Index Values

Shape Index Values	Before Land Consolidation		After Land Consolidation	
	Number of Parcels	%	Number of Parcels	%
1.09533 - 1.52771	926	66.52	655	60.04
1.52772 - 1.96009	288	20.69	285	26.12
1.96010 - 2.39247	96	6.90	110	10.08
2.39248 - 2.82484	53	3.81	32	2.93
2.82485 - 3.25722	21	1.51	9	0.82
3.25723 - 3.68960	7	0.50	0	0.00
3.68961 - 4.12198	1	0.07	0	0.00

Before consolidation, the total area of cadastral parcels in Özyurt village was calculated as 16184.10 decares. The total area of parcels created by leaving a buffer of 50 cm inside the parcel border to calculate the lost area was 15809.76 decares. The difference between the two areas was calculated as 374.34 decares. In other words, in the old situation, 374.34 decares of land could not be used conveniently because agricultural machinery could not approach the parcel border. The total area after consolidation was calculated as 15679.71 decares. The arable area after consolidation was calculated as 15357.70 decares. The difference between the two areas was 322.01 decares, representing the area that could not be used after consolidation. The pre-project situation of the study area is given in Figure 4, and the post-project situation is given in Figure 5.

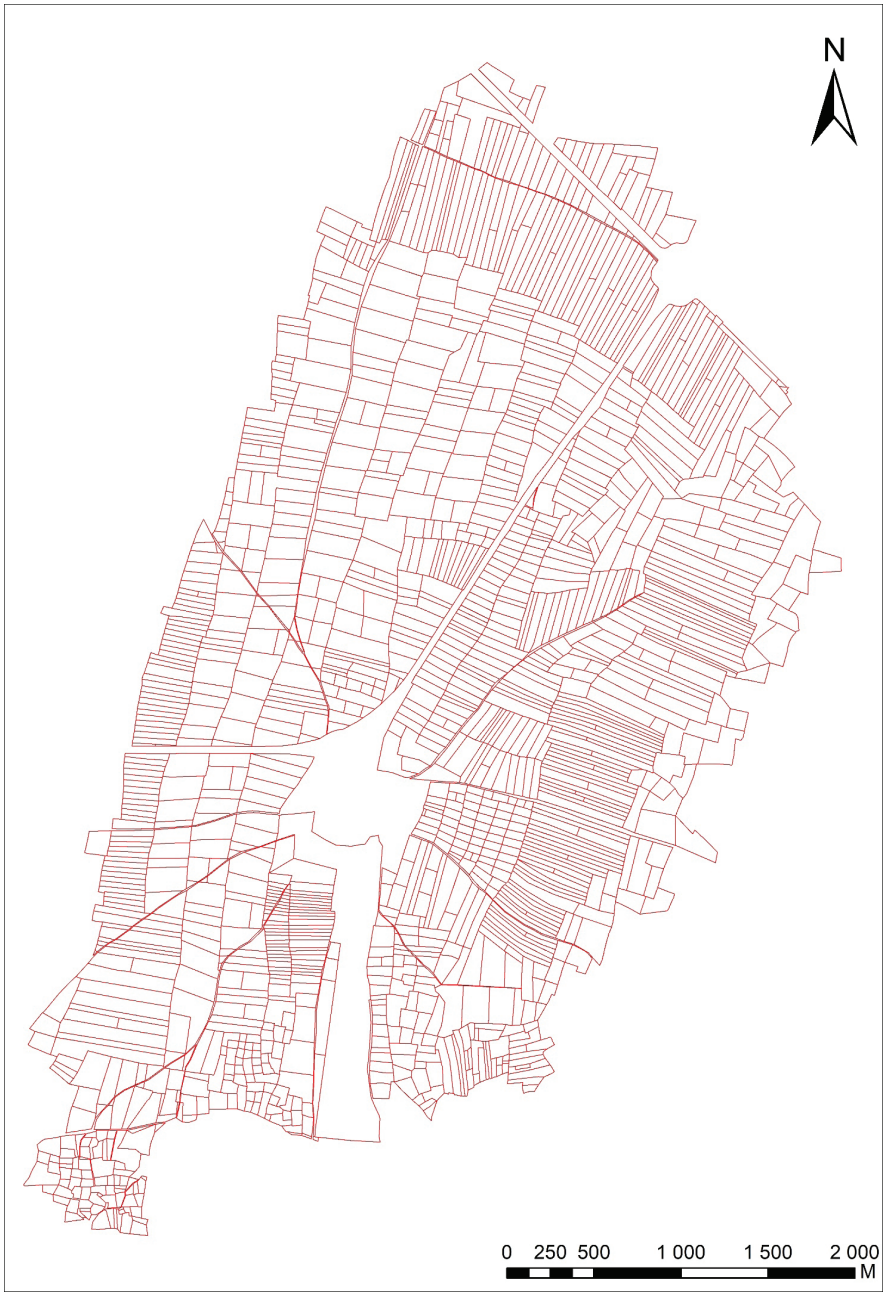

Figure 4. Özyurt Village Pre-Project Situation Map

Figure 5. Özyurt Village Post-Project Situation Map

CONCLUSION

Land consolidation projects allow spatial changes on a parcel basis in agricultural production areas. Along with the locations of the parcels, arrangements are also made in their shapes and sizes. Geometric shapes in agricultural areas are considered an adequate criterion in production costs from plowing to harvesting operations. It is known that the ideal parcel geometry for agricultural production minimizes labor and fuel costs. In this context, it is important to evaluate consolidation projects' contribution to agricultural production and conduct post-project research.

In the study area, the geometric shape of the parcels was mainly trapezoidal before the project, but after the project, it shifted to rectangular parcels. Although the parcel geometry was corrected to a large extent, there are still trapezoidal triangles and irregular parcels. This problem is caused by the fact that village/neighborhood border correction processes are not carried out or cannot be carried out, as well as the fixed facilities in the project area, the topographic structure of the land, and the existing road transportation network. In this context, while planning, more linear block planning should be made in the creation of block shapes, and border neighboring villages or neighborhoods should be included in the consolidation, and border correction processes should be made. This will contribute to the increase in the number of ideal parcel shapes.

As a result of the analyses made according to the parcel shape index, it has been revealed that the parcel geometry has been corrected to a great extent. When the values obtained before and after the project are compared, while the general parcel distribution before the project was between 1.09 and 4.12, the parcel distribution after the project is between 1.09 and 3.25. Although it is seen that there is an improvement in the most problematic parcel shapes in the index values of the parcel shapes after the project, it is seen that the expected benefit has not been provided in the general situation.

A consolidation rate of 21.62% was reached in the project carried out in Özyurt village. Scattered and fragmented lands belonging to the same enterprise were brought together and combined, but it is seen that it is insufficient. This situation also showed its effect on the parcel shape index. The average parcel size in the project area increased from 11.61 decares to 14.37 decares. Proportionally, the average parcel size has increased by approximately 24%. By bringing parcels together, the total parcel boundary length decreases, and the usable area for agricultural production increases. The area loss before and after the project has decreased by approximately 52 decares. If the consolidation rate reaches higher values, the parcel geometric shapes will become more suitable for agricultural mechanization,

the average parcel size will increase, and the amount of arable land will increase.

When the land consolidation study in Özyurt village is compared to the pre-project situation, the number of parcel shapes suitable for agricultural production generally increases, and the amount of land that cannot be used for agricultural production decreases. It is anticipated that the amount of production in the project area will increase, and production costs will decrease compared to the pre-project period.

REFERENCES

Acar, Ö., Bengin, E. (2018). Yozgat (Baştürk Köyü) Arazi Toplulaştırma Projesinin Bölgesel Kalkınma Açısından Değerlendirilmesi, III. Uluslararası Bozok Sempozyumu, 3-5 Mayıs, Bozok Üniversitesi, Yozgat.

Acar, Ö., ve Akdeniz, H. B., (2023). Arazi Toplulaştırma Projelerinin Parsel Şekil Değişimine Etkisinin Analizi: Manyas/Salur Köyü Örneği, Türkiye. Tarımsal Eski Sorunlara Yeni Yaklaşımlar (s. 81–101). İksad yayınevi. https://doi.org/10.5281/zenodo.8373721

Akdeniz, H. B., ve Acar, Ö., (2023). Arazi Toplulaştırma Projelerinin Arazi Parçalanması Değişimine Etkisi Bakımından Değerlendirilmesi: Manyas / Yeniköy Köyü Örneği, Türkiye. Tarımsal Eski Sorunlara Yeni Yaklaşımlar (s. 103–121). İksad Yayınevi. https://doi.org/10.5281/zenodo.8373751

Akdeniz, M., & Temizel, K. E. (2018). Arazi toplulaştırma projelerinde başarının değişik göstergelere göre değerlendirilmesi. Anadolu Tarım Bilimleri Dergisi, 33(2), 149-161. https://doi.org/10.7161/omuanajas.412040

Arslan, F., Degirmenci, H., Akkaya, S., & Jürgenson, E. (2021). A new approach to measure parcel shapes for land consolidation. Kahramanmaraş Sütçü İmam Üniversitesi Tarım ve Doğa Dergisi, 24(5), 1059-1067.

Bengin, E., Acar, Ö. (2018). Yozgat İlinin Tarımsal Kalkınmasında Kırsal Alan Düzenlemesinin Önemi, III. Uluslararası Bozok Sempozyumu, 3-5 Mayıs, Bozok Üniversitesi, Yozgat.

Boztoprak, T. (2015). Kamulaştirmanin Parsel Sayisi ve Ortalama Parsel Büyüklüğüne Etkisi. Selçuk Üniversitesi Mühendislik, Bilim ve Teknoloji Dergisi, 3(2), 10-17.

Cengiz, N., (2021). Bursa- Karacabey Ovası Toprak Toplulaştırması. İksad Yayınevi, Ankara. ISBN: 978-625-8423-29-7

Demetriou, D., Stillwell, J., & See, L. (2012). Land consolidation in Cyprus: why is an integrated planning and decision support system required?. Land use policy, 29(1), 131-142.

Demetriou, D., See, L., & Stillwell, J. (2013). A parcel shape index for use in land consolidation planning. Transactions in GIS, 17(6), 861-882.

Demirtaş, E. İ., & Sarı, M. (2016). ARAZİ TOPLULAŞTIRMASI. Derim, 20(1), 48-58.

Dengiz, O., Özcan, H., Güntürk, A., & Köşker, Y. (2007). Tarımsal amaçlı fiziksel arazi değerlendirme çalışmalarında bilgisayar model yaklaşımı (TOSATADEM-2005). Anadolu Tarım Bilimleri Dergisi, 22(1), 55-63.

FAO, 2020. Legal Guide on Land Consolidation, Based on Regulatory Practices in Europe. Food and Agricultural Organization of the United Nations, Rome. FAO Legal Guide 3. https://www.fao.org/publications/card/en/c/CA9520EN/ (Access Date: 20.11.2024).

Guo, B., Jin, X., Yang, X., Guan, X., Lin, Y., & Zhou, Y. (2015). Determining the effects of land consolidation on the multifunctionlity of the cropland production system in China using a SPA-fuzzy assessment model. European Journal of Agronomy, 63, 12-26.

Hiironen, J., & Riekkinen, K. (2016). Agricultural impacts and profitability of land consolidations. Land Use Policy, 55, 309-317.

Janus, J., & Markuszewska, I. (2017). Land consolidation–A great need to improve effectiveness. A case study from Poland. Land Use Policy, 65, 143-153.

Jiang, Y., Tang, Y. T., Long, H., & Deng, W. (2022). Land consolidation: A comparative research between Europe and China. Land Use Policy, 112, 105790.

Kangethe, A. W. (2024). The Changing Dynamics of Agricultural Land Use in Kenya: Legal responses to address the threat of food insecurity from land fragmentation. Journal of Academics Stand Against Poverty, 4(Special Issue), 1-9.

Karamatov, O., & Sadykova, G. (2018). Bağımsızlık Yıllarında Özbekistan Cumhuriyeti'nin Toprak ve Tarım Politikası. Asya Araştırmaları Uluslararası Sosyal Bilimler Dergisi, 2(1), 57-65.

Kirmikil, M., & Arici, I. (2013). The use of landscape metrics to assess parcel conditions pre-and post-land consolidation. Journal of Food, Agriculture & Environment, 11(2), 985-989.

Knippenberg, E., Jolliffe, D., & Hoddinott, J. (2020). Land fragmentation and food insecurity in Ethiopia. American Journal of Agricultural Economics, 102(5), 1557-1577.

Kocur-Bera, K., Rapiński, J., Siejka, M., Leń, P., & Małek, A. (2023). Potential of an Area in Terms of Pro-Climate Solutions in a Land Consolidation Project. Sustainability, 15(12), 9306.

Küsek, G. (2014). Türkiye'de arazi toplulaştırmasının yasal durumu ve tarihsel gelişimi. Çukurova Üniversitesi Ziraat Fakültesi Dergisi, 29(1), 1-6.

Latruffe, L., & Piet, L. (2014). Does land fragmentation affect farm performance? A case study from Brittany, France. Agricultural systems, 129, 68-80.

Li, Y., Wu, W., & Liu, Y. (2018). Land consolidation for rural sustainability in China: Practical reflections and policy implications. Land use policy, 74, 137-141.

Long, H., Zhang, Y., & Tu, S. (2019). Rural vitalization in China: A perspective of land consolidation. Journal of Geographical Sciences, 29, 517-530.

Mayele, J. M., Kolleh, J. B., & Saburi, J. E. (2024). The Impacts and Causes of Land Fragmentation on Farm Productivity: Case Review of East African Countries. Open Journal of Ecology, 14(5), 455-482.

McGarical, K. and Marks, B.J. (1995). FRAGSTATS: spatial pattern analysis program for quantifying landscape structure. Washington, D.C., U.S. Department of Agriculture, Forest Service, General Technical Report No PNW-GTR-351.

Niroula, G. S., & Thapa, G. B. (2005). Impacts and causes of land fragmentation, and lessons learned from land consolidation in South Asia. Land use policy, 22(4), 358-372.

Ntihinyurwa, P. D., & de Vries, W. T. (2021). Farmland fragmentation, farmland consolidation and food security: Relationships, research lapses and future perspectives. Land, 10(2), 129.

Orea, L., Perez, J. A., & Roibas, D. (2015). Evaluating the double effect of land fragmentation on technology choice and dairy farm productivity: A latent class model approach. Land Use Policy, 45, 189-198.

Postek, P. (2018). Differences in spatial structure of villages of commune ksiezpol with regard to parcel shape index. Engineering for Rural Development, 17, 611-616.

Seyyar, E. K. (2019). Arazi toplulaştırma çalışmalarının sosyal ve ekonomik yönden analizi: Kırıkkale Ili–Delice Ilçesi köy toplulaştırma çalışma örneği. Yüksek Lisans Tezi, Ankara Üniversitesi, Fen Bilimleri Enstitüsü, Ankara.

Shaw, D. J. (1963). The problem of land fragmentation in the Mediterranean area: a case study. Geographical Review, 53(1), 40-51.

Shi, Y., Cao, X., Fu, D., & Wang, Y. (2018). Comprehensive value discovery of land consolidation projects: An empirical analysis of Shanghai, China. Sustainability, 10(6), 2039. https://doi.org/10.3390/su10062039

Stręk, Ż., Leń, P., Wójcik-Leń, J., Postek, P., Mika, M., & Dawid, L. (2021). A proposed land exchange algorithm for eliminating the external plot patchwork. Land, 10(1), 64.

Su, Y., Xuan, Y., Zang, L., & Zhang, X. (2024). Is Land Fragmentation Undermining Collective Action in Rural Areas? An Empirical Study Based on Irrigation Systems in China's Frontier Areas. Land, 13(7), 1041.

Presidency of Strategy and Budget of the Republic of Turkey (2023), Twelfth Development Plan: 2024-2028, Presidency of Strategy and Budget Publication, Ankara, http://www.sbb.gov.tr (Access Date: 20.11.2024)

Republic of Turkey Official Gazette, 2019. Land Consolidation and On-Farm Development Services Implementation Regulation, 30679, www.resmigazete.gov.tr (Access Date: 10.11.2024)

Tan, S., Heerink, N., & Qu, F. (2006). Land fragmentation and its driving forces in China. Land use policy, 23(3), 272-285.

Tezcan, A., Büyüktaş, K., & Aslan, Ş. T. A. (2020). A multi-criteria model for land valuation in the land consolidation. Land use policy, 95, 104572.

Thapa, G. B., & Niroula, G. S. (2008). Alternative options of land consolidation in the mountains of Nepal: An analysis based on stakeholders' opinions. Land use policy, 25(3), 338-350.

Tran, T. Q., & Van Vu, H. (2021). The impact of land fragmentation on food security in the North Central Coast, Vietnam. Asia & the Pacific Policy Studies, 8(2), 327-345.

Vitikainen, A. (2004). An overview of land consolidation in Europe. nordic Journal of Surveying and real Estate research, 1(1).

Chapter 14

CFD MODELING OF BATTERY COOLING SYSTEMS FOR ELECTRIC VEHICLES: ENHANCING THERMAL MANAGEMENT EFFICIENCY

Yasin Furkan GORGULU

Mehmet Akif KUNT[2]

1. INTRODUCTION

Thermal management systems play a critical role in the operation, performance, and safety of electric vehicles (EVs), particularly in relation to the lithium-ion battery packs that power them. The efficiency and lifespan of these batteries are highly dependent on maintaining an optimal temperature range, as excessive heat can accelerate degradation, reduce battery capacity, and in extreme cases, lead to thermal runaway, a dangerous condition that can cause fire or explosion. Thus, effective thermal management is indispensable for ensuring both the longevity of the battery and the overall safety of the vehicle. The need for robust battery thermal management arises primarily from the non-uniform heat generation within the battery cells during charge and discharge cycles. Lithium-ion batteries, widely used in EVs due to their high energy density, are prone to significant heat generation, particularly under high load conditions, such as fast charging or heavy acceleration (Garud et al. 2023; Oh et al. 2023). Failure to dissipate this heat efficiently can lead to uneven temperature distributions across the battery pack, which not only reduces the performance of individual cells but also compromises the pack's overall performance. Moreover, thermal gradients can lead to differing rates of aging among the cells, resulting in imbalances that further reduce efficiency (Falcone et al. 2021).

Numerous studies have demonstrated that maintaining battery temperatures within an optimal range (typically 20-40°C) is crucial for maximizing efficiency and extending the battery's operational life (Garud et al. 2023). Effective thermal management also ensures the battery operates within safe thermal limits, thereby preventing the risk of thermal runaway. Research shows that maintaining a uniform temperature distribution within the battery pack can prevent localized overheating and improve the safety of electric vehicles. Additionally, excessive cooling, while potentially mitigating thermal risks, can result in energy inefficiencies, making it important to balance cooling effectiveness with energy consumption (Carello et al. 2023). The implementation of thermal management systems in EVs typically involves active cooling solutions, such as liquid cooling systems, or passive approaches, such as phase change materials (PCMs). While air cooling was initially adopted due to its simplicity, liquid cooling has become the preferred method in high-performance EVs, owing to its superior heat transfer characteristics (Chen et al. 2019; Murali et al. 2021; Thakur et al. 2020; Zhao et al. 2023). Furthermore, advanced cooling techniques like immersion cooling, where batteries are submerged in a dielectric liquid, have shown promise in maintaining uniform temperatures even under high power loads, enhancing both safety and performance. Thermal management is not only a technical necessity for the optimal performance of electric vehicles but also a key factor in ensuring the longevity and safety

of the battery systems. The ongoing development of more efficient cooling technologies, coupled with advances in computational fluid dynamics (CFD) modeling, continues to drive improvements in this critical area of electric vehicle design.

CFD is a tool used in the analysis and optimization of battery thermal management systems (BTMS) for EVs. As electric vehicle batteries generate significant heat during operation, managing this heat becomes crucial for maintaining performance, extending battery life, and ensuring safety. CFD allows for detailed simulations of heat transfer and fluid flow, providing insights that are difficult to obtain through experimental methods alone. Through the use of numerical methods, CFD can simulate how heat is generated and transferred both inside individual battery cells and across the entire pack, considering various cooling configurations like air, liquid, or immersion cooling. This ability to predict temperature behavior at such a detailed level has made CFD invaluable in optimizing BTMS designs. Recent studies have demonstrated the effectiveness of CFD in comparing different cooling strategies for electric vehicle batteries (Akinlabi and Solyali 2020; Aswin Karthik et al. 2020; Behi et al. 2020; Deng et al. 2018; Dhisale 2021; Falcone et al. 2021; Murali et al. 2021; Roe et al. 2022; Zhao et al. 2023). For example, researchers have used CFD to analyze the performance of liquid cooling systems compared to traditional air-cooling methods, showing that liquid cooling provides superior temperature control, particularly under high load conditions. Moreover, advanced CFD models can simulate innovative cooling techniques such as immersion cooling, where batteries are immersed in dielectric fluids, demonstrating significant improvements in thermal regulation by maintaining uniform temperatures across the battery pack (Carello et al. 2023; Oh et al. 2023; Roe et al. 2022).

2. OVERVIEW OF BATTERY THERMAL MANAGEMENT SYSTEMS

1.1. Air Cooling Systems

Air cooling systems are one of the earliest and most straightforward methods used to manage the thermal load in EV battery packs. This method typically involves the circulation of ambient air or forced convection of cooled air through battery modules to dissipate heat generated during operation (Akinlabi and Solyali 2020). Air cooling is favored in some applications due to its simplicity, relatively low cost, and the absence of additional components like heat exchangers or liquid pumps. However, as energy densities in modern EV batteries continue to rise, the limitations of air cooling have become more pronounced. One of the primary limitations of air cooling is its relatively low heat transfer efficiency. Air, compared to liquids, has a lower thermal conductivity and specific heat capacity,

making it less effective at removing large amounts of heat quickly. Another significant drawback of air cooling is the difficulty in maintaining uniform temperature distribution across the battery pack. Air cooling systems often struggle to prevent localized hotspots, especially in densely packed battery modules where air may not flow evenly through all cells. Hotspots can lead to uneven aging of battery cells, reducing the overall performance and lifespan of the battery pack. Additionally, temperature gradients within the battery can cause imbalances between cells, leading to efficiency losses and potentially dangerous conditions like thermal runaway. Furthermore, air cooling systems become increasingly inefficient at higher energy densities, where the amount of heat generated per unit volume is greater. In such cases, air cooling requires more powerful fans or blowers, which not only increase the energy consumption but also generate more noise and occupy additional space—factors that can negatively affect the overall design and user experience of electric vehicles.

1.2. Liquid Cooling Systems

Liquid cooling has emerged as a more advanced and efficient alternative to air cooling for battery thermal management in EVs. This method typically uses a combination of water and glycol-based coolants, which are circulated through channels embedded in or around battery modules to absorb and dissipate heat (Wu et al. 2019). The higher thermal conductivity and heat capacity of liquids compared to air allow for more effective and uniform temperature control, making liquid cooling particularly suitable for high-performance and high-energy-density EVs. One of the key advantages of liquid cooling systems is their superior heat transfer efficiency. Liquids like water and glycol can absorb significantly more heat than air before their temperature rises, allowing them to remove larger amounts of heat from the battery pack in a relatively short period of time. This increased heat transfer capacity is especially important in modern EVs, where batteries generate substantial heat during fast charging and discharging cycles. Liquid cooling can maintain the battery pack within the optimal temperature range, thus preventing performance degradation, extending battery life, and minimizing the risk of thermal runaway. In addition to heat transfer efficiency, liquid cooling systems offer more precise temperature control and uniformity across the battery pack. The use of coolant channels ensures that heat is distributed evenly throughout the system, reducing the occurrence of hotspots and thermal gradients between individual cells. This uniformity is critical for maintaining the overall balance of the battery pack, as uneven temperatures can lead to cell degradation and performance losses over time . Liquid cooling systems also provide the flexibility to incorporate different design configurations, such as direct and indirect cooling. In direct liquid cooling, the coolant comes into direct contact with the battery cells or their

casings, maximizing heat transfer efficiency. In indirect cooling, the coolant circulates through separate channels or plates, providing a thermal barrier between the coolant and the cells. While direct cooling offers better heat removal, indirect cooling is often preferred for its reduced risk of leakage and contamination. However, liquid cooling systems are not without their challenges. They require additional components, such as pumps, heat exchangers, and sealing mechanisms, which increase system complexity, cost, and maintenance requirements. Moreover, the energy consumed by these systems to circulate the coolant must be carefully managed to avoid offsetting the overall energy efficiency gains.

1.3. Immersion Cooling Technologies

Immersion cooling represents a relatively new and highly effective approach to battery thermal management, offering superior heat dissipation compared to traditional air and liquid cooling methods. In this technique, battery cells are directly immersed in a dielectric fluid, which has high thermal conductivity and is electrically non-conductive, allowing for direct contact with battery components without the risk of short circuits (Roe et al. 2022). Immersion cooling has demonstrated significant advantages in terms of maintaining uniform temperatures across the battery pack, enhancing both efficiency and safety. Dielectric fluids such as Novec™ 649 and mineral oils are commonly used in immersion cooling systems due to their ability to efficiently absorb and transfer heat (Oh et al. 2023). Unlike water/glycol mixtures, these fluids are non-conductive, which enables them to be in direct contact with sensitive battery components, thus maximizing heat transfer without the risk of damaging electrical circuits. The superior thermal properties of dielectric fluids allow for rapid heat dissipation, making immersion cooling particularly effective during high-demand operations such as fast charging or rapid acceleration. One of the main advantages of immersion cooling is its ability to maintain a highly uniform temperature distribution throughout the battery pack. Traditional air and liquid cooling systems often struggle to eliminate localized hotspots, which can lead to uneven aging of cells and reduced battery performance. In contrast, immersion cooling effectively eliminates these thermal gradients, ensuring that all cells remain within the desired temperature range. This uniform temperature control not only enhances battery performance but also prolongs the operational life of the cells by preventing uneven wear . Another critical benefit of immersion cooling is the increased safety it provides, particularly in preventing thermal runaway—a dangerous condition where excessive heat generation can cause a battery to ignite or explode. The direct immersion of cells in a dielectric fluid helps to contain and dissipate the heat quickly, reducing the risk of thermal runaway even under extreme conditions. Furthermore, many dielectric fluids used

in immersion cooling, such as Novec™ 649, are specifically designed to suppress flames and prevent fire propagation, adding an extra layer of safety for electric vehicle batteries. However, the implementation of immersion cooling systems also comes with challenges, such as the need for highly specialized fluids and complex sealing systems to prevent fluid leakage. Additionally, the cost of dielectric fluids is typically higher than that of traditional coolants, which may increase the overall cost of the battery system.

3. CFD MODELING METHODOLOGIES FOR BATTERY COOLING

1.1. Governing Equations and CFD Fundamentals

The foundation of any CFD analysis lies in solving a set of partial differential equations that govern the behavior of fluid flow and heat transfer. For battery thermal management, CFD models focus on accurately simulating the heat dissipation and cooling effects within the battery pack. The primary equations used in these simulations are the Navier-Stokes equations for fluid flow, the continuity equation for mass conservation, and the energy equation for heat transfer. These equations work together to describe how heat is generated, transferred, and removed within the cooling system. The Navier-Stokes equations describe the motion of fluid substances and are essential for understanding the fluid flow in a cooling system. These equations are based on Newton's second law, which balances the rate of change of momentum in the fluid with the forces acting on it. In their incompressible form (often assumed for liquids used in battery cooling), the Navier-Stokes equations can be written as (Gorgulu 2024a):

$$\rho\left(\frac{\partial \mathbf{v}}{\partial t} + \mathbf{v}.\nabla\mathbf{v}\right) = -\nabla p + \mu\nabla^2\mathbf{v} + \mathbf{f} \quad (1)$$

Where:

ρ is the fluid density,

is the velocity field,

is the pressure,

is the dynamic viscosity,

f represents external forces (e.g., gravity).

In battery cooling applications, the fluid velocity distribution and pressure gradients are critical for ensuring effective heat removal from the battery cells. The Navier-Stokes equations allow the CFD model to simulate the flow patterns of the coolant around the battery, determining whether sufficient cooling is achieved across the entire system. The continuity equation represents the conservation of mass in the fluid system, ensuring

that mass cannot be created or destroyed within the flow field. For an incompressible fluid, the continuity equation simplifies to (Gorgulu 2024b):

$$\nabla . v = 0 \tag{2}$$

This equation ensures that the flow of the coolant remains consistent throughout the system, which is essential for preventing localized areas of insufficient cooling, commonly known as hot spots. In battery cooling, it is important to ensure that the coolant flows uniformly, especially in regions with high heat generation. The energy equation governs the transfer of heat within the system. It is essential for modeling how heat is generated within the battery cells and how it is transferred to the coolant for removal. The energy equation is expressed as (Gorgulu 2024b):

$$\rho c_p \left(\frac{\partial T}{\partial t} + v . \nabla T \right) = k \nabla^2 T + q \tag{3}$$

Where:

is the temperature,

is the specific heat capacity of the fluid,

is the thermal conductivity,

q represents the heat source term, such as heat generated by the battery cells during operation.

The energy equation is central to the thermal analysis in battery cooling systems because it directly models how much heat is being generated by the battery and how efficiently the coolant is removing that heat. Accurate modeling of the temperature field ensures that the battery cells are maintained within safe operational limits. In addition to the governing equations, proper boundary and initial conditions must be specified to achieve accurate CFD results. Typical boundary conditions include specifying inlet and outlet conditions for the coolant (e.g., velocity or temperature), thermal boundary conditions on the battery surface (e.g., heat flux or temperature), and wall conditions that affect how the fluid interacts with solid surfaces. In battery cooling simulations, the governing equations are tightly coupled. The Navier-Stokes equations describe how the coolant moves through the system, while the energy equation governs how heat is transferred between the battery cells and the coolant. The continuity equation ensures mass is conserved throughout the system. Solving these equations simultaneously is necessary to accurately predict the temperature distribution and fluid flow in the battery thermal management system. The successful application of CFD to battery cooling requires solving the

Navier-Stokes, continuity, and energy equations in a coordinated manner. These fundamental equations form the backbone of thermal management simulations, providing insights into how to optimize cooling strategies for electric vehicle batteries.

1.2. CFD Setup and Boundary Conditions for Battery Cooling

Setting up a CFD simulation for battery thermal management involves several key steps, including selecting appropriate models, defining the geometry, setting boundary conditions, and determining the meshing strategy. The accuracy of a CFD simulation is highly dependent on how well these factors are configured, especially the boundary conditions that govern fluid flow and heat transfer between the battery and its cooling medium. The first step in CFD setup is defining the geometry of the battery pack and its cooling system. The model typically includes battery cells (cylindrical or prismatic), the cooling channels, and the surrounding fluid region. Depending on the cooling method (air, liquid, or immersion cooling), the geometry may include air ducts, liquid channels, or an immersed fluid volume. In battery cooling simulations, accurately representing the battery's internal structure and the placement of the cooling system is crucial for capturing the thermal behavior across the entire battery pack. For instance, in air cooling, this would involve defining the airflow paths and inlets/outlets around the battery cells. In liquid and immersion cooling, the cooling channels or the fluid domain that surrounds the battery pack need to be modeled in detail. For air cooling, boundary conditions are typically set at the inlets and outlets of the cooling ducts, where air enters and exits the system. Inlet boundary conditions usually define the air velocity or flow rate, along with its temperature. Common inlet conditions may specify a velocity-inlet or a mass-flow inlet, depending on the airflow characteristics. At the outlet, a pressure-outlet boundary condition is often applied, allowing the air to exit at atmospheric or specified pressure. Walls and other solid surfaces are set as no-slip conditions, meaning the velocity at the wall is zero. The temperature distribution on the battery surfaces exposed to the air must be carefully modeled. Typically, the battery's external surfaces are assigned a heat flux or temperature boundary condition to reflect the amount of heat being dissipated through convection to the surrounding air. The convective heat transfer coefficient (based on the airflow and battery surface characteristics) needs to be accurately calculated to ensure the heat is removed efficiently from the battery. The inlet and outlet boundary conditions for liquid cooling are usually similar to air cooling but involve the liquid coolant. The velocity-inlet or mass-flow inlet conditions specify the coolant's flow rate and temperature, while the outlet is again modeled using pressure-outlet or a specified back pressure. These boundary conditions help control the flow rate and pressure drop across the cooling system.

For liquid-cooled systems, it is important to account for thermal contact resistance between the battery cells and the cooling plates or channels. The boundary condition between the battery surface and the cooling channels can be modeled using a conjugate heat transfer approach, where heat transfer between the solid (battery) and liquid (coolant) is coupled directly. A volume of fluid (VOF) approach (Jaafar et al. 2017) may be used to model the interaction between the battery surface and the surrounding dielectric fluid. For immersion cooling systems, the boundary conditions focus on ensuring the fluid's temperature and velocity profiles are maintained at steady-state levels throughout the simulation. Inlets for fresh dielectric fluid may be set with velocity-inlet conditions, and the battery surfaces are assigned a heat generation rate based on the internal heat generated during operation. The outlet boundary is similarly configured to allow the heated fluid to exit or recirculate back into the system. Meshing plays a critical role in determining the accuracy of the CFD simulation. A finer mesh is typically applied near the battery cells and cooling channels to capture the detailed flow and heat transfer behaviors, while a coarser mesh can be used in regions where gradients are less pronounced. Choosing the right turbulence model is essential for simulating the flow of coolant in battery cooling systems. The k-ε or k-ω SST models are commonly used in battery cooling applications, as they provide a good balance between accuracy and computational efficiency in turbulent flows (Akinlabi and Solyali 2020).

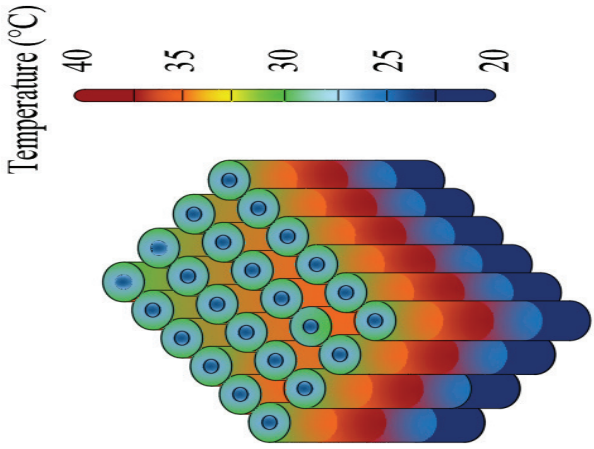

Figure 1. *Thermal distribution contours of cylindrical lithium-ion battery cells.*

Figure 1. shows a thermal contour plot of cylindrical lithium-ion battery cells, illustrating temperature distribution ranging from 20°C to 40°C. The contour colors indicate cooler regions in blue and progressively warmer regions in red. The visualization effectively highlights how heat is distributed across the battery cells, with distinct thermal gradients. This

kind of analysis is critical for evaluating cooling strategies in battery thermal management systems, as it helps identify areas prone to overheating and guides improvements in cooling designs to maintain optimal operating conditions.

4. COMPARATIVE ANALYSIS OF COOLING STRATEGIES USING CFD

Air cooling is a simple and widely adopted strategy in BTMS due to its cost-effectiveness and straightforward design. However, the limited heat transfer capacity of air often becomes a constraint in applications where high energy densities are required or extreme conditions are present. Studies indicate that air-cooling strategies, both natural and forced, are more suited for smaller battery systems or mild operational environments. Forced air cooling, despite its better heat dissipation, still struggles to manage temperature gradients effectively, resulting in reduced energy efficiency and uneven cell temperatures (Akinlabi and Solyali 2020). Liquid cooling, on the other hand, provides significantly higher heat transfer efficiency due to the greater thermal conductivity and specific heat capacity of liquids like water/glycol mixtures. Liquid cooling systems can manage large heat loads and offer superior cooling performance, which is essential for high-power EV batteries. Various configurations such as direct liquid cooling, cold plates, and indirect methods have been explored to optimize heat removal. Research by Zhao et al. demonstrates the effectiveness of liquid cooling systems in achieving lower temperature differentials and maintaining battery performance even under demanding conditions (Zhao et al. 2023).

Immersion cooling techniques involve submerging battery modules in dielectric fluids, offering direct contact between the coolant and the battery cells. This method drastically improves heat dissipation compared to air and traditional liquid cooling systems, due to the elimination of thermal barriers and the high thermal conductivity of dielectric fluids. Immersion cooling, especially in two-phase systems, leverages the latent heat of evaporation, leading to enhanced convective heat transfer through boiling and turbulent flow mechanisms. Hong et al. have shown that immersion cooling can achieve a 10,000-fold improvement in heat transfer efficiency compared to passive air cooling, effectively preventing thermal runaway and ensuring battery safety (Hong et al. 2024).

When evaluating cooling strategies, performance metrics such as maximum temperature, temperature uniformity, and cooling efficiency are critical. Liquid cooling systems typically exhibit a more uniform temperature distribution within battery packs, reducing thermal stresses that contribute to capacity fade and safety risks (Tete, Gupta, and Joshi 2021). Immersion

cooling, with its high heat transfer coefficients, demonstrates better temperature regulation, especially under high discharge rates or rapid charging conditions, minimizing hotspots and prolonging battery life.

5. FUTURE TRENDS IN BATTERY THERMAL MANAGEMENT

As EV technology continues to evolve, new and innovative cooling technologies are being developed to meet the increasing demands of high-performance batteries. Among these, PCMs and nano-coolants are gaining significant attention due to their potential to enhance thermal management systems. PCMs are designed to absorb and store large amounts of heat as they change from a solid to a liquid phase. This latent heat storage capability allows PCMs to maintain battery temperatures within safe limits without the need for additional active cooling components. PCMs have shown great promise in providing passive thermal management, especially in applications where space and energy efficiency are critical. They can be integrated into battery modules, where they absorb heat during high-load operations, such as fast charging or heavy discharging, and release it slowly once the demand decreases. However, challenges remain in selecting the right PCM with appropriate thermal properties and integrating it efficiently into EV systems. Nano-coolants, which are conventional fluids enhanced with nanoparticles, offer another cutting-edge approach to improving heat transfer in battery thermal management systems. These nanoparticles (e.g., copper, aluminum oxide, or carbon-based materials) significantly increase the thermal conductivity of the coolant, allowing for more efficient heat dissipation from the battery cells. Nano-coolants can be used in both liquid and immersion cooling systems, offering better performance without drastically increasing energy consumption.

As fast-charging infrastructure becomes more widespread, BTMS must adapt to the increased heat generation associated with rapid charging. Fast charging, particularly at rates of 150 kW or more, generates significant thermal stress on the battery cells, which can lead to overheating and reduced battery lifespan if not properly managed. To handle these high thermal loads, BTMS designs must be optimized to dissipate heat more rapidly while maintaining uniform temperatures across the battery pack. Advanced cooling technologies such as direct liquid cooling and immersion cooling are becoming increasingly important for fast-charging applications. These systems ensure that the heat generated during rapid charging cycles is efficiently removed, maintaining safe battery operating temperatures.

6. CONCLUSION

In this study, the importance of effective thermal management for EV batteries was thoroughly analyzed using various cooling strategies. Through CFD modeling, it was demonstrated that air cooling, while cost-effective

and simple, is limited by its lower heat transfer capacity and inability to maintain uniform temperature distribution, particularly in high-energy-density applications. Liquid cooling methods, employing water-glycol mixtures, proved to be significantly more effective due to their superior thermal conductivity and capacity to handle larger heat loads. Different configurations of liquid cooling, such as direct and indirect systems, were explored, showing improved performance and temperature regulation capabilities. Immersion cooling is a promising strategy, achieving a temperature uniformity and safety. By submerging battery modules in dielectric fluids, direct heat transfer was enabled, eliminating thermal barriers and achieving higher efficiency. Immersion cooling systems demonstrated not only enhanced cooling performance but also critical safety benefits, such as mitigating the risk of thermal runaway. The insights gained from the comparative analysis underscore the need for tailored cooling strategies depending on the specific requirements of the EV battery system. Air cooling remains a viable solution for smaller-scale or low-power applications, while liquid and immersion cooling are recommended for high-performance and high-power systems. The exploration of advanced cooling methods like PCMs and nano-coolants indicates the future direction of battery thermal management. The integration of such innovative solutions with fast-charging infrastructure will be crucial in meeting the increasing demands of next-generation electric vehicles. Ultimately, the application of CFD in optimizing cooling systems has proven to be invaluable in enhancing battery safety, efficiency, and lifespan. Continued research and development in thermal management technologies will play a key role in the evolution of electric vehicles, paving the way for more reliable and high-performance battery systems.

REFERENCES

Akinlabi, A. A. Hakeem, and Davut Solyali. 2020. "Configuration, Design, and Optimization of Air-Cooled Battery Thermal Management System for Electric Vehicles: A Review." *Renewable and Sustainable Energy Reviews* 125(February):109815. doi: 10.1016/j.rser.2020.109815.

Aswin Karthik, Chandrasekaran, Pankaj Kalita, Xujian Cui, and Xiongbin Peng. 2020. "Thermal Management for Prevention of Failures of Lithium Ion Battery Packs in Electric Vehicles: A Review and Critical Future Aspects." *Energy Storage* 2(3):1–15. doi: 10.1002/est2.137.

Behi, Hamidreza, Danial Karimi, Mohammadreza Behi, Morteza Ghanbarpour, Joris Jaguemont, Mohsen Akbarzadeh Sokkeh, Foad Heidari Gandoman, Maitane Berecibar, and Joeri Van Mierlo. 2020. "A New Concept of Thermal Management System in Li-Ion Battery Using Air Cooling and Heat Pipe for Electric Vehicles." *Applied Thermal Engineering* 174(March):115280. doi: 10.1016/j.applthermaleng.2020.115280.

Carello, Massimiliana, Massimo Bovio, Federico Ricci, Simone Dall'Acqua, Daniele Isidoro Strano, and Alessandro Rizzello. 2023. "CFD Simulation and Modelling of a Battery Thermal Management System: Comparison between Indirect and Immersion Cooling."

Chen, Jingwei, Siyi Kang, Jiaqiang E, Zhonghua Huang, Kexiang Wei, Bin Zhang, Hao Zhu, Yuanwang Deng, Feng Zhang, and Gaoliang Liao. 2019. "Effects of Different Phase Change Material Thermal Management Strategies on the Cooling Performance of the Power Lithium Ion Batteries: A Review." *Journal of Power Sources* 442(October):227228. doi: 10.1016/j.jpowsour.2019.227228.

Deng, Yuanwang, Changling Feng, Jiaqiang E, Hao Zhu, Jingwei Chen, Ming Wen, and Huichun Yin. 2018. "Effects of Different Coolants and Cooling Strategies on the Cooling Performance of the Power Lithium Ion Battery System: A Review." *Applied Thermal Engineering* 142(June):10–29. doi: 10.1016/j.applthermaleng.2018.06.043.

Dhisale, Manthan. 2021. *CFD Simulation of Thermal Management System (Immersion Cooling) of Lithium Ion Batteries in EVs*. Bombay. doi: 10.13140/RG.2.2.19948.69767.

Falcone, Morena, Eleonora Palka Bayard De Volo, Ali Hellany, Claudio Rossi, and Beatrice Pulvirenti. 2021. "Lithium-Ion Battery Thermal Management Systems: A Survey and New CFD Results." *Batteries* 7(4):86. doi: 10.3390/batteries7040086.

Garud, Kunal Sandip, Le Duc Tai, Seong-Guk Hwang, Nghia-Huu Nguyen, and Moo-Yeon Lee. 2023. "A Review of Advanced Cooling Strategies for

Battery Thermal Management Systems in Electric Vehicles." *Symmetry* 15(7):1322. doi: 10.3390/sym15071322.

Gorgulu, Yasin Furkan. 2024a. "CFD Analysis of Parallel Flow in Double Pipe Heat Exchangers: Evaluating Thermal Performance and Effectiveness." Pp. 53–61 in *15th INTERNATIONAL CONGRESS SCIENTIFIC RESEARCH, CHINA TO ADRIATIC*. Baku.

Gorgulu, Yasin Furkan. 2024b. "Shell and Tube Heat Exchanger Optimization for Enhanced Swimming Pool Heating Efficiency Using CFD Analysis." Pp. 414–25 in *5. BİLSEL International World Scientific and Research Congress*. İstanbul.

Hong, Hanchi, Xu Shi, Luigi D`Apolito, and Qianfan Xin. 2024. *Immersion Cooling for Lithium – Ion Batteries at High Discharging Rates*. doi: 10.21203/rs.3.rs-4169021/v1.

Jaafar, Mohamad Ali, Daniel R. Rousse, Stéphane Gibout, and Jean-Pierre Bédécarrats. 2017. "A Review of Dendritic Growth during Solidification: Mathematical Modeling and Numerical Simulations." *Renewable and Sustainable Energy Reviews* 74:1064–79. doi: 10.1016/j.rser.2017.02.050.

Murali, G., G. S. N. Sravya, J. Jaya, and V. Naga Vamsi. 2021. "A Review on Hybrid Thermal Management of Battery Packs and It's Cooling Performance by Enhanced PCM." *Renewable and Sustainable Energy Reviews* 150:111513. doi: 10.1016/j.rser.2021.111513.

Oh, In-Taek, Ji-Su Lee, Jin-Se Han, Seong-Woo Lee, Su-Jong Kim, and Seok-Ho Rhi. 2023. "Li-Ion Battery Immersed Heat Pipe Cooling Technology for Electric Vehicles." *Electronics* 12(24):4931. doi: 10.3390/electronics12244931.

Roe, Charlotte, Xuning Feng, Gavin White, Ruihe Li, Huaibin Wang, Xinyu Rui, Cheng Li, Feng Zhang, Volker Null, Michael Parkes, Yatish Patel, Yan Wang, Hewu Wang, Minggao Ouyang, Gregory Offer, and Billy Wu. 2022. "Immersion Cooling for Lithium-Ion Batteries – A Review." *Journal of Power Sources* 525(January):231094. doi: 10.1016/j.jpowsour.2022.231094.

Tete, Pranjali R., Mahendra M. Gupta, and Sandeep S. Joshi. 2021. "Developments in Battery Thermal Management Systems for Electric Vehicles: A Technical Review." *Journal of Energy Storage* 35(September 2020):102255. doi: 10.1016/j.est.2021.102255.

Thakur, Amrit Kumar, Rajendran Prabakaran, M. R. Elkadeem, Swellam W. Sharshir, Müslüm Arıcı, Cheng Wang, Wensheng Zhao, Jang-Yeon Hwang, and R. Saidur. 2020. "A State of Art Review and Future Viewpoint on Advance Cooling Techniques for Lithium–Ion Battery System of Electric Vehicles." *Journal of Energy Storage* 32(October):101771. doi: 10.1016/j.est.2020.101771.

Wu, Weixiong, Shuangfeng Wang, Wei Wu, Kai Chen, Sihui Hong, and Yongxin Lai. 2019. "A Critical Review of Battery Thermal Performance and Liquid Based Battery Thermal Management." *Energy Conversion and Management* 182(January):262–81. doi: 10.1016/j.enconman.2018.12.051.

Zhao, Gang, Xiaolin Wang, Michael Negnevitsky, and Chengjiang Li. 2023. "An Up-to-Date Review on the Design Improvement and Optimization of the Liquid-Cooling Battery Thermal Management System for Electric Vehicles." *Applied Thermal Engineering* 219(PB):119626. doi: 10.1016/j.applthermaleng.2022.119626.

Chapter 15

A DECISION-MAKING FRAMEWORK FOR ECO-INDUSTRIAL PARK SITE SELECTION IN ISTANBUL USING THE ANALYTIC HIERARCHY PROCESS (AHP)

Mirac Nur Ciner

Emine Elmaslar Özbaş

H. Kurtulus Ozcan, Doğa Aydın, Burcu Arife Ayakçı

İstanbul Üniversitesi- Cerrahpaşa, Mühendislik Fakültesi, Çevre Mühendisliği Bölümü
Istanbul University-Cerrahpasa, Engineering Faculty, Environmental Engineering Department
mirac.ciner@iuc.edu.tr, elmaslar@iuc.edu.tr, hkozcan@iuc.edu.tr, doga.aydin@ogr.iuc.edu.tr, burcuarife.ayakci@ogr.iuc.edu.tr

Introduction

Eco-industrial parks (EIPs) are defined as innovative industrial zones designed to promote environmental sustainability, economic development, and social cohesion. These parks are based on the principles of industrial ecology, aiming to minimize environmental impacts through systems that encourage waste reuse and practices like energy sharing (Veiga & Magrini, 2009). The site selection process is critically important for the successful establishment of EIPs, as the right location directly influences the environmental and economic performance of these parks (Uscha et al., 2021).

Today, multi-criteria decision-making (MCDM) methods have become indispensable for the effective planning and management of EIPs. These methods, when integrated with technologies such as geographic information systems (GIS), enable the optimal siting of industrial parks. As a strategic metropolis, Istanbul plays a central role in Turkey's economic and industrial development and holds great significance for environmental sustainability and infrastructure planning. In this context, the establishment of an EIP in Istanbul would not only support local environmental sustainability but also significantly contribute to the implementation of national environmental policies. Such an initiative would facilitate achieving goals like improving energy efficiency, enhancing waste management, and reducing the carbon footprint, while also strengthening Turkey's capacity to fulfill its international environmental commitments.

In this study, the districts of Arnavutköy, Çatalca, and Silivri in Istanbul were evaluated for the site selection of an EIP using the Analytic Hierarchy Process (AHP) methodology. AHP provides a suitable approach for complex decision-making processes by systematically evaluating multiple criteria. The primary objective of this study is to identify the district in Istanbul that aligns best with the principles of environmental sustainability and economic development, thereby determining the most ideal location for the establishment of an EIP.

Eco-Industrial Park

Planning and constructing the environment with a sustainable and ecological approach is crucial. This requires urban design and transformation projects to cause less harm to nature compared to previous practices. Furthermore, these projects should meet their energy, water, and nutrient needs both within and around their ecosystems. It is equally important to use healthier materials in such developments.

Globally, the number of ecological settlement examples is rapidly increasing. In these settlements, the storage, conservation, and reuse of

energy and water hold significant importance. Eco-settlements are designed using safe, reusable, and healthy materials. To ensure livable urbanization, social, economic, and demographic developments must progress in a balanced manner.

Industrial symbiosis is defined as a long-term partnership where two or more economic operations, typically functioning independently, collaborate to enhance both environmental performance and competitive advantage, facilitated by their physical proximity (Walls & Paquin, 2015).

In this context, environmental management systems developed for industrial zones such as organized industrial zones (OIZs) enable by-products, residues, and waste produced by one company to be used as raw materials by another. Industrial symbiosis should be applied within traditional industrial systems to promote the efficient shared use of existing resources. Following this application, the system is expected to require inter-company collaboration and provide a recyclable mutual benefit mechanism for both producers and consumers (Gümüş, 2016).

The environmental protection strategies implemented by manufacturing companies not only reduce environmental impacts but also enhance production efficiency and contribute to the economy. To achieve sustainable economic growth in OIZs, it is essential to promote and expand clean production by employing eco-friendly and innovative methods, and to establish an industrial symbiosis network capable of implementing the principles of a circular economy.

EIPs are defined as industrial zones where producers of goods and services collaborate to enhance their economic, environmental, and social performance while advancing their collective interests. Through collaborative networks among different sectors, these organized structures provide companies with not only economic and environmental benefits but also strategic advantages such as increased competitiveness, risk management, production continuity, and value creation (Valenzuela-Venegas et al., 2020). EIPs aim to foster sustainable growth by reducing negative environmental impacts (Hong & Gasparatos, 2020).

Eco-Industrial Parks Around the World

When examining EIPs worldwide, the symbiotic system established in the Kalundborg EIP demonstrates significant environmental and economic benefits. Through recycling and reuse practices, the park achieves annual energy savings equivalent to the electricity consumption of over 75,000 households. Additionally, it saves 45,000 tons of oil, 15,000 tons of coal, 90,000 tons of gypsum, and 3 million cubic meters of water each year. As a

result, emissions of over 240,000 tons of CO_2, 10,200 tons of SO_2, and 4,500 tons of S^{2-} have been prevented. The system processes over 30 types of waste, transforming materials such as wastewater, waste heat, and ethanol into various products, including biogas, enzymes, and gypsum board. This symbiotic network, which began in 1961, now comprises 18 different facilities and features a resource-sharing network with 30 interconnections (Özsoy, 2018).

The businesses operating in the Gladstone Industrial Region account for 10% of Australia's total exports. Within the region, companies from various sectors have established the Gladstone Investment Corporation (GAIN). The region primarily hosts industries in mining (aluminum, coal), cement production, chemical manufacturing (ammonium nitrate, sodium cyanide, chlorine), petroleum, energy production, and a thermal power plant. It is noteworthy that in the Gladstone Region, the administrative responsibility for symbiosis formation is observed to be undertaken by the private sector (Uslu, 2019).

The Tianjin TEDA EIP is another significant eco-park. Established in 1984, TEDA was recognized in 2008 by the Chinese government as one of the top three EIPs in China. The park has made substantial environmental advancements, fostering numerous symbiotic relationship networks. Located in Tianjin, one of China's low-carbon pilot cities, all facilities in the EIP operate using electricity generated from green energy sources. As of 2020, Tianjin TEDA EIP hosts 146 green factories and 14 state-level green supply chain management enterprises (Esenlikci, 2023).

Ulsan, located in the southeastern part of the Republic of Korea along the coast of the Sea of Japan, is the country's seventh-largest metropolitan area. This metropolis stands out as an industrial powerhouse in Korea, employing over 100,000 people and hosting more than 1,000 companies. Ulsan's EIP plays a significant economic role, housing notable companies such as the world's largest automobile assembly plant (Hyundai Motor Group), the world's largest shipyard (Hyundai Heavy Industries Group), and the world's second-largest refinery (SK Energy). The annual profits shared by companies operating in the EIP exceed the investment costs for infrastructure planning and construction. For instance, the Sung-am Municipality Waste Incineration Plant and Hyosung Company shared revenues of $6,500,000 after an investment of $4,500,000. Similarly, Yoosung Company and Hankook Paper Factory achieved a shared profit of $2,100,000 from a joint investment of $800,000 (T.R. MSIT, 2015).

Eco-Industrial Parks in Türkiye

In recent years, numerous studies have been conducted in Turkey regarding EIPs. A 2020 study examined the potential for transforming industrial zones in Turkey into EIPs by adopting the concept of industrial symbiosis in line with sustainability principles (Genç, 2020). Additionally, a theoretical prototype EIP was developed within the framework of the construction industry to guide the design of newly planned industrial zones as EIPs.

In a study conducted by Yalman Akcengiz (2020), the transformation of conventional industrial parks into EIPs was investigated to enhance resource efficiency in production under changing global competition conditions. The research involved a virtual park created by 10 companies located in OSTİM OIZ. Using simulation programs, the study compared the input materials and output products of a conventional park operating with traditional methods and an EIP utilizing raw material and waste sharing (Yalman Akcengiz, 2020).

In a study conducted by Temiz and Sağlık (2021), green business parks were defined, emphasizing their benefits for human and community health, accompanied by examples from around the world. These parks aim to adopt the concept of sustainable cities, providing comfortable spaces for users and strengthening the connections between the built environment and humans (Temiz & Sağlık, 2021).

Materials and Methods

Analytic Hierarchy Process (AHP)

The Analytic Hierarchy Process AHP), developed by Thomas Saaty, is a method that enables decision-makers to make more accurate and effective decisions in complex decision-making problems. It is recognized as one of the most widely used MCDM approaches (Saaty, 2008). AHP is defined as a decision support tool that organizes goals, criteria, and alternatives within a hierarchical structure. This process utilizes pairwise comparison matrices, reflecting both subjective and objective considerations of the decision-maker (Triantaphyllou & Mann, 1995). To ensure the decisions are more consistent, a consistency check is applied during these comparisons (Saaty, 2008).

AHP is effectively utilized in environmental engineering across various fields such as waste management, risk assessment, and environmental impact analyses (Stypka et al., 2016; Topuz & van Gestel, 2016; Upadhyay, 2017). Particularly in scenarios requiring MCDM, the systematic and consistent approach offered by AHP plays a critical role in solving environmental problems.

Steps of the Analytic Hierarchy Process (AHP):

Step 1: Structuring the Hierarchical Model

This step involves the creation of a hierarchical structure. During this phase, the decision problem is designed in a hierarchical order, which is considered one of the most critical elements of the decision-making process. At the top level of the hierarchy, the decision-making goal is placed. The criteria to be evaluated are located at the middle level, while the alternatives are positioned at the bottom level (Bhushan & Rai, 2004).

Step 2: Constructing the Pairwise Comparison Matrix

This step involves the creation of a pairwise comparison matrix for evaluating the criteria. A square matrix is constructed, where the diagonal elements are always assigned a value of 1 (Bhushan & Rai, 2004). The criteria are compared pairwise based on their relative importance, using the importance scale provided in Table 1 (Saaty, 2008). This scale facilitates a systematic evaluation of the criteria based on their significance.

Table 1. Importance Scale

Importance Values	Definition of Values
1	The situation where both factors have equal importance
3	The situation where the 1st factor is more important than the 2nd factor
5	The situation where the 1st factor is significantly more important than the 2nd factor
7	The situation where the 1st factor has much stronger importance compared to the 2nd factor
9	The situation where the 1st factor has absolute superior importance compared to the 2nd factor
2,4,6,8	Intermediate values

Step 3: Determining the Eigenvector Values of Criteria

The pairwise comparison matrix represents the relative importance of the criteria. At this stage, the eigenvector value for each criterion, representing its proportion in the total weight, is calculated. This calculation is performed using Formula 1 (Bhushan & Rai, 2004). The eigenvector values serve as the priority weights of the criteria, providing a numerical basis for their relative significance in the decision-making process.

$$\frac{1}{n} \cdot \sum \frac{aij}{\sum aij} \qquad (1)$$

Step 4: Calculating the Consistency Ratio (CR)

Due to the subjective nature of pairwise comparisons, the Consistency Ratio (CR) is calculated to assess the reliability of these judgments. The CR is determined using Formula 2, Formula 3, and the Random Index Table (Table 2) (Bhushan & Rai, 2004). The CR value is considered acceptable if it is below 10% (0.1). If the CR exceeds this threshold, the pairwise comparison matrix must be revisited, and each step should be reviewed and repeated to improve consistency (Triantaphyllou & Mann, 1995). This ensures that the comparisons remain logical and reliable for decision-making.

$$\text{Consistency Ratio (CR)} = \frac{\text{Consistency Index (CI)}}{\text{Random Index (RI)}} \quad (2)$$

$$\text{Consistency Index (CI)} = \frac{\lambda max - n}{n - 1} \quad (3)$$

Table 2. Random Index Table (RI)

n	3	4	5	6	7	8	9
Values	0.58	0.9	1.12	1.24	1.32	1.41	1.45

Application

To select a suitable location for an EIP, it is first necessary to identify alternative regions and then define the relevant criteria to facilitate the selection process among these regions. In this study, potential locations for EIPs were evaluated using the AHP. The selection criteria were determined through a literature review, and the weights of these criteria were calculated using the AHP method.

In Türkiye, the districts of Arnavutköy, Çatalca, and Silivri were evaluated for EIP site selection using the AHP methodology. The potential of each district was analyzed based on sub-criteria grouped under four main categories: environmental, economic, socio-cultural, and technological criteria.

Alternative regions for the establishment of the EIP were identified based on expert opinions. For the selected regions, factors such as land ownership conditions and environmental suitability were examined in collaboration with local governments and relevant public institutions. Particular attention was given to public lands and areas that support environmental sustainability, leading to the identification of three

alternative locations: Arnavutköy, Çatalca, and Silivri.

As a result of the literature review, the criteria to be used for EIP site selection were identified, comprising a total of 4 main criteria and 24 sub-criteria. These criteria are presented in Table 3.

Table 3. Criteria

Main Criteria	Sub-criteria
Environmental Criteria	Availability of adequate water resources
	Water quality and purity
	Wastewater treatment capabilities
	Possession of fertile soils
	Proximity to natural parks, reserves, or protected areas
	Potential risk of ecosystem damage
	Air quality
	Provision of clean air
	Wind direction and velocity
Economic Criteria	Accessibility to road, rail, maritime, and air transport networks
	Availability of a skilled workforce
	Energy infrastructure
	Access to electricity, gas, heating, and other energy sources
	Land acquisition costs
	Construction costs
	Operational costs
Social and Cultural Criteria	Support and engagement of local communities
	Compatibility with historically and culturally significant sites
	Preservation of heritage areas
	Access to healthcare and educational institutions
	Services supporting human health and well-being
Technological Criteria	Proximity to research and development centers
	Technological infrastructure capabilities
	Innovation supports and incentives

Considering that each criterion does not have the same level of importance and their degrees of significance vary, the AHP method was employed to calculate the weight of each criterion. In the first stage, a pairwise comparison matrix was developed, and the criteria were compared pairwise to determine which criterion is more important or dominant relative to the other. This comparison matrix was formed based on face-to-face interviews conducted with three academics specializing in environmental engineering and sustainability in the Istanbul region, as

well as an environmental engineer from relevant public institutions. The resulting pairwise comparison matrix is presented in Table 4.

Table 4. Main Criterion Pairwise Comparison Matrix

	Environmental Criteria	Economic Criteria	Social and Cultural Criteria	Technological Criteria
Environmental Criteria	1	0,333	0,25	0,5
Economic Criteria	3	1	2	2
Social and Cultural Criteria	4	0,5	1	3
Technological Criteria	2	0,5	0,333	1

Since the CR of the comparison matrix is below 0.10, the resulting decision matrix is deemed consistent. The percentage importance distributions for each main and sub-criterion are presented in Table 5

Table 5. Percentage Importance Distributions for Main and Sub-Criteria

Criteria	Percentage Importance Distributions of the Criteria	Sub-criteria	Percentage Importance Distributions of the Sub-Criteria	Arnavutköy	Çatalca	Silivri
Environmental Criteria	0.097	Availability of adequate water resources	0.235	0.548	0.241	0.211
		Water quality and purity	0.188	0.698	0.277	0.154
		Wastewater treatment capabilities	0.087	0.232	0.662	0.779
		Possession of fertile soils	0.053	0.765	0.344	0.131
		Proximity to natural parks. reserves. or protected areas	0.041	0.236	0.844	0.597
		Potential risk of ecosystem damage	0.085	0.715	0.262	0.169
		Air quality	0.122	0.765	0.277	0.145
		Provision of clean air	0.058	0.332	0.332	0.332
		Wind direction and velocity	0.132	0.236	0.844	0.597

Criteria	Percentage Importance Distributions of the Criteria	Sub-criteria	Percentage Importance Distributions of the Sub-Criteria	Arnavutköy	Çatalca	Silivri
Economic Criteria	0.399	Accessibility to road. rail. maritime. and air transport networks	0.064	0.537	0.268	0.195
		Availability of a skilled workforce	0.089	0.240	0.753	0.467
		Energy infrastructure	0.113	0.340	0.820	0.182
		Access to electricity. gas. heating. and other energy sources	0.112	0.463	0.232	0.232
		Land acquisition costs	0.206	0.530	0.232	0.201
		Construction costs	0.162	0.463	0.232	0.232
		Operational costs	0.255	0.323	0.323	0.323
Social and Cultural Criteria	0.339	Support and engagement of local communities	0.122	0.187	0.234	0.579
		Compatibility with historically and culturally significant sites	0.122	0.202	0.234	0.524
		Preservation of heritage areas	0.203	0.329	0.329	0.329
		Access to healthcare and educational institutions	0.310	0.413	0.302	0.329
		Services supporting human health and well-being	0.243	0.603	0.302	0.302
Technological Criteria	0.165	Proximity to research and development centers	0.195	0.539	0.164	0.297
		Technological infrastructure capabilities	0.267	0.539	0.164	0.297
		Innovation supports and incentives	0.538	0.539	0.164	0.297

Discussion and Conclusion

Examples of eco-settlements are rapidly increasing worldwide. In these settlements, the storage, conservation, and reuse of energy and water, along with household-level food production systems in the immediate vicinity, constitute a critical component of planning. For urbanization to remain livable, social, economic, and demographic developments must advance in a balanced manner.

In this study, the weights of various criteria and sub-criteria were determined according to their respective degrees of importance in an investment evaluation process. The findings serve as a critical guide for understanding how environmental, economic, social and cultural, and technological criteria affect investment decisions. The significance of each main criterion and sub-criterion is discussed below:

Environmental criteria account for 9.7% of the overall weight, with "Availability of Adequate Water Resources" (23.5%) being the most

significant sub-criterion in this category. This finding highlights the critical role of water resources, particularly in terms of sustainability and environmental compatibility for investment decisions. "Water Quality and Purity" (18.8%) and "Wind Direction and Velocity" (13.2%) also stand out as important environmental factors. However, other sub-criteria, such as "Proximity to Natural Parks and Protected Areas," have relatively lower importance (4.1%).

Economic criteria, accounting for 39.9% of the overall weight, emerge as the most dominant category in investment decisions. Notably, "Operational Costs" (25.5%) and "Land Acquisition Costs" (20.6%) are the most significant sub-criteria within this category. This finding underscores the considerable importance that investors place on minimizing total costs. Criteria related to energy, such as "Energy Infrastructure" (11.3%) and "Access to Electricity, Gas, Heating, etc." (11.2%), also stand out in economic evaluations. However, transportation infrastructure factors like "Accessibility to Road, Rail, Maritime, and Air Transport Networks" (6.4%) are assigned relatively lower priority.

Social and cultural criteria, accounting for 33.9% of the overall weight, emerge as the second most significant category after economic criteria. Among these, "Access to Healthcare and Educational Institutions" holds the highest weight at 31.0%, suggesting that access to community well-being is a critical determinant in investment decisions. Other important sub-criteria include "Services Supporting Human Health and Well-being" (24.3%) and "Preservation of Heritage Areas" (20.3%). These findings emphasize the influence of social sustainability on investment decisions.

Technological criteria comprise 16.5% of the overall weight, thus having a lower priority compared to the other criteria. However, the sub-criterion "Innovation Supports and Incentives," at 53.8%, holds the highest importance in this category by a considerable margin. This finding indicates that promoting and incentivizing innovation serves as a significant driving force in modern investments. Other sub-criteria, such as "Technological Infrastructure Capabilities" (26.7%) and "Proximity to Research and Development Centers" (19.5%), carry relatively lower priority.

When each district is evaluated according to the criteria, Arnavutköy exhibits notable advantages for EIP site selection, outperforming other districts due to the combined strength of its environmental, economic, social, and technological factors. The standout features of Arnavutköy, based on the criteria established in this study, have been examined in detail.

Arnavutköy has demonstrated a strong performance in terms of environmental criteria. Specifically, it achieved high scores on the sub-criteria "Availability of Adequate Water Resources" and "Water Quality

and Purity," placing it ahead of other districts in terms of environmental sustainability. From an economic standpoint, Arnavutköy's levels of "Land Acquisition Costs" and "Construction Costs" are found to be favorable. In addition, the district's high score on the "Accessibility to Road, Rail, Maritime, and Air Transport" criterion indicates a strategic position regarding transportation infrastructure, offering logistical advantages and attractive opportunities for investors.

Upon evaluating the social and cultural dimensions, Arnavutköy was observed to perform strongly in areas such as "Services Supporting Human Health and Well-being" and "Access to Healthcare and Educational Institutions." These criteria notably contribute to securing local community support and fostering social cohesion. From the perspective of technological and innovative capacities, Arnavutköy also stands out in the sub-criteria "Technological Infrastructure Capabilities" and "Innovation Supports and Incentives." This demonstrates that the district offers a long-term, sustainable solution for an industry- and technology-focused EIP.

This study has clearly demonstrated the varying degrees of importance among different criteria for investment decisions. The consideration of social and environmental sustainability factors is critically significant for long-term investment strategies. Although technological criteria receive a relatively lower weight, the prominence of innovation incentives as the leading factor in this category suggests that future investments may grow in this field. These findings can be utilized to guide investors and policymakers in allocating resources most effectively. In particular, a more balanced assessment of the relative importance of various criteria can lead to healthier outcomes, both in terms of short-term gains and long-term sustainability.

REFERENCES

Bhushan, N., & Rai, K. (2004). Strategic decision-making. In *Strategic Decision Making: Applying the Analytic Hierarchy Process* (pp. 3-10). London: Springer London.

Esenlikci, A. C. (2023). Türkiye'de Organize Sanayi Bölgelerinin Yeşil Dönüşümü: Yeşil Organize Sanayi Bölgesi Projesi. Nevşehir Hacı Bektaş Veli Üniversitesi SBE Dergisi, 13(1), 337-357 *(in Turkish).*

Genç, O. (2020). Doğadan ilham alan sürdürülebilir eko-endüstriyel park gelişimi ve tasarımı *(in Turkish).*

Gümüş, T. Ç. (2016). *Eko-endüstriyel parklar için temiz üretim ve endüstriyel simbiyoz karar destek sisteminin geliştirilmesi (in Turkish)* (Master's thesis, TOBB University of Economics and Technology, Graduate School of Natural and Applied Sciences).

Hong, H., & Gasparatos, A. (2020). Eco-industrial parks in China: Key institutional aspects, sustainability impacts, and implementation challenges. *Journal of Cleaner Production*, *274*, 122853.

Özsoy, T. (2018). Endüstriyel Ekolojiyi Anlamak Adına Endüstriyel Ortakyaşarlık Örneklerinin İncelenmesi. Artıbilim: Adana Bilim ve Teknoloji Üniversitesi Sosyal Bilimler Dergisi, 1(2), 22-34 *(in Turkish).*

Saaty, T. L. (2008). Decision making with the analytic hierarchy process. *International journal of services sciences*, *1*(1), 83-98.

Stypka, T., Flaga-Maryanczyk, A., & Schnotale, J. (2016). Application of the AHP method in environmental engineering: Three case studies. *Applications and Theory of Analytic Hierarchy Process-Decision Making for Strategic Decisions*.

T.R. Ministry of Science, Industry and Technology (MSIT) (2015). New generation industrial zones. Retrieved December 12, 2024, from https://edergi.sanayi.gov.tr/File/Journal/2015/9/9_2015.pdf

Temiz, M., & Sağlık, A. (2021). Sürdürülebilir kentler: Yeşil iş parkları. *Türkiye Peyzaj Araştırmaları Dergisi*, *4*(1), 1-12 *(in Turkish).*

Topuz, E., & van Gestel, C. A. (2016). An approach for environmental risk assessment of engineered nanomaterials using Analytical Hierarchy Process (AHP) and fuzzy inference rules. *Environment international*, *92*, 334-347.

Triantaphyllou, E., & Mann, S. H. (1995). Using the analytic hierarchy process for decision making in engineering applications: some challenges. *International journal of industrial engineering: applications and practice*, *2*(1), 35-44.

Upadhyay, K. (2017). Application of analytical hierarchy process in evaluation of best sewage treatment plant. *International Journal of Science and Research*, *6*(6), 259-264.

Uscha, C. M., Cahyo, R. N., & Farizal, F. (2021, May). Proposed Site Selection Criteria for Eco-Industrial Park in Indonesia. In *Proceedings of the 4th Asia Pacific Conference on Research in Industrial and Systems Engineering* (pp. 419-424).

Uslu, G. (2019). *Bir sürdürülebilir kalkınma modeli olarak endüstriyel simbiyoz ve KOBİ'lerde endüstriyel simbiyoz uygulamaları üzerine öneriler (in Turkish)* (Master's thesis, Namık Kemal University)

Valenzuela-Venegas, G., Vera-Hofmann, G., & Díaz-Alvarado, F. A. (2020). Design of sustainable and resilient eco-industrial parks: Planning the flows integration network through multi-objective optimization. *Journal of cleaner production*, *243*, 118610.

Veiga, L. B. E., & Magrini, A. (2009). Eco-industrial park development in Rio de Janeiro, Brazil: a tool for sustainable development. *Journal of cleaner production*, *17*(7), 653-661.

Walls, J. L., & Paquin, R. L. (2015). Organizational perspectives of industrial symbiosis: A review and synthesis. *Organization & Environment*, *28*(1), 32-53.

Yalman Akcengiz, P. (2020). *Eko endüstriyel parklarda enerji yönetimi: OSTİM OSB örneği (in Turkish)* (Master's thesis, Başkent University, Graduate School of Natural and Applied Sciences).